# Advancing Catalysis by Colloidal Metal Nanoparticles: Process Intensification and Beyond

Zur Erlangung des akademischen Grades eines

**Dr.-Ing.**

von der Fakultät Bio- und Chemieingenieurwesen
der Technischen Universität Dortmund
genehmigte Dissertation

vorgelegt von

**M.Sc. Florian Lehmann**

aus

Werne

Tag der mündlichen Prüfung: 15.06.2026

1. Gutachter: Prof. Dr. Dieter Vogt
2. Gutachter: Prof. Dr. Hannsjörg Freund

**Dortmund 2026**

„1.21 Gigawatt! Tom Edison, wie erzeugt man so viel Strom?“
— Doc E.L. Brown in *Zurück in die Zukunft I*

***Danksagung***

Das Gelingen dieser Arbeit wäre ohne Unterstützung unterschiedlichster Art durch eine Vielzahl von Personen nicht möglich gewesen.

Ich danke Prof. Dr. Dieter Vogt für die Möglichkeit, diese Arbeit an seinem Lehrstuhl anfertigen zu können, das offene Ohr und das entgegengebrachte Vertrauen sowie die Freiheit zur selbstständigen Arbeit. Prof. Dr. Hannsjörg Freund danke ich für die freundliche Übernahme des Zweitgutachtens sowie Prof. Dr. Christoph Held für die Mitwirkung in der Prüfungskommission.

Herzlichst danken möchte ich PD Dr. Thomas Seidensticker für die enge inhaltliche Betreuung und die stets angeregten Diskussionen sowie eingeworfenen Ideen. Sie haben die Gestalt dieser Arbeit wesentlich geformt und waren wertvolle Hilfen und Inspirationen für den gesamten Verlauf der Bearbeitung dieses Projekts.

Ein weiterer großer Dank geht an zwei Arbeitsgruppen der Universität Duisburg-Essen, deren intensive Kooperation die Grundsteine für diese Arbeit gelegt haben. Hier danke ich zum einen PD Dr. Sven Reichenberger und Dr. Theo Fromme vom Lehrstuhl Technische Chemie I für zahlreiche Stunden am Laser sowie zugehörige fachliche Diskussionen. Zum anderen danke ich Prof. Dr. Matthias Epple vom Fachbereich Anorganische Chemie mit seinen Mitarbeitern Dr. Niklas Kost, Rui Guo und Dr. Kateryna Loza sowie Dr. Marc Heggen vom Forschungszentrum Jülich für die enge Zusammenarbeit bei der Untersuchung der nasschemisch hergestellten Partikel.

Ein besonderer Dank geht an alle Kollegen vom Lehrstuhl Technische Chemie, die das tägliche Lehrstuhlleben und auch die Zeit abseits der Uni bereichert und bei Bedarf mit Rat und Tat zur Seite gestanden haben: Maxi, mein Bürokollege Justus, Alex, Thomas, Tim, Bernd, Niclas, Christian, Kevin, Johanna, Hannes, Dominik, Jerome, Arno, Thilo, Nadine, Jan-Niklas, Franzi, Daniel, Tobi, Jonas, Anna, Till, Saqib, Milan und Fabian.

Ebenfalls danke ich den technischen Angestellten Andreas, Marén, Justin und Iris sowie den Azubis Deniz, Till, Sidonie, Claudia und Lucia für ihre Unterstützung.

Ohne die Mitarbeit einiger von mir betreuter Studierender hätten Teile dieser Arbeit nicht realisiert werden können, deshalb danke ich Janik A., Isa, Nikita, Lennard, Thilo, Moritz, Take, Dagmar, Sebastian und Simon, vor allem aber Peter, Karl Steffen, Flavia, Janik H., Tobias und Merlin für ihre geleistete Arbeit sowie Nils für beigesteuerte Versuche zur Methoxycarbonylierung.

Abschließend geht ein großer Dank an meine Freunde und meine Familie, insbesondere meine Eltern, die mich zu jeder Zeit während des gesamten Studiums und der anschließenden Promotion voll unterstützt haben, sodass die Anfertigung der Arbeit in dieser Form überhaupt erst möglich wurde.

# Table of Contents

# Zusammenfassung

Die signifikante Verbesserung der Kosten-, Energie- und Materialeffizienz von chemischen Prozessen ist das Ziel der Prozessintensivierung, wobei unter anderem Katalyse eine herausragende Rolle spielt. Dafür werden immer neue Katalysatoren entwickelt und initial getestet. Ein sehr aktives Forschungs-Teilgebiet ist dabei die Herstellung von Nanopartikeln und deren katalytische Anwendung im Labormaßstab. Ein Übertrag zu kontinuierlichen Prozessen bleibt aber meistens aus.

Trotz langer Entwicklungsarbeit verbleiben spezifische Problemstellungen für einige katalytische Umsetzungen. Ein Beispiel ist die selektive Teilhydrierung von Polyenen und Alkinen. Mit neu entwickelten Katalysatoren bzw. deren Herstellmethoden ist dabei eine nie dagewesene Innovation in der Entwicklung und Intensivierung neuer chemischer Produktionsprozesse möglich. Die vorliegende Arbeit nutzt daher die Kombination von teils neuartig hergestellten kolloidalen, lösungsmittelstabilisierten Nanokatalysatoren mit Elementen der vier verschiedenen Ebenen der Prozessintensivierung in einem ganzheitlichen hierarchischen Entwicklungsansatz. Für mindestens einen Beispielfall soll ein kontinuierlicher Reaktorbetrieb ermöglicht werden.

Zunächst werden auf der molekularen Ebene verschiedene kolloidale Nanokatalysatoren in ihrer Anwendbarkeit in selektiven Teilhydrierungen verschiedener Substrate getestet. Zum Teil werden strukturelle Veränderungen des Katalysatormaterials untersucht.

Auf der Phasenebene wird anschließend eine alternative Heizmethode mit Mikrowellen für Suzuki-Kupplungen mit einem ähnlichen Katalysatorsystem betrachtet.

Das vielversprechendste Katalysatorsystem wird danach zur Etablierung einer Reaktionssequenz auf der Ebene einer Prozesseinheit genutzt. Insbesondere wird dabei die selektive Teilhydrierung mehrfach ungesättigter Fettsäuremethylester untersucht. Diese wird dann in einem tandemkatalytischen System mit einer isomerisierenden Methoxycarbonylierung kombiniert und detailliert auf die Vereinbarkeit beider Reaktionsschritte hinsichtlich Lösungsmittel, Gasphasenwechsel und Aktivierung für den zweiten Reaktionsschritt untersucht.

Zuletzt wird auf der Anlagenebene die Reaktoreinheit mit einer Stoffübertragungseinheit kombiniert: In einem Kapillarreaktor mit Gas-Flüssig-Slug-Flow wird die selektive Teilhydrierung von Fettsäuremethylestern mit der kontinuierlichen Gasnachförderung durch Permeation kombiniert. Dies soll ermöglichen, die vorteilhaften Eigenschaften des Slug-Flows über die gesamte Reaktorlänge beizubehalten. Dieses Konzept bietet eine Übertragbarkeit auf ähnliche Reaktionen mit homogenen Flüssigphasen und Reaktionsgas.

# Abstract

The significant improvement of cost, energy, and material efficiency in chemical processes is the goal of process intensification, with catalysis playing a crucial role. To achieve this, new catalysts are continuously developed and initially tested. A highly active research subtopic focuses on the synthesis of nanoparticles and their catalytic application on a laboratory scale. However, transfer to continuous processes often remains unrealized.

Despite extensive development efforts, specific challenges persist for certain catalytic transformations like selective partial hydrogenations of polyenes and alkynes. Newly developed catalysts and preparation methods enable unprecedented innovation in the design and intensification of novel chemical production processes. The present work combines the use of partly newly synthesized colloidal, solvent-stabilized nanocatalysts with elements of all levels of process intensification. In a holistic, hierarchical development approach, operation in a continuous reactor shall be enabled.

At the molecular level, various colloidal nanocatalysts are tested for their applicability in the selective partial hydrogenation of different substrates. Investigations into structural changes of the catalyst material are included.

At the phase level, an alternative microwave-based heating method for Suzuki couplings using a similar catalytic system is examined.

The most promising catalyst system is then applied to establish a reaction sequence at the process-unit level. In a tandem catalytic system, the selective hydrogenation of fatty acid methyl esters followed by isomerizing methoxycarbonylation is analyzed regarding compatibility of both reaction steps in terms of solvent choice, gas-phase change, and subsequent catalyst activation.

At the plant level, the combination of a reactor with a mass-transfer unit is realized: Selective partial hydrogenation of fatty acid methyl esters in a capillary reactor with gas-liquid slug flow is coupled with continuous gas replenishment via permeation. This should maintain favorable slug-flow characteristics along the entire reactor length, offering transferability to similar reactions involving homogeneous liquid phases with reactive gases.

# Publications and Conference Contributions

**Publications**

1. (Publication I) N. Kost, F. Lehmann, R. Guo, K. Loza, M. Heggen, T. Seidensticker, M. Epple, “Catalytic Activity of Water-Dispersed Palladium Nanoparticles with Different Sizes and Shapes in the Semihydrogenation of Alkynes”, *ChemCatChem* **2025**, *17*, e01164, DOI: 10.1002/cctc.202501164.
2. (Publication II) F. Lehmann, H. W. Wegener, N. Brede, T. Seidensticker, “Combining Partial Hydrogenation of Soybean-Derived Biodiesel and Methoxycarbonylation Using a Single Palladium Source”, *Eur. J. Lipid Sci. Technol.* **2025**, *127*, e70073, DOI: 10.1002/ejlt.70073.
3. (Publication III) F. Lehmann, N. von Vietinghoff, P. Pey, K. S. Wulle, T. Seidensticker, “Integrating Gas Permeation with Gas-Consuming Reactions in Slug-Flow Capillaries: Continuous and Selective Hydrogenation of Biodiesel”, *ACS Sustainable Chem. Eng.* **2025**, *13*, 20242–20252, DOI: 10.1021/acssuschemeng.5c09302.
4. (Publication IV) T. Fromme, M. L. Spiekermann, F. Lehmann, S. Barcikowski, T. Seidensticker, S. Reichenberger, “Preferential enrichment and extraction of laser-synthesized nanoparticles in organic phases”, *Beilstein J. Nanotechnol.* 2025, *16*, 254–263, DOI: 10.3762/bjnano.16.20.
5. (Publication V) J. Diekamp, A. Schmidt, F. Lehmann, L. Küsel, C. Strohmann, D. Vogt, T. Seidensticker, "Selective Transfer Hydrogenation of Polyenes to Monoenes Catalysed by Shvo´s Catalyst", *Adv. Synth. Catal.*, accepted.
6. (Review I) F. Lehmann, T. Seidensticker, "Stoffliche Nutzung von Pflanzenölen im Non-Food-Bereich" in *Warenkunde Ölpflanzen und Pflanzenöle*. *Anbau, Verarbeitung, Vermarktung, Verwendung,* (Eds.: B. Matthäus, E.-W. Münch), Erling, Clenze, **2024**.

Only the first three publications are considered in this thesis.

**Poster Presentations**

1. F. Lehmann, N. von Vietinghoff, T. Nakai, L. Nebel, P. Pey, K.S. Wulle, D. Vogt, T. Seidensticker, “Continuous selective FAME hydrogenation utilizing a microcapillary reactor”, 12th Workshop on Fats and Oils as Renewable Feedstocks for the Chemical Industry, Dortmund, June 2023
2. F. Lehmann, N. von Vietinghoff, T. Nakai, L. Nebel, P. Pey, K.S. Wulle, D. Vogt, T. Seidensticker, “Strategies to counteract gas shortage in microcapillaries for multiphase hydrogenation reaction“, 57. Jahrestreffen Deutscher Katalytiker, Weimar, March 2024
3. F. Lehmann, N. von Vietinghoff, T. Nakai, L. Nebel, P. Pey, K.S. Wulle, D. Vogt, T. Seidensticker, “Strategies to counteract gas shortage in microcapillaries for multiphase hydrogenation reaction“, Annual Meeting on Reaction Engineering and Electrochemical Processes 2024, Würzburg, May 2024

4. F. Lehmann, N. von Vietinghoff, T. Nakai, L. Nebel, P. Pey, K.S. Wulle, D. Vogt, T. Seidensticker, “Selective Hydrogenation in Multiphase Microcapillary Reactors: A Valuable Tool to Harmonize Feedstocks in Lab Scale”, DGMK Conference Energy and Material Flows in Sustainable Petrochemistry, Hamburg, November 2024
5. F. Lehmann, N. von Vietinghoff, T. Nakai, P. Pey, K.S. Wulle, D. Vogt, T. Seidensticker, “Integration of Gas Permeation with Gas-Consuming Reactions in a Slug Flow Capillary Reactor“, GeCatS Infoday "From Flow Chemistry to Continuous Processes: New Alternatives for Chemical Production on Laboratory and Ton Scale", Frankfurt a.M., December 2025

# List of Abbreviations and Symbols

| symbol or abbreviation | meaning | unit |
|---|---|---|
| $\Delta p_{perm}$ | permeation pressure difference | kPa or bar |
| $\varepsilon_{gas,polymer}$ | permeation coefficient | $cm^3$ mm $cm^{-2}$ $kPa^{-1}$ $s^{-1}$ |
| $\varphi_{FAME}$ | volume fraction of fatty acid methyl esters in the reaction mixture | mL $mL^{-1}$ |
| $\varphi_{H2O}$ | volume fraction of water in catalyst solution | % (V/V) |
| $\tau$ | residence time | min |
| A | area | $m^2$ or $cm^2$ |
| CO:$H_2$ | molar carbon monoxide to hydrogen ratio | mol $mol^{-1}$ |
| $c_{H2,solvent}$ | solubility of hydrogen in a solvent | mol $m^{-3}$ |
| $c_{Pd}$ | catalyst loading | mol% |
| $c_{Rh,total}$ | Rh concentration in the reaction solution | mmol $L^{-1}$ |
| $c_{substrate,toluene}$ | concentration of the substrate in toluene | mol $L^{-1}$ |
| $d_{Feret}$ | Feret-diameter | nm |
| $f_{stirrer}$, ω | rotational speed | $min^{-1}$ |
| $k'$ | molar rate constants | $s^{-1}$ |
| $k_l a$ | volumetric mass transfer coefficient of gas in liquid | $s^{-1}$ |
| l | length of the reactor | m |
| L:Pd | molar ligand:palladium ratio | mol $mol^{-1}$ |
| $l_{p,0m}$ | length of gas bubbles at the reactor inlet | m |
| $l_{p,i}$ | length of gas bubbles after each reactor segment | m |
| $l_{segment,i}$ | length of the segment | m |
| M | molar mass | g $mol^{-1}$ |
| n | molar amount | mmol |
| $n_{H2,GC}$ | hydrogen uptake calculated from gas chromatography | mmol |
| p | pressure | bar |
| P:Rh | molar phosphorus:rhodium ratio | mol $mol^{-1}$ |
| PC:solvent | volumetric ratio of propylene carbonate to an additional solvent | mL $mL^{-1}$ |
| q | permeation flux | mL $s^{-1}$ |
| s | wall thickness | mm |
| S | selectivity | mol $mol^{-1}$ |
| S:C | molar substrate:catalyst ratio | mol $mol^{-1}$ |
| S:Pd | molar substrate:palladium ratio | mol $mol^{-1}$ |
| STY | space-time yield | g $h^{-1}$ $mL^{-1}$ |
| T | temperature | K or °C |
| t | time | min or h |
| $TOF_{20}$ | turnover frequency at 20% substrate conversion | $h^{-1}$ |
| $TOF_{20,H2}$ | turnover frequency at 20% targeted hydrogen conversion | $h^{-1}$ |
| $T_{start}$ | start temperature of the reaction | °C |
| V | volume | mL |
| $\bar{\dot{V}}$ | averaged total volume flow | mL $min^{-1}$ |

| symbol or abbreviation | meaning | unit |
|---|---|---|
| $\dot{V}_{cat}$ | volume flow of (diluted) catalyst solution | mL min$^{-1}$ |
| $\dot{V}_{FAME}$ | volume flow of fatty acid methyl esters | mL min$^{-1}$ |
| $\dot{V}_{G}$ | volume flow of the gas at the inlet | mL min$^{-1}$ |
| $\dot{V}_{H_2,T}$ | volume flow of hydrogen introduced at the reactor inlet | mL min$^{-1}$ |
| $\dot{V}_{L}$ | volume flow of the liquid | mL min$^{-1}$ |
| $\dot{V}_{liq,total}$ | total liquid volume flow | mL min$^{-1}$ |
| $V_{measured,max}$ | maximum hydrogen uptake measured by mass flow controller | mLn |
| $V_{measured}$ | time-dependent hydrogen uptake measured by mass flow controller | mLn |
| $V_R$ | reactor volume | mL |
| $\dot{V}_{total}$ | total volume flow at the reactor inlet | mL min$^{-1}$ |
| w | mass fraction of a catalyst metal in a solvent | ppm (w/w) |
| X | conversion | mol mol$^{-1}$ |
| x | mole fraction | mol mol$^{-1}$ |
| Y | yield | mol mol$^{-1}$ |
| 1,2-DTBPMB | 1,2-bis[(di-tert-butylphosphino)methyl]benzene | |
| 1,2-DTBPMB(OTf)$_2$H$_2$ | 1,2-bis[(di-tert-butylphosphino)methyl]benzene triflate | |
| B1D | butane-1,4-diol | |
| B2D | 2-butene-1,4-diol | |
| B3D | 2-butyne-1,4-diol | |
| BuOH | 1-butanol | |
| $C_{11}$-ME | methyl-10-undecenoate | |
| C16:0 | methyl palmitate | |
| C18:0 | methyl stearate | |
| C18:1 | methyl octadecenoates | |
| C18:2 | methyl octadecadienoates | |
| C18:3 | methyl octadecatrienoates | |
| C20:0 | methyl arachidate | |
| CDA | cyclododecane | |
| CDD | cyclododecadiene | |
| CDE | cyclododecene | |
| CDT | cyclododecatriene | |
| CML | conjugated methyl linoleate | |
| COA | cyclooctane | |
| COD | cyclooctadiene | |
| COE | cyclooctene | |
| CV | coefficient of variation | |
| DC | disc centrifuge | |
| DCS | differential centrifugal sedimentation | |
| DFT | density functional theory | |
| DLS | dynamic light scattering | |
| DLVO | Derjaguin-Landau-Verwey-Overbeek | |
| DMA | dimethylacetamide | |
| DMF | dimethylformamide | |

| symbol or abbreviation | meaning | unit |
|---|---|---|
| dppe | 1,2-bis(diphenylphosphino)ethane | |
| dtbpx | 1,2-bis[(di-tert-butylphosphino)methyl]benzene | |
| FAME | fatty acid methyl ester | |
| FEP | fluorinated ethylene-propylene | |
| g/l | gaseous/liquid | |
| GC-FID | gas chromatography with flame ionization detector | |
| GC-MS-EI | gas chromatography with electron impact mass spectrometer | |
| GSH | glutathione | |
| HHDMA | hexadecyl-(2-hydroxyethyl)dimethyl ammonium dihydrogenphosphate | |
| HRTEM | high-resolution transmission electron microsopy | |
| iCML | isomerized conjugated methyl linoleate | |
| ICP-MS | inductively coupled plasma mass spectrometry | |
| ICP-OES | inductively coupled plasma optical emission spectrometry | |
| IL | ionic liquid | |
| iMC | isomerizing methoxycarbonylation | |
| IPA | isopropanol | |
| l/l | liquid/liquid | |
| MBA | methyl-butane-2-ol, tert-amylalcohol | |
| MBE | 2-methyl-3-butene-2-ol | |
| MBY | 2-methyl-3-butyne-2-ol | |
| ML | methyl linoleate | |
| MMA | methyl methacrylate | |
| MO | methyl oleate | |
| MTBE | methyl-tert-butyl ether | |
| MUFA | monounsaturated fatty acids | |
| MU-FAME | monounsaturated FAME | |
| NMR | nuclear magnetic resonance (spectroscopy) | |
| NP | nanoparticle | |
| PC | propylene carbonate (4-methyl-1,3-dioxolan-2-one) | |
| PLAL | pulsed laser ablation in liquids | |
| PUFA | polyunsaturated fatty acids | |
| PU-FAME | polyunsaturated FAME | |
| PVC | polyvinylchloride | |
| PVP | polyvinylpyrrolidone | |
| SEM | scanning electron microscopy | |
| TEM | transmission electron microsopy | |
| TMEDA | tetramethylethylenediamine | |
| TOF | turnover frequency | |
| XPS | X-ray photoelectron spectroscopy | |
| XRD | X-ray diffraction | |

# 1 Motivation

The chemical industry is of superior importance for everyday life and economics, since the production of chemicals is the fourth-largest industry sector in the European Union. However, it is also one of the most energy- and resource-intensive sectors with a very high impact on the environment. Therefore, this industry is heavily stressed, with the need to become more sustainable and still remain competitive. However, the European Commission expects the importance of the location Europe to decrease from being the second-most-important chemical producer worldwide in 2018 to the third place in 2030. As a solution, inherently safe and sustainable chemicals are expected to restore competitiveness.[1] As a second measure, the Green Deal was introduced, superficially as an engagement to overcome climate and environmental challenges, to establish a resource-efficient and competitive economy. The elimination of net $CO_2$ emissions by 2050 plays a central role there.[2] Therefore, the chemical industry is forced to save energy and resources and reduce $CO_2$ emissions.

The origin of the educts and their energy demand for sourcing, production, and purification has a major contribution to the sustainability of the product and its $CO_2$ emission, numerically expressed as Scope 3 emissions[3],[4]. Especially for incorporated fossil carbon, Scope 3 emissions contribute by 1/3 to 2/3 to the total emissions of the product[4]. While decarbonization is not possible due to the inherent structure of all organic molecules, defossilization is highly desirable, reducing the use of fossil resources[4]. These aspects raise the urgent need for more efficient processes and for a transition towards renewable resources in the near future.

To enable this transformation, continuous research in central fields of chemistry, like catalysis, is demanded[4]. However, due to practical, logistical, economic, and institutional reasons, a parallel optimization of existing, non-sustainable products and processes is also necessary[3]. This can be achieved by means of process intensification and catalysis as well, still contributing to the overall transformative process.

**Catalysis** is essential for modern life, since most of the industrially produced chemicals, which are also required for consumer goods directly or indirectly, include catalytic reaction steps[5]. Moreover, catalysis also plays a central role in environmental technologies, with exhaust gas treatment being one prominent example[6]. In total, catalysis is involved in more than 80% of all produced goods[5]. As a consequence, catalysis offers to reduce the environmental impact and total production costs of these goods, underlining its enormous impact on the whole planet[5]. At the same time, it offers attractive opportunities for technological development and resulting economic benefits[6]. As a consequence, catalysis was identified as a fundamental technology in the field of process intensification – aiming at significant improvements of chemical processes, e.g., a significantly reduced waste amount per product amount – and green chemistry[7],[8]. Green chemistry targets the reduction of environmental pollution and the reduction of the use of hazardous substances in chemical manufacturing and application[8]. This further includes aspects like the highest possible incorporation of all educt atoms in the product and the utilization of renewable resources[8].

At the same time, even small improvements of known **reaction** pathways – like yield increased by a few percentage points or temperature lowered by a few Kelvin – already show superior economic effects (especially for large-scale processes)[6] as well as positive ecological impacts. Therefore, such measures are highly desired, independent of the type of reaction.

Accordingly, the development of catalytic systems with ever-increasing selectivity and activity is a vital research area for various catalytic conversions, aiming to achieve even more cost- and material-efficient synthesis capabilities. This might be enabled by ongoing variations in synthesis routes or even completely novel synthesis strategies for both, catalysts and products. Innovative approaches to catalysts will, in a further step, create new opportunities for intensified processes. Several types of catalytic materials can be considered for this. As one of those possibilities, the synthesis of nanoparticles for catalytic purposes receives much attention in scientific literature, with a special focus on the use of bio-based materials as either part of the catalyst, such as a stabilizer, or as the substrate[9]. In combination with the use of “green” solvents in synthesis or as a reaction medium, the applicability of a vast range of nanomaterials for various efficient organic transformations was already shown[9]. Several general synthesis routes towards nanoparticles are known. However, typical wet-chemical approaches to nanoparticles are tedious and include several synthesis and work-up steps. Therefore, faster and more reliable synthesis methods are demanded, which can be found in physical processes like pulsed laser ablation in liquids. Although this is, in principle, a well-known tool for the preparation of nanoparticles, the application of the resulting particles in catalytic reactions has been only sparsely investigated[10].

At the same time, a literature review reveals that the synthesis and application of nanoparticles is predominantly performed from a very chemistry- and materials science-based position: The focus is often set on precise synthesis steps and first applications only in standard (often glass) laboratory equipment. The subsequent application of catalytically active nanoparticles under industrially relevant conditions is only scarcely considered, but is highly demanded to enable the application of nanocatalysis on a larger scale towards a more industrially viable implementation.

Therefore, this thesis will focus on an engineering perspective on nanocatalysis throughout all different levels of **process intensification**. Its combination with the synthesis and application of novel, highly selective catalysts (e.g., for the industrially strongly relevant selective partial hydrogenation) is a powerful tool for a more sustainable chemical industry and will be addressed in this work in-depth. By doing so, it is intended to enable the full potential of the applied catalysts in technically relevant scales and setups (Figure 1).

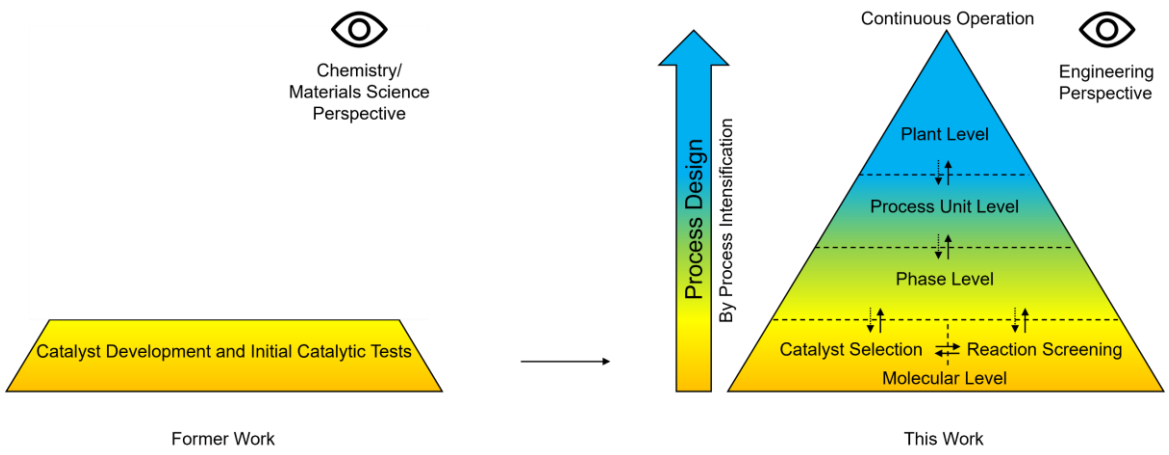


Figure 1: Different viewpoints on nanocatalyst development and resulting processes.

Like in existing literature, the investigations need to start at the basic layer of catalyst development and initial catalytic tests. This should be followed by measures on higher levels (Figure 1, right) to ultimately establish more sustainable processes with catalytically active colloidal nanoparticles. For the general investigations on synthesis strategies and the applicability of nanoparticles in various reactions, the molecular level should be divided into separate sections, focusing on catalyst selection and reaction screening individually. For the identification of an optimal catalyst (class), the consideration of both, wet-chemical and physical approaches to the catalyst material tested in an exemplary reaction seems appropriate for a systematic and overall evaluation of the potentials of all investigated synthesis routes and the resulting particles. The application of colloidal nanocatalysts synthesized by pulsed laser ablation in a stabilizing liquid was found to be a valuable tool for the hydrogenation of alkenes[11]; hence, broadening the applicability of this physical approach to catalytically active colloidal nanoparticles for further reactions and variations of the particles is of high interest. Moreover, selective partial hydrogenation offers possibilities to enable further functionalizations of polyunsaturated substrates and to access above-lying process intensification levels like the process unit level and the plant level: With this technique, resulting products derived from renewable substrates offer to be further converted into value-added products for direct use or as an alternative to fossil-based raw materials by means of generally known, but innovatively applied, homogeneous catalysis steps[12]. Especially for a continuous laboratory reactor operation with suitable, catalytically active colloidal nanoparticles, the design and commissioning of innovative reactor setups need to be performed to combine the benefits from both reaction engineering and nanocatalysis. For future-oriented chemistry, the application of renewable substrates also has to be considered repeatedly throughout this work.

With the following investigations, the typical development procedure for nanocatalysts is expected to be drastically extended and covered in a holistic approach (see Figure 1) by taking into account every hierarchical level of process intensification for a more sustainable chemical industry.

# 2 Theoretical Background

To address every level depicted in Figure 1, several methods are applied, which are introduced in this chapter. These methods range from different catalytic reactions like hydrogenations and C-C bond forming reactions on the molecular level, distinct heating and transport phenomena at the phase level, to the implementation in apparatuses and processes at the process unit level and plant level.

## 2.1 Selected Aspects of Catalysis

Most of the applied catalysts in this thesis are novel colloidal nanocatalysts. Therefore, the concept of nanocatalysis, possible synthesis strategies, and particle characterization methods are introduced first. Afterwards, essentials for all other catalytic systems will be presented.

### 2.1.1 Nanocatalysis: At the Interface Between Homogeneous and Heterogeneous Catalysis

#### *2.1.1.1 Classification*

Nanocatalysis represents an intermediate region between homogeneous and heterogeneous catalysis[9],[13]. It involves particles containing between 10 to $10^6$ atoms or possessing radii from 1 to 100 nm, while some literature defines 10 nm as the upper limit[14],[15]. Consequently, nanocatalysts occupy a size range that locates them between homogeneous and heterogeneous catalysts (Figure 2).

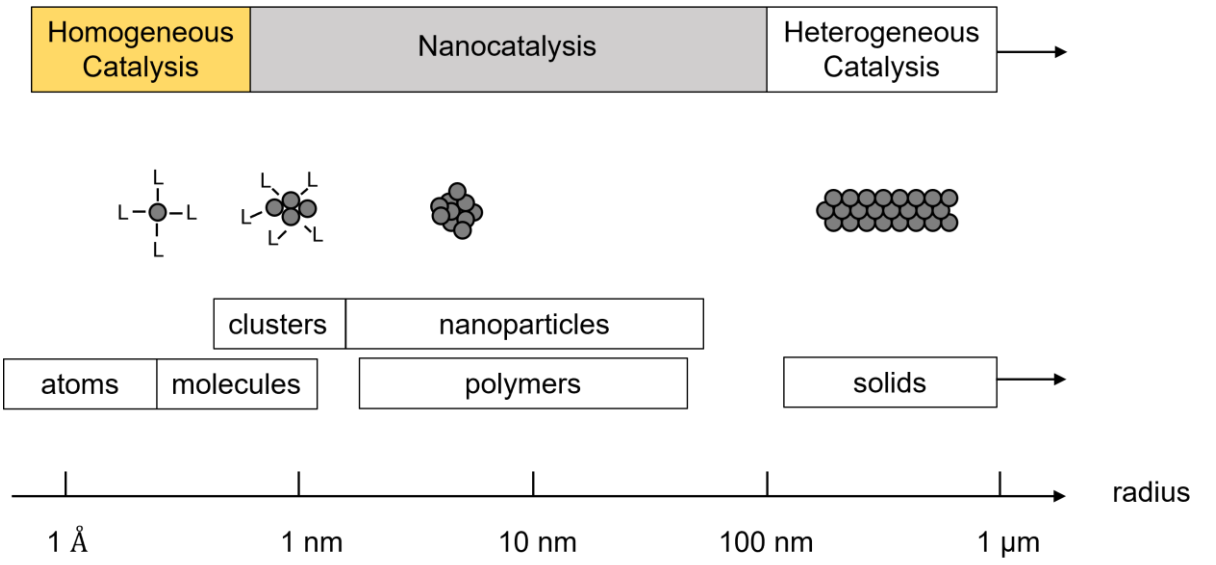


Figure 2: Size comparison of metal catalysts and differentiation between types of catalysis, adapted from[9],[13]–[15].

When suspended in liquid, they can be handled like homogeneous catalysts; however, their operating principle resembles heterogeneous catalysis. Notably, supports are not necessarily required for nanocatalysts. Furthermore, their major advantage over truly homogeneous catalysts is that their separation from reaction mixtures is generally more feasible due to their larger size and weight, allowing for filtration or centrifugation methods.[13],[16]

A clear distinction must be made between clusters and nanoparticles: Clusters are defined as polymetallic assemblies that can include ligands and possess a known X-ray crystallographic structure. In contrast, nanoparticles are characterized as polydisperse larger nanoclusters, with their size distribution typically defined through transmission electron microscopy (TEM) histograms.[9] This thesis will only deal with nanoparticles due to their high degree of variability in properties governed by spatial structures and stabilizing agents (see chapter 2.1.1.2), offering several opportunities for efficient catalysis.

Nanocatalysts possess a significant number of catalyst atoms located on their surface[15]. In theory, a high dispersion is particularly advantageous, as smaller particle dimensions lead to an increased surface area. Consequently, a substantial proportion of atoms becomes accessible for interaction with substrates.[14],[16],[17] These characteristics facilitate rapid and selective chemical conversions with very high yields, along with simple catalyst separation and recovery[17].

To achieve these benefits, the following major requirements are set in literature: Synthesis must be reliable to ensure reproducible particle properties. Therefore, the particles must exhibit a uniform size with well-defined surface composition. Finally, their high catalytic activity in solution must be maintained for a long catalyst lifetime with reproducible performance.[14]

### *2.1.1.2 Properties of Catalytically Active Nanoparticles*

Nanoparticles (NPs) in general possess a variety of unique physical and chemical properties that differ from those of bulk metals and can exhibit size-dependent behavior[9],[15],[18]. Their properties depend on factors such as size, size distribution, and shape[9],[17],[18]. Accordingly, catalytic aspects like activity and selectivity are significantly influenced by these factors as well as by the presence (or absence) of supports.[16]

The general impact of accessibility to specific structural features – such as steps, corners, and edges – is well recognized[16]. Exposed sites on NPs can exhibit varying reactivities due to markedly different coordination numbers associated with these locations[9]. Additionally, the crystal structure plays a crucial role in catalysis since different facets may possess distinct catalytic properties[9].

Colloidal NPs are only kinetically and not thermodynamically stable – meaning only for a limited amount of time –, accordingly, necessitating appropriate stabilization for convenient and reproducible usage[19]. An alternative approach involves the use of supports; however, this corresponds to conventional heterogeneous catalysis and will thus not be considered in this work[13]. The underlying reason for the instability is that thermodynamically, surface energy should be minimized[13]. Overall, two states of particle assembly can occur, being agglomeration and aggregation. Aggregates are dense assemblies, and their primary particles cannot be separated once aggregated, whereas the individual particles of agglomerates can still be separated, because they are more weakly bound[20]. Aggregates or even big agglomerates lose the beneficial properties of nanoparticles and may be insufficiently stabilized in the surrounding medium, leading to precipitation[13]. Currently, there is no universally applicable metric for

assessing stability[13]. However, high temperatures negatively impact stability, as particles move more vigorously and rapidly, making it easier for them to overcome energy barriers. Additionally, high concentrations adversely affect stability due to the increased likelihood of collisions among particles.[20]

In general, a small interparticle distance leads to attractive forces governed by van-der-Waals interactions, which necessitate the presence of repulsive forces to prevent particle aggregation. The fundamental stabilization mechanisms can be mathematically described by the DLVO theory (Derjaguin-Landau-Verwey-Overbeek). This theory provides energy-distance curves that delineate stable and unstable regions; however, an in-depth exploration of this theory is beyond the scope of this discussion.[14],[21]

To counteract the interparticle attraction, several mechanisms of particle stabilization are known, but the definition and underlying principles may vary slightly within literature. In the following, the mechanisms according to Roucoux are presented and depicted in Figure 3[14].

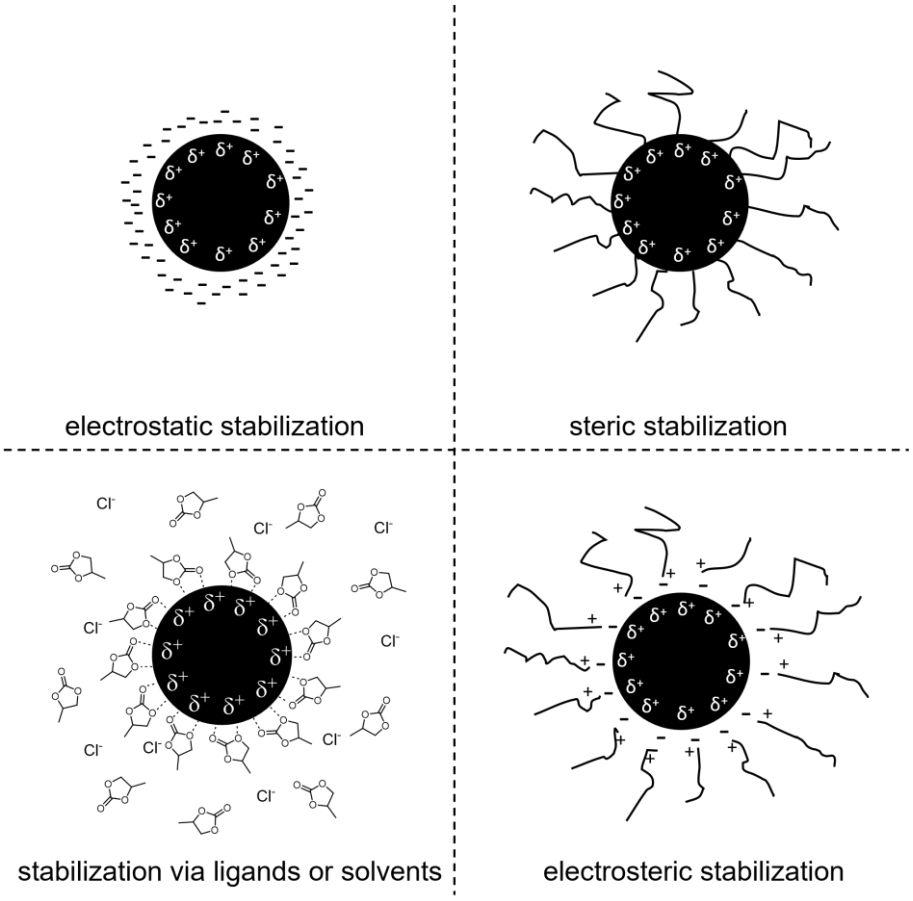


Figure 3: Principles of different stabilizing mechanisms, adapted from[13],[14],[22].

In *electrostatic stabilization*, an electric double layer around particles occurs due to the presence of ions originating from synthesis, leading to coulombic repulsion. This double layer is highly sensitive to any factors that may influence its stability, particularly ionic strength and (thermal) motion. The phenomenon is primarily observed in aqueous media.

For *steric stabilization*, macromolecules, such as oligomers or polymers, serve as ligands. They can adsorb onto surfaces through their oxygen, nitrogen, or sulfur atoms[23], forming a protective layer. The

movement within the interparticle region becomes restricted, resulting in a decrease in entropy and an increase in free energy. When the protective layers of two macromolecules penetrate each other, an osmotic repulsion occurs, macroscopically resulting in stabilization. The length and nature of the macromolecules determine the thickness of the protective layer and consequently influence the magnitude of the repulsive forces. Here, the medium is irrelevant.

*Stabilization via ligands or solvents*: This is a special type of steric stabilization, with the major difference that the stabilizing molecule is not an oligomer or polymer, but a ligand or solvent[13]. Typical ligands for complex catalysts like phosphines, thiols, amines, CO, or 1,10-phenantroline can coordinate to the surface via their respective donor atoms and may also influence or even completely hinder catalysis, see also chapter 2.1.1.3[13]. When the coordinating molecule is a solvent molecule, these systems are called “solvent-stabilized colloids”. One example is Pd nanoparticles in propylene carbonate as synthesized by Behr and coworkers[22].

*Electrosteric stabilization* is a combination of steric and electrostatic stabilization and uses ionic surfactants as stabilizing agents. Their polar headgroup forms the electric double layer on the particle surface, whereas the lipophilic group is responsible for the steric repulsion.

Stabilizers or strongly adsorbed reaction residues can adversely affect reactions by creating barriers or poisoning the catalyst[24]. On the one hand, highly pure and ligand-free surfaces are preferred for interactions with adsorbates. On the other hand, ligand-free nanospecies may not always serve as optimal catalysts since ligands can improve or alter chemoselectivity. Therefore, ligands are not only important for stabilization but can also be selectively chosen to influence surface properties through steric or electronic effects, with thiols and phosphines serving as notable examples.[9] Moreover, catalytic activity depends on the particle diameter, with four possibilities of dependence: constant activity, decreasing activity with increasing radius, increasing activity with increasing radius, or the exhibition of an activity optimum.[25] However, no universally valid relationship can be established, as the dependence is highly system- and substrate-specific, according to the literature.

During catalysis or even long shelf-life, colloidal NPs may undergo aging processes. One possibility is that atoms might dissolve, thus their native particles shrink in size. Particles may also aggregate due to less good stabilization, ultimately leading to sedimentation. Furthermore, Ostwald-ripening may occur: Here, small particles become disintegrated, followed by the integration of their atoms into larger particles[26].[27]

#### *2.1.1.3 Experimental Differentiation Between Homogeneous and Heterogeneous Catalysis*

Although the surface of the nanocatalysts was stated above as the catalytically active species, several authors discuss the possibility of metal atoms leaching into the liquid. Consequently, these leached atoms are the real catalytically active species for some reactions, like in homogeneous catalysis, especially investigated for Pd in coupling reactions[28]. This may happen due to Ostwald ripening. During this process, the reaction solution contains dissolved atoms that, in turn, might contribute to catalysis[29].

In order to certainly differentiate between homogeneous and nanocatalysis, multiple experiments are necessary, since every method has its limitations. Furthermore, not all tests are suitable for every type of reaction. A first indicator for in situ nanoparticle formation is a sigmoidal reaction profile observed for reactions starting from metal precursors. While TEM can visualize clusters or particles, it cannot determine whether these particles actually catalyze the reaction or whether the reaction is catalyzed by other species. Additionally, imaging of particles smaller than 1 nm using TEM is particularly challenging due to poor contrast.[30]

As complementary tests, two catalyst poisoning strategies can be applied. The first one is selective poisoning: This test aims to deactivate only one specific catalyst species, while others are not influenced. Depending on which species is deactivated, a change in reaction rate indicates the respective activity in the investigated reaction. To investigate for nanoparticles, mercury is often utilized as a testing agent. The addition of mercury allows for two possible interactions: adsorption onto the surface or amalgamation of the metal. Mercury forms amalgams with various (mostly zero-valent) metals, including palladium, making this test particularly effective. However, a significant excess of mercury and thorough mixing are essential for optimal results. During the mercury test in hydrogenation reactions, approximately 50% conversion should be permitted before releasing pressure and adding mercury, followed by reintroducing gas.[30]–[32] The test is complicated by the fact that different catalysts require different amounts of excess mercury[32]. Mercury has been shown to have the potential to alter complexes (that are mostly believed not to be influenced by mercury), leading to the formation of either free ligands along with an amalgam or a mercury complex combined with an amalgam. Thus, incorrect conclusions can arise from these tests.[32]

The second poisoning test is quantitative poisoning, applying strongly binding ligands like $CS_2$, 1,10-phenanthroline, $P(OCH_3)_3$, tetramethylurea, thiols, or phosphines[9],[30],[31],[33]. If significantly less than one equivalent of poison with regard to the total metal amount of catalyst atoms is sufficient for a drastic reduction of the reaction rate, nanoparticles are the prevalent catalyst, since only surface atoms are active, whose number is less than the total applied metal amount. If one equivalent of poison or more is needed, catalysis is expected to proceed via soluble metal atoms. However, in so-called dynamic catalysis (meaning simultaneous formation of clusters or single atoms from reservoirs during reaction, see also Scheme 7), effective poisoning depends on the reaction rates of leaching, aggregation, poisoning, and reaction. Hence, in this case, quantitative poisoning can deliver incorrect results.[30],[31]

Further tests include the addition of filter aids with a high surface area, such as Celite, to the reaction solution with subsequent filtration through a glass frit. The residue obtained can then be used in catalytic reactions. Ideally, the filtrate is also applied in the reaction. This allows to distinguish whether the active species is adsorbable (thus being likely a heterogeneous catalyst) or not. Filtration tests are primarily suitable for bulk metals, while the behavior of clusters remains unclear.[30]

Light scattering techniques may be applied, but require a minimum quantity of material. Differently sized particles scatter light to varying extents; thus, this test reveals the presence of particulate matter. Centrifugation is another method employed; however, it presents challenges because quantitative separation of sediment from liquid is difficult, potentially leaving residual reactivity. If only a small amount of a highly active catalyst is present, sediment formation may not be visually apparent. Furthermore, smaller clusters or particles tend to sediment less effectively.[30]

## 2.1.2 Synthesis Strategies for Colloidal Nanoparticles

The following sections give an overview of possible synthesis strategies for colloidal nanoparticles and will thereafter focus on relevant routes for this work, followed by a brief overview of tools for characterization of the obtained particles.

### *2.1.2.1 Overview*

Colloidal metal nanoparticles can, in principle, be synthesized by two different approaches. In bottom-up approaches, the NPs are synthesized from single atoms.[13] Bottom-up approaches include the reduction of metal salts, thermal, sonochemical, or photochemical decomposition of precursors, ligand reduction or displacement, sol-gel methods, and electrochemical synthesis[14],[17],[19]. Contrary, top-down approaches disintegrate bulk metal into NPs[13]. Top-down approaches include metal vapor deposition and laser ablation of solid targets[13],[14],[19].

The applied synthesis strategy significantly influences the properties of the resulting catalysts[15]. For instance, chemisorption of capping ligands prevents particle growth and aggregation, allowing for control over particle size and even shape[34]. Capping ligands also affect the catalytically usable surface area, electronic structure of the surface, and thus local reaction environment, all of which play crucial roles in catalytic activity. For example, polyvinylpyrrolidone (PVP) is a commonly used ligand that can inadvertently poison the catalyst by reducing the number of accessible surface sites.[16] Accordingly, stability can be enhanced through tailored synthesis methods that enable precise control over size, shape, and morphology[35]. For catalysis, strongly binding surfactants should be removed after synthesis[35].

In the following, relevant synthesis techniques used in this work are presented in more detail.

### *2.1.2.2 (Auto-)reductive Methods*

As stated in chapter 2.1.2.1, reductive methods are applicable bottom-up approaches to synthesize NPs. Reduction of metal salts in solution is a very common tool for producing metal colloids. Hydrogen is one of the most widely used reducing agents for transition metal nanoparticles, often in conjunction

with various stabilizers. Boron hydrides, particularly $NaBH_4$ or $KBH_4$, are the most frequently employed hydrides in aqueous solutions. Other reducing agents, such as hydrazine and its derivatives, as well as sodium citrate, are also utilized occasionally. An alternative approach involves using oxidizable alcohols that can be converted into ketones or aldehydes; accordingly, tertiary alcohols are not suitable for this approach.[14]

As a modification, “auto-reduction” of metal precursors like $Pd(OAc)_2$ in various organic solvents under elevated temperature without adding any further reagents or stabilizers was presented by Behr and Lux[22] and Tano et al.[36]. Clearly, electron transfer must happen, but the exact mechanism remains unclear[22]. Early literature confirms acetic acid as the main decomposition product in the case of $Pd(OAc)_2$, necessitating an unknown external electron donor[36]. As a result, this approach is classified by Roucoux et al. as a thermal decomposition of the precursor rather than a reductive method[14].

### *2.1.2.3 Pulsed Laser Ablation in Liquids*

The concept of Pulsed Laser Ablation in Liquids (PLAL, or short: laser ablation) was first presented in 1987 for Fe particles in water[5]. This method exhibits several major opportunities over wet-chemical approaches: properties like size and composition may be controlled independently by the operational parameters. During the fast synthesis, no surfactants or additional stabilizers are required, which is beneficial for subsequent catalysis, because the surface is better accessible for reactants, which should result in a higher catalytic activity[37]. Adversely, decomposition products of the liquid emerge that might act as weak ligands. This is also valid for the stabilizing solvent.[5] The purity of the laser-ablated NPs is only dependent on the purity of the target material, as well as of the surrounding medium[18].

During laser ablation, an extremely high amount of energy from a laser beam is concentrated on a very small spot of a light-absorbing surface. The physical-chemical processes are highly complex and are, to date, not fully understood. However, two mechanisms for ablation were identified, depending on the pulse length and power density of the laser beam. For long pulses and low power density, molten nanodroplets and fragments are directly ejected with a broad size distribution, resulting in a rugged surface of the target that complicates or disables long-term operation due to dilution of the power density of the beam on the resulting surfaces.[38]

In the other mechanism, short laser pulses with high power density result in the formation of vapor and plasma[38]: After a critical power is exceeded[39], this energy concentration results in a rapid increase in the temperature of the irradiated spot until the target evaporates, interacting with its surrounding until molecules decompose into electrons and ions, finally forming a plasma plume. The structure of the plasma always depends on the target, laser parameters, pressure, and its surrounding, including the solvent. Thus, the structure of the plume influences the ablation result.[39] The plasma plume results in the formation of a gaseous cavitation bubble at the interface between plasma and liquid, which collapses due to rapid cooling from temperatures beyond 5000 K to room temperature (or any other operating temperature) within less than 50 µs, leading to shockwaves in the liquid. During the cool-down, NPs begin to form and grow by supersaturated vapor nucleation at the edge of the plume and inside the cavitation bubble. By the collapse of the cavitation bubble, the particles get ejected into the surrounding

liquid that immediately stabilizes them (Figure 4).[5],[18],[38] Thus, PLAL allows for the production of ultrasmall nanoparticles without the need for additional stabilizers if the solvent is chosen properly, providing the stabilizing effects itself[37].

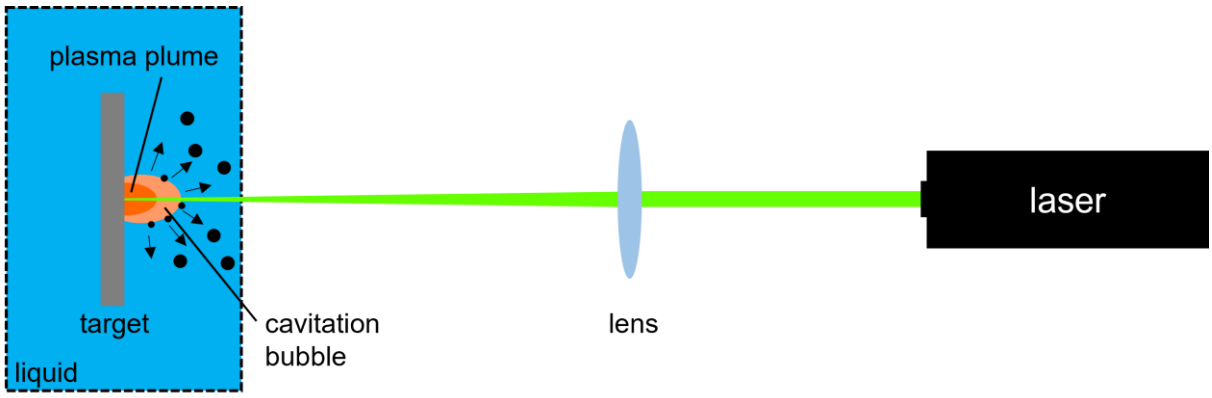


Figure 4: Working principle of PLAL without development over time, adapted from[18],[38].

Physical nanoparticle syntheses lead to broader particle size distributions than chemical routes; therefore, particles resulting from physical methods may be less preferred for catalysis (see also chapter 2.1.1)[14]. In line with this notion, after PLAL, bimodal particle-size distributions are often observed, resulting from plasma dynamics. Laser fragmentation (laser irradiation of existing small particles) is frequently employed to reduce the size of existing nanoparticles, allowing for a more uniform particle size distribution. However, this process requires higher fluences (beam energy per area) to be effective.[5],[20] Particle size distribution and concentration are easily adjustable through variation of laser parameters like fluence or operation time[24]. The ablation result is further influenced by the chemical composition of target and liquid, refractive index of the liquid, laser wavelength, laser pulse length, pulse repetition rate, length of operation time, density, and height of the liquid layer, as well as heat capacity, thermal conductivity, and polarity of the solvent[5],[37],[39].

The resulting particles always possess defect sites[20]. Furthermore, carbonaceous deposits may occur due to the decomposition of the solvents. Elements with a higher amount of empty d-orbitals may also form carbides.[37],[40],[41] Accordingly, appropriate particle characterization is important.

### *2.1.2.4 Particle Characterization*

After the successful synthesis of nanoparticles, a characterization must be performed. Numerous methods are available, of which a selection is presented in the following. As stated earlier, TEM or high-resolution TEM (HRTEM) may be performed. This allows for obtaining information about several aspects, like particle size, particle size distribution, information about atom rows and defects, shell formation, and phase segregation. Alternatively, scanning electron microscopy (SEM) can be applied to gain information about size and morphology of particles that are at least 5-10 nm in diameter. Dynamic light scattering (DLS) allows for determining the hydrodynamic particle size and also performs an estimation of the resulting particle size distribution. Particle size may also be determined via disc centrifuges (DC). To measure the concentration of certain elements in a sample, inductively coupled plasma mass spectrometry (ICP-MS) or inductively coupled plasma optical emission spectrometry (ICP-

OES) analyses can be conducted. Furthermore, several X-ray analysis methods like X-ray diffraction (XRD) and X-ray photoelectron spectroscopy (XPS) can be applied to identify atomic arrangements and distances, surface composition, and the surface oxidation state. Nuclear magnetic resonance (NMR) spectroscopy helps to identify organic molecules bound to surfaces.[19],[20]

## 2.2 Catalytic Reactions

Catalysis is a key element in nearly 80% of all chemical processes and makes a huge contribution to the world economy[13]. The present work deals in its core with several different catalytic reactions. Their fundamentals will be introduced in the following chapter.

### 2.2.1 Hydrogenation

#### *2.2.1.1 Overview*

Hydrogenation is one of the most important reactions in commercial organic chemistry, i.e., in the synthesis of pharmaceuticals, agrochemicals, and fine chemicals like fragrances and flavors[42]–[47]. In general, hydrogenation refers to the addition of hydrogen to C-C, C-O, C-N, N-O multiple bonds and related ones, which is usually exothermic[48]. Particularly, the selective partial hydrogenation of polyunsaturated species or C≡C triple bonds is essential, as the remaining double bond is often required for further conversions.[49] Furthermore, it has been shown that polyunsaturated species hinder catalyst activity in certain desired homogeneously catalyzed consecutive reactions by the formation of stable, unreactive catalyst complexes[12],[50].

In principle, many noble metals are capable of hydrogenating C=C double bonds[51]. Industrially relevant metals include Ni, Cu, Co, Pt, Pd, Rh, and Ru, while typically metals of the Pt group are more active and thus allow milder reaction conditions and less catalyst use[47]. This may be explained by the interatomic distance of Ni, Cu, Pt, and Pd atoms, which is around 2.7 Å and allows a C=C double bond with a bond length of ca. 1.5 Å to fit in well[52]. Especially, Pd shows a superior versatility regarding applicable substrate classes[42]. The majority of commercially employed catalysts are mostly heterogeneous[13].

Considering the existing literature, Pd nanoparticles appear to be highly promising catalysts for hydrogenation of polyunsaturated compounds and alkynes and have therefore been studied extensively with varying stabilizers, solvents, and substrates[44],[53]–[59]. Details on selected hydrogenations are presented in the following.

#### *2.2.1.2 Selective Partial FAME Hydrogenation*

The first application of heterogeneous hydrogenation of edible oils was conducted by Wilhelm Normann in 1901, with a patent granted in 1903[60],[61]. This process, commonly known as (fat) hardening, predominantly utilizes Raney-Nickel as a catalyst[48].

Selective hydrogenation of fats and oils, as well as of their derivatives like fatty acid methyl esters (FAME), has been a long-standing research topic with numerous examples. The conversion of polyunsaturated fatty acids (PUFA) or their derivatives to monounsaturated fatty acids (MUFA) or

derivatives (shown in Scheme 1 for the corresponding methyl esters) represents a critical step for food applications, biodiesel production, and as a platform chemical for sustainable chemistry.[62] This can be explained by the following examples.

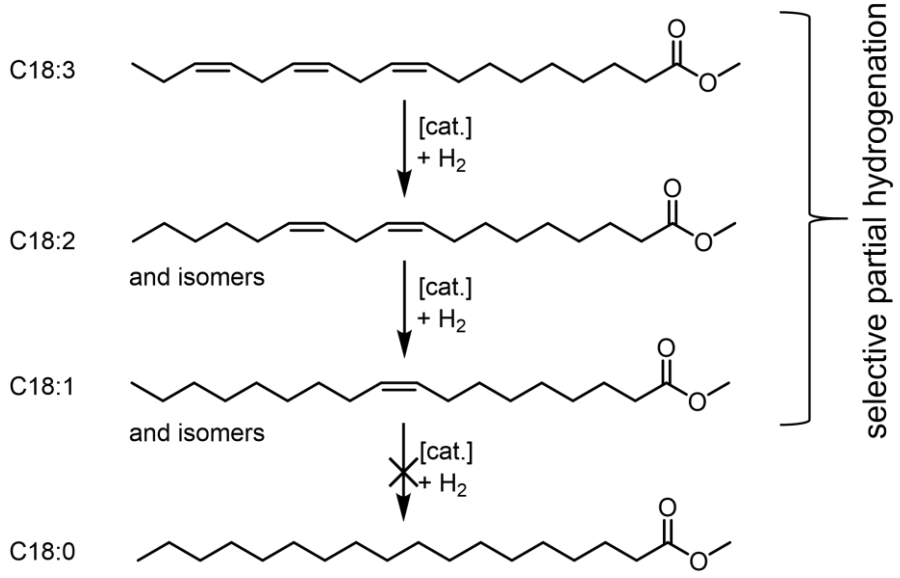


Scheme 1: Reaction scheme for the selective partial hydrogenation of FAME.

FAME are among the most promising alternative fuels due to their biodegradability, high cetane numbers, and low emissions of $SO_2$, CO, and soot. On the one hand, increased unsaturation in FAME leads to higher oxidation sensitivity. On the other hand, a high degree of saturation can result in issues related to flow behavior at low temperatures; thus, the best compromise is found with cis-monounsaturated FAME[63].[64] Furthermore, selective hydrogenation of FAME followed by subsequent isomerization and metathesis also has potential applications as biodiesel[65].

Apart from fuel uses, fatty acid derivatives can be used for sustainable chemistry[62]: Reactions involving fatty acid chains include oxidation, hydroformylation, hydroxy- and methoxycarbonylations, metathesis, various C-C bond formations, and diverse addition reactions[66]. Recent studies have demonstrated that selectively hydrogenated FAME undergo isomerizing methoxycarbonylation and ethenolysis more effectively than unhydrogenated FAME[12].

The reactivity order of noble metals for the selective partial hydrogenation is Pd > Rh > Pt > Ir > Ru > Ni; however, when considering activity towards isomerization, the order shifts to Pd > Rh > Ru > Pt[67]. Accordingly, Pd is the most active element for both processes, which may not be beneficial for all intended purposes.

One of the most successful systems for selective partial hydrogenation of fatty acid derivatives to date is unmodified colloidal Pd in propylene carbonate (PC), which operates as a biphasic system. Dimethylformamide (DMF) instead of PC was also found to be an alternative, but PC is preferred due to safety and sustainability reasons. Both systems were patented in 1990 resp. 1991 and published in 1993, but received until now only little attention.[62],[68]–[70] The reaction can be conducted under mild conditions, with temperatures up to 150 °C and pressures of around 1 atm, nevertheless achieving rapid

reaction rates[70]. Increasing the pressure to 5 bar significantly reduces the reaction time to as low as 7 minutes. Remarkably, very high substrate-to-palladium ratios of up to 100,000:1 are achievable with just 100 ppm of Pd in PC, while only minimal over-hydrogenation takes place and residual trace amounts of linoleic acid remain.[68]

Numerous metrics have been developed to describe the reaction performance of selective partial hydrogenations of fatty acid derivatives, with some based on kinetic parameters and others relying on compositional information, such as the trans/cis resp. cis/trans ratio. It is virtually impossible to completely avoid the formation of trans isomers. Hence, a pure cis-configured hydrogenation product is ruled out.[62] As an example, hydrogenation can be considered selective if the ratio $\frac{k_{C18:2\rightarrow C18:1}}{k_{C18:1\rightarrow C18:0}}$ is greater than 10[71].

The hydrogenation of polyunsaturated species compared to monounsaturated fatty acids occurs rapidly due to the preferential adsorption of polyenes to any catalyst surface[71]. Since the 1950s, it has been known that PUFA exhibit stronger surface adsorption than derivatives with a lower degree of unsaturation[52]. Accordingly, the hydrogenation of PUFA is a consecutive process, as shown in Scheme 1 [72]. Both insights explain the known different reactivities with respect to the degree of unsaturation, which follow the order C18:3 > C18:2 > C18:1[73]. In an attempt to mathematically further describe the reaction network, a pseudo-first-order model was able to effectively fit the reaction profiles of canola and sunflower oil hydrogenation using a Lindlar catalyst[74]. Some studies also indicate that conjugated C18:2 isomers are present that react preferentially[71]. The reaction of conjugated 9,11-C18:2 proceeds an order of magnitude faster than that of linoleic acid (9,12-C18:2), suggesting that pre-conjugation could serve as an alternative mechanism approach to the typically applied Horiuti-Polanyi mechanism that will be explained in the following[71]. As a consequence, the prevailing mechanism should always be considered for each system individually.

The substrate adsorption characteristics for Pd and Pt are assumed to be similar to those of Ni due to comparable d-electron configurations of these elements[71]. This suggests that the Horiuti-Polanyi mechanism, which was originally established for hydrogenations over Ni[75], may also be applicable for Pd and Pt. This mechanism enables the explanation of the impacts of the reaction conditions on the product composition, see Figure 5.

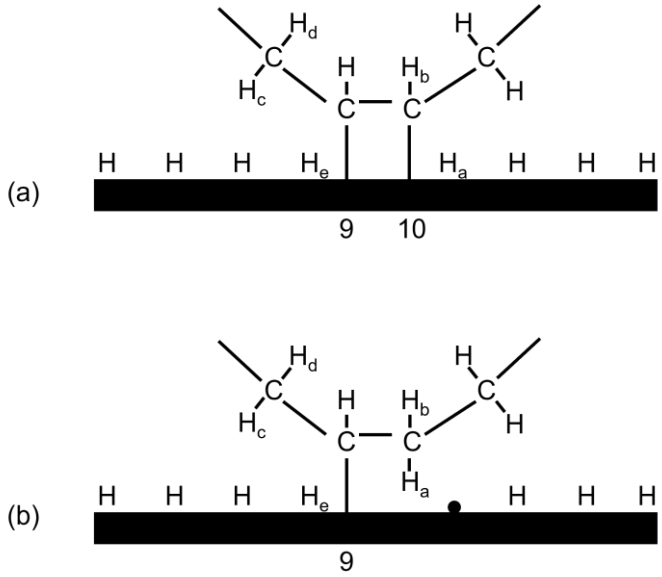


Figure 5: Horiuti-Polanyi mechanism, adapted from[73].

Initially, hydrogen chemisorbs on the catalyst surface, and the hydrogen molecule gets split into two atoms. In the next step, a substrate molecule binds via one double bond to the catalyst surface (a). Subsequently, one hydrogen atom ($H_a$) is incorporated and a partially hydrogenated state (b) forms, which can undergo four possible evolutions:[72],[73],[75]

1. A second hydrogen atom from the surface (e.g., $H_e$) binds to the carbon chain, saturating the double bond. The hydrogenated product leaves the catalyst.
2. The hydrogen atom initially occupied by the carbon chain ($H_a$) returns to the catalyst surface, and the original molecule desorbs.
3. The hydrogen atom $H_b$ returns to the surface due to a rotation around the single C-C bond, after which the molecule desorbs, leading to cis-trans isomerization.
4. Hydrogen atoms $H_c$ or $H_d$ bind to the surface like in steps 2 or 3. Following desorption, this results in a double bond that is shifted by one carbon atom compared to the original state. Depending on which hydrogen atom from the chain is transferred to the catalyst surface, the formation of the cis and trans isomer can occur.

A high hydrogen surface coverage leads to rapid hydrogenation with reduced selectivity. Conversely, a low hydrogen surface coverage results in pronounced isomerization against hydrogenation. The degree of hydrogen surface coverage can be influenced by process parameters such as pressure, temperature, stirring intensity, and catalyst concentration.[73] Increased temperatures also thermodynamically favor the formation of trans isomers[63].

### *2.2.1.3 Selective Hydrogenation of Alkynes and Polyenes*

Beyond the hydrogenation of fatty acid derivatives, other selective partial hydrogenation reactions are also of considerable interest. The selective partial hydrogenation of alkynes to produce disubstituted Z-alkenes is a frequently performed reaction[76]. Often, the already mentioned Lindlar catalyst is used, which is a $CaCO_3$-supported Pd catalyst that is deliberately poisoned with a Pb co-catalyst and

quinoline[76],[77]. This is done in order to reduce the hydrogenation activity to enable the reaction termination at the alkene stage, thus preventing overhydrogenation to the alkane[76],[77]. The major drawback is the presence of the Pb co-catalyst, which causes environmental and safety issues and needs to be completely removed from products used for fine chemicals and the pharmaceutical industry[44],[76],[77].

The so-derived alkenes are important products in fine chemistry, polymers, and pharmaceuticals: 2-Methyl-3-butene-2-ol (MBE), for example, is a key substance for the synthesis of artificial terpenes used in flavorings[78]. It is also utilized in the production of vitamins A and E, as well as linalool[44],[46]. Other noteworthy examples include cis-butene-1,4-diol (B2D), which serves as a precursor for vitamin A, vitamin B6, and polybutenediol, and cis-3-hexene-1-ol, which is a valuable product for use in consumer chemicals and as an edible flavor[44],[79]. Additionally, ethylene purification for polymerization purposes by selective acetylene hydrogenation benefits from this transformation[49].

The selection of metals for this reaction type poses specific challenges: Metals that facilitate easy hydrogen activation often lead to over-hydrogenation, while those with less hydrogen activation tend to be more selective but necessitate harsher reaction conditions. Palladium represents a suitable compromise; however, controlling selectivity at nearly full conversion remains challenging.[53],[80] Notably, Pd is the only metal exhibiting significant alkene selectivity in alkyne and diene hydrogenation. The use of promoters or selective poisoning agents (such as CO, phosphines, or Pb with quinoline in the case of the Lindlar catalyst) can further enhance selectivity.[6],[33] Other examples for promoters include nitrogen-containing additives, as they may compete for free sites on the surface; examples include ethylenediamine or piperazine, as well as quinoline[43],[53],[80],[81].

Besides the choice of the appropriate metal, the structure of the substrate also influences the catalytic behavior. Internal alkynes exhibit a higher selectivity than terminal alkynes, as those are significantly more reactive due to steric effects and resulting accessibility to the surface, which favors over-hydrogenation.[53],[80] Furthermore, internal alkynes possess intrinsic stereoselectivity toward cis-configured products due to syn-addition to the catalyst, making the targeted production of trans-alkenes from alkynes challenging[82]. In general, the strength of adsorption follows the order: alkane < alkene < alkyne[54]. This is due to the electron density of the double resp. triple bond and is also valid for dienes, allowing them to displace alkene products, as long as reactant residues are still present[6]. Several structural relationships for alkyne hydrogenation on Pd were found: Density functional theory (DFT) calculations for Pd indicate that the (100) surface preferentially binds alkynes, thus facilitating the easier displacement of the formed alkene. Only after complete conversion of the alkyne, the alkene binds to the (100) surface and undergoes hydrogenation.[54] Pd edges were shown to exhibit an increased adsorption strength for alkenes, thus significantly promoting over-hydrogenation[54] Accordingly, over-hydrogenation is more pronounced for Pd particles with a variety of facets[54]. Studies involving different sizes and shapes of nanoparticles stabilized with PVP in water have shown that the hydrogenation of 2-methyl-3-butyne-2-ol (MBY) to MBE occurs primarily on planar surfaces, regardless whether they are (111) or (100) oriented, with over-hydrogenation mainly occurring at the edges[56].

As a result, structural dependencies in metal nanoparticles have garnered significant attention over recent decades: Since the ratio of one active site to another is highly size-dependent, both size and shape influence the catalytic behavior. Hence, it was shown that the turnover frequency (TOF) for MBY is a function of particle size, particularly within the range of 3 - 20 nm.[56] In particles smaller than or equal to 3 nm, changes in surface morphology are most pronounced[57]. In contrast to MBY, longer-chain alkynes up to C8 do not demonstrate any size-dependent selectivity across particle sizes ranging from 1 - 14 nm[57]. Concluding, it has to be noted that any possible structural dependence must be evaluated individually for each catalytic system[56]. Referring to chapter 2.1.2, these dependencies can be controlled, to some extent, by an appropriate choice of the exact synthesis route of the particles.

The overall situation becomes increasingly complex by the fact that small alkynes can oligomerize with up to 40% selectivity during partial hydrogenation[53],[80]. Moreover, it has been shown for Pd black that the modification of near-surface Pd regions is crucial as well, since the occupation of subsurface sites by carbon or hydrogen atoms plays another role. Unselective hydrogenation occurs via a hydrogen-saturated hydride phase. Innerparticulate near-surface processes are a highly complex topic under active research and will not be further explored here.[83]–[88]

Numerous approaches for selective partial alkyne hydrogenation catalysts apart from the Lindlar catalyst have been tested in literature, but only the NanoSelect catalysts by BASF have reached market readiness. These catalysts consist of supported Pd colloids, with hexadecyl-(2-hydroxyethyl)dimethyl ammonium dihydrogenphosphate (HHDMA) serving as a stabilizer[77],[89]. NanoSelect and Lindlar catalysts exhibit similar activity and selectivity when hydrogenating 3-hexyn-1-ol, even though the palladium loading in NanoSelect is approximately one-tenth that of Lindlar[77]. This discrepancy may be attributed to the fact that only about 10% of the palladium used in a Lindlar catalyst is actually active[90].

Apart from alkynes, monounsaturated compounds can also be synthesized from various polyenes. Here, the type and degree of substitution at the double bond to be hydrogenated significantly influences the hydrogenation activity, following this order: monosubstituted > 1,1-disubstituted ≈ cis-1,2-disubstituted > trans-1,2-disubstituted > trisubstituted > tetrasubstituted, Scheme 2 [91].

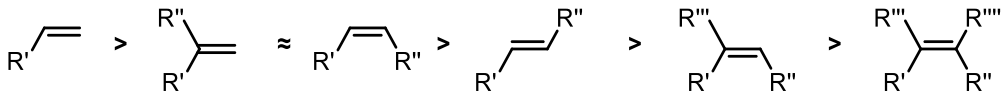


Scheme 2: Structure-specific activity in the hydrogenation of different substituted alkenes[91].

Acyclic double bonds are generally more reactive than endocyclic double bonds. Specific examples for selective polyene hydrogenation beyond fats and oils include terpenes (such as limonene and β-myrcene), which may also feature conjugated systems. Further examples are non-conjugated cyclic structures such as 1,5-cyclooctadiene (1,5-COD) and 1,5,9-cyclododecatriene (1,5,9-CDT). Partially hydrogenated terpenes serve as intermediates for fragrances, flavors, and polymers. The hydrogenation of β-myrcene has been studied since the 1930s, utilizing catalysts such as palladium on activated carbon and Raney-Nickel[92]. The selective hydrogenation of 1,5-COD and 1,5,9-CDT is particularly relevant, as both educts can yield monounsaturated compounds useful for synthesizing aliphatic dicarboxylic acids, ketones, cyclic alcohols, and lactones. For 1,5-COD, homogeneous palladium complexes provide good

results; however, heterogeneous palladium systems exhibit significantly higher activity while maintaining similar selectivity. The partial hydrogenation of 1,5,9-CDT is notably more complex than that of 1,5-COD due to the presence of a third double bond and a greater potential for isomerization, resulting in a significantly broader range of possible products compared to 1,5-COD. Most reactions involving 1,5,9-CDT are conducted using solid palladium catalysts.[91]

## 2.2.2 Selected Carbonylations

Double bonds might not only be hydrogenated; in theory, lots of other addition reactions are possible. In the following, the addition of CO (carbonylation) in two different reactions, namely (isomerizing) methoxycarbonylation and hydroformylation, will be presented.

### *2.2.2.1 Isomerizing Methoxycarbonylation of Oleochemicals*

#### *2.2.2.1.1 General*

Methoxycarbonylation is a 100% atom-economical reaction, involving the addition of CO and methanol to double bonds to form methyl esters[93]. Typically, systems that generate $Pd^{II}$ complexes in situ from $Pd^0$ are employed in methoxycarbonylation, such as $Pd_2(dba)_3$, together with a diphosphine ligand and an acid, since Pd-based systems are generally the most active ones in methoxycarbonylation[94],[95]. A suitable diphosphine ligand for this conversion is 1,2-bis[(di-tert-butylphosphino)methyl]benzene (1,2-DTBPMB, sometimes also called dtbpx[95]), which was first mentioned in 1976[93]. Lucite uses this ligand to produce 710,000 tons per year of methyl methacrylate (MMA) by a methoxycarbonylation of ethylene to methyl propanoate, followed by aldol condensation with formaldehyde to yield MMA, which is used for polymers (Scheme 3)[13],[93],[96]. The applied ligand 1,2-DTBPMB is sterically demanding and electron-rich[95].

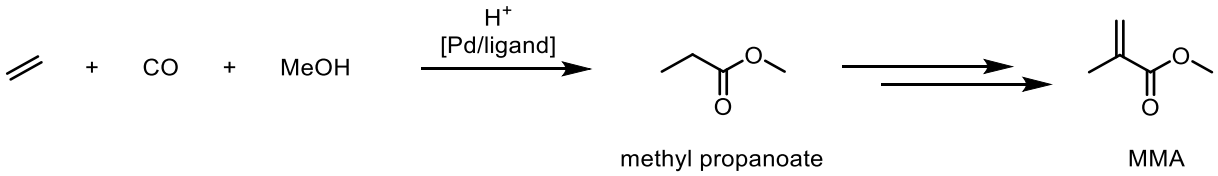


Scheme 3: Methoxycarbonylation of ethylene to methylpropanoate for MMA synthesis[13].

Deactivation poses a significant challenge for transition metals in positive oxidation states within reducing environments, including the applied $Pd^{II}$ under CO atmosphere, leading to the formation of $Pd^0$ and uncoordinated, protonated ligand. The deactivation process involves various intermediates ranging from clusters and nanoparticles to bulk metal (Scheme 4), but is, in this special case, completely reversible.[95]

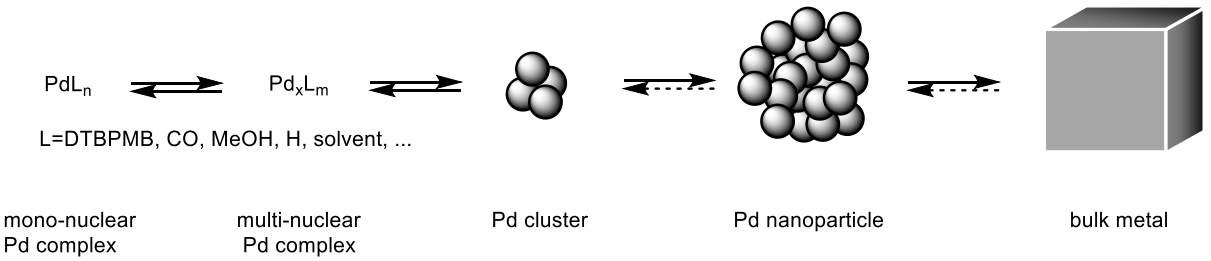


Scheme 4: Deactivation of the applied $Pd^{II}$-complex under reducing conditions, adapted from [95].

An excess of the protonated version of the ligand, 1,2-bis[(di-tert-butylphosphino)methyl]benzene triflate (1,2-DTBPMB$(OTf)_2H_2$), helps to prevent catalyst decomposition. Even the formation of active palladium species from different heterogeneous $Pd^0$ sources by means of the protonated ligand has been demonstrated based on these findings. Notably, as the size of the metal piece increases, the reaction time extends; meanwhile, selectivity tends to decrease slightly.[95]

### *2.2.2.1.2 Isomerizing Methoxycarbonylation of Oleochemicals*

Fatty acids represent a unique feedstock for chemical production due to their long methylene sequences. Polyesters derived from a $C_{19}$-diester obtained from isomerizing methoxycarbonylation of methyl oleate exhibit polyethylene-like characteristics owing to their long carbon chain structure[96]. Work regarding the isomerizing methoxycarbonylation of oleochemicals like methyl-10-undecenoate and methyl oleate has particularly been carried out by Mecking and co-workers as well as Seidensticker and co-workers. Their work includes additional product purification by crystallization, reaching purities suitable for polycondensation (> 99%) for the linear $C_{19}$-diester and ≥ 99.9% for the linear $C_{12}$-diester, see Scheme 5[12],[94]–[98].

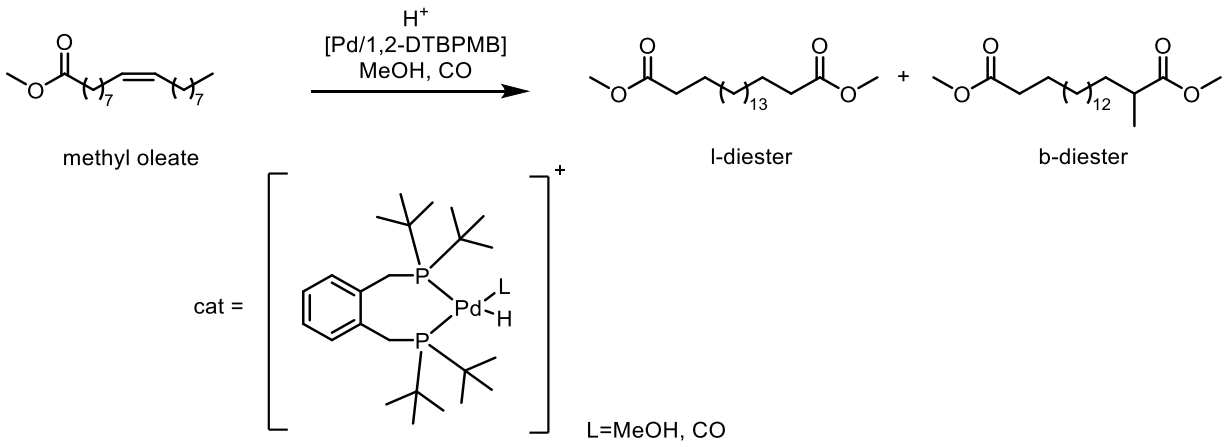


Scheme 5: Isomerizing methoxycarbonylation of methyl oleate to $C_{19}$-diesters[13],[97].

In the isomerizing methoxycarbonylation of monounsaturated oleochemicals, steric hindrance caused by the diphosphine ligand is crucial for the productivity and the selectivity to linear products. The formation of linear alkyl species is favored when using sterically demanding diphosphines. Isomerization of the double bond along the chain is energetically easily possible. CO insertion is reversible and shows minimal influence from ligand variation. The rate-limiting step, characterized by the highest energy barrier, is the methanolysis of the palladium acyl species, releasing the final product. Among all acyl

species, the methanolysis of the linear acyl species has the lowest energy barrier, making it the preferred pathway. Hence, the reaction preferentially generates the linear product. Shorter alkenes react more readily, while the position of the double bond within the carbon chain does not exert any influence on the total reaction rate. Conversely, the alcoholysis of higher alcohols becomes slower with increasing chain length. Because the formation of terminal olefins is, in principle, thermodynamically less favored compared to internal ones, the isomerizing methoxycarbonylation is a kinetically controlled reaction. Furthermore, polyunsaturated fatty acids form terminal palladium allyl species, and subsequent carbonylation occurs significantly slower than isomerizing methoxycarbonylation of monounsaturated substrates.[99]

Recently, it was shown that the isomerization of polyunsaturated species with the same Pd/1,2-DTBPMB catalyst leads to conjugation of the double bonds with a broad distribution of resulting double bond positions that is oriented towards the omega position. During isomerizing methoxycarbonylation of predominantly monounsaturated FAME with 12% of C18:2, a significant decrease in conversion was observed compared to pure monounsaturated FAME at identical reaction times.[97] It has been shown that the yield of isomerizing methoxycarbonylation of canola and soybean-based feedstocks can be increased by up to 80% through previous selective partial hydrogenation of the polyunsaturated species[12].

As a consequence, an attempt to combine both reaction steps (selective partial hydrogenation and isomerizing methoxycarbonylation) in a one-pot reaction sequence of highly polyunsaturated FAME has already been reported: Selective partial hydrogenation of C20:5 methyl ester as a model compound for microalgae oil using palladium on alumina (5% (w/w); 0.4 mol%) without additional solvent yielded 80% of C20:1 at 3% remaining C20:2 species and 17% C20:0. The hydrogenation was followed by the activation of the supported palladium with the protonated ligand 1,2-DTBPMB$(OTf)_2H_2$ in methanol. The selectivity and activity of the resulting catalyst were comparable to complexes freshly derived from $Pd(dba)_2$ and $[(dtbpx)Pd(OTf)_2]$, resulting in an almost complete dissolution of the supported Pd particles as elucidated by a filtration test. In this one-pot approach, the isomerizing methoxycarbonylation achieved 80% yield of the desired diester with 92% selectivity towards the linear product, leading to an overall yield of 60%. However, for actual algal oil, a higher catalyst loading was required. In the case of tall oil, the 1,19-diester could be obtained with a total selectivity of 71%. After 18 h reaction time, 81% conversion in methoxycarbonylation was observable; only after three days, 98% conversion was achieved, showing a drastic decrease in reaction rate at high conversions.[100]

### 2.2.2.2 Hydroformylation of Terpenes

#### 2.2.2.2.1 General

Alkene hydroformylation plays a significant role in the chemical industry, producing more than 12 million tons of aldehydes annually[101],[102]. These products are essential for bulk chemicals, pharmaceuticals, and flavoring agents[103]. Hydroformylation was discovered by Roelen at Ruhrchemie Oberhausen in 1938.[103] The typical starting material for this reaction is an olefin that reacts with synthesis gas, a mixture of hydrogen and CO[103]. With only few exceptions, mixtures of linear and branched aldehydes are obtained (Scheme 6)[104]. During the reaction, preceding isomerization of the double bond may occur[104]. In addition to the main reaction, several side reactions can take place, including hydrogenation of either the alkene or the product aldehyde, as well as aldol addition and aldol condensation[103].

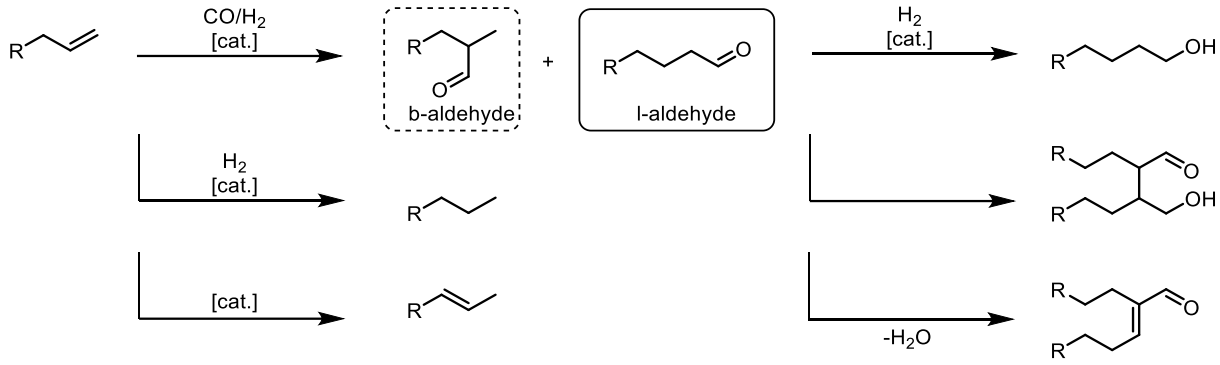


Scheme 6: Reaction network of mono-unsaturated alkene hydroformylation[103],[104].

For unmodified metal carbonyl complexes, the following order of activity applies: Rh >> Co > Ir > Ru > Os = Tc > Pt > Pd > Mn > Fe > Ni >> Re[103]. Currently, only rhodium and cobalt are utilized industrially[103],[104]. Cobalt exhibits greater robustness against poisons in the feedstock and higher temperatures, but also has a higher hydrogenation activity and can directly lead to a high alcohol yield (which may be desired); however, it requires harsher conditions, making the whole process more expensive.[104] Rhodium is up to 1000 times more active than cobalt, allowing for lower synthesis gas pressure and reduced temperatures during reactions. A significant challenge associated with the utilization of Rh is its price volatility and generally high cost, which is largely dictated by demand from the automotive industry.[103],[104]

Many laboratory hydroformylations utilize $Rh(acac)(CO)_2$ as the catalyst precursor in combination with ligands. Ligands allow for broad modification of the electronic and steric properties of the resulting metal carbonyl complex and are mostly mono- or bidentate. They can either accelerate or inhibit the specific steps in the catalytic cycle, as well as promote side and consecutive reactions that are shown in Scheme 6. The concentration of the ligand, its coordination properties, and the partial pressure of CO influence the position of equilibria within the whole catalytic system. Therefore, it is essential to identify optimal reaction conditions specific to each system.[103] Particularly, electron-withdrawing substituents on the ligands enhance reaction rates by favoring CO dissociation and alkene association[105]. Phosphorus ligands in rhodium hydroformylation increase the thermal stability and may contribute to catalytic activity, and will be presented more closely in the following section.

### *2.2.2.2.2 Phosphorus Ligands*

Phosphites are superior π-acceptors compared to phosphines, offering significant potential in hydroformylation. They are easier to synthesize and exhibit reduced susceptibility to sulfur and oxidative agents compared to phosphine ligands. Additionally, electron-withdrawing phosphites promote the formation of linear products.[105] Phosphines and phosphites contain trivalent phosphorus that can be oxidized by air, trace amounts of oxygen, or hydroperoxides. Impurities arising from ligand synthesis, such as acids, bases, and water, can promote ligand decomposition. Additionally, there are general catalyst poisons such as $H_2S$, COS, HCl, HCN, hydroperoxides, $CO_2$, water, enones, alkynes, and butadiene[104]. These can be introduced through the feed or solvents.[103] Furthermore, phosphites can react with water, alcohols, acids, and bases under degradation[103]. The water can also result from aldol condensation of the product[106]. The bulkier the phosphite, the less susceptible it is to hydrolysis. For example, the bulky phosphite tris(2,4-di-tert-butylphenyl)phosphite begins to hydrolyze in water at 60 °C only after more than 400 hours.[106]

Bulky phosphite derivatives can exhibit high activities, attributed to the exclusive formation of a complex with only one phosphite (with the other ligands being CO, H, and occasionally the substrate). The high reactivity of bulky phosphites is leveraged in the hydroformylation of natural product derivatives that are typically not very reactive.[106] Especially, phosphites with additional tert-butylphenyl groups are particularly well-suited for less reactive substrates such as limonene, cyclohexene, and methylenecyclohexane[107].

### *2.2.2.2.3 Hurdles for Terpenes*

Diene hydroformylation has been a long-standing research topic, with the objective of producing bifunctional molecules for bio-based fine chemicals and polymers. As an example, the hydroformylation of the challenging substrate β-myrcene often results in product mixtures due to side and consecutive reactions. Therefore, controlling chemoselectivity (and successive regioselectivity) is crucial in these reactions.[102] In general, terminal double bonds react more quickly than internal double bonds. Additionally, the presence of tri-substituted carbon atoms is disadvantageous, as described by Keuleman's rule, since they are rather unreactive in hydroformylation.[103]

Hydroformylation of various aliphatic cyclic terpenes and β-myrcene was demonstrated as early as 1965; however, in the case of β-myrcene, only saturated high-molecular-weight compounds and other unknown high-boilers were produced. The reasons for the relatively low reactivity of β-myrcene remained unclear at that time.[108] Recent findings indicate that for polyunsaturated oleochemicals, conjugated species form during the hydroformylation with the bulky tris(2,4-di-tert-butylphenyl)phosphite, which are bound in $\eta^3$-complexes that are only slowly converted. As the ratio of C18:2 to C18:1 increases, the reaction becomes more inhibited due to the higher availability of C18:2 species to form these $\eta^3$-complexes, and migration of double bonds, as well as cis-trans isomerization increase. Only after conversion of the polyunsaturated species, the overall reaction rate accelerates.[50] Similar observations have been made with $Rh_4(CO)_{12}$ during hydroformylation of alkenes containing traces of dienes. A significant reduction in reaction rate is noted when diene traces are present. As

observed through infrared spectroscopy, the affinity of the catalyst for dienes was found to be considerably higher than for alkenes under identical conditions. Multiple species are formed simultaneously, which the authors suggest to include $\eta^3$-allyl and sigma-allyl complexes.[109]

Besides β-myrcene, a variety of terpenes have been hydroformylated since 1965 for use in fragrances, with some products undergoing further transformations such as acetalization. Notable examples include dihydromyrcene, limonene, and linalool.[110]–[113] The ligand P(O-*o*-*tert*-BuPh)$_3$ significantly accelerates the hydroformylation process for all these substrates compared to $PPh_3$[110],[114]. In the case of dihydromyrcene, the reaction occurs exclusively at the terminal double bond[115]. For hydroformylation of conjugated systems, initial experiments utilized 1,2-bis(diphenylphosphino)ethane (dppe), and it was later demonstrated that a substantial excess of $PPh_3$ also leads to enhanced reactivity[115].

For the successful hydroformylation of terpenes containing conjugated double bonds like β-myrcene, a high excess of $PPh_3$ is required (with a molar ratio of P:Rh = 20-40 at 80 °C and under high-pressure conditions of 80 bar), resulting in the formation of double unsaturated aldehydes[112]. A similar approach applies to isoprene hydroformylation[103]. Hydroformylation of α-farnesene has been conducted using $PPh_3$ over extended periods of 70 hours[115]. Under different conditions, dppe yielded the best results for diene systems, along with TPP and several other ligands, while tris(tert-butylphenyl)phosphite performed poorly[116]. Recent research enabled a significantly more efficient hydroformylation of β-myrcene using Rh/dppe under optimized conditions, achieving TOFs as high as 9590 $h^{-1}$, which represents an improvement by an order of magnitude over previously reported TOFs[102].

In summary, several (sometimes specialized) ligands can be applied for terpene hydroformylation, but harsh conditions are sometimes required. However, bulky phosphites are well-suited for efficient hydroformylation of rather unreactive substrates in theory and practice.

## 2.2.3 C-C Coupling Reactions

### *2.2.3.1 Overview*

Coupling reactions are important organic transformations in fine chemistry, pharmaceuticals, and related fields[29]. Various types of coupling reactions exist that include Suzuki(-Miyaura), Negishi, Stille, Kumada, and Hiyama couplings for the formation of C-C single bonds, as well as (Mizoroki-)Heck for C=C double bonds and Sonogashira(-Hagihara) for C≡C triple bonds. Typically, aryl halides are coupled homogeneously with either metal alkyls or aryls or with alkenes, alkynes, or boronic acids. Aryl chlorides are the least expensive option but often exhibit low reactivity; in contrast, aryl iodides are the most reactive. Instead of halides, other leaving groups such as triflates, acid chlorides, sulfonyl chlorides, or azocompounds can also be utilized.[13]

Although these coupling reactions are never fully atom-economical, this drawback is generally acceptable in the context of fine chemistry and pharmaceuticals. The most commonly used catalyst metal is Pd; however, other metals such as Ni, Co, Cu, and Fe can also be employed.[13] The separation of the catalyst (most commonly complexes are used) is tedious and difficult; thus, strategies to prevent high Pd loadings in the reaction, as well as separation strategies, are demanded[29],[117]. Alternatives to homogeneous complex catalysts are the application of clusters or nanoparticles[117].

### *2.2.3.2 Suzuki Coupling*

Metal-catalyzed Suzuki couplings of aryl, vinyl, or alkyl halides or pseudohalides are among the most efficient methods for the formation of C-C single bonds, leading to their widespread application in organic synthesis[29]. This significant contribution to chemistry was recognized with the Nobel Prize for A. Suzuki, together with R.F. Heck and E. Negishi for their respective coupling reactions[13]. The reaction involves boronic acids and requires the presence of a base[13]. Boronic acids are non-toxic and stable in air and moisture, making them easy to handle[13]. The reactions are generally conducted under mild conditions, and water is often unproblematic and sometimes even advantageous[118]. Suzuki couplings are often homogeneously catalyzed using Pd complexes with phosphorus-based ligands[29],[118]. The underlying catalysis mechanisms are controversially discussed, since it remains unclear whether it proceeds via ionic or neutral intermediates[13].

It has also been shown that ligand-free systems can effectively couple aryl iodides and aryl bromides containing electron-withdrawing groups with high turnover numbers. In contrast, less reactive aryl chlorides and tosylates require bulky and electron-rich phosphines for successful coupling. A significant drawback of ligand-free systems is the tendency for agglomeration, necessitating the use of appropriate stabilizers.[29] As an example, de Vries and co-workers employed dissolved $Pd(OAc)_2$ for Suzuki and Heck reactions, achieving catalytic activity at Pd loadings as low as 0.01 mol%, which is referred to as "homeopathic Pd catalysis". This approach allows for the utilization of various substrates containing iodine and bromine, along with several boronic acids.[119] Later, it was shown for Heck reactions from $Pd^{II}$ precursors that the catalysis itself very likely proceeds via monomeric or dimeric anionic species,

while temperatures above 120 °C lead to a fast reduction of $Pd^{II}$ to $Pd^0$ that strongly tends to colloid formation. Furthermore, it was shown that catalysis with molecular $Pd^0$ is always in competition with the formation of Pd clusters and Pd black, while all Pd species can transform into each other.[120] This means that clusters act as a reservoir for soluble Pd species that are the actual catalyst (depicted in Scheme 7). This finding was verified not only for the Heck reaction but has also been verified for the Suzuki reaction, among others.[121] While further insights into the catalytic mechanism for nanoparticles are missing, the presented behaviour can be explained by Ostwald ripening.

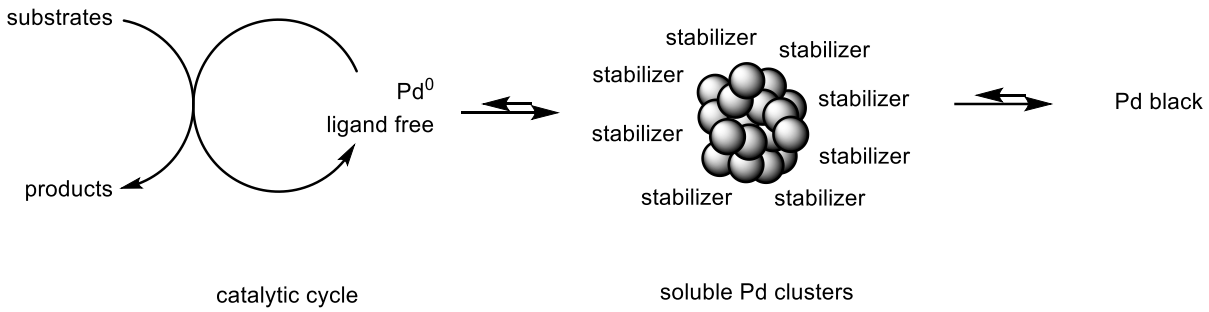


Scheme 7: Soluble Pd clusters as storage for single-atom $Pd^0$ species for Suzuki and Heck reactions, adapted from [121].

However, works for other catalytic Pd systems show that the catalytic conversion happens on the particle surface. The whole topic is thus controversially discussed.[29] The situation is further obscured by the fact that many authors do not consider the identity of the active species at all or provide only educated guesses[117]. A comprehensive review concludes that the active species is indeed always system-specific; thus, generalizable statements are not feasible. However, in most cases, the presented behavior is likely to apply.[117]

As a consequence, each catalytic system for Suzuki couplings demands a combination of several tests to enable a precise conclusion regarding the nature of the true catalytic species, as has already been described in chapter 2.1.1.3. Notably, some of the proposed tests bear weaknesses specific to Suzuki couplings[117]: During the filtration test, leaching species may recombine if the duration of the filtration process exceeds the time required for dissolution and recombination. Furthermore, the catalytically necessary metal amounts can be so low that they become undetectable. The conclusions from the mercury test must be limited to the following: If mercury shows no effect, it indicates that there is no unprotected $Pd^0$ present in any form within the catalytic cycle. Conversely, if mercury does have an impact, it suggests that a $Pd^0$ intermediate is present; however, no conclusions can be drawn regarding its location in the reaction mixture or state.[117]

Despite the many difficulties that may arise in the quest for the true catalytically active species, a lot of work has been conducted in synthesizing and applying Pd NP in Suzuki couplings to address the shortcomings regarding separation and activity mentioned in the beginning[29],[122],[123].

## 2.3 Process Intensification

If certain aspects of chemical processes are improved drastically, this can be regarded as process intensification. Examples of those aspects include specific energy consumption, numbers or sizes of apparatuses, or specific waste-per-product amounts.[7]

### 2.3.1 General Aspects

The term “process intensification” is commonly used to describe any measures aiming at significant enhancements of the efficiency of chemical processes. However, there is no standardized definition for this term, making it challenging to distinguish from traditional process optimization. While several different distinctions can be made, e.g., based on the type of underlying mechanisms, a commonly used classification involves hierarchical levels, see Figure 6.[7],[124],[125]

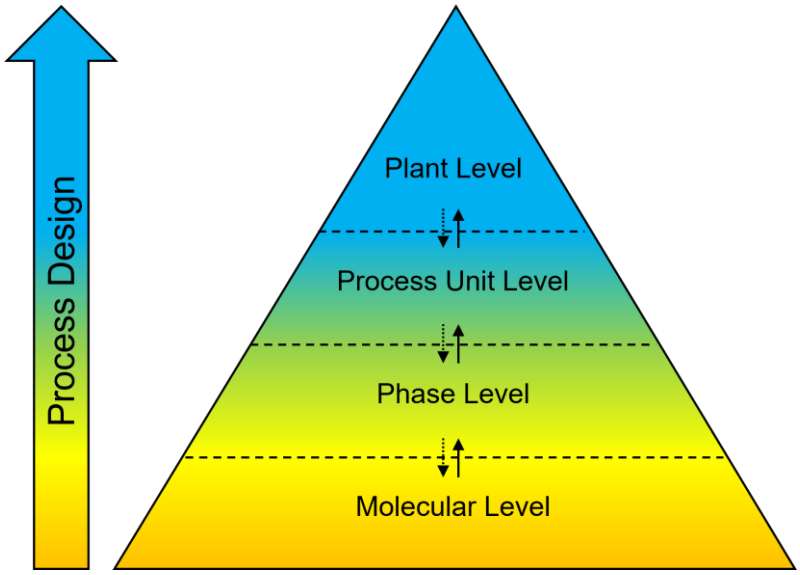


Figure 6: Levels of Process Intensification and direction of Process Design, adapted from Freund and Sundmacher[7].

On the *Molecular Level,* phenomena occurring at the molecular scale are described. The *Phase Level* considers processes of assemblies of molecules that form a distinct phase. In the superordinate *Process Unit Level,* phases within enclosed process spaces, such as apparatuses, are examined. Lastly, in the *Plant Level*, the overall picture of all process spaces is depicted. This level examines connections between individual process units and often integrates multiple unit operations into multifunctional process units.[7],[124],[125]

Changes at one level frequently lead to alterations at mostly higher levels. Hence, intensification in chemical processes is more easily achievable through modifications at the molecular level than through traditional optimization methods, since those are situated more closely at the upper levels. As a consequence, catalysis, located at the molecular level, plays a key role in process intensification.[7]

## 2.3.2 Mass and Energy Transfer

At the phase level, non-thermodynamic ("kinetic") methods can enhance reaction rates. Traditional heat transfer devices such as oil baths, sand baths, or heating jackets tend to operate slowly and can create temperature gradients within the reaction medium, bearing the risk of local overheating. As an alternative approach, microwave radiation can be used. Microwave radiation only heats solvents and reagents rather than the walls of the apparatus itself, resulting in a uniform increase in temperature. It has to be noted that microwave radiation cannot commence reactions by itself, as its radiation energy is lower than the chemical bond energies.[126]

The reduction of mass transport pathways through geometric modification is a phenomenon occurring at the process unit level, since the geometry of the process unit is often crucial for determining the specific surface area and interfacial area[127]. For example, in the hydrogenation of fats and oils, interfacial mass transfer is typically the rate-limiting step; therefore, it is essential to determine the volumetric mass transfer coefficient of the gas in the liquid, $k_l a$ [71]. This value is derived from the two-film theory and is applicable if the reaction takes place almost exclusively in the core of the liquid phase[128]. In this case, mass transfer controls the reaction rate and can be treated as a preceding operation[128]. The $k_l a$ value describes the gas mass transfer from the gas phase across the phase interface into the liquid phase[128]. In mechanically stirred reactors, its value depends on numerous parameters, including stirrer dimensions, position of the stirrer in the reactor and the medium, operating conditions, and the physicochemical properties of the liquid phase[129]. For instance, in the hydrogenation of fats and oils, an increased stirring speed leads to a higher concentration of hydrogen in the liquid phase, which in turn enhances the reaction rate and reduces trans-isomer formation as explained in chapter 2.2.1.2[71]. Pressure does not significantly affect the $k_l a$ value, unless it has a strong impact on surface tension[129]. It is important to note that the $k_l a$ value has to be determined in the absence of any chemical reaction[71].

In practice, miniaturization of equipment is an important option for process intensification in terms of increased mass and energy transport, happening on the process unit level and enabled by e.g., microreactors like capillary reactors that will be explained in detail in the next section[127].

## 2.3.3 Capillary Reactors

### *2.3.3.1 General Aspects*

Microprocess technology is part of process intensification and Green Chemistry and refers to chemical processing carried out using reactors and additional equipment with at least one dimension of 1 mm or less. Microprocess technology features small reaction volumes, typically utilizing round channels, although other shapes are possible. Specifically, capillary reactors fall under the superordinate term of microprocess technology and are flow chemistry reactors with continuous liquid delivery and removal.[130]

Microreactors in general can be employed for the investigation of specific phenomena at the laboratory scale, the identification of optimal process parameters, and the production of small quantities of specialty chemicals[127]. Microstructured equipment allows the transfer from batch processes to continuous ones, thereby simplifying subsequent process design and scale-up[127],[131]. Scale-up of distinct microreactor systems is typically achieved through parallel replication (numbering up) rather than by increasing the size of individual units[132]. However, numbering up in multiphase reactions presents challenges due to high demands for equipment and process control[131]. Additional disadvantages of microreactors include high pressure drops, low throughput, susceptibility to blockage by solids, and sometimes complex miniaturization of measurement and control elements[131].

Despite those possible drawbacks, microreactors are particularly attractive for highly exothermic or endothermic reactions. They help to avoid hotspots by rapid heat removal and facilitate effective heating due to a high energy transfer, which can be increased by a factor of ca. 1,000 compared to conventional reactors.[127] Furthermore, they are advantageous for very rapid, heterogeneously catalyzed reactions that are prone to mass transport limitations[127]. As mass transport often becomes the rate-determining step in multiphase reactions, those reactions can benefit from microfluidics due to increased interfacial areas[133]. Typical reactions that are mass transport-limited and may become hazardous in batch processes, yet are suitable for capillary systems, include hydrogenations, sulfonations with oleum, or nitrations with nitric acid[132]. The high energy and mass transfer characteristics of microreactors allow for better control over these highly intensive reactions, ultimately leading to optimal yields and selectivities[132].

Reactions that present significant selectivity challenges or require high selectivity benefit from well-defined residence times of microreactors: The small lateral dimensions of capillaries result in short characteristic diffusion times, enabling ideal radial mixing through diffusion. This allows for plug-flow-like behavior despite laminar flow conditions, even in monophasic systems.[127] Flow characteristics of biphasic capillary flow will be introduced in the next section.

#### *2.3.3.2 Slug Flow*

In biphasic flow, mostly liquid/liquid (l/l) or gaseous/liquid (g/l) flow is employed[134]. Several flow regimes exist for biphasic flows in capillaries, dependent on several parameters like channel geometries, flow rates, and properties of the surrounding material and both liquids[134]. Examples for resulting flow patterns include bubbly flow, churn flow, slug flow, and annular flow and intermediate patterns. The most often investigated one is slug flow.[134]–[137] Slug flow, also called Taylor flow or segmented flow, is applicable for both g/l or l/l multiphase systems and is, in a simple case, achievable through suitable adjustments of the individual feed flow rates[127]. Furthermore, material properties of the capillary material as well as geometrical parameters at the mixing zone influence slug lengths, thus slug lengths can be adjusted independently from the ratio of the liquid flow rates[138],[139]. In this flow regime, the axial length of the individual phase exceeds the channel diameter[138]. Wall friction of the liquid phase(s) induces secondary flow, leading to internal circulation within the liquid slug, known as Taylor vortices,

see Figure 7[127],[132],[135]. The recirculation time depends on the superficial velocity of the slug, its length, channel diameter, and the ratio of the viscosities of both fluids[139]. This phenomenon significantly enhances radial and tangential mass transfer within each liquid slug[127],[132],[135]. In comparison to monophasic flow, mass transport can be increased by one order of magnitude[127]. Due to the segmented flow and strong internal mass transport within the liquid slugs, the whole flow regime exhibits a plug flow characteristic[127]. In case the second phase is a gas phase, the gas slugs form a disperse phase nearly filling the whole cross-section, leaving only a thin liquid wall film[127]. In Taylor flow, the mass transport rate across the gas-liquid interface is nearly linearly dependent on the frequency of vortex circulation[135].

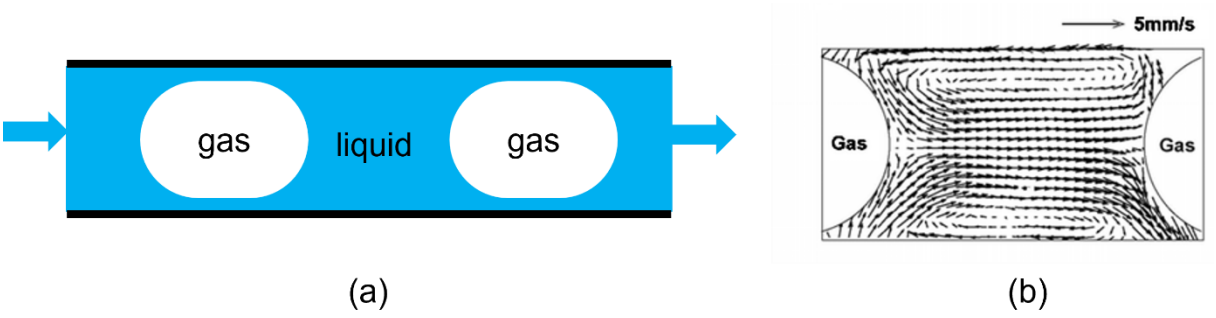


Figure 7: Schematic g/l slug flow (a) and measurement of the relative velocity field inside a liquid slug moving through a rectangular microchannel in g/l slug flow (b)[136].

The slug length is influenced by factors such as viscosity, flow velocity, channel geometry, and surface properties, and thus can be adjusted by these[132]. It is a crucial parameter for mass transport as it affects the interfacial area and hydrodynamics of the individual segments[138]. Excessively long slugs can lead to stagnant zones and reduced mass transfer efficiency, and are therefore undesirable[138].

In g/l reactions without additional gas slugs (meaning a monophasic system with only dissolved gas), there is typically insufficient gas solubility for complete conversion[140]. Even with the presence of additional gas slugs, the density difference between gas and liquid results in varying substance amounts in the gas resp. liquid slugs[141]. As a viable solution to this issue, the gas replenishment by permeation through the capillary wall has been recently presented and will be explained more closely in the following section[141].

#### *2.3.3.3 Permeation*

The concept of permeation utilizes the solubility of certain gases in polymeric materials. Conceptually, the reaction gas is supplied from the outside of the reaction/fluid zone through specialized polymer materials (such as the highly specialized Teflon AF2400 and the more conventional fluorinated ethylene-propylene, FEP) that have high permeation coefficients. However, permeation coefficients vary among these polymer materials, with FEP having lower permeation coefficients compared to Teflon AF2400, i.e., by a factor of at least 160 for hydrogen at room temperature[142]. In the literature, this gas supply setup typically involves an inner capillary surrounded by a concentric outer tube. This configuration is referred to as the "tube-in-tube" concept and is schematically shown in Figure 8.[141]

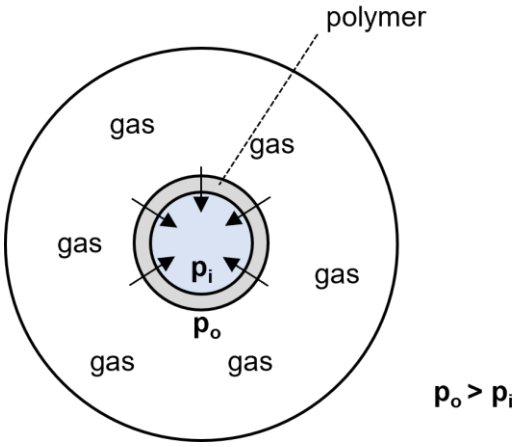


Figure 8: Tube-in-tube concept for the permeation of gases through polymers.

The permeation flux of a gas can theoretically be calculated using the temperature-dependent permeation coefficient, specific to the investigated gas and polymer $\varepsilon_{\mathrm{gas,polymer}}$, as well as the permeation pressure difference $\Delta p_{\mathrm{perm}}$, the wall thickness $s$ and surface area $A$ according to equation (1).[141]

$$q_{\mathrm{gas}} = \varepsilon_{\mathrm{gas,polymer}}(T) \cdot \frac{A}{s} \cdot \Delta p_{\mathrm{perm}} \qquad (1)$$

The applicability of gas permeation in an existing slug flow without reaction has already been demonstrated, resulting in an enlargement of the already existing gas slugs. However, there are currently only a few examples of reactions in slug flow utilizing permeation. These investigations are moreover often limited to short capillaries and never investigate the development of the gas slug sizes or influences of the permeation on flow stability.[141]

# 3 Objectives

The overall objective of this work is the extension of the development and application of catalytic colloidal nanoparticles in a holistic engineering approach, as introduced in detail in Figure 1 in chapter 1. This should be achieved in a broad range of reactions or processes by means of all four levels of process intensification. Catalysis, as one of the most powerful tools for process intensification and green chemistry, will play the central role in this work. As first-principle catalytic applications contribute to the molecular level as introduced in chapter 2.3, all above-lying levels will be subsequently covered and examined in more detail (see Figure 9). It will start from the synthesis, evaluation, and selection of colloidal nanocatalysts, followed by applications in several catalytic reactions, up to the implementation of intensified processes for selected reactions. The ultimate goal is to establish an intensified, continuous process for a catalytic conversion using nanoparticles. The selective partial hydrogenation is a highly promising tool to achieve further functionalizations of formerly unreactive or less reactive substrates and will be used extensively to reach this topmost goal. Throughout most of the levels, the applicability of renewable resources as raw material is examined to support the transformation towards defossilized products, where fatty acid methyl esters are used as a recurring substrate.

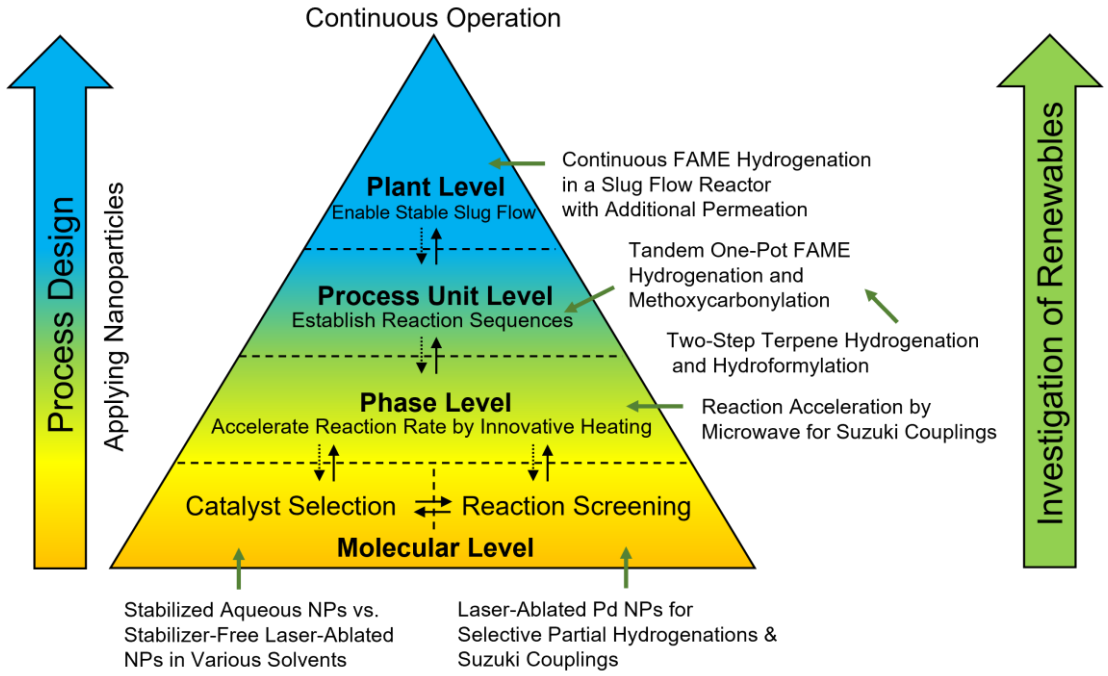


Figure 9: Visualization of the objectives of this work on each level of process intensification.

In the first part of this work, process intensification at the molecular level should be achieved by first-principle investigations of several nanocatalytic approaches. For this, the molecular level will be divided into two major sections, focusing on a catalyst screening and selection on one side. A screening of different applicable reactions and substrates for one highly promising class of colloidal nanocatalysts will be performed on the other side. The catalyst selection segment should answer the following questions: What is the applicability and reactivity of various types of Pd nanoparticles in aqueous media produced by conventional wet-chemical approaches for the hydrogenation of selected substrates, and what structural changes do these particles undergo as a result of the catalytic conversions? In a second,

contrary step in this section, solvent-stabilized transition metal nanoparticles will be synthesized using pulsed laser ablation in liquids as a top-down approach. Here, PLAL is examined as an intensification method for the production process of the particles, aiming to enable a fast and reliable synthesis route. What are, for specific applications, optimal metals and solvents, and what initial insights into the underlying reaction mechanisms can be gained?

In the reaction and substrate screening section, the applicability of the optimized catalyst system synthesized by the intensified approach of PLAL will be investigated in several different catalytic reactions in more detail. What kind of reactions are these particles suited for? For each reaction type, a substrate screening will be performed alongside, considering especially industrially relevant substrates (for the optimization of existing processes as introduced in chapter 1) and renewable substrates (for the transition towards a defossilized industry). In parts, the phase level will be examined by the question of the effect of an intensified energy transfer on the reaction rate. Furthermore, an inherent catalyst separation strategy by a liquid biphasic reaction system will be considered.

In the next step towards the process unit level, the implementation of reaction sequences will be performed in order to present applicability studies for advanced product usage and in order to verify the robustness and versatility of the chosen type of nanocatalyst. At first, a sequential reaction sequence is to be performed, including the utilization of selective partial hydrogenations of conjugated terpenes and subsequent hydroformylations, with the need for intermediate workup, as the hydroformylation of untreated terpenes is challenging. Can selective partial hydrogenation overcome this hurdle to enable the use of polyunsaturated terpenes for value-added products?

In an even more advanced reaction sequence, an integrated tandem one-pot approach without intermediate workup with one catalyst metal performing two different types of reaction is desired, being the selective partial hydrogenation of FAME and a subsequent isomerizing methoxycarbonylation. This approach is fully located at the process unit level. How is the compatibility of the individual reaction steps in terms of solvent, catalyst amount, and gas change? To date, only conditions for the individual reaction steps have been established independently. In both reaction sequences, stable catalyst colloids are expected to play central roles, but these sequences have never been performed before.

Insights gained at the molecular level at the beginning of this work will ultimately be applied as a basis for a continuous selective partial FAME hydrogenation in a capillary reactor utilizing the beneficial slug flow regime. In this stage, particularly improvements in reactivity caused by intensified mass transport supported by additional gas permeation are expected and examined, along with effects of the permeation on the flow stability. To date, permeation has only been applied without simultaneous reaction. So the first question is: can permeation be combined with a continuous reaction in slug flow? What implications arise with the concept of permeation? And most importantly, can permeation prevent flow destabilization? This final approach aims at process intensification at the plant level by the integration of a mass transfer unit into a reaction unit, resulting in a multifunctional process unit for continuous operation, supported, for the first time, by colloidal catalytic nanoparticles in an exemplary reaction with a renewable substrate.

# 4 Catalytic Activity of Water-Dispersed Palladium Nanoparticles with Different Sizes and Shapes in the Semihydrogenation of Alkynes

This chapter was published as

N. Kost, F. Lehmann, R. Guo, K. Loza, M. Heggen, T. Seidensticker, M. Epple, “Catalytic Activity of Water-Dispersed Palladium Nanoparticles with Different Sizes and Shapes in the Semihydrogenation of Alkynes”, *ChemCatChem* **2025**, *17*, e01164, DOI: 10.1002/cctc.202501164.

Citation style and numbering, as well as Figure and Table numbering, were changed to a sequential mode to fit the document style.

**Author contributions:** The conceptualization leading to this publication and manuscript preparation including formal analysis, writing, and visualization, was performed by N. Kost and me equally; therefore, we share first authorship. N. Kost and R. Guo prepared and analyzed the nanoparticle solutions (apart from electron microscopy) that were investigated in the hydrogenations by me. K. Loza contributed the HRTEM and SEM images, together with M. Heggen. T. Seidensticker and M. Epple acquired funding, supervised this project, and reviewed and edited the manuscript.

## 4.1 Abstract

Palladium nanoparticles of different sizes and shapes dispersed in water, stabilized by either polyvinylpyrrolidone or glutathione, were studied in both monophasic and biphasic alkyne hydrogenation reactions at 50 bar hydrogen pressure. Spherical nanoparticles of 2 and 5 nm diameter as well as cubic nanoparticles of 18 and 28 nm edge length were investigated. Structural changes in the particles before and after the catalytic reactions were assessed with respect to agglomeration and particle size. The particle size had the strongest effect on the catalytic efficiency, i.e., spherical nanoparticles of 5 nm were the most active and spherical nanoparticles of 2 nm were the least active. The nanocubes had intermediate catalytic activities. Semihydrogenation occurred within minutes at low palladium loadings. The highest turnover frequencies of about 183,000 $h^{-1}$ were achieved with 5 nm palladium nanoparticles. Mass transport limitations constrained the reaction rates in aqueous biphasic systems with larger nanoparticles.

## 4.2 Introduction

Metallic nanomaterials have found many applications in catalysis due to their remarkable properties compared to the bulk phases. This is mainly due to their high specific surface area.[143]–[145] Palladium nanoparticles are especially important in heterogeneous catalysis, e.g. for hydrogenation[146],[147] and cross-coupling reactions[148]. Ultrasmall nanoparticles, i.e., smaller than 3 nm in diameter, have a particularly high surface area with good colloidal stability.[144],[145] Therefore, they behave like

homogeneous catalysts while simultaneously acting as heterogeneous catalysts. This dual nature bridges the gap between homogeneous and heterogeneous catalysis, combining the high activity, selectivity, and mild reaction conditions of homogeneous catalysts with the easy catalyst retrieval (e.g., by membrane filtration) of heterogeneous systems. This opens up new avenues for more efficient and sustainable catalytic processes.[13],[53]

Various larger palladium nanoparticles have been investigated in catalysis, with studies exploring the influence of particle size, shape, and stabilizing ligands, particularly in alkyne hydrogenation, which is a key reaction in fine chemistry and polymer production.[53] Palladium is the preferred metal for alkyne hydrogenation, although it is usually applied in supported form.[53] Both nanoparticle size and shape have been shown to affect the catalytic performance, usually ascribed to differences of the active sites on the particle surface.[56] Planar crystal faces were identified as the most important for hydrogenation catalysis. Crystal edges and corners lead to selective alkyne-to-alkene hydrogenation, but at high conversions, they also catalyze the hydrogenation of alkene to the corresponding alkane.[56] The catalytic behavior of palladium nanoparticles is influenced not only by their shape and size, which determine turnover frequency (TOF) and selectivity, but also by their capping agents, which can alter their surface properties and restrict the access of a substrate to the metal surface.[55] For example, the polymer poly(N-vinylpyrrolidone) (PVP), which is frequently used as capping agent for nanoparticles[54],[56],[149]–[151] initially inhibits the catalytic activity by covering the active surface sites, but gradually desorbs to expose more catalytically active parts of the surface.[26],[152],[153] On the other hand, glutathione (GSH) is a smaller capping agent that has a strong stabilizing effect on metal particles of different size and shape.[34],[154],[155] Therefore, it is another promising choice to coat catalytically active palladium nanoparticles.[146]

Ultrasmall palladium nanoparticles have been synthesized but rarely tested for their catalytic activity.[144],[146],[151],[154],[156]–[158] Usually, palladium nanoparticles larger than 5 nm were used in alkyne hydrogenation.[57] It appears to be an attractive option to use ultrasmall palladium nanoparticles with their very high specific surface area as catalysts to reduce the amount of necessary palladium. Only two reports have addressed the hydrogenation of alkynes or alkenes by ultrasmall colloidally dispersed nanoparticles so far.[57],[146]

The hydrogenation of alkynes with palladium nanoparticles is usually carried out at low hydrogen pressure (1 to 4 bar) in liquid single-phase systems,[54]–[57],[59],[159]–[161] with the only exception of Telkar et al. who used 24 bar.[162] Hydrogen pressures above 24 bar were never applied together with dispersed catalytically active nanoparticles. Furthermore, palladium nanoparticles have not yet been applied in the aqueous biphasic hydrogenation of alkynes.

Closing this gap in knowledge, we report here on the catalytic activity of palladium nanoparticles of well-defined and uniform size, shape, and surface functionalization in high-pressure hydrogenation, focusing on their high specific surface area and resource-efficient material use. We compare their catalytic activity in alkyne hydrogenation in a monophasic as well as in a biphasic system. Besides the assessment of

the catalytic efficiency, we isolated the particles after the reaction and analyzed them by transmission electron microscopy to shed light on possible changes that occurred during the catalytic reaction.

## 4.3 Experimental Section

All chemicals were obtained with a purity of at least 98% and used without further purification (see chapter 11.1).

For the preparation of spherical ultrasmall palladium nanoparticles (2 nm),[144] disodium tetrachloropalladate ($Na_2PdCl_4$, 60 mg, 1 eq.) was dissolved in 230 mL water in a 500 mL round bottom flask. Glutathione (GSH, 128 mg, 2 eq.) dissolved in 10 mL cold water was added. The solution changed its colour from light-yellow to orange within 2 min. After 10 min, a freshly prepared solution of sodium borohydride (46 mg, 6 eq.) in 10 mL cold degassed water was quickly added. The color of the solution rapidly changed to brown-black. After 12 h, the glutathione-coated ultrasmall black palladium nanoparticles were isolated by spin filtration (5 kDa SpinX UF 20 centrifuge filters; 45 min, 4,000 rpm). Finally, the nanoparticles were washed several times with 15 mL water each by spin filtration. In an earlier study, the number of GSH ligands on a similar type of palladium nanoparticles was determined to 117 GSH ligands on each 1.8 nm particle.[144] For the larger palladium nanoparticles, the number of ligands on the surface is not known because NMR spectroscopy is not applicable in this case.[163] PVP-coated spherical palladium nanoparticles (5 nm) were prepared according to a published procedure.[151] The ligand exchange of PVP to GSH in 5 nm nanoparticles was carried out by dispersing the palladium nanoparticles (10.6 mg, 100 µmol palladium content) in 190 mL water. 1 g glutathione dispersed in 10 mL water was added and the dispersion was stirred for 24 h. The particles were isolated by spin filtration in 30 kDa SpinX UF 20 centrifuge filters (45 min, 4,000 rpm).

PVP-coated palladium nanocubes (18 nm) were prepared according to a published procedure.[149],[150] PVP-coated palladium nanocubes (28 nm) were prepared as follows: 18 nm PVP-coated palladium nanocubes were used as seeds for the on-growth of palladium. This involved the dissolution/dispersion of $PVP_{55}$ (55 kDa, 150 mg), ascorbic acid (90 mg), potassium bromide (450 mg), and palladium nanocubes (18 nm, 1.8 mg) in a 50 mL round-bottom flask in 12 mL water, followed by vigorous shaking. Subsequently, the mixture was heated to 40 °C for 10 min. Then, a solution of $Na_2PdCl_4$ (0.02 M in 5 mL water) was added, and the mixture was stirred at 40 °C for 24 h. Then, the reaction mixture was quenched with an ice bath. The particles were isolated by centrifugation (14,200 rpm; 21,190 g; 30 min) and washed twice with water. For the ligand exchange of PVP to GSH, 18 or 28 nm Pd-PVP nanocubes (5 mL, 2.5 mg Pd) were dispersed in 2.5 mL water, respectively, and mixed with glutathione (200 mg, dissolved in 2.5 mL water). The reaction mixtures were stirred for 12 h. The nanoparticles were isolated by centrifugation (14,200 rpm; 21,190 g; 30 min) and washed twice with water.

Transmission electron microscopy (TEM) was performed with an FEI TEM 80–300 instrument with an accelerating voltage of 300 kV.[164] The nanoparticle dispersions were deposited onto copper grids that were coated with an ultrathin amorphous carbon film and dried in air. The size of the 2 nm nanoparticles was determined by the program ANTEMA.[165] The size of the 5 nm nanoparticles was determined

manually with the program ImageJ.[166] Scanning electron microscopy (SEM) was performed with an Apreo S LoVac instrument (Thermo Fisher Scientific, USA) with nanoparticles prepared as for TEM. The size of the nanocubes was determined manually with the program ImageJ.[166]

Differential centrifugal sedimentation was carried out with a CPS Instruments DC 24,000 disc centrifuge, operating at 24,000 rpm and 29,000 g. A density gradient was obtained by overlaying with two sucrose solutions of 8 and 24 wt%, respectively. Dodecane (0.5 mL) was added to the top layer to prevent evaporation. Prior to each measurement, a calibration standard of polyvinylchloride (PVC) with a defined hydrodynamic diameter of 263 nm dispersed in water was measured. The volume of the added aqueous nanoparticle dispersion was 100 µL. The hydrodynamic diameter of the nanoparticles was calculated with the density of elemental palladium (12.023 g $cm^{-3}$). Hydrodynamic particle size distributions were also determined by dynamic light scattering (DLS) with a Malvern Zetasizer Nano ZS ZEN 3600 instrument with nanoparticles in aqueous dispersion.

For the ICP analysis, the sample was dried at 150 °C and then digested with 8 mL 67% $HNO_3$ in a CEM Mars 6 microwave instrument. Afterwards, the sample was dispersed in 3 mL deionized water and measured in an ICP-OES instrument (Plasma Quant PQ9000 Elite, Analytik Jena).

For hydrogenation at 1 atm, the concentrated nanoparticle dispersions were ultrasonicated for 5 min. Then, an aliquot was diluted to the desired content of palladium with deionized water, followed by stirring for 5 min. Reactions at 1 atm hydrogen were conducted in round bottom flasks with stopcock that were flushed with argon under stirring at 1,400 rpm for at least 5 min after the diluted catalyst solution had been added. A constant hydrogen supply was realized with a hydrogen balloon. To exchange argon by hydrogen, the flask was flushed with one complete balloon without stirring. Next, the nanoparticles were preformed for 10 min under stirring at 1,400 rpm. The substrate was added with a syringe, any possible overpressure was released, and a new balloon was attached with subsequent short flushing. For reactions at elevated temperatures, the reaction time was started after the desired temperature was reached. Aliquots were taken with a syringe and rapidly quenched.

A 120 mL stainless steel reactor was sealed, flushed with argon, and evacuated for high-pressure reactions. This was repeated three times. The catalyst dispersion was introduced into the reactor in argon counterflow; subsequently, the substrate container was charged by applying argon counterflow. Afterwards, the reactor was pressurized to 50 bar hydrogen under constant stirring at 1,500 rpm. After reaching a constant pressure, a preforming time of 10 min was allowed before the substrate was added to the preformed catalyst solution. During the reaction, aliquots were taken and rapidly quenched with liquid N2-frozen glassware. In the hydrogenation experiment with the Lindlar catalyst, the catalyst was placed inside the reactor prior to sealing, and no water was added.

All samples were analyzed by GC analysis with an FID detector and *tert*-butanol or *o*-xylene as external standards for quantitative analysis. For the biphasic hydrogenation, additional GC-MS-EI and NMR analyses were performed to exclude the formation of positional isomers.

## 4.4 Results and Discussion

### 4.4.1 Nanoparticle Characterization

Different types of palladium nanoparticles were prepared as potential catalysts: three types of spherical nanoparticles, i.e., 2 nm GSH-coated nanoparticles (denoted as ultrasmall nanoparticles in the following) and 5 nm PVP- or GSH-coated nanoparticles. The affinity of PVP to the palladium surface is weaker than that of the thiol-containing ligand GSH, a fact that may influence the catalytic activity.[146]

The diameter of the metal core was determined by high-resolution transmission electron microscopy (HRTEM; Figure 10). The average diameter of the ultrasmall nanoparticles was 1.5 ± 0.4 nm. The larger PVP-stabilized spherical nanoparticles (5 nm) had an average diameter of 4.4 ± 0.7 nm. Note the crystallographic well-developed faces of the 5 nm nanoparticles.

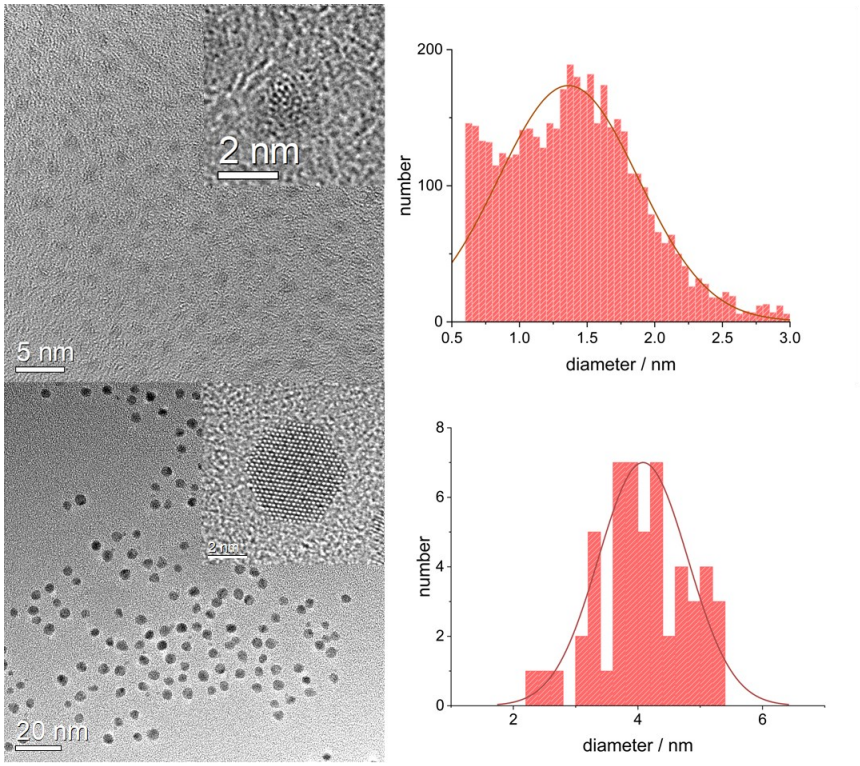


Figure 10: **Top:** HRTEM images of GSH-coated ultrasmall palladium nanoparticles (2 nm), together with the particle size distribution (>2,000 particles were analysed, average diameter: 1.5 ± 0.4 nm). **Bottom:** HRTEM images of larger PVP-coated palladium nanoparticles (5 nm), together with the particle size distribution (50 particles were analysed; average diameter: 4.4 ± 0.7 nm).

Differential centrifugal sedimentation (DCS) gave the hydrodynamic diameter of water-dispersed nanoparticles (Figure 11). Note that ultrasmall particles appear smaller in DCS because their effective density is lower than that of the metal core due to the surrounding ligand shell.[167]

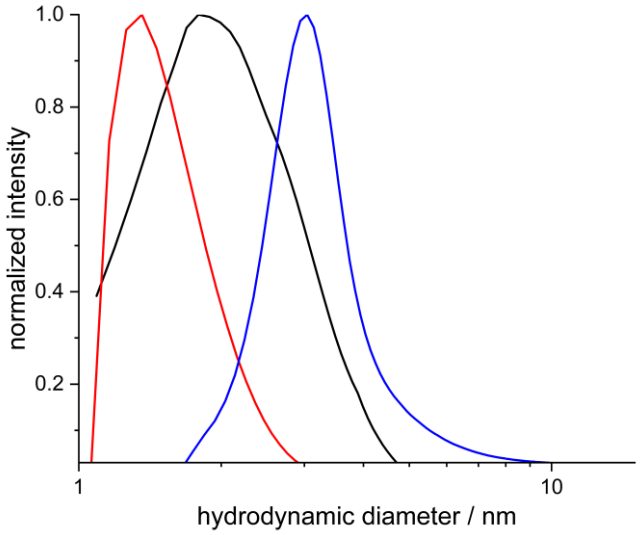


Figure 11: Differential centrifugal sedimentation (DCS) of GSH-coated ultrasmall palladium nanoparticles (2 nm, **red**), PVP-coated larger palladium nanoparticles (5 nm, **blue**), and GSH-coated larger palladium nanoparticles (5 nm, **black**), dispersed in water. The average diameter of the ultrasmall nanoparticles was 1.5 ± 0.4 nm. The average diameter of the PVP-coated larger nanoparticles was 3.1 ± 0.6 nm. The average diameter of the GSH-coated larger nanoparticles was 2.1 ± 0.9 nm.

A complementary method is dynamic light scattering (DLS), which was applicable only to the 5 nm nanoparticles because the ultrasmall nanoparticles do not scatter the light (Figure 12).

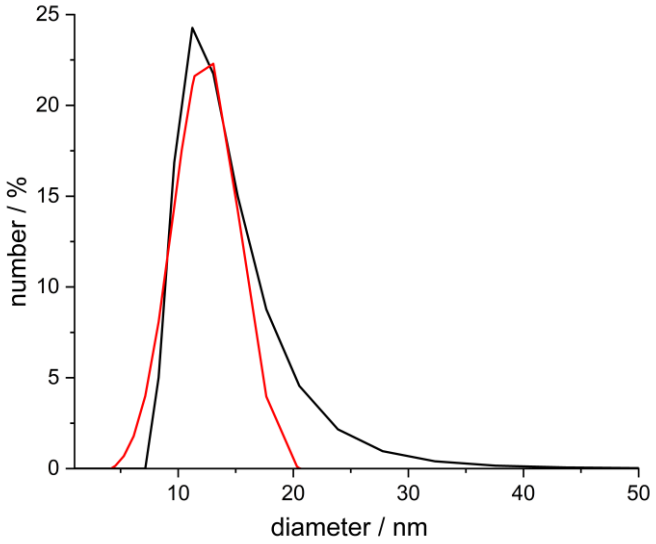


Figure 12: Dynamic light scattering (DLS) of PVP-coated larger palladium nanoparticles (5 nm), dispersed in water. The average diameter was 12 ± 3 nm (**black**). DLS of GSH-coated larger palladium nanoparticles (5 nm), dispersed in water. The average diameter was 7 ± 1 nm (**red**).

Two different sizes of palladium nanocubes were prepared with edge lengths of 18 and 28 nm, respectively, coated either with PVP or with GSH. The HRTEM images of the smaller nanocubes showed uniform cubes with slightly rounded corners. The HRTEM images of the larger nanocubes showed uniform cubes with minor surface defects (Figure 13). Scanning electron microscopy gave average edge lengths of 18 ± 2 and 28 ± 2 nm, respectively (Figure 14). The 18 nm cubes are mostly regular but the 28 nm cubes have concave faces. Although this is difficult to assess in a quantitative

way, it indicates that the exposed crystallographic faces are different for both types of cubes which may also influence their catalytic activity.

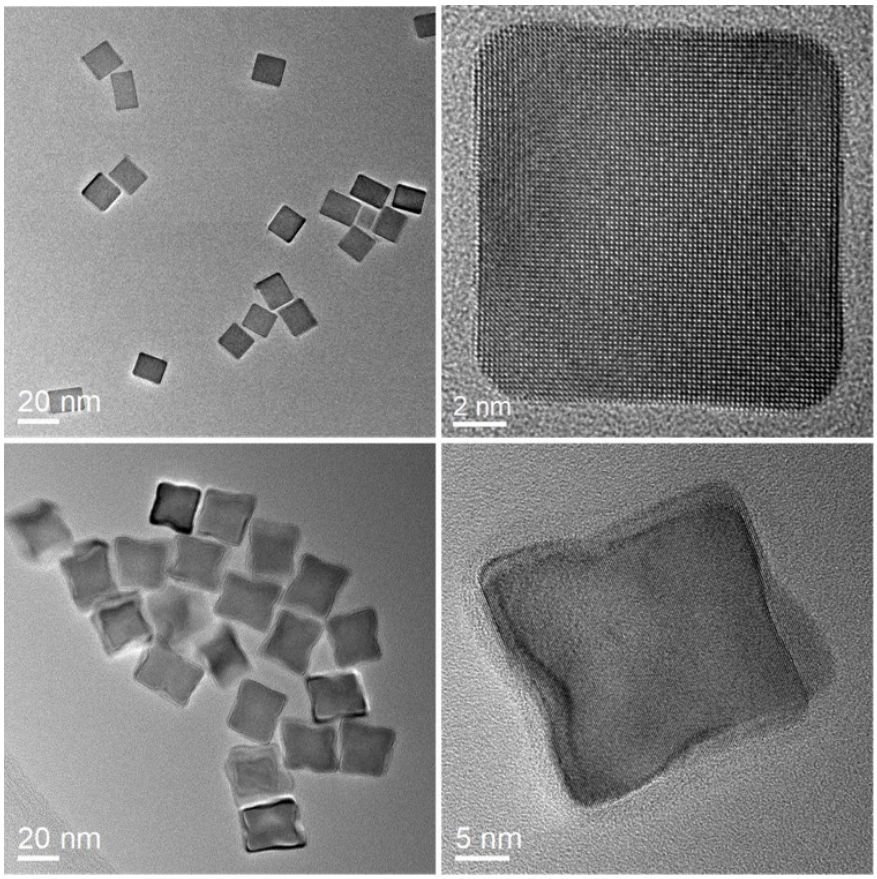


Figure 13: **Top:** HRTEM image of smaller PVP-coated palladium nanocubes (18 nm). **Bottom:** HRTEM image of the larger PVP-coated palladium nanocubes (28 nm).

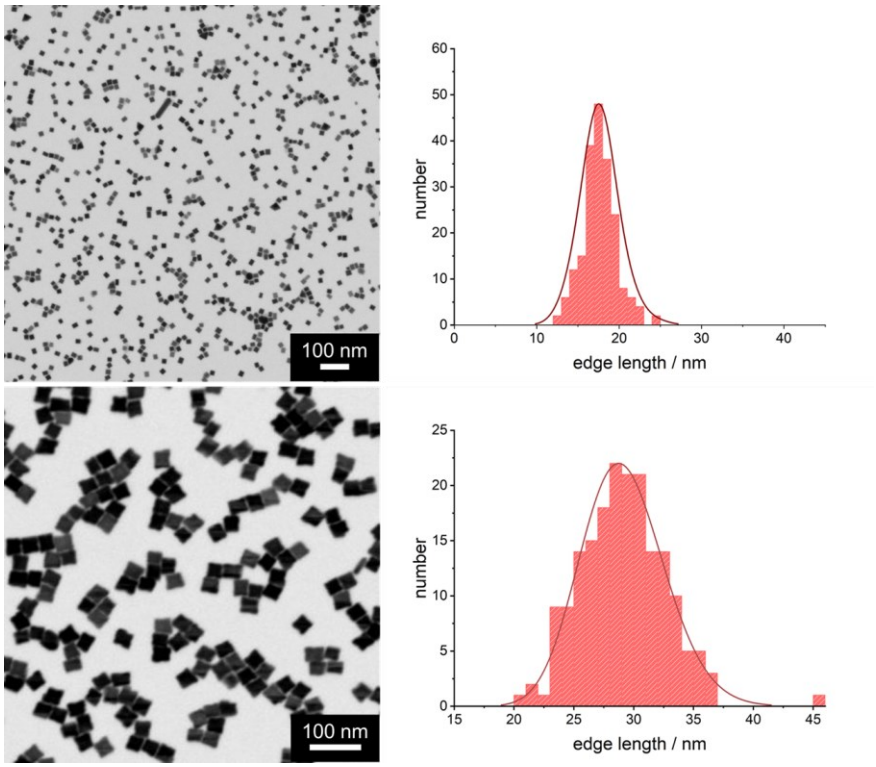


Figure 14: **Top:** Scanning electron microscopy of smaller PVP-coated palladium nanocubes (18 nm), together with their particle size distribution (203 particles were analysed, average edge length: 18 ± 2 nm). **Bottom:** Scanning electron microscopy of larger PVP-coated palladium nanocubes (28 nm), together with their particle size distribution (185 particles were analysed, average edge length: 28 ± 2 nm).

DCS (Figure 15) and DLS (Figure 16) gave the hydrodynamic diameters of the water-dispersed nanocubes, both with GSH and PVP-coating. The higher hydrodynamic diameter by DLS in comparison to the core diameter by TEM indicates a moderate degree of agglomeration. Table 1 summarizes all size characterization data of the nanoparticles.

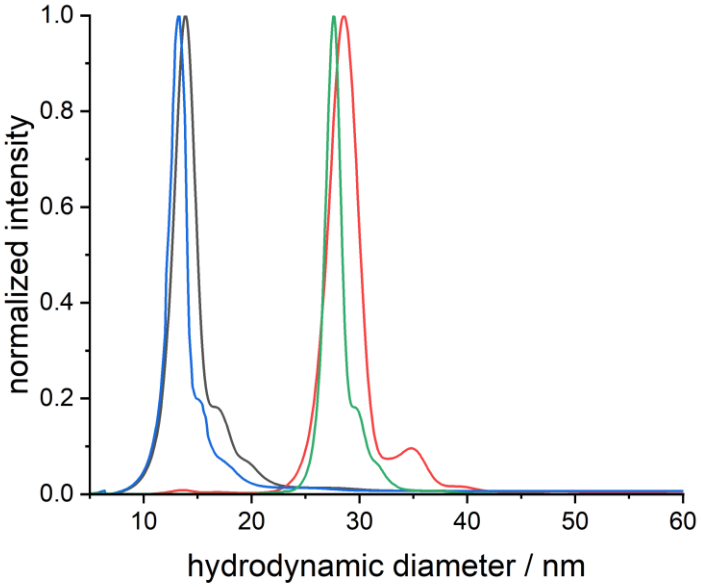


Figure 15: Differential centrifugal sedimentation (DCS) of smaller (18 nm) and larger (28 nm) palladium nanocubes, coated with either PVP or GSH. The GSH-coated nanoparticles had hydrodynamic diameters of 13 nm (**blue**) and 26 nm (**green**). The PVP-coated palladium nanoparticles had hydrodynamic diameters of 15 nm (**black**) and 28 nm (**red**), respectively.

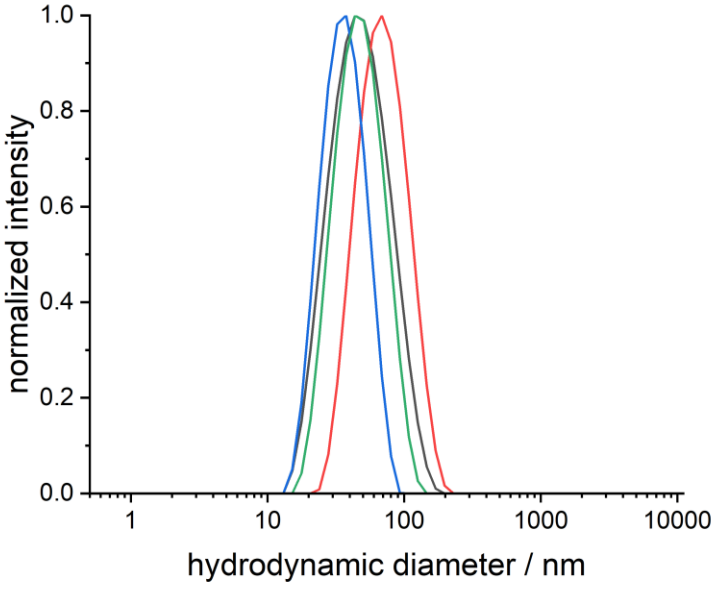


Figure 16: Dynamic light scattering (DLS) data of smaller (18 nm) and larger (28 nm) palladium nanocubes, coated with either PVP or GSH. The PVP-coated nanocubes had hydrodynamic diameters of 47 nm (**black**) and 68 nm (**red**), respectively. The GSH-coated nanocubes had hydrodynamic diameters of 35 nm (**blue**) and 47 nm (**green**), respectively.

Table 1: Characterization data of all palladium nanoparticles used for hydrogenation catalysis.

| Coating | Shape | Particle core diameter or edge length by electron microscopy / nm | Hydrodynamic diameter by DCS / nm | Hydrodynamic diameter by DLS / nm |
|---|---|---|---|---|
| **GSH** | Spheres (2 nm) | 1.5 ± 0.4 | 1.5 ± 0.4 | - |
| **GSH** | Spheres (5 nm) | 4.4 ± 0.7 | 2.1 ± 0.9 | 7 ± 1 |
| **GSH** | Cubes (18 nm) | 18 ± 2 | 13 ± 1 | 35± 4 |
| **GSH** | Cubes (28 nm) | 28 ± 2 | 26 ± 1 | 47± 5 |
| **PVP** | Spheres (5 nm) | 4.4 ± 0.7 | 3.1 ± 0.6 | 12 ± 3 |
| **PVP** | Cubes (18 nm) | 18 ± 2 | 15 ± 1 | 47 ± 5 |
| **PVP** | Cubes (28 nm) | 28 ± 2 | 28 ± 2 | 68 ± 7 |

After the detailed characterization of the particles, they were tested in the semihydrogenation reaction of alkynes. Figure 17 illustrates the relative dimensions of the molecular substrates 2-methyl-3-butyne-2-ol **1** and 1-octyne **2** in comparison to the palladium nanoparticles. The substrate 1-octyne has a similar size as the ultrasmall palladium nanoparticles.

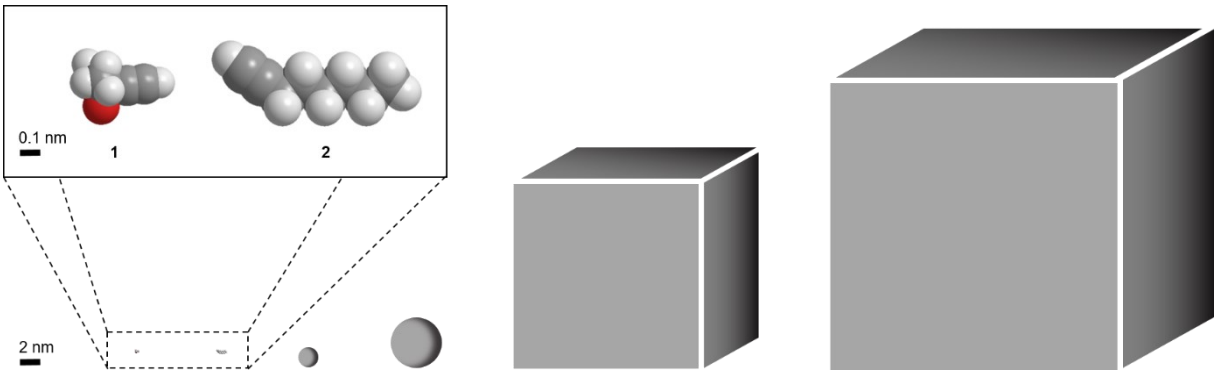


Figure 17: Schematic size comparison of the substrates (**1**: 2-methyl-3-butyne-2-ol, **2**: 1-octyne) with all palladium nanoparticles used for heterogeneous catalysis.

### 4.4.2 Hydrogenation of 2-Methyl-3-butyne-2-ol (Monophasic)

First, the GSH-coated ultrasmall nanoparticles were applied in the monophasic semihydrogenation of 2-methyl-3-butyne-2-ol (**1**, Scheme 8) to identify suitable reaction conditions.

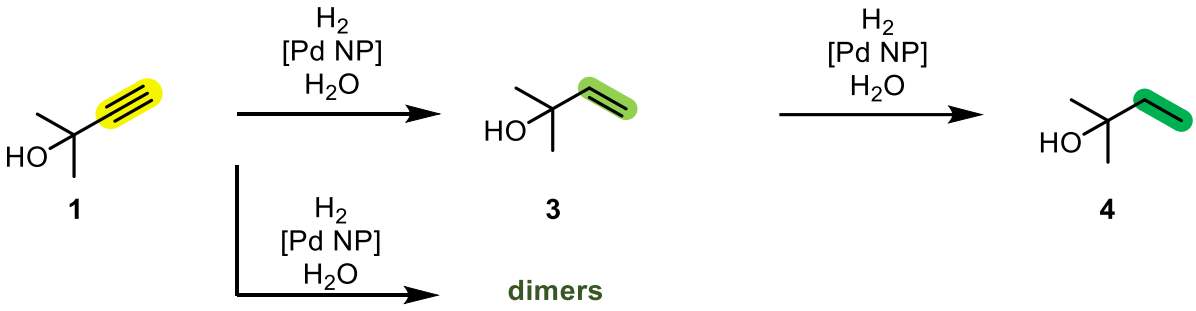


Scheme 8: Reaction network of the hydrogenation of 2-methyl-3-butyne-2-ol (**1**), catalyzed by palladium nanoparticles.

Initially, a standard approach was used, conducting the experiment at 1 atm hydrogen pressure with variable catalyst loadings and at variable temperature. Catalyst loadings as low as 0.016 mol% Pd were found to be catalytically active. However, the maximum conversion of **1** never exceeded 45%, regardless of the catalyst concentration and the temperature (see Figure S 1 and Figure S 2). Furthermore, TEM analysis of the ultrasmall palladium nanoparticles recovered after the hydrogenation reaction of **1** at 1 atm $H_2$, 25 °C and 0.016 mol% Pd showed strongly aggregated nanoparticles (Figure S 3). Therefore, the hydrogen pressure was increased to 50 bar to achieve a full substrate conversion. We found that at all investigated catalyst loadings, the hydrogenation of **1** to **3** at 50 bar and room temperature occurred within a few minutes (Figure 18). Notably, a selectivity of 84% toward the desired alkenol **3** was observed when approaching full conversion. Over-hydrogenation to *tert*-amyl alcohol **4** and dimer formation occurred only in minor amounts in that case. As expected, alkynes were hydrogenated significantly faster than alkenes.[56]

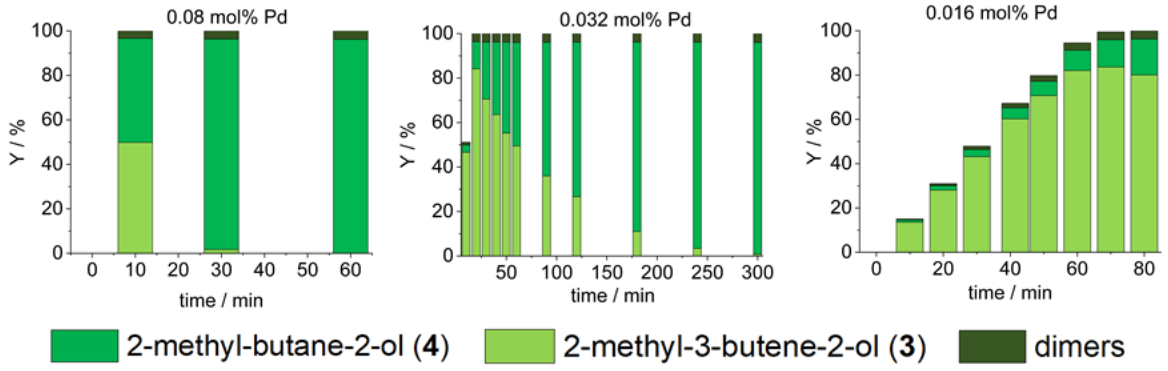


Figure 18: *Y*,*t*-plots of the hydrogenation of **1** at 50 bar $H_2$ catalyzed by GSH-coated ultrasmall palladium nanoparticles (2 nm) at different catalyst loadings. General conditions: $n_{substrate}$ = 50 mmol, $p_{H2}$ = 50 bar, $f_{stirrer}$ = 1500 rpm, $T_{start}$ = RT, $V_{total}$ = 58.1 mL, $t_{preforming}$ = 10 min, semibatch conditions; **left**: $c_{Pd}$ = 0.08 mol%, $w_{Pd,H2O}$ = 80 ppm; **center:** $c_{Pd}$ = 0.032 mol%, $w_{Pd,H2O}$ = 32 ppm; **right:** $c_{Pd}$ = 0.016 mol%, $w_{Pd,H2O}$ = 16 ppm.

At full conversion, a temperature maximum was reached, which decreased during over-hydrogenation (Figure 19). This can be explained by the different reaction enthalpies associated with the conversions from alkyne to alkene and from alkene to alkane of the same species,[168] coupled with different rates of

the individual reaction steps, and heat exchange across the reactor wall. This was also reported by Brunet et al.[59] Thus, the reaction progress was monitored non-invasively by monitoring the temperature in the reactor. Aliquots were taken toward the end of the plateau phase for analysis. Taking into account the reaction rate and the selectivity, 0.016 mol% Pd was chosen as the catalyst loading for all further experiments. The selectivity at complete conversion (X ≥ 99%) is particularly relevant because it correlates with the maximum yield. This underscores the intrinsic selectivity of this catalyst configuration because over-hydrogenation is expected to become more prominent at an excess of alkenes over alkynes.[53],[54],[56]

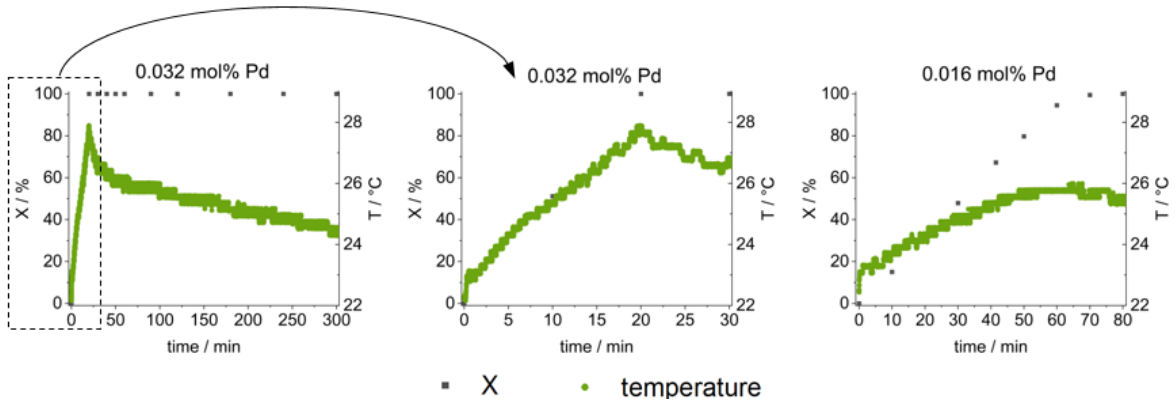


Figure 19: Development of reactor temperature and conversion during the hydrogenation of **1** at 50 bar $H_2$ with GSH-coated ultrasmall palladium nanoparticles (2 nm) at different catalyst loadings. General conditions: $n_{substrate}$ = 50 mmol, $p_{H2}$ = 50 bar, $f_{stirrer}$ = 1500 rpm, $T_{start}$=RT, $V_{total}$ = 58.1 mL, $t_{preforming}$ = 10 min, semibatch conditions; **left:** $c_{Pd}$ = 0.032 mol%, $w_{Pd,H2O}$ = 32 ppm, **center:** enlarged section of the left image, **right:** $c_{Pd}$ = 0.016 mol%, $w_{Pd,H2O}$ = 16 ppm.

Further monophasic hydrogenation experiments of **1** catalyzed by the other types of palladium nanoparticles were performed under the same conditions. The results are shown in Table 2.

Table 2: Overview of hydrogenation reactions of **1** (monophasic). Conditions: $n_{substrate}$ = 50 mmol, $p_{H2}$ = 50 bar, $f_{stirrer}$ = 1500 rpm, $c_{Pd}$ = 0.016 mol%, $T_{start}$= RT, $w_{Pd,H2O}$ = 16 ppm, $V_{total}$ = 58.1 mL, $t_{preforming}$ = 10 min, semibatch conditions.

| Entry | Coating | Shape | $d_{core/edge\ length,\ before}$ / nm | $d_{core/edge\ length,\ after}$ / nm | $S^a$ / % | $t_{T,max}$ / s | *TOF* / $h^{-1}$ | Pd recovery[b] / ppm |
|---|---|---|---|---|---|---|---|---|
| **2.1** | GSH | Spheres (2 nm) | 1.5 ± 0.4 | 1.5 ± 0.3 | 84 | 3,866-4,061 | 4,400 | full |
| **2.2** | GSH | Spheres (5 nm) | 4.4 ± 0.7 | 3.6± 0.6 | 84 | 125-132 | 177,000 | full |
| **2.3** | GSH | Cubes (18 nm) | 18 ± 2 | 17 ± 2 | 88 | 634-684 | 27,000 | full |
| **2.4** | GSH | Cubes (28 nm) | 28 ± 2 | 26 ± 2 | -[c] | 3,812-4,271[d] | 3,000[d] | 10 |
| **2.5** | PVP | Spheres (5 nm) | 4.4 ± 0.7 | 3.4 ± 0.6 | 76 | 122-138 | 183,000 | full |
| **2.6** | PVP | Cubes (18 nm) | 18 ± 2 | 13 ± 2 | 88 | 2,233-2,307[d] | 4,100[d] | full |
| **2.7** | PVP | Cubes (28 nm) | 28 ± 2 | 24 ± 3 | 81 | 1,402-1,713 | 15,000 | 4 |

[a] at full conversion; [b] the theoretical recovery is 14.85 ppm Pd at maximum; "full" indicates values between 12-17 ppm; [c] full conversion was not reached; [d] could be even lower, see SI for details.

The ultrasmall nanoparticles showed the lowest reaction rate (entry 2.1). Notably, a complete conversion was not achieved for the large GSH-coated nanocubes (entry 2.4), and the reaction significantly slowed down with time. The selectivity at full conversion was high in all cases, ranging from 76% to 88%. The 5 nm particles showed the highest reaction rate, regardless of the capping ligand (GSH or PVP, entries 2.2 and 2.5). ICP analysis gave very high recoveries for most types of palladium nanoparticles, suggesting that palladium remained well dispersed in the liquid phase. Only for PVP-coated 28 nm nanocubes, lower retrieval rates were observed.

A possible change of the shape and structure of the palladium nanoparticles during the hydrogenation of **1** at 50 bar hydrogen pressure was assessed by analyzing the retrieved nanoparticles by HRTEM (Figure 20). The crystallinity of the ultrasmall palladium particles had significantly increased due to the high hydrogen pressure (reduction of initially present PdO[144] to metallic palladium). This was confirmed by the treatment with hydrogen in the absence of the organic substrate. The particle core size remained unchanged. After retrieval, the ultrasmall nanoparticles were still well colloidally dispersed without noticeable agglomeration.

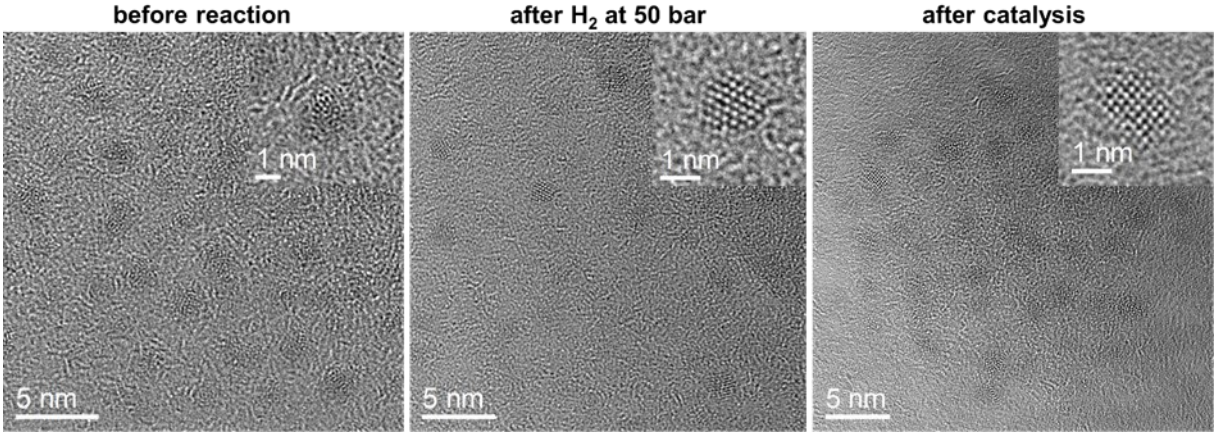


Figure 20: HRTEM images of ultrasmall GSH-coated palladium nanoparticles (2 nm) before the catalytic reaction (**left,** same as Figure 10), retrieved after stirring at 50 bar hydrogen pressure for 1 h (**center**), and retrieved after the hydrogenation reaction of **1** (**right**). Conditions: $n_{substrate}$ = 50 mmol, $p_{H2}$ = 50 bar, $f_{stirrer}$ = 1500 rpm, $c_{Pd}$ = 0.016 mol%, $T_{start}$ = RT, $w_{Pd,H2O}$ = 16 ppm, $V_{total}$ = 58.1 mL, $t_{preforming}$ = 10 min, semibatch conditions.

The corresponding HRTEM images of the larger GSH-coated palladium nanoparticles (5 nm) (entry 2.2) are shown in Figure 21. They had formed loose aggregates of approximately 30 nm in diameter, consisting of the original particles. In contrast, the nanocubes showed a pronounced aggregation but retained their original shape and size. Very similar results were obtained for PVP-stabilized nanoparticles (see Figure S 4).

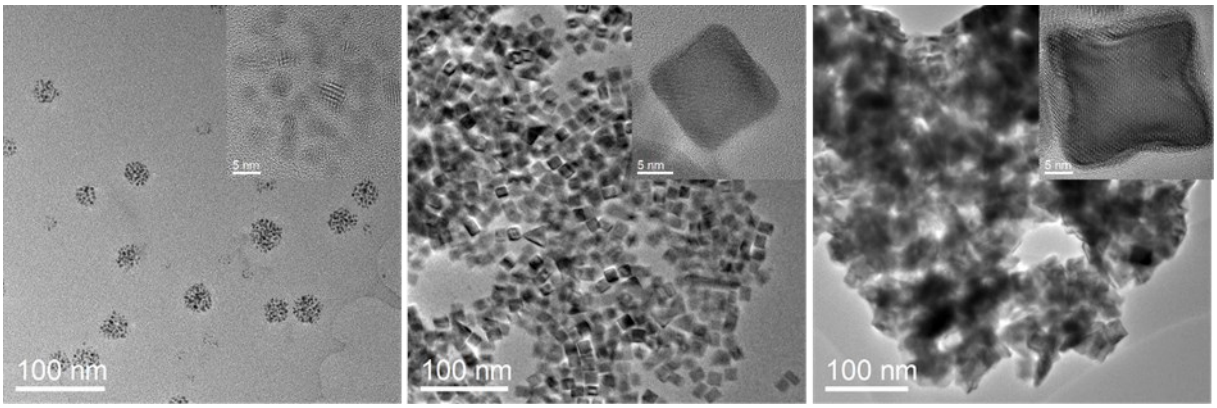


Figure 21: Overview and magnified HRTEM images of larger GSH-coated spherical palladium nanoparticles (5 nm) (**left**), smaller palladium nanocubes (18 nm) (**center**), and larger palladium nanocubes (28 nm) (**right**) after hydrogenation of **1** at 50 bar hydrogen pressure. Conditions: $n_{substrate}$ = 50 mmol, $p_{H2}$ = 50 bar, $f_{stirrer}$ = 1500 rpm, $c_{Pd}$ = 0.016 mol%, $T_{start}$ = RT, $w_{Pd,H2O}$ = 16 ppm, $V_{total}$ = 58.1 ml, $t_{preforming}$ = 10 min, semibatch conditions.

A benchmark hydrogenation experiment of **1** with a Lindlar catalyst at the same pressure, catalyst concentration, and initial temperature gave 83% selectivity after a reaction time of 33 min (Figure S 6), i.e., an intermediate reaction rate with a selectivity comparable to the nanoparticles. Thus, the nanoparticles are a lead-free alternative to the Lindlar catalyst.

### 4.4.3 Hydrogenation of 1-Octyne (Biphasic)

Next, a biphasic hydrogenation reaction was tested (Figure 22). 1-Octyne **2** was used as water-immiscible substrate. In such a biphasic system, the initially water-dispersed particles may agglomerate and deposit on the walls of the reactor or on the phase interface. Furthermore, they may also leach from the aqueous phase into the product phase (Figure 23). Table 3 gives the results of the biphasic hydrogenation catalysis.

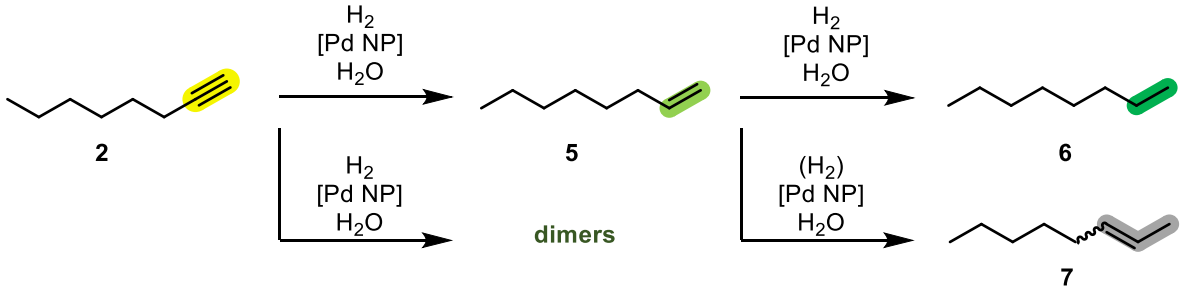


Figure 22: Reaction pathway of the biphasic hydrogenation of 1-octyne **2**, catalyzed by palladium nanoparticles.

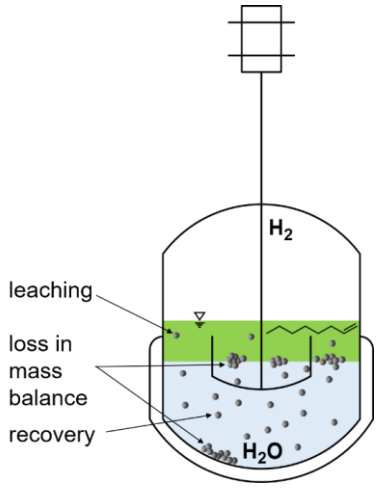


Figure 23: Possible processes that may occur with palladium nanoparticles in a biphasic oil-water system during catalysis.

Table 3: Results of hydrogenation reactions of **2** (biphasic). Conditions: $n_{substrate}$ = 50 mmol, $p_{H2}$ = 50 bar, $f_{stirrer}$ = 1500 rpm, $c_{Pd}$ = 0.016 mol%, $T_{start}$ = RT, $w_{Pd,H2O}$ = 16 ppm, $V_{total}$ = 60.6 mL, $t_{preforming}$ = 10 min, semibatch.

| Entry | Coating | Shape | $d_{core/edge\ length,\ before}$ / nm | $d_{core/edge\ length,\ after}$ / nm | $S^a$ / % | $t_{T,max}$ / s | *TOF* / $h^{-1}$ | Pd leaching / % | Pd mass balance / % |
|---|---|---|---|---|---|---|---|---|---|
| **3.1** | GSH | Spheres (2 nm) | 1.5 ± 0.4 | 1.6 ± 0.3 | 77 | 6,800-8,925 | 1,000[b] | 2 | +2 |
| **3.2** | GSH | Spheres (5 nm) | 4.4 ± 0.7 | 4.0 ± 0.5 | 51 | 594-781 | 21,000 | 54 | -40 |
| **3.3** | GSH | Cubes (18 nm) | 18 ± 2 | 16 ± 2 | 83 | 1,283-1,396 | 12,000 | 1 | -86 |
| **3.4** | GSH | Cubes (28 nm) | 28 ± 2 | 25 ± 2 | 88 | 1,171-1,465 | 16,600 | 1 | -80 |
| **3.5** | PVP | Spheres (5 nm) | 4.4 ± 0.7 | 3.2 ± 0.3 | 80 | 460-490 | 38,000 | 7 | -87 |
| **3.6** | PVP | Cubes (18 nm) | 18 ± 2 | 13 ± 2 | 77 | 1,484-1,780 | 13,000 | 3 | -66 |
| **3.7** | PVP | Cubes (28 nm) | 28 ± 2 | 20 ± 3 | 83 | 1,485-1,929 | 11,000 | 3 | -85 |

[a] at full conversion; [b] induction period within regression time frame leading to imprecise linearization

In the biphasic hydrogenation, the ultrasmall nanoparticles showed a significantly slower reaction rate compared to the monophasic system (entry 3.1), requiring approximately 2.5 h for completion. Again, all other particles had a higher activity than the ultrasmall nanoparticles. The 5 nm nanoparticles gave the highest reaction rate (entries 3.2 and 3.5). However, this was accompanied by an increased rate of isomerization in the case of the GSH-coated particles, resulting in a decrease in selectivity to 51% (entry 3.2). All cubic particles (entries 3.3, 3.4, 3.6, and 3.7) had a similar reaction rate, possibly due to additional mass transport limitations during the biphasic reaction. In the same line, the 5 nm particles had a significantly lower reaction rate compared to the monophasic hydrogenation of **1,** suggesting mass transport limitation.

The loss of palladium was considerable for all particles except for the ultrasmall nanoparticles. The particles showed a pronounced accumulation of palladium at the phase interface, independent of their

surface coating. Strong brown deposits were visually observed on the interface and also on the reactor surface.

The ultrasmall nanoparticles could not be recovered. The 5 nm GSH-coated nanoparticles (entry 3.2) were almost unchanged after hydrogenation in the two-phase system. The GSH-coated nanocubes (entries 3.3 and 3.4) were aggregated but mostly unchanged in size and shape (Figure 24). Similar results were obtained for PVP-coated particles (Figure S 5).

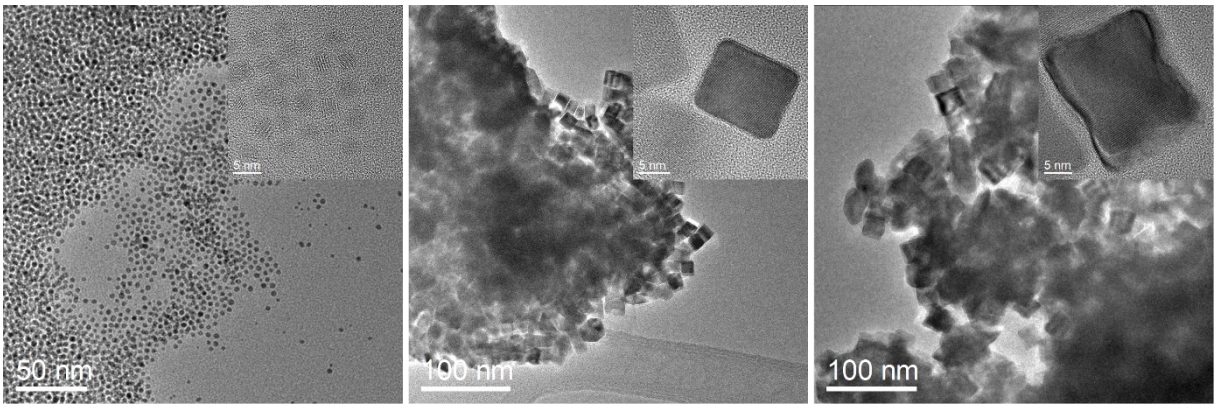


Figure 24: Overview and magnified HRTEM images of larger GSH-coated spherical palladium nanoparticles (5 nm) (**left**), smaller palladium nanocubes (18 nm) (**center**), and larger nanocubes (28 nm) (**right**) after biphasic hydrogenation of **2** with 50 bar hydrogen. Conditions: $n_{substrate}$ = 50 mmol, $p_{H2}$ = 50 bar, $f_{stirrer}$ = 1500 rpm, $c_{Pd}$ = 0.016 mol%, $T_{start}$ = RT, $w_{Pd,H2O}$ = 16 ppm, $V_{total}$ = 60.6 mL, $t_{preforming}$ = 10 min, semibatch conditions.

Figure 25 depicts the relative reaction rates for both substrates and all types of palladium nanoparticles. In all cases, the 5 nm nanoparticles were the most efficient (shortest reaction time) and the 2 nm ultrasmall nanoparticles the least efficient (longest reaction time). The nanocubes gave intermediate reaction rates. For a possible explanation, we have computed the specific surface area of all catalysts samples used and also the number of accessible palladium atoms on the particle surface (Table 4). In relative terms and normalized to the catalyst mass, the palladium atoms on the particle surface are of the ratio 21:10:1.5:1 for spheres (2 nm):spheres (5 nm):cubes (18 nm):cubes (28 nm). This clearly illustrates that the catalytic efficiency is not proportional to the number of palladium atoms on the particle surface.

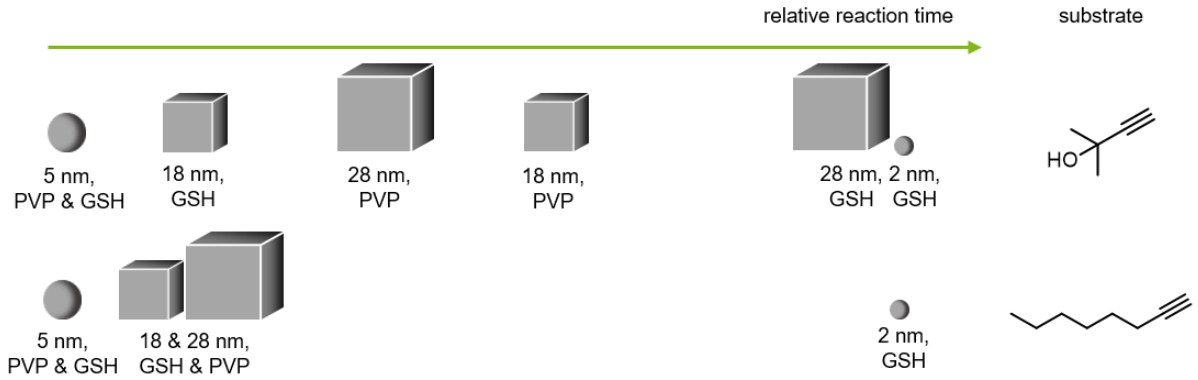


Figure 25: Comparison of the relative reaction times for monophasic (**top row**) and biphasic reactions (**bottom row**).

Table 4: Properties of all nanoparticle catalysts, based on geometrical considerations.

| Particle shape | Mass of one particle / g | Surface area of one particle / $m^2$ | Specific surface area of catalyst / $m^2\ g^{-1}$ | Number of particles in 1 g catalyst | Number of palladium atoms in one particle[c] | Number of palladium atoms on the surface of one particle[d] | Number of palladium atoms on the surface in 1 g catalyst |
|---|---|---|---|---|---|---|---|
| **Spheres (2 nm)[a]** | $4.77 \cdot 10^{-20}$ | $1.26 \cdot 10^{-17}$ | 264 | $2.10 \cdot 10^{19}$ | 270 | 170 | $3.54 \cdot 10^{21}$ |
| **Spheres (5 nm)[a]** | $7.45 \cdot 10^{-19}$ | $7.85 \cdot 10^{-17}$ | 105 | $1.34 \cdot 10^{18}$ | 4,200 | 1,260 | $1.69 \cdot 10^{21}$ |
| **Cubes (18 nm)[b]** | $6.64 \cdot 10^{-17}$ | $1.94 \cdot 10^{-15}$ | 29 | $1.51 \cdot 10^{16}$ | 375,000 | 17,300 | $2.60 \cdot 10^{20}$ |
| **Cubes (28 nm)[b]** | $2.50 \cdot 10^{-16}$ | $4.70 \cdot 10^{-15}$ | 19 | $4.00 \cdot 10^{15}$ | 1,413,000 | 42,000 | $1.68 \cdot 10^{20}$ |

[a] The particles were assumed to be perfect spheres with the given diameter.

[b] The particles were assumed to be perfect cubes with the given edge length.

[c] To compute the number of palladium atoms in one particle, the particle volume was divided by the volume of one palladium atom (0.0115 $nm^3$) and assuming a packing density (fcc) of 74%.

[d] To compute the number of palladium atoms on the surface of spherical particles, a surface layer of 0.28 nm thickness (diameter of one palladium atom) was assumed. The number of palladium atoms in this layer was approximated by dividing it by the volume of one palladium atom and assuming a packing density (fcc) of 74%.

As the catalytic efficiency is not simply proportional to the specific surface area, other effects must be responsible. A possible explanation is that ultrasmall nanoparticles have a very rugged surface and therefore lack distinct crystallographically defined faces and therefore give lower reaction rates.[56],[57] Furthermore, the lower reaction rates observed for the investigated nanocubes agree with simulations conducted by Crespo-Quesada et al. for nanoparticles of different size.[56] The surface coverage with the capping ligands (GSH and PVP) and the surface dynamics (desorption and re-adsorption) certainly have a major effect on the catalytic efficiency, like the turnover frequencies (TOF). Unfortunately, these data are not available for the initial particles. It can be underscored that all particles were thoroughly washed and purified by centrifugation, therefore, we can safely assume that the ligands are well attached to the nanoparticle surface before catalysis. However, it is not known what is happening with the ligand shell under catalytic conditions, e.g. in different solvents, at elevated temperature, and elevated hydrogen pressure. The fact that some particles were strongly agglomerated after the catalysis suggests that the ligand shell could be influenced. Unfortunately, there are no analytical methods available that can address this question in a quantitative way.

For transition-metal catalysts such as palladium, there is a strong ecological and economic incentive for facile separation, ideally in their active form, so that the catalysts can be reused after recovery. Biphasic systems have proven to be a useful concept for molecular catalysts, therefore, we aimed to transfer this concept to the present catalyst system. However, when introducing a second phase, distribution phenomena inevitably occur, since a certain degree of cross-solubility must be expected, even if small.

The nonpolar nature of the substrate leads, upon coordination to the active surface, to a competition with the ligands that otherwise stabilize the particles in water. As the substrate itself is nonpolar, the particles exhibit an increased tendency to disperse in nonpolar media, which results in a destabilization of the aqueous suspension. This effect is further enhanced by the intense stirring required to ensure sufficient mass transfer for high catalytic activity, which additionally enlarges the interfacial area. Our experimental results support this interpretation: Spherical 5 nm particles displayed higher activity, i.e., a more effective substrate coordination and increased turnover, but consequently also a stronger destabilization. In contrast, 2 nm particles showed a lower affinity of the substrate to the surface, resulting in reduced activity but at the same time improved stability. In purely aqueous systems, where the substrate is an alcohol and thus water-soluble, these destabilizing effects are far less pronounced, resulting in a more stable catalytic system overall.

## 4.5 Conclusions

Palladium nanoparticles of various sizes and shapes in water, stabilized by either PVP or GSH, are active in the monophasic and biphasic semihydrogenation of alkynes. For biphasic alkyne semihydrogenation, this is the first report of a application of palladium nanoparticles. The ultrasmall nanoparticles had a low efficiency both at 1 and 50 bar hydrogen pressure. The nanoparticles were analyzed before and after the catalytic reaction by electron microscopy to assess possible structural changes. The internal crystallinity of the ultrasmall nanoparticles increased due to reduction by hydrogen but the particles did not agglomerate. In contrast, all larger particles showed a significant aggregation after catalysis but did not significantly change their size and shape.

The semihydrogenation was fast for most particles and never took longer than about 2.5 h to completion. Regarding reaction rates, several trends emerged for both monophasic and biphasic reaction conditions: The ultrasmall particles were always the least efficient with turnover frequencies of 1000 - 4,000 $h^{-1}$, while the 5 nm particles were consistently the most efficient, reaching remarkably high TOFs of up to 183,000 $h^{-1}$. In biphasic catalysis, mass transport limitations led to similar reaction rates for all larger particles with TOFs around 12,000 $h^{-1}$. The selectivity was comparable in most cases with about 80%. There was no significant effect of the coating agent (GSH or PVP) on either selectivity or activity in hydrogenation catalysis, indicating that the surface of the palladium nanoparticles is easily accessible in all cases for the substrates.

In monophasic catalysis, most of the palladium could be recovered. In contrast, in biphasic catalysis, a significant palladium loss was found except for the ultrasmall nanoparticles which were fully recovered. In conclusion, nanoparticles with diameter of 5 nm turned out to be most efficient in hydrogenation catalysis. However, the chosen biphasic approach is not suitable for the present catalyst system. Instead, future work should focus on carrying out the reaction in a monophasic aqueous medium (potentially with co-solvents), followed by a downstream separation step such as liquid–liquid extraction.

## 4.6 Acknowledgments

The authors thank the networking program “Sustainable Chemical Synthesis 2.0” (SusChemSys 2.0) for support and fruitful discussions across disciplines. The authors also thank I. Henkel, M. Schwandt and J. Ufer for ICP-OES measurements. N.K. thanks the Konrad-Adenauer-Stiftung for a Ph.D. scholarship.

Open access funding enabled and organized by Projekt DEAL.

# 5 Solvent and Metal Selection for FAME Hydrogenation with Laser-Ablated Nanoparticles

**Author contributions:** The concept and ideas for this project were provided by me. PLAL was performed together with T. Fromme; TEM images were taken by R. Jerusalem and J. Jakobi. T. Ahlers, F. Bajro, L. Nebel, and I. Heintz contributed some of the hydrogenation experiments as parts of their bachelor's or master's theses or internships under my supervision. Further experiments, overall analyses, visualization, and writing were performed by me. T. Seidensticker acquired funding and supervised this project.

## 5.1 Introduction

The previous chapter shows promising results for hydrogenation reactions with spherical, small (but not ultra-small), and very uniform Pd nanoparticles of ca. 5 nm, while the bigger and ultra-small ones exhibit lower reactivity. To avoid the elaborative synthesis strategy applied there, the intensification of NP synthesis using laser ablation and fragmentation is applied in the following. A broad range of solvents and metals can, in theory, be applied for this process. Thus, a selection must be made, which is done in the following sections. After synthesis and characterization of the particles, selective partial FAME hydrogenation (Scheme 9) will be applied as a model reaction. Afterwards, influences of reaction conditions on the reaction performance in the chosen hydrogenation reaction will be investigated, also in comparison with similar catalyst systems. Finally, structure-specific relationships for several similar substrates are used to shed some light on the underlying possible catalysis mechanism.

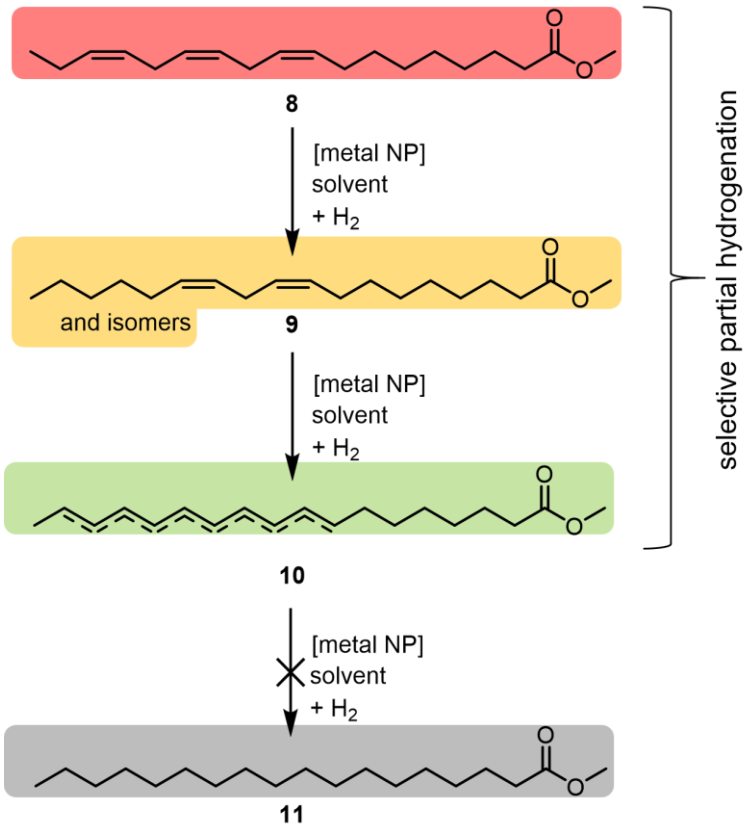


Scheme 9: Reaction scheme of the intended selective partial FAME hydrogenation with laser-ablated NPs in an appropriate solvent.

## 5.2 Experimental

All laser-ablated catalyst solutions were obtained by PLAL with subsequent laser fragmentation using Nd:YAG lasers (IS400-1-L, Edgewave or RSM 100D, ROFIN-SINAR) at a power output of 50 W resp. 27 W, wavelengths of 532 nm resp. 1064 nm, and a repetition rate of 5 kHz according to otherwise known methods[169],[170]. A schematic setup can be found in Figure 26. The collection of the product colloid in the substrate container during operation enables further irradiation cycles and thus laser fragmentation of the freshly produced particles.

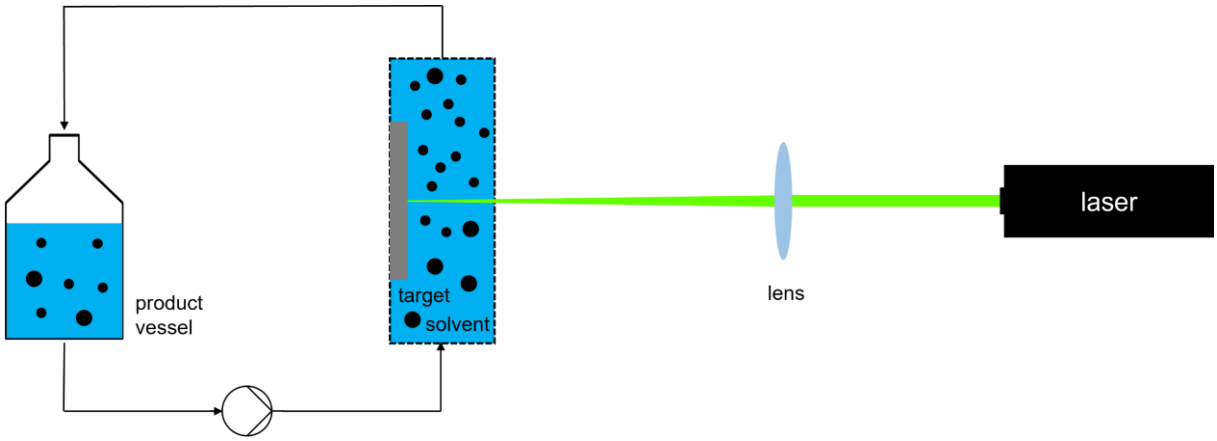


Figure 26: Schematic setup for PLAL as used in this chapter.

Particle analysis for particle size distributions of laser-ablated particles was performed with the software Fiji and the ParticleSizer plugin. All solutions were measured using ICP-OES for their Pd contents (in ppm, w/w) prior to first use as described in chapter 4.3. The only exception was made for glycerol due to safety concerns during sample preparation. Here, glycerol was removed in high vacuum at elevated temperatures, and the digestion with $HNO_3$ was subsequently performed in reflux at 90 °C for 30 minutes in the bottom flask from evaporation.

Pd in PC was also prepared according to the autoreductive method by Lux and Behr[22]: $Pd(OAc)_2$ was dissolved in PC and stirred under reflux at 80 °C for 2 h. The resulting particles are known to exhibit sizes in the range of 5-12 nm[22]. Furthermore, Pd in PC and DMF was prepared reductively based on the method by Lux and Behr[22]: $Pd(OAc)_2$ was dissolved in 100 ml of the solvent to give stock solutions of 34 ppm Pd content. The reaction was carried out for 2.5 h at 80 °C and 10 bar hydrogen in the glass reactors to a similar workflow as described below.

All hydrogenation experiments were performed in 120 mL stainless steel or 250 mL glass reactors with mostly gas impeller stirrers, substrate containers, and a hydrogen dosing system. The vessels were at most half-filled to ensure sufficient mixing behavior. In the metal screening and in selected further experiments on mixing behaviors, additional baffles were inserted into the stainless steel reactors. For all high-boiling solvents, the catalyst solution was introduced into the reactor, and the reactor was sealed afterwards. The whole system was then inertized via an alternation of argon supply (ca. 10 bar) and vacuum degassing for at least three cycles. The stainless steel reactors also allowed for the introduction of the catalyst solution via syringe in argon counterflow after inertization. As an exception, the catalyst solution with 1-butanol was added through the substrate container after inertization in argon counterflow. Then, the substrate was added to the substrate container using a syringe. Afterwards, the system was pressurized, stirring was initiated, and heating started for the preformation of the catalyst. The 120 mL reactor also allowed preheating of the substrate. For the glass reactors, preheated substrate was introduced shortly before reaction start in order to enable a high uniformity of the temperature of the whole (biphasic) reaction system. After reaching the constant reaction temperature, the pressure

equalization valve was opened. After pressure equalization, the substrate was added to start the reaction. Hydrogen was constantly fed by a mass flow controller so that the pressure remained constant throughout the reaction. Blind activities of the reactors were ruled out for most of the substrates under relevant conditions. FAME samples were withdrawn and quenched in pre-cooled Falcon tubes and degassed with bubbled-through argon or helium to strip soluble hydrogen. Biphasic samples were subsequently centrifuged for 3 minutes at 1,000 $min^{-1}$. All other samples were collected in l-$N_2$ freezed glassware. All collected product phases were diluted and measured on GC-FIDs. Catalyst solutions were not measured since the solubility of the products was found to be negligible. Turnover frequencies were calculated at 20% targeted hydrogen conversion ($TOF_{20,H2}$). Further details on sample analyses can be found in chapter 11.2.2. For comparison with literature, available data were used to calculate conversion, selectivity, and the trans/cis ratio in the same way as for own data.

$k_la$ values and hydrogen solubilities were measured by pressure loss due to hydrogen absorption in the liquid according to the method described by Dietrich et al.[129]. Therefore, the 120 mL reactors at room temperature were used with mixtures of the same composition as the corresponding reaction mixtures, just without Pd.

## 5.3 Results and Discussion

### 5.3.1 Solvents for Laser-Ablated Nanoparticles

In literature-investigations on Pd NPs synthesized by reductive methods, a broad solvent screening was performed. There, the solvents with the longest NP shelf life were methyl-isobutylketone, DMF and especially five-membered cyclic molecules with N or O heteroatoms, such as PC, N-methyl pyrrolidone, or THF. Other polar solvents also exhibited good stabilization, while very short-chain alcohols and apolar hydrocarbons were less suitable.[22],[36] In order to use „green“ solvents in this work, PC and the even more polar derivative glycerol carbonate were chosen from the group of five-membered heterocycles[171]. Although several short-chain alcohols were proven by Lux to be unsuitable at least at 100 ppm metal loading, the diol ethylene glycol, the straight-chain 1-butanol, and the highly polar glycerol were not tested in previous work and thus will be evaluated here[22],[36],[172].

PLAL of Pd in the mentioned solvents with subsequent laser fragmentation was performed according to the described procedure. The resulting colloids were examined by TEM; the obtained $q_0$ particle size distributions are shown in Figure 27. The resulting mean diameters are summarized in Table 5.

Table 5: Mean particle sizes for laser-ablated Pd in various solvents, determined by TEM.

| solvent | $d_{Feret}$ [nm] | annotations |
|---|---|---|
| **propylene carbonate** | 3.6 ± 2.0 | - |
| **glycerol carbonate** | 4.9 ± 1.9 | - |
| **1-butanol** | 3.8 ± 1.6 | Few and small agglomerates |
| **ethylene glycol** | 6.4 ± 3.9 | Many small agglomerates |
| **glycerol** | 7.6 ± 3.8 | Many aggregates in a loose structure |

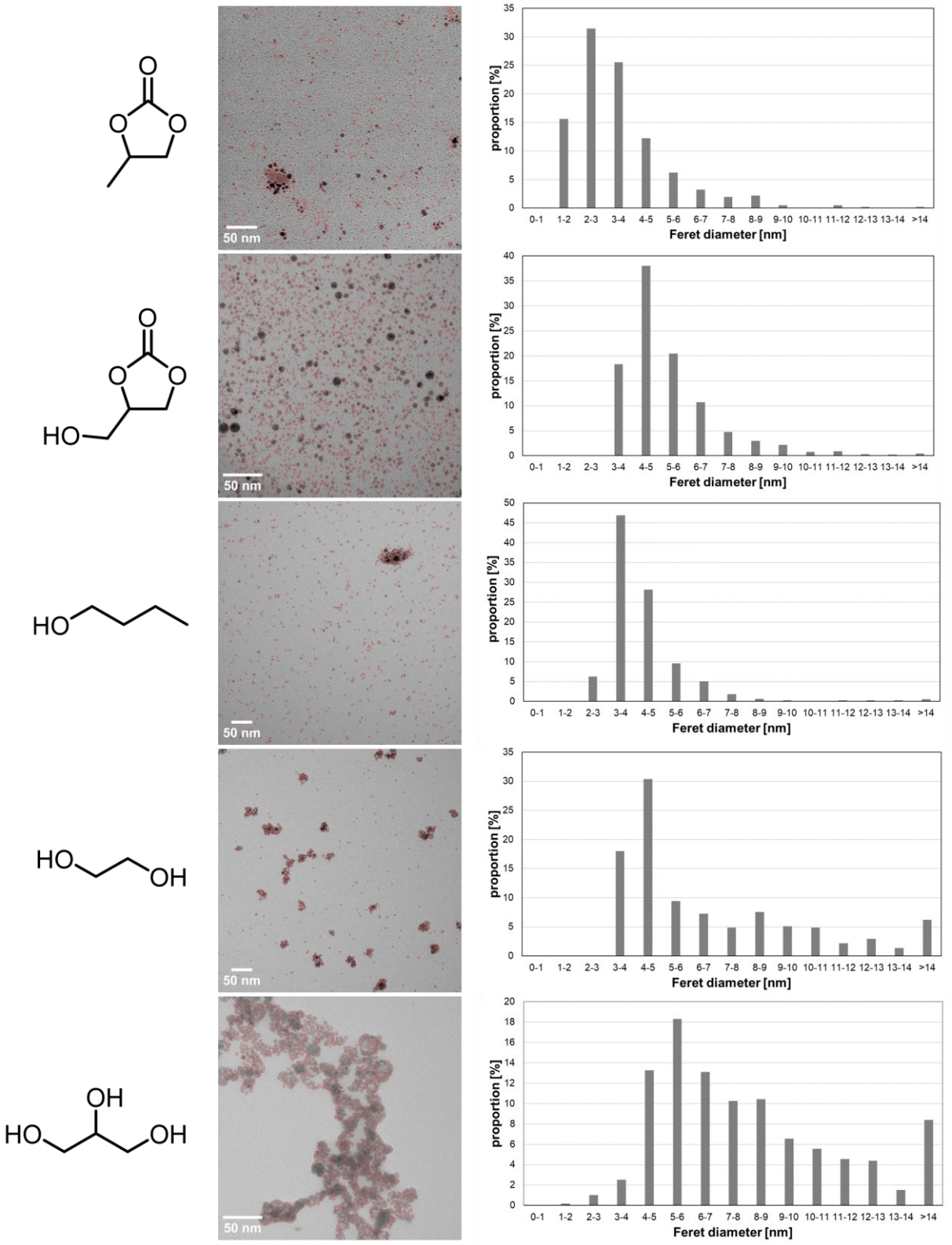


Figure 27: TEM images of the solvent-stabilized Pd colloids produced by PLAL in propylene carbonate, glycerol carbonate, 1-butanol, ethylene glycol, and glycerol. Counted particles are outlined in red.

The obtained particle size distributions tend to overestimate the mean particle size, as primarily the right half of a Gaussian-like curve is detected, while particles less than ca. 2 nm are only barely detectable by the software due to low contrast with the background. As can be seen from Figure 27, 1-butanol contains a small amount of agglomerates, but the image recognition can still determine the sizes of most of its single particles. Rather loosely bound agglomerates are also detectable for ethylene glycol. Even though single particles of some agglomerates or aggregates are sometimes not detected and the whole assembly is counted instead, monomodal particle size distributions in a size range around 5 nm are obtained for all particles as expected, except for glycerol: here, all particles form larger aggregates of irregular shapes that are rather loosely bound itself, but individual primary particles are only hardly distinguishable. Thus, the particle size distribution of glycerol is strongly broadened towards bigger particles.

During the ablation process, glycerol and glycerol carbonate had to be heated to lower the viscosity, and foam was detected. Hence, they are not preferred solvents for PLAL in terms of handling, and for glycerol also in terms of the resulting particles.

However, the obtained particles with average size ranges of 4-8 nm are expectedly highly active and selective in hydrogenations, as can be extrapolated from aqueous Pd NPs used for selective partial alkyne hydrogenations [56]. To investigate this, hydrogenation of FAME as a less reactive substrate instead of alkynes was carried out afterwards. The results are shown in Figure 28 and indicate the highest activity of NPs in the organic carbonates PC and glycerol carbonate. Selectivity in glycerol carbonate is high and counts 90%, but is less than the excellent selectivity of 96% for PC. All alcohols perform poorly, necessitating strongly prolonged reaction times of 20-22 h (as derived from the evolution of the total hydrogen uptake). At the same time, most of them show pronounced overhydrogenation at incomplete conversion of polyunsaturated species. This results in selectivities of 88-90% for the alcohols. Therefore, the only reasonable solvents in terms of activity and selectivity are PC and glycerol carbonate, followed by 1-butanol.

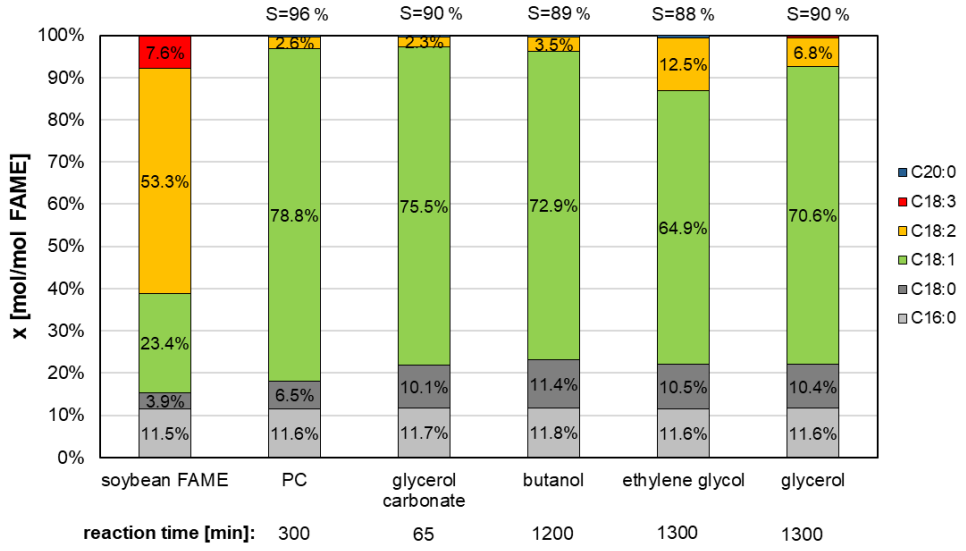


Figure 28: Composition of samples of the selective partial hydrogenation of soybean FAME at 10 bar with laser-ablated Pd in various solvents. Reaction conditions: S:C= 100,000:1, T= 50 °C, $f_{stirrer}$ = 3,400 rpm, $p_{H2}$= 10 bar, $w_{Pd,solvent}$= 5 ppm, t as stated, $V_{total}$= 100 mL, semibatch. Glycerol was diluted with deionized water to reach the desired Pd concentration for viscosity reasons.

Under the chosen conditions (including 5 ppm Pd within the solvent), the use of PC and glycerol carbonate leads to the formation of a biphasic system, with the product forming the upper phase. In these cases, the Pd leaching into the product phase was determined as 1 ppm or below for PC and glycerol carbonate, thus being at the limit of quantification. FAME with 1-butanol forms a monophasic system, whereas ethylene glycol and glycerol form emulsions that do not allow precise statements regarding Pd leaching.

The particle size distributions cannot be the reason for these drastic differences in activity and selectivity, since all average diameters are very similar. Although aggregates and agglomerates are visible in the TEM images (Figure 27), for the alcohols, the activity should be in a different order, with the particles in glycerol being the worst catalyst. Apparently, this is not the case. Hydrogen solubilities in the solvent (at 1 bar and 25 °C, see Table 6) can also not explain the different reaction rates, since the glycerol/water mixture has the highest hydrogen solubility, followed by PC.

Table 6: Hydrogen solubilities in the investigated solvent (mixtures) at 1 bar and 25 °C, mostly calculated from solubility constants like the Henry coefficient and their errors.

| solvent | $c_{H2,solvent}$ [mol m$^{-3}$] |
|---|---|
| **propylene carbonate**[173],[174] | 14.1 ± 1.7; 16.6 |
| **glycerol carbonate**[a] | <14.1 |
| **1-butanol**[175] | 3.0 ± 0.06 |
| **ethylene glycol**[175] | 0.7 ± 0.014 |
| **glycerol+water**[173] | 20.8 ± 0.06 |

a: not literature-known and from conducted experiments only uncertainly determinable, but in comparison less than for PC

Furthermore, $k_la$ values at room temperature were measured for each system (apart from 1-butanol, where the method was surprisingly not applicable despite repeated attempts) at the same composition as for hydrogenation. However, all $k_la$ values were very similar (see Table 7), and no clear trend was observable either.

Table 7: Determined $k_la$ values at room temperature for genuine reaction compositions from Figure 28 with volumes of 55 mL in the stainless steel autoclaves according to the method of Dietrich et al.[129] for one set of measurements.

| solvent | $k_la$ [$s^{-1}$] |
|---|---|
| **propylene carbonate** | 0.516 |
| **glycerol carbonate** | 0.319 |
| **1-butanol** | -[a] |
| **ethylene glycol** | 0.304 |
| **glycerol+water** | 0.280 |

a: Linearization of measured data and thus the whole method not applicable

While the number and exact structure of defect sites and carbonaceous species may be solvent dependent[41],[170] due to individual physico-chemical properties that affect the formation of the plasma plume during ablation, this cannot be elucidated from the given TEM images and requires a substantially higher resolution. The last and most probable option is different adsorption strengths of solvents and hydrogen and their competition with the adsorption of the substrates. Similar effects were already observed for the hydrogenation of MBY on Pd surfaces, where MeOH and EtOH competed with hydrogen for adsorption sites[58]. Thus, for other small alcohols such as those used in this investigation, this mechanism also appears to be very likely. Further work on the elucidation of different adsorption behaviors would require the measurement of adsorption enthalpies and the number of adsorption sites. However, the necessary presence of solvents complicates or even excludes typical measurements like the Brunauer-Emmett-Teller method.

As a conclusion, PC and glycerol carbonate remain the solvent of choice to produce catalytically highly active NPs by laser-ablation. However, the lower selectivity with glycerol carbonate compared to PC at a different C18:2 residue demands further analysis that will be performed in chapter 5.3.3.1, which also includes a comparison of results originating from different synthesis routes. Since the availability of glycerol carbonate is lower than for PC, PC will be used in the following to investigate the most suitable metal for highly active hydrogenation catalysts of this type.

### 5.3.2 Metals for Laser-Ablated Nanoparticles

A metal screening is intended to identify the optimal catalyst metal for the given task of selective partial FAME hydrogenation. From the typically investigated metals for selective partial FAME hydrogenation (Pd, Rh, Pt, Ir, Ru, and Ni) introduced in chapter 2.2.1.2, Pd, Ir, and Pt were chosen for this task, since they are the most active ones, together with Rh, which is difficult to purchase in pure form as ablation target. Furthermore, silica-supported Cu was shown to give extraordinary selectivities in selective partial FAME hydrogenation[176],[177]. Therefore, colloidal Cu NPs were also included in the metal screening. TEM images were taken from exemplary samples, and corresponding $q_0$ particle size distributions were obtained, see Figure 29 and Table 8.

Table 8: Mean particle diameters of various laser-ablated metals in PC, determined by TEM.

| metal | $d_{Feret}$ [nm] | Annotations |
|---|---|---|
| **Pd** | 3.6 ± 2.0 | - |
| **Pt** | 4.8 ± 3.0 | bad image qualities |
| **Ir** | 3.2 ± 1.2 | - |
| **Cu** | 2.9 ± 1.1 | low contrast |

While PLAL of Pd, Ir, and Cu in PC yielded well-dispersed NPs with narrow particle size distributions and similar mean particle sizes, Pt in PC forms partially dense aggregates, where single particles cannot be distinguished anymore. In combination with the facts that the image quality of these particles is low and that only a few particles are detectable, the broadened particle size distribution with a second mode around 10 nm can be explained. Nevertheless, all nanoparticles exhibit a reasonable size range and are thus used for catalytic experiments in the selective partial hydrogenation of FAME.

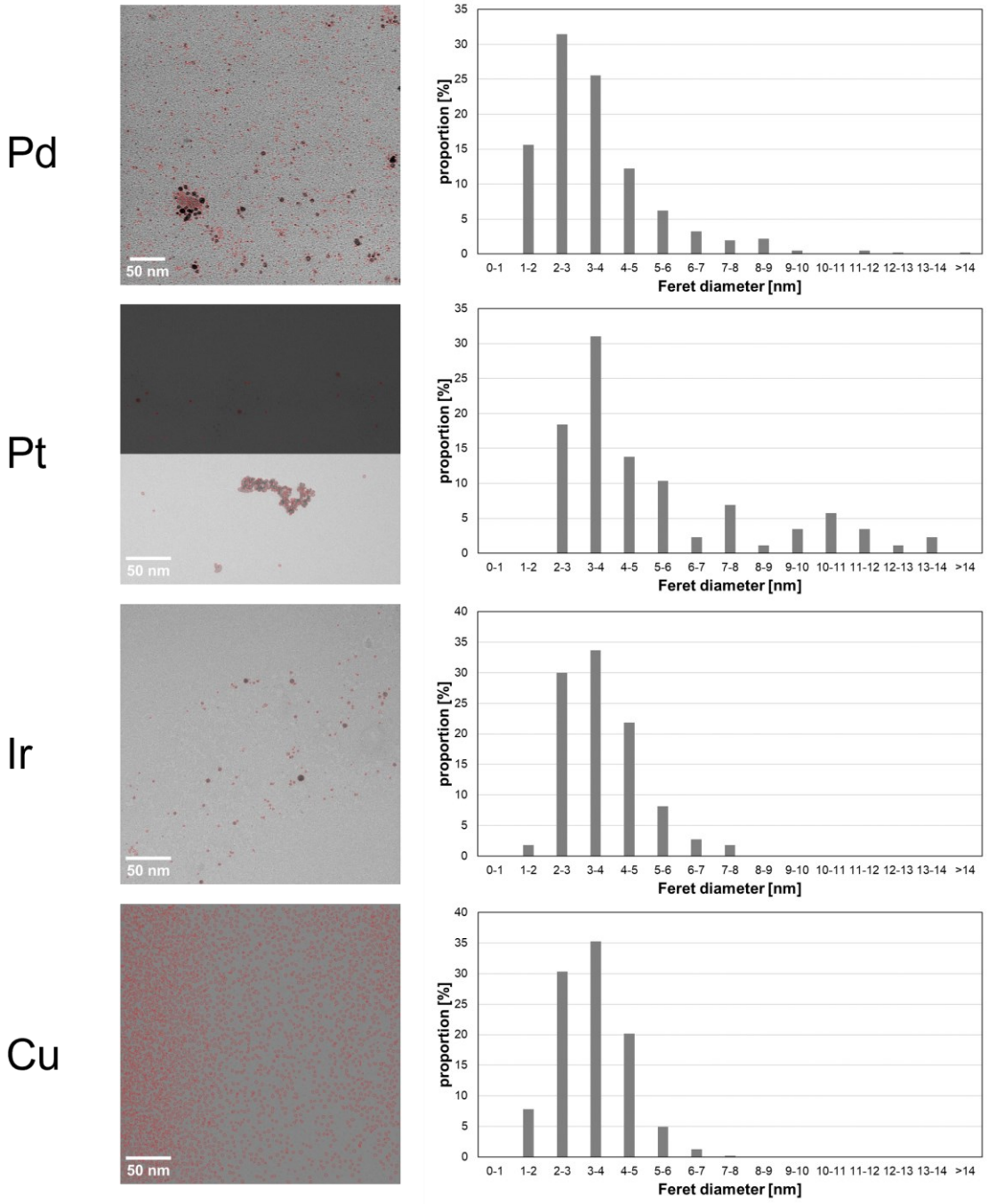


Figure 29: TEM images of the solvent-stabilized colloids produced by PLAL of various metals in PC. Counted particles are outlined in red.

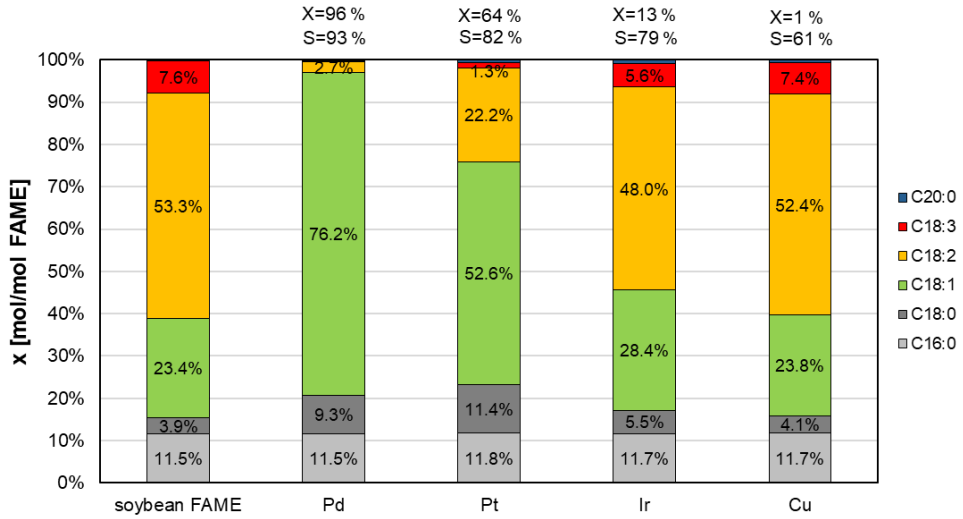


Figure 30: Composition of samples of the selective partial hydrogenation of soybean FAME at 10 bar with laser-ablated Pd in various solvents. General reaction conditions: $f_{stirrer}$ = 3,500 rpm, t= 180 min, $V_{total}$= 55 mL, semibatch
Pd: S:C= 100,000:1, T= 50 °C, $p_{H2}$= 50 bar, $w_{Pd,PC}$= 12 ppm,
Pt: S:C= 5,000:1, T= 190 °C, $p_{H2}$= 51 bar, $w_{Pt,PC}$= 82 ppm, reactor equipped with baffles
Ir: S:C= 5,000:1, T= 150 °C, $p_{H2}$= 51 bar, $w_{Ir,PC}$= 22 ppm, reactor equipped with baffles
Cu: S:C= 5,000:1, T= 150 °C, $p_{H2}$= 51 bar, $w_{Cu,PC}$= 57 ppm, reactor equipped with baffles.

The literature-known order of activity is also valid for the investigated transition metal NPs in PC (see Figure 30). Maximum achievable reaction conditions in the system were applied for each metal, except for Pd, due to sufficient results already at 50 °C. Pd in PC shows by far the highest activity already at mild conditions and low metal usage and exhibits the highest selectivity at the same time. Pt shows a drastically reduced activity and selectivity, leading to strong overhydrogenation at incomplete conversion. Furthermore, Pt is the only metal where intermediate conjugated species are present. Ir shows an even lower activity. The promising Cu does not show relevant catalytic activity at all, although temperature, pressure, and reaction time were chosen according to literature[176]. The acidity of the support was found in literature to be a crucial factor[177]. Thus, a further test with slightly acidified Cu to mimic the acid influence of the support was also carried out, but showed no reactivity either. Hence, apart from the S:C ratio – which is ca. 36 times higher for the supported Cu catalysts[176] – the presence of a suitable support may be the most crucial factor for the selective partial hydrogenation with Cu. Further experiments with laser-ablated Cu NPs that are more concentrated or subsequently supported on silica would need to be carried out to unravel the exact influence. Since supported NPs are not considered in this work, Cu was excluded from further experiments with laser-ablated NPs in PC. Moreover, all other elements apart from Pd were excluded due to worse activity and selectivity.

### 5.3.3 FAME Hydrogenation in Batch with Pd Nanoparticles

Many batch experiments on the selective partial hydrogenation of FAME with colloidal Pd nanoparticles at different reaction conditions were carried out in this work and are analyzed in the following regarding condition-dependent selectivity. Furthermore, the investigated different solvents are compared to PC, and the variation of the metals in PC is compared to Pd. Afterwards, a comparison with literature will be

presented. Finally, tests regarding structure-effect relationships were carried out to obtain first insights into the underlying catalytic mechanism.

### *5.3.3.1 X,S- and X,trans/cis-Plot*

Conversion-selectivity plots show limits that known catalysts cannot overcome and thus allow for the comparison of different catalysts for the same reaction, regardless of the applied reaction conditions and reaction time. Examples for various selective oxidations were already given by Batiot and Hodnett in 1996.[178] A similar depiction is shown in Figure 31a for batch hydrogenations with laser-ablated Pd in PC at varying reaction conditions, together with the results for the other investigated solvents glycerol carbonate, ethylene glycol, 1-butanol, and glycerol, as well as the results of the other metals in PC. Figure 31b shows the behavior of the trans/cis ratio during the corresponding reactions.

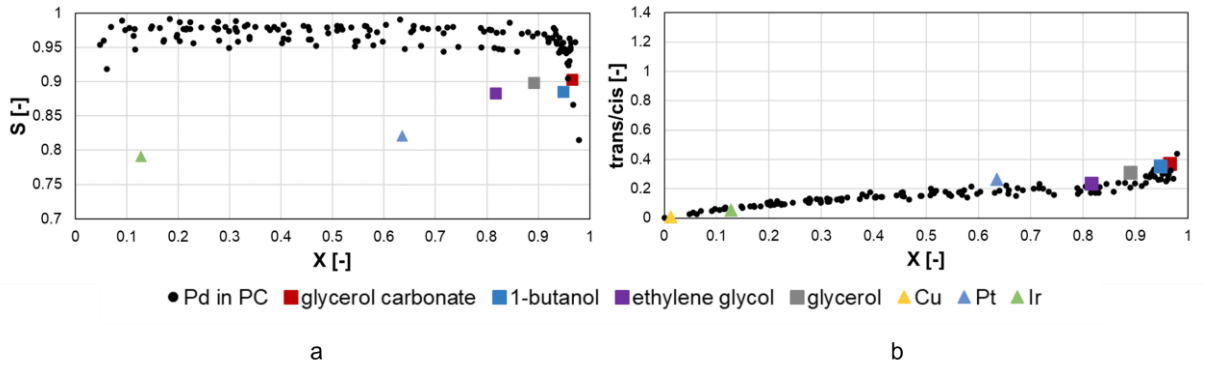


Figure 31: X,S- (a) and X,trans/cis-plot (b) for the selective partial hydrogenation of soybean-derived FAME with laser-ablated Pd in PC and the other solvents from chapter 5.3.1. Reaction conditions for Pd: S:C= 20,000:1 or 100,000:1, T= 50 or 85 °C, $f_{stirrer}$ = 600 or 2,250 or 3,400 or 3,500 rpm, $p_{H2}$= 10 or 11 or 50 or 51 bar, $w_{Pd,solvent}$= 5 or 11 or 12 or 24 ppm, $V_{total}$= 55 or 100 mL, semibatch, mostly without baffles and mostly with gas injection stirrer. For conditions of the other metals, see Figure 30.

For Pd in PC, the reaction always gives similar results in terms of selectivity, ranging above 95% until 90% conversion, except for slight fluctuations, regardless of the applied conditions. After 90% conversion, a steep decrease in selectivity is observable due to pronounced overhydrogenation. The other metals were shown in Figure 30 to give drastically lower selectivities even already at low conversion, and Figure 31 confirms that it is always below the selectivity of Pd. Pd in other solvents performs better than other metals in PC, but no trend is observable within the solvents. Instead, some of the lowered selectivities in Figure 28 (for glycerol carbonate and 1-butanol) are only the result of high conversions and thus lie on the trend for Pd in PC.

Interestingly, the trans/cis ratio is not affected by any variations in solvent, metal, or reaction conditions and always follows the same trend. Again, after 90% conversion, trans/cis begins to increase. Thus, the resulting amount of trans-configured species cannot be varied by adjusting reaction conditions in the investigated operational window and is more likely thermodynamically driven.

Accordingly, the alternative beneficial solvent glycerol carbonate is confirmed by Figure 30, which also suggests 1-butanol as suitable. Nevertheless, both solvents are excluded from further usage in selective

partial FAME hydrogenation due to the known reasons of long reaction times and single-phase operation (1-butanol) resp. worse availability (glycerol carbonate).

Comparing the behavior of Pd in PC for natural soybean-derived FAME with a different soybean-derived FAME mixture that was additionally slightly pre-hydrogenated by the manufacturer, similar trends are observable (Figure 32).

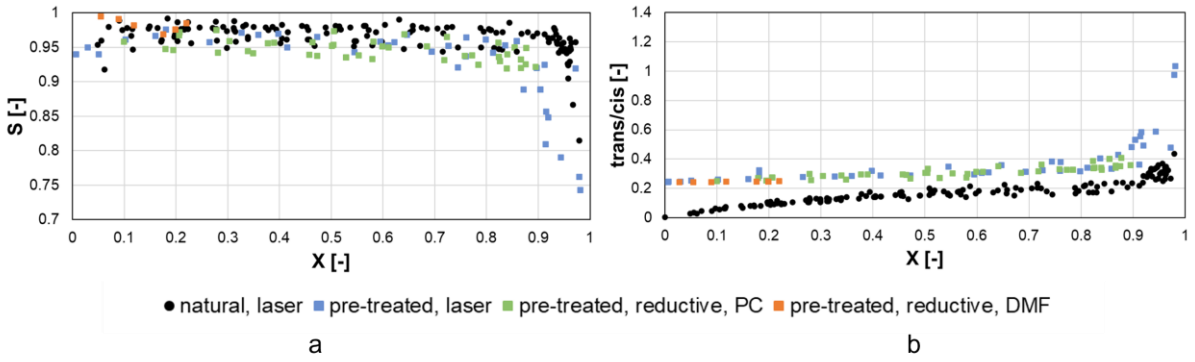


Figure 32: X,S- (a) and X,trans/cis-plot (b) for the selective partial hydrogenation of soybean-derived FAME with laser-ablated Pd in PC in comparison with different substrate mixtures and NPs produced by reductive methods. For conditions for natural soybean-derived FAME, see Figure 31. Additional reaction conditions for pre-treated soybean-derived FAME: S:C= 10,000:1 or 50,000:1 or 100,000:1 or 500,000:1, T= 50 or 65 °C, $f_{stirrer}$ = 3,400 rpm, $p_{H2}$= 10 bar, $w_{Pd,solvent}$= 11 or 28.65 or 35 ppm, $V_{total}$= 100 mL, $\varphi_{H2O}$= 0 or 2.5 or 5 or 10%, semibatch.

At first, the selectivity trends are similar, but pronounced overhydrogenation starts already from ca. 80% conversion for the pre-hydrogenated FAME mixture, although the decrease in selectivity is not as steep as for the natural soybean FAME, independent of the applied catalyst solution. This shows that laser-ablated Pd NPs in PC exhibit the same selectivity as NPs from reductive synthesis methods. Here, DMF is confirmed as an alternative solvent (which is known from works by Behr et al.[68],[69]), although only limited data points are available. These experiments reveal furthermore that water is tolerated as co-solvent, which has been applied up to 10% (V/V) here. Pre-experiments for chapter 9 confirmed the tolerance of several other polar co-solvents. Again, the trans/cis-ratio is not influenced by any change in reaction conditions, but the resulting curve is different from the one for natural soybean FAME (Figure 32b).

Comparing these findings to data calculated from literature for various other catalytic systems and substrates (Figure 33), the investigated system shows an outstanding selectivity even at high conversion, also in regard of a minimum amount of trans-configured species: Most of the literature data contains colloidal or homogeneous catalysts and shows earlier overhydrogenation and trans/cis ratios that are up to 3 times as high as for the applied natural soybean FAME with Pd NPs in PC. No clear trends in the literature data are observable. However, several positional isomers occur during hydrogenation, and their analytical identification is challenging; systematic errors can never be excluded for all data points. The only system that constantly outperforms the reaction system from this work is the already mentioned Cu on $SiO_2$, but information on the trans/cis ratios is not available[176],[179]. Instead, also in light of Figure 32, all results may strongly be influenced by the applied substrate. This may be attributable to trace impurities of other constituents in the respective FAMEs, like sulfur- or phosphorus-containing compounds, whereas the applied natural FAME mixture is with 1 ppm nearly S-free and

therefore does not poison the catalyst as much. Information on individual trace impurities is not given in the respective literature. Future work could further elucidate the influences of trace impurities on the obtainable selectivity and trans/cis ratio for the given reaction system.

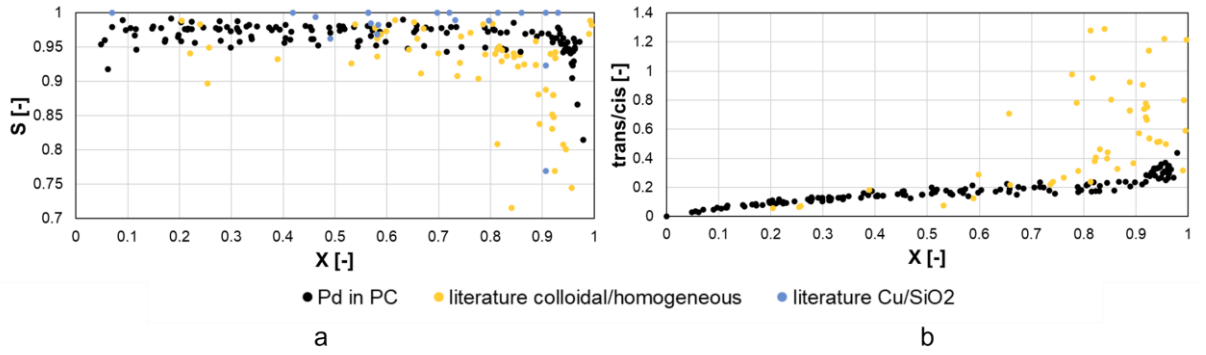


Figure 33: X,S- (a) and X,trans/cis-plot (b) for the selective partial hydrogenation of soybean-derived FAME with laser-ablated Pd in PC (black) in comparison with data calculated from literature (Cu on $SiO_2$ is coloured blue for distinction, all other literature data is yellow). For conditions for soybean-derived FAME see Figure 31. Literature data calculated from [176],[179]–[183].

### *5.3.3.2 Structure-Specific Impacts on Activity*

In order to find structure-specific impacts of the substrates on the activity of Pd NPs in PC and to gain first insights into the catalytic mechanism, several similar, but slightly different substrates were selectively hydrogenated with Pd in PC from the autoreductive approach. Applied substrates include FAMEs with varying amounts of double bonds, with and without pre-conjugation, as well as a monoterpene with conjugated double bonds (β-myrcene, **14**) that is examined in more detail in chapter 6.3.4. The resulting hydrogen consumption curves are depicted in Figure 34.

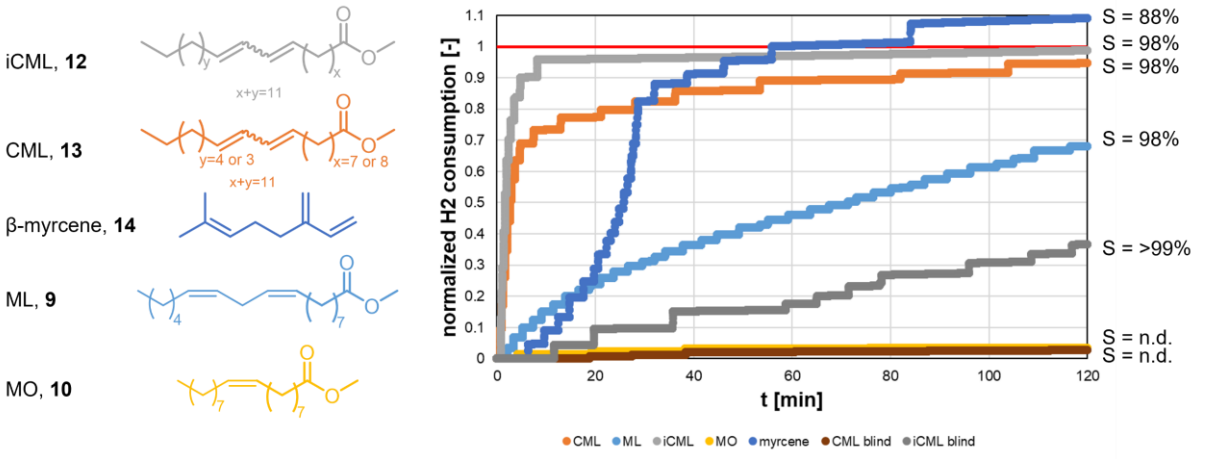


Figure 34: Normalized hydrogen uptake curves for the selective partial hydrogenation of various substrates with Pd NPs in PC from the autoreductive approach. Reaction conditions: $n_{substrate}$= 25 mmol, S:C= 10,000:1 (blind reactions are carried out with PC, but without Pd), T= 50 °C, $f_{stirrer}$ = 3,500 rpm, $p_{H2}$= 50 bar, $w_{Pd,PC}$= 12 ppm, t=120 min, $V_{total}$= 22.2-28.5 mL, semibatch. Reactions performed in the same reactor vessel. The red line corresponds to one equivalent of hydrogenated double bonds. S = n.d.: measurement error too high for precise calculation due to very low conversion.

All substrates with conjugated double bonds (**12**, **13**, **14**) show nearly full conversion within the given time frame, with only the equivalent of one double bond being hydrogenated, resulting in excellent selectivity for **12** and **13**. The position of the double bonds within the fatty acid chain influences the reactivity, since isomerized conjugated methyl linoleate (iCML, **12**) with double bonds more towards the ω-end reacts significantly faster than conjugated methyl linoleate (CML, **13**) with double bonds in middle positions, although **12** also contains ca. 25-30% double bonds that are located towards the α-end, which should accordingly react more slowly. Turnover frequencies at 20 % targeted hydrogen conversion ($TOF_{20,H2}$) are in the range of 90,000 $h^{-1}$ – 110,000 $h^{-1}$ for these substrates. Although Pd cannot fully be removed during the preparation of **12** (1.5 ppm Pd remain in **12** from the isomerisation with a Pd complex), it plays a negligible role in the hydrogenation process, as observable from the corresponding blind experiment with **12**, since the real hydrogenation is finished after less than 5% blind conversion. A similar conclusion can be made for **13**; accordingly, blind activity can be neglected for all substrates in the given time frame. Thus, the observable hydrogen uptake is always caused by the catalytic reaction with the Pd NPs in PC.

Non-conjugated methyl linoleate (ML, **9**) reacts much more slowly than systems with conjugated double bonds, but with similar selectivity of 98%. Its $TOF_{20,H2}$ is with ca. 8,500 $h^{-1}$ one order of magnitude lower than that for its conjugated isomers **12** and **13**, as expected from the literature[71]. After 2 hours, mainly C18:1 (Δ9 c) and C18:1 (Δ12 c) isomers form in a ratio of $\frac{\text{C18:1 (Δ9 c)}}{\text{C18:1 (Δ12 c)}} = \frac{55}{45}$. This confirms the observation that double bonds towards the ω-position are more readily hydrogenated. Especially, conjugated species are not visible, thus no conjugation prior to or during hydrogenation appears. In comparison, methyl oleate (MO, **10**) shows nearly no reaction, confirming literature-known reactivity differences concerning the degree of unsaturation[73].

β-Myrcene (**14**) can be converted completely within the given time frame with sufficient selectivity of 88% in this initial approach, and only the 1,3-diene structure is affected. However, **14** is the only investigated substrate with an induction period, resulting in a $TOF_{20,H2}$ of ca. 7,000 $h^{-1}$. The structural diene motif should not be an issue here, since it is terminal, thus readily accessible. Instead, the solubility of the substrates in the catalyst phase or Pd leaching into the substrate phase might become relevant. By $^1$H-NMR spectroscopy, it was shown that all FAME substrates can be found with 2-3.6% (w/w) in the catalyst phase after the reaction time, while no β-myrcene is observable in the catalyst phase. Thus, all substrates show low solubilities in the catalyst phase, although the more apolar substrate **14** is even more disfavored. However, Pd leaching into the substrate phase was always similar (4-8% due to ICP-OES measurement increments). Concluding, the differences in solubility may be the reason for the induction period for **14**. Further analyses of the reaction products of **14** and the underlying mechanism can be found in chapter 6.3.4. It will be shown there that conjugated dienes show a specific product isomer pattern that is by no means observable for **9** here. Therefore, the experiments refute a sometimes discussed pre-conjugation prior to hydrogenation or conjugation during the reaction. Instead, the proposed Horiuti-Polanyi mechanism can explain the product compositions for the hydrogenation of non-conjugated substrates with Pd NPs in PC. Nevertheless, further experiments are needed to verify a heterogeneous pathway.

## 5.4 Conclusions

In summary, PLAL of various metals in PC and PLAL of Pd in various solvents was performed, leading mostly to monomodal particle size distributions with similar mean diameters around 5 nm. Selective partial FAME hydrogenation was used to evaluate the applicability of the resulting particles for further catalytic conversions. For the chosen reaction system, Pd in PC exhibited the highest activity and selectivity, even at high conversions. The interaction of the solvent with the catalyst surface during ablation and reaction is the most probable reason for varying catalyst activities and selectivities. Other promising solvents that enable similar results are 1-butanol and glycerol carbonate, but these solvents were rejected for different reasons. Regarding other metals, the literature-known trend for activity was confirmed. The catalytic behavior of Pd in PC was further elucidated: selectivities of more than 95% are achievable up to 90% conversion of the excess double bonds, independent of the investigated reaction conditions. Only at even higher conversion, pronounced overhydrogenation is observable. The trans/cis ratio was found to be completely unaffected by any variations in reaction conditions, even regarding other metals and solvents, rising pronouncedly only after 90% conversion is exceeded. Indeed, in comparison with literature and another substrate mixture, the chosen catalyst and substrate perform superior to most of the other systems. The applied substrate is expected to influence the whole reaction performance due to its trace impurities.

Pd NPs in PC hydrogenate preferentially conjugated species over non-conjugated ones. If only one double bond or highly separated double bonds remain in the product, hydrogenation drastically slows down, in accordance with literature. Furthermore, the heterogeneous Horiuti-Polanyi mechanism was not refuted and is instead able to explain the product compositions for non-conjugated species, although further experiments are needed to verify a true heterogeneous pathway. An induction period is visible for the strongly apolar β-myrcene that may be attributed to different solubilities of substrates in the catalyst phase. On the contrary, Pd leaching is rather substrate-independent.

With these findings, a robust basis is laid for the implementation of colloidal Pd nanocatalysts in several catalytic reactions and their applications in further process intensification measurements.

# 6 Laser-Ablated Pd Nanoparticles as Versatile Catalysts for Selective Partial Hydrogenation

**Author contributions:** The concept and ideas for this project were provided by me. PLAL was performed together with T. Fromme. D. Ljatifi contributed selected hydrogenation experiments as part of his apprenticeship under my supervision. N. Tkatschenko initially screened reaction conditions for alkynes as part of his bachelor's thesis under my supervision, which is not presented here. F. Bajro and J. Herrmann contributed hydrogenation and/or hydroformylation experiments of terpenes as parts of their bachelor's theses under my supervision. Further experiments, overall analyses, visualization, and writing were performed by me. T. Seidensticker acquired funding and supervised this project.

## 6.1 Introduction

This chapter aims to combine the advantages of the reactivity of Pd NPs with sizes around 5 nm introduced in chapter 4 with the approach of pulsed laser ablation in liquids from the previous chapter to obtain highly active nanoparticles for the selective hydrogenation of various unsaturated substrates apart from FAME. As Pd in PC was found to be a highly promising candidate, this system will be used for the following investigations. Although a broad range of tested synthesis routes for colloidal Pd NPs and their application in hydrogenation of a broad substrate base are known[22],[51],[54]–[57],[59],[79],[158]–[162],[172],[184]–[203], the application of Pd nanoparticles obtained by PLAL has so far only been tested in the hydrogenation of alkenes and fatty acid derivatives[11],[204] although these particles enable to completely avoid any further stabilizing molecules or ions and allow a fast and reproducible synthesis[38].

To begin, alkynes shall be selectively hydrogenated to the corresponding alkenes (Scheme 10). Here, Pd is a particularly meaningful choice, since it poses an optimal compromise between selectivity and activity, both originating from the hydrogen activation (splitting) by the metal that is well balanced for Pd. Nevertheless, selectivity control at high or full conversion remains a crucial factor. If further improvement is desired, it could be achieved by the addition of auxiliaries (typically containing nitrogen) that compete for free surface sites with the substrates and increase electron density at the metal to lower alkene adsorption.[80],[81] However, this stands in contrast to the objective of achieving the cleanest possible surfaces and systems, as outlined in chapter 2.1.1.2.

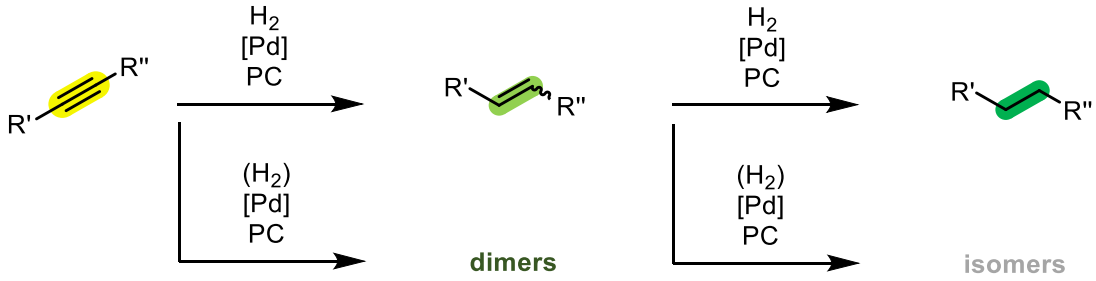


Scheme 10: Reaction network for the selective partial hydrogenation of alkynes to alkenes.

To further test the selectivity of the chosen catalyst system in the hydrogenation of activated double bonds, like in the presence of carbonyl groups, examples of α,β-unsaturated aldehydes are investigated. Here, different products might form, with the allyl alcohol being the desired product. However, the saturated carbonyl compound is thermodynamically more stable than the allyl alcohol and can be formed from the latter by double bond isomerization and subsequent keto-enol-tautomerization (Scheme 11).[6],[205]

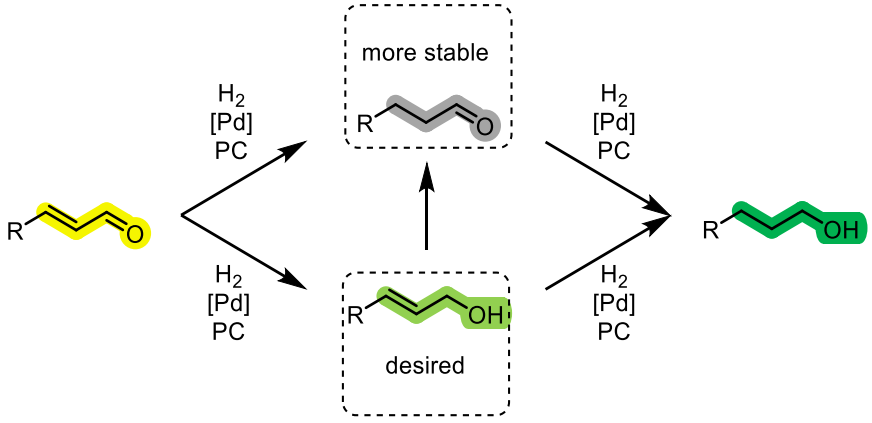


Scheme 11: Reaction network for the selective partial hydrogenation of α,β-unsaturated aldehydes.

As further substrates, both common cyclic butadiene oligomers (1,5-cyclooctadiene and 1,5,9-cyclododecatriene) are subjected to the selective partial hydrogenation (Scheme 12), since especially the selective hydrogenation of 1,5,9-cyclododecatriene is of industrial relevance[206]. The influence of the cyclic nature of the applied substrates, as well as the second separating methylene group between the double bonds on the reaction performance is to be shown.

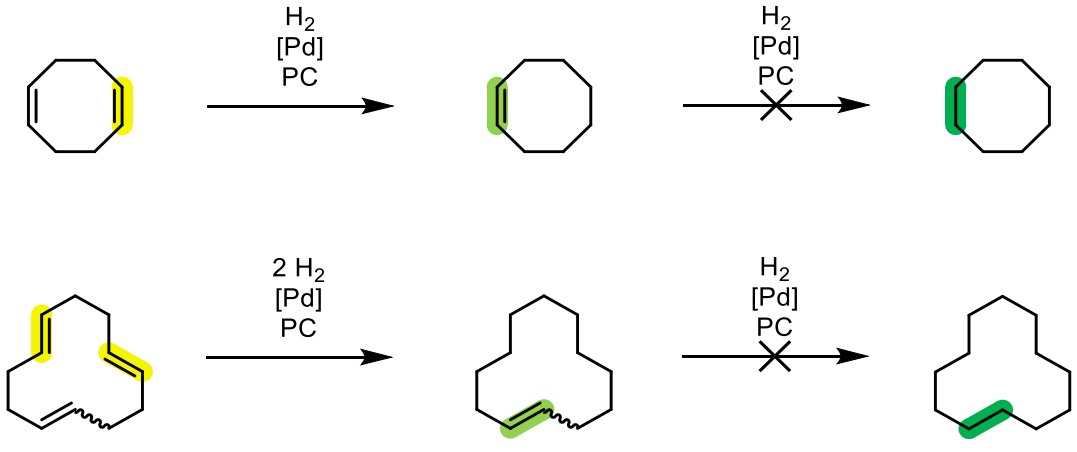


Scheme 12: Intended reactions with cyclic non-conjugated dienes.

At last, the innovative catalyst system is applied for sustainable chemistry, utilizing renewable resources with conjugated double bonds to produce renewable platform chemicals for further functionalization. Terpenes are promising candidates, avoiding the use of edible resources, hence decoupling the

chemical industry from nutritional purposes. Further functionalisation of untreated terpenes is only scarcely investigated. One reason is that they often contain conjugated double bonds that hamper catalysts for further functionalisation like hydroformylation[50],[60],[103]. Pd is known to be the only metal for high alkene selectivity in alkyne and diene hydrogenation[6], further underlining the suitability of the chosen catalyst system (shown in Scheme 13 for conjugated double bonds).

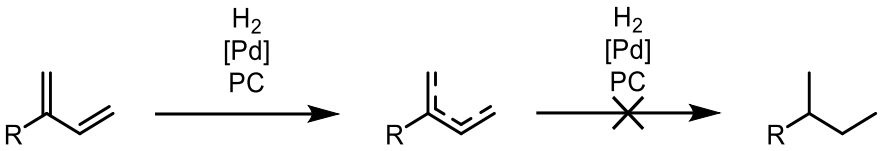


Scheme 13: Reaction network for selective partial hydrogenation of conjugated double bonds like in terpenes.

The hydrogenated products are then subjected to a subsequent hydroformylation to obtain new bifunctional value-added products (either unsaturated monoaldehydes or saturated dialdehydes) based on renewable resources, e.g. for the fragrance industry[103].

## 6.2 Experimental

All chemicals were purchased from commercial suppliers and used as received, except for farnesenes: These were purified of any possible peroxides by percolation with cyclohexane through neutral alumina prior to use. Subsequently, cyclohexane was removed in vacuo at 50 °C and 350 mbar for at least 1 h.

Pd in PC was produced in two batches by PLAL with subsequent laser fragmentation using a Nd:YAG-laser (IS400-1-L, Edgewave) at a power output of 50 W, a wavelength of 532 nm, and a repetition rate of 5 kHz, as already explained in chapter 5.2. Pd contents (in ppm, w/w) of the obtained solutions were measured using ICP-OES prior to first use as described in chapter 4.3.

All hydrogenation experiments were performed in 120 mL stainless steel or 250 mL glass reactors with gas injection stirrers, substrate containers, and a hydrogen dosing system. The vessels were at most half-filled to ensure sufficient mixing behavior. For all liquid substrates, the catalyst solution was introduced into the reactor, which was sealed afterwards. The whole system was then inertized via an alternation of argon supply and vacuum degassing for at least three cycles. Then, liquid substrates (and cyclohexane as solvent whenever necessary) were introduced into the substrate container using a syringe. Cyclohexane was chosen, since miscibility with PC is very low and the respective substrates are not miscible with PC either; thus, biphasic systems with very low cross-solubilities were investigated. However, hydrogenations were carried out without any further solvent, unless the liquid level was too low. Especially within each substrate class, comparable liquid levels were targeted for comparable gas supply and mixing behavior.

Afterwards, the system was pressurized, stirring was initiated, and heating was started if necessary to preform the catalyst. The 120 mL reactor also allowed preheating of the substrate. When applying heating, the pressure setpoint was set below its final value until preheating was finished to allow compensation of any possible pressure changes during preheating. After reaching constant conditions,

the substrate was added, and the reaction started. Hydrogen was constantly fed by a mass flow controller so that the pressure remained constant throughout the reaction.

For the hydrogenation of 2-butyne-1,4-diol, the solid substrate was added into the vessel with the catalyst solution and stirred for ca. 60 s without hydrogen to allow dissolution. Then, inertisation was carried out. While pressurizing, the solution was not stirred to minimize the risk of an uncontrolled reaction start. The reaction was started by initiating stirring after reaching a constant pressure.

The blind activities of the reactors were tested with most substrates under their individually applied conditions and were found to be non-existent or below 4% conversion within the reaction time frame.

Hydrogenations at ambient pressure were conducted in round-bottom flasks with a gas balloon filled with hydrogen. The catalyst solution was introduced, then the flask was flushed with argon. Afterwards, the balloon was attached, and the flask was purged with one complete balloon filled with hydrogen. A new balloon was installed, and the catalyst was preformed for several minutes under stirring at 1,400 rpm. Afterwards, the substrate was introduced through the septum using a syringe, overpressure was released, and a new balloon was attached. Samples were withdrawn as indicated via a syringe, and a new balloon was attached after sample withdrawal.

For the hydroformylation, all substrates were purified by percolation through alumina with cyclohexane, which was evaporated afterwards at 50 °C and 0.35 mbar for at least one hour. Hydrogenated β-myrcene and farnesenes were obtained from the hydrogenation experiments by phase separation. The hydroformylation experiments were performed in the same 120 mL stainless steel reactors as the hydrogenations. The reactor, as well as a Schlenk tube, were inertized via an alternation of argon supply and vacuum degassing for at least three cycles. $Rh(acac)(CO)_2$, ligand, and toluene were introduced into the Schlenk flask under argon counterflow and sonicated for 30 minutes to dissolve precursor and ligand. Purified substrate was introduced into the substrate container under argon counterflow using a syringe. Subsequently, an appropriate amount of the catalyst solution was introduced into the reactor vessel using a syringe under argon counterflow to meet the required substrate-to-catalyst ratio (S:C). Afterwards, heating and stirring were initiated, and pressure was adjusted to approximately 5 bar below the intended reaction setpoint. Preforming was conducted for one hour after all setpoints were reached. After 30 minutes of preforming, heating of the substrate container was initiated. After preforming, the desired reaction pressure was applied to the whole system. Upon reaching stable values, the reaction was initiated. Converted synthesis gas was constantly replenished by the mass flow controller.

Samples were withdrawn and cooled in liquid $N_2$-freezed glassware or precooled Falcon tubes. They were measured via GC-FID after standard addition and, for biphasic reactions, phase separation and dilution. All turnover frequencies refer to ca. 20 % substrate conversion and were calculated either by hydrogen uptake ($TOF_{20,H2}$) or from GC data in cases where sufficient hydrogen uptake data were not available ($TOF_{20}$). Further details on analyses and the calculation of reaction performance indicators can be found in chapter 11.3.2.

## 6.3 Results and Discussion

### 6.3.1 Alkynes

To achieve a selective partial hydrogenation of alkynes to the corresponding alkenes at high selectivities, suitable reaction conditions must be applied. In a first step, typical conditions for Pd in PC from wet-chemical approaches were taken from literature and adjusted to constraints of the system: In the present case, PLAL yields only highly diluted Pd in PC with maximum concentrations of 35 ppm (w/w). A typical particle size distribution was already shown in Figure 27. For comparison, in the wet-chemical approach, 100 ppm are typically employed [172],[185]. Room temperature and intermediate catalyst loading (S:C of 7,000-10,000) were tested. While literature typically utilizes atmospheric pressure, this is not sufficient for complete conversion even for highly active substrates under the given conditions: the hydrogenation of 25 mmol 2-methyl-3-butyne-2-ol (**1**) at room temperature and 1 atm of hydrogen results in a stagnant conversion of 86% after 24 h at the latest. Accordingly, all reactions were conducted at elevated pressures of 50 bar for all alkynes to overcome this hurdle, which is the result of a preceding optimization.

2-Butyne-1,4-diol (**15**) was chosen as a simple and available model substrate. The resulting alkenediol **16** is of industrial relevance in the production of vitamins A and B6, as well as for poly(butenediol)[44],[79]. The selective partial hydrogenation of **15** proceeds very fast, showing quantitative conversion after only 30 minutes with a selectivity of 96% (Table 9, entry 1). A turnover frequency at 20% targeted hydrogen conversion ($TOF_{20,H2}$) of 8,300 $h^{-1}$ was obtained. Trans-configured species were not clearly visible in this experiment and are thus negligible. After approaching maximum yield, overhydrogenation towards the saturated diol **17** proceeds, although at a slightly lower rate (Figure 35, evolution of the green entries).

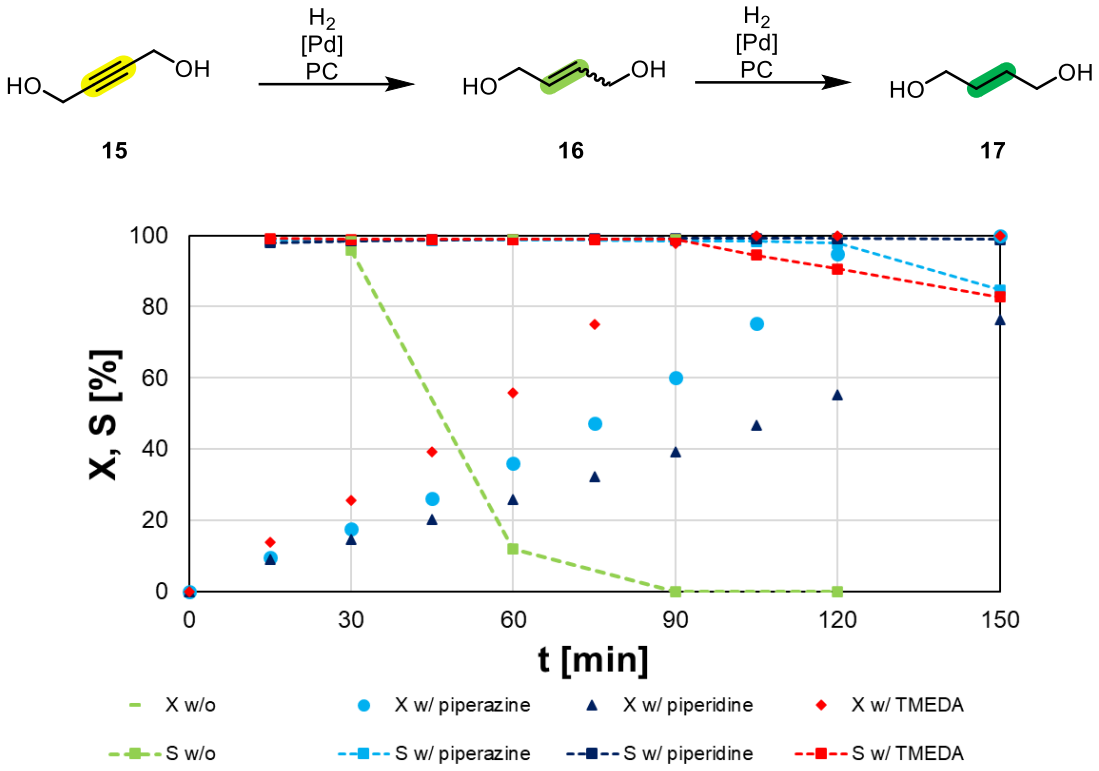


Figure 35: Development of selectivity towards **16** in the selective partial hydrogenation of **15** with different additives at 50 bar $H_2$. Conditions: $n_{substrate}$= 50 mmol, S:C= 7,000:1, $T_{start}$= 22-24 °C (29 °C for TMEDA), $f_{stirrer}$ = 1,500 rpm, $p_{H2}$= 50 bar, $w_{Pd,PC}$= 16 ppm, $n_{additive}$:$n_{substrate}$= 1:1, semibatch. Lines are for visualization purposes only.

In an attempt to maintain selectivity or even improve it at high conversion, three different N-containing additives (piperazine, tetramethylethylenediamine (TMEDA), piperidine) were investigated (also Figure 35), since promoting effects are expected from literature (see chapters 2.2.1.3 and 6.1). When using those additives, the reactions are slowed down compared to the reaction without an additive, with reduced $TOF_{20,H2}$ of 2,600-3,800 $h^{-1}$. However, selectivities are always comparable at low to intermediate conversions, regardless of the presence of an additive. TMEDA gives 94.5% selectivity at full conversion. For piperazine, a similar selectivity at nearly complete conversion is obtained, while piperidine lacks sufficient data for conversions greater than 80%. With these promising results, further substrates were investigated without N-containing additives, since they only lower turnover frequencies and thus productivity without relevant effects on selectivity. Accordingly, the particles show an intrinsic thermodynamic selectivity behavior in the selective partial hydrogenation of alkynes.

Phenylacetylene (**18**) serves as an example of an aromatic alkyne substrate in comparison to the aliphatic diol **15**. It shows drastically improved reaction times of ca. 5 minutes for full conversion and a $TOF_{20,H2}$ of 88,000 $h^{-1}$, an increase by an order of magnitude. However, the selectivity is reduced to 88% due to the parallel rise of overhydrogenation to **20** (Figure 36). Hydrogenation of the aromatic ring was not observable in accordance with the literature[11].

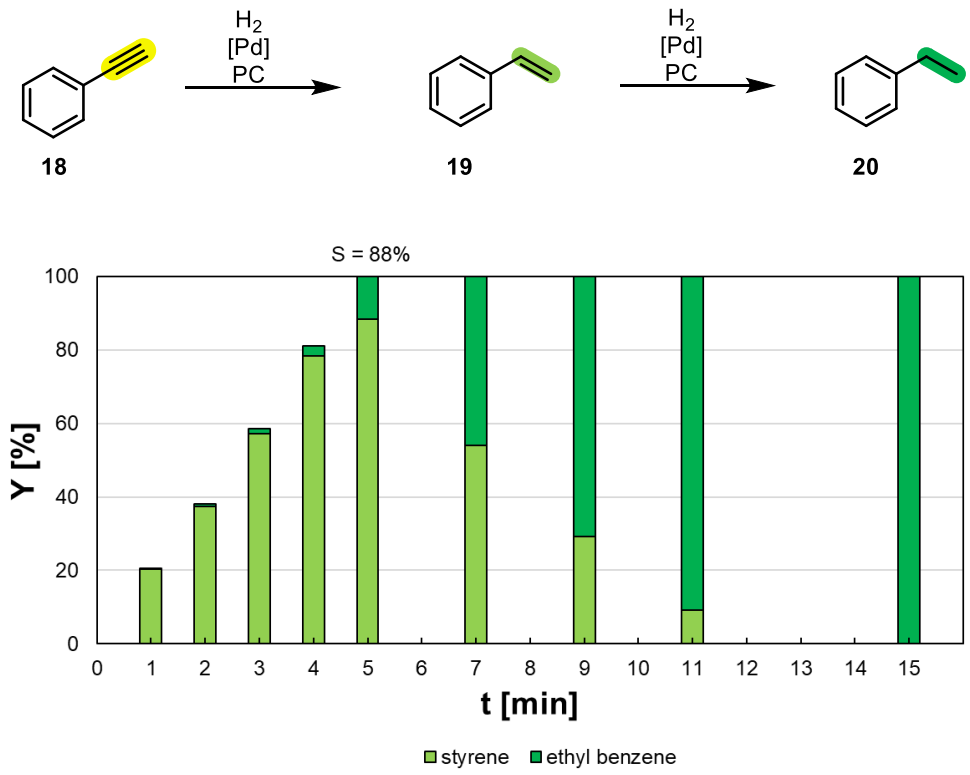


Figure 36: Yields in the selective partial hydrogenation of **18** at 50 bar $H_2$. Conditions: $n_{substrate}$= 50 mmol, S:C= 7,000:1, $T_{start}$= 22 °C, $f_{stirrer}$ = 1,500 rpm, $p_{H2}$= 50 bar, $w_{Pd,PC}$= 16 ppm, semibatch.

Both reactions show that conversion of the alkyne is indirectly observable through temperature development, with maximum temperature at full alkyne conversion (Figure 37). This is in line with literature findings that alkyne and alkene hydrogenation of the same structural motif possess different reaction enthalpies, and is strengthened by observed different reaction rates for alkyne and alkene hydrogenation[168].

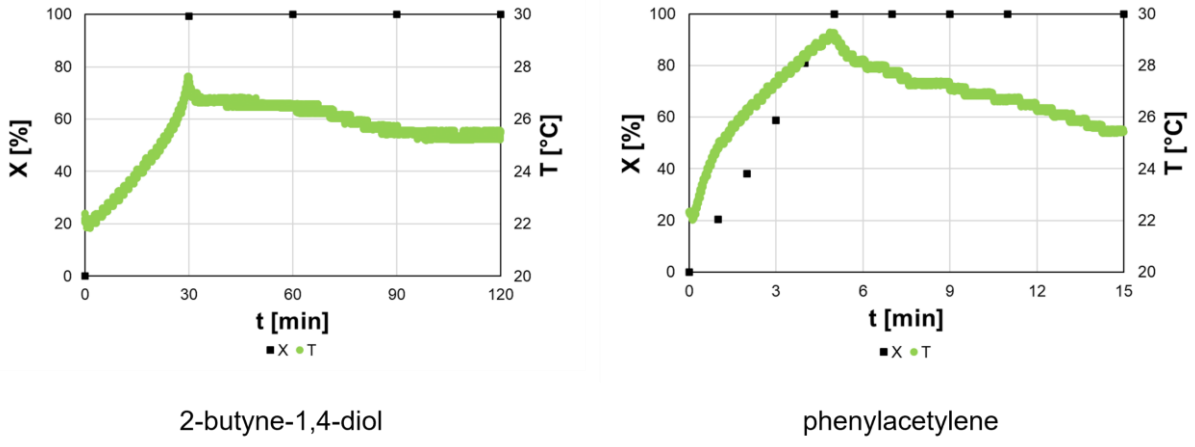


Figure 37: Evolution of conversion and temperature in the selective partial hydrogenation of **15** (left) and **18** (right) at 50 bar $H_2$. Conditions: $n_{substrate}$= 50 mmol, S:C= 7,000:1, $T_{start}$= 22 °C, $f_{stirrer}$ = 1,500 rpm, $p_{H2}$= 50 bar, $w_{Pd,PC}$= 16 ppm, semibatch.

To elucidate the influence of the triple bond's position on the chemoselectivity and to show the applicability of a biphasic reaction system approach, all n-octyne isomers (see also Table 9, entries 3-6) were subjected to selective partial hydrogenation, forming a second, immiscible liquid phase. Because reactions involving more internally located double bonds require longer reaction times for full conversion, sample time stamps are also included (Figure 38).

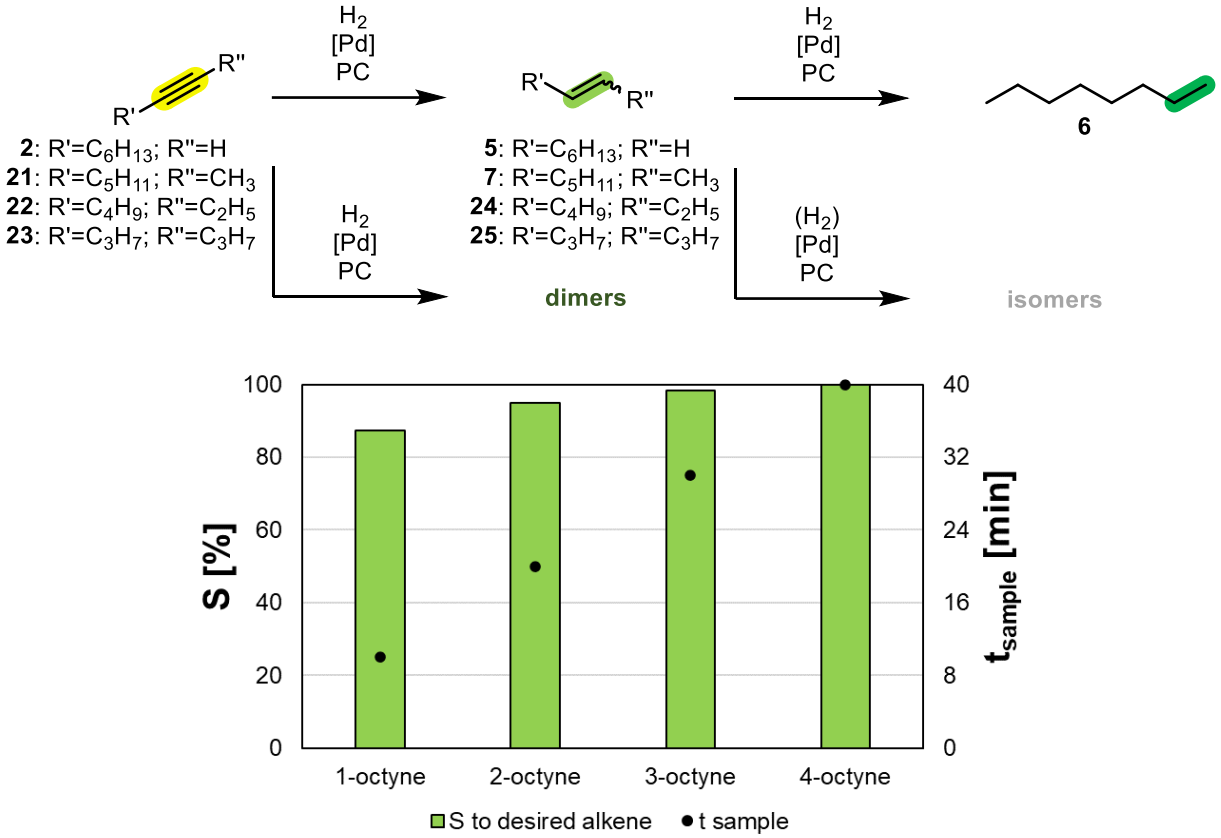


Figure 38: Selectivities at full conversion in partial hydrogenation of **2**, **21**, **22**, **23** at 50 bar $H_2$ with additional indication of sample withdrawal times. Conditions: $n_{substrate}$= 25 mmol (21.7 mmol for **2**), S:C= 10,000:1 (8,700:1 for **2**), $T_{start}$= 19-22 °C, $f_{stirrer}$ = 1,500 rpm, $p_{H2}$= 50 bar, $w_{Pd,PC}$= 11 ppm, t as stated, $V_{cyclohexane}$= 16.5 mL (17 mL for **2**), semibatch.

In all cases, selectivity is high with 87% for the terminal octyne **2** and even higher than 95% for all internal n-octynes (**21**-**23**). Literature typically uses sterical considerations to explain the higher reactivity of terminal alkynes[53]. However, it is also known that the electron density of the Pd surface and in the substrate influences their interaction: Here, a high electron density of the surface leads to less interaction with electron-rich substrates.[207] From this, it can be concluded for a defined adsoption site that inductive effects cause less reactivity of the internal substrates **21**-**23** and their products **7**, **24**, and **25** in the observed manner. This also leads to higher selectivity. Apart from overhydrogenation to **6**, selectivity is determined by dimer formation and isomerization of the double bond. All three effects are especially observable in the hydrogenation of **2**. TOFs can be estimated from hydrogen consumption resp. sample withdrawal to be 41,000 $h^{-1}$ for **2** ($TOF_{20,H2}$) and more than 27,000 $h^{-1}$ for the internal n-octynes **22** ($TOF_{20,H2}$) and **23** ($TOF_{20}$), while **21** lacks sufficient data. To evaluate product contamination with Pd in

this biphasic approach, ICP-OES measurements were performed that revealed Pd concentrations at the quantification limit of 1 ppm (w/w) and thus indicate nearly catalyst-free products.

Industrial alkyne hydrogenation utilizes a Lindlar catalyst, e.g., for the production of **3**, a key intermediate for artificial terpenes, obtained from the selective partial hydrogenation of **1**[45],[78]. The Lindlar catalyst contains Pd on $CaCO_3$, partially poisoned with toxic Pb and quinoline. As a result, only ca. 10% of the applied Pd mass is catalytically active.[46],[90] Applying laser-ablated nanoparticles as a lead-free alternative at the standard S:C ratio of 10,000:1 results in an exceptionally rapid reaction within less than 3 minutes required for nearly complete conversion and a resulting $TOF_{20,H2}$ of 570,000 $h^{-1}$. In this short time frame, precise sampling is not possible; thus, selectivity at approaching full conversion cannot be given here. Accordingly, for better reaction control, the S:C ratio was increased to 50,000:1, which still results in less than 1 h reaction time with a maximum yield of **3** of 84%. This corresponds to 87% selectivity and a $TOF_{20}$ of 69,000 $h^{-1}$ (Figure 39 and Table 9, entry 7). The outstanding activity may be explained by the structure of **1**: The vicinity of the electron-withdrawing -OH group to the terminal triple bond results in reduced electron density at the triple bond, probably leading to increased reactivity due to the same effects discussed for the n-octynes.

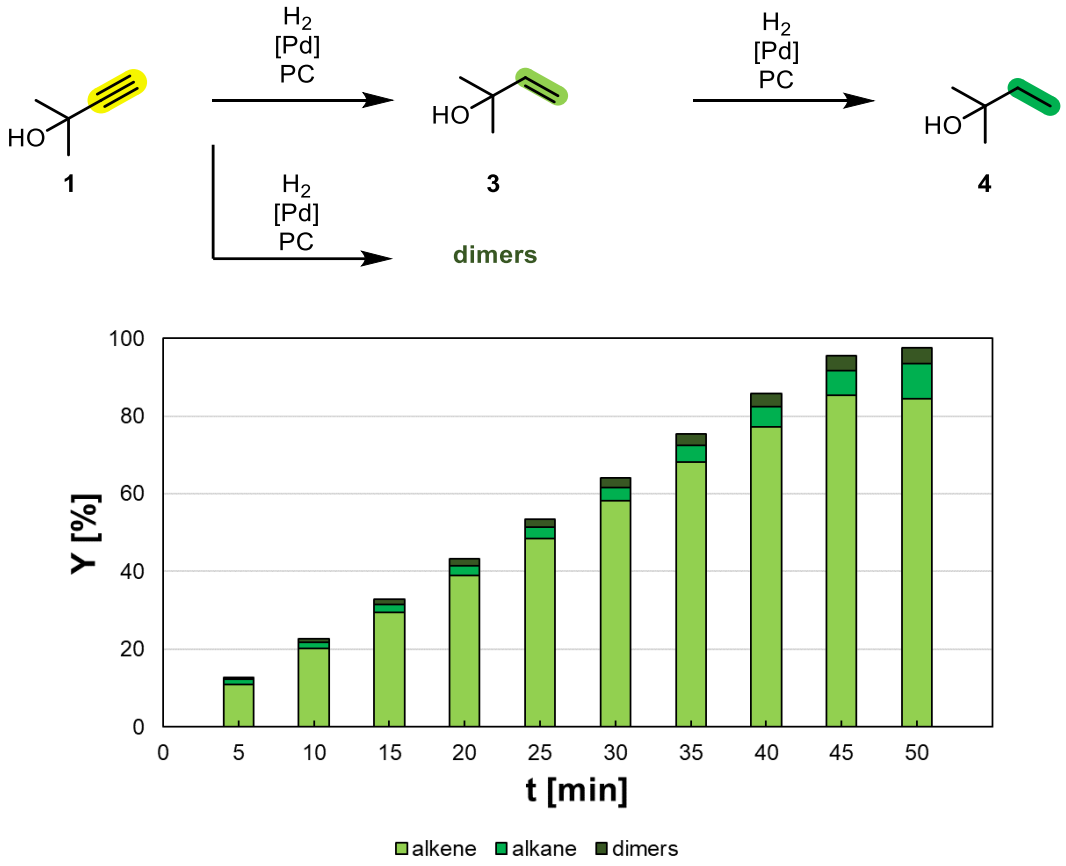


Figure 39: Yields in the selective partial hydrogenation of **1** at 50 bar $H_2$ and increased S:C. Conditions: $n_{substrate}$= 50 mmol, S:C= 50,000:1, $T_{start}$= 20 °C, $f_{stirrer}$ = 1,500 rpm, $p_{H2}$= 50 bar, $w_{Pd,PC}$= 11 ppm, semibatch.

Applying a Lindlar catalyst under standard conditions with S:C of 10,000:1 results in reaction times of around 70 minutes for full conversion and a slightly lower selectivity of 83% at a maximum yield of **3** of 81%. The resulting $TOF_{20}$ is 6,700 $h^{-1}$, thus one magnitude lower than for Pd in PC at reasonable

conditions. As a consequence, laser-ablated Pd nanoparticles in PC outperform the Lindlar catalyst not only in environmental considerations and manufacturing cost but especially in catalytic performance, thereby posing themselves as a lead-free alternative to the Lindlar catalyst that is of significant industrial relevance.

Overall, high selectivities at very high to full conversion are achievable for all investigated alkynes with varying substituents in a time range of minutes and thus at very high turnover frequencies of mostly several 10,000 $h^{-1}$. The chosen catalyst system shows low to no hydrogenation activity with regard to monounsaturated alkenes. As a consequence, further substrate classes with activated and/or several double bonds per molecule are investigated next.

Table 9: Overview of the selective partial hydrogenation of alkynes with laser-ablated Pd in PC. General conditions if not stated otherwise (for details, see above): $n_{substrate}$= 50 mmol, S:C= 7,000 or 10,000:1, $T_{start}$= 19-24 °C, ω= 1,500 rpm, $p_{H2}$= 50 bar, $w_{Pd,PC}$= 11-16 ppm, semibatch.

| entry | substrate | product | byproducts (observed) | S[a] [%] | $TOF_{20(,H2)}$ [$h^{-1}$] | trans/cis[a] [mol $mol^{-1}$] |
|---|---|---|---|---|---|---|
| **1** |  **15** | 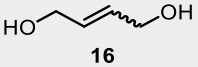 **16** | 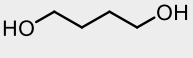 **17** + unknown | 96 | 8,300 | n.d. |
| **2** | 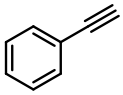 **18** | 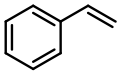 **19** | 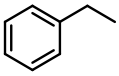 **20** | 88 | 88,000 | - |
| **3**[b] | 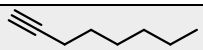 **2** | 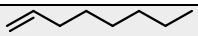 **5** | 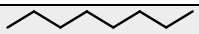 **6** + **7** + dimers | 87 | 41,000 | - |
| **4**[c] | 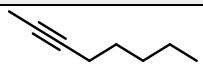 **21** | 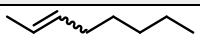 **7** | 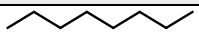 **6** + **5** + dimers | 95 | n.d.[e] | 0.03 |
| **5**[c] | 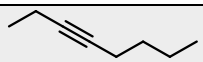 **22** | 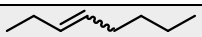 **24** | 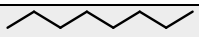 **6** + **7** + **25** + dimers | 98 | 27,000 | 0.09 |
| **6**[c] | 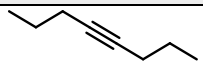 **23** | 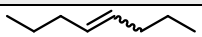 **25** | 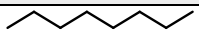 **6** + **7** + **24** + dimers | >99 | ≥28.000[e] | 0.07 |
| **7**[d] | 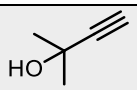 **1** | 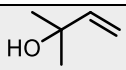 **3** | 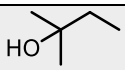 **4** + dimers | 87[f] | 69,000 | - |

a: at full conversion if not stated otherwise, b: $n_{Substrate}$= 21.7 mmol, $V_{cyclohexane}$= 16.5 mL, S:C= 8,700:1, c: $n_{substrate}$= 25 mmol, $V_{cyclohexane}$= 16.5 mL, d: S:C= 50,000:1, e: insufficient data for determination, f: @ 97.5% X

### 6.3.2 α,β-Unsaturated Aldehydes

One example of activated double bonds can be found in α,β-unsaturated aldehydes. According to Scheme 11, the thermodynamically challenging hydrogenation of the carbonyl group instead of the C=C double bond is of academic interest. Two different α,β-unsaturated aldehydes were investigated to elucidate the influence of an aromatic system compared to an aliphatic chain for this alternative activated substrate class. t-Cinnamaldehyde (**26**) is a typically applied substrate in literature[6],[205], and thus used here for initial tests. Conditions used for alkyne hydrogenation cannot be applied here, as cinnamaldehyde shows no reactivity at alkyne conditions. Accordingly, temperature and stirring rate were increased. Despite those measures, the reaction still progressed rather slowly in comparison to the former results, with a stagnant conversion of 98% after 52 h. Although in the present case the reaction drastically slows down towards the end, a $TOF_{20}$ of ca. 2,500 $h^{-1}$ is achieved, because the catalyst loading is still very low with a S:C ratio of 10,000:1 (0.01 mol%). Selectivity is perfectly constant over the whole reaction, with values of 96% towards the saturated aldehyde **28** and 4% towards the saturated alcohol **29**, c.f. Figure 40. Therefore, the applied particles allow for the highly selective production of **28** with a thermodynamically determined selectivity. Comparing this to literature results for Pd/C catalysts shows superior performance of laser-ablated Pd in PC, since in the benchmark systems, selectivity is in the range of 90% at most and highly dependent on solvents and additives[208],[209].

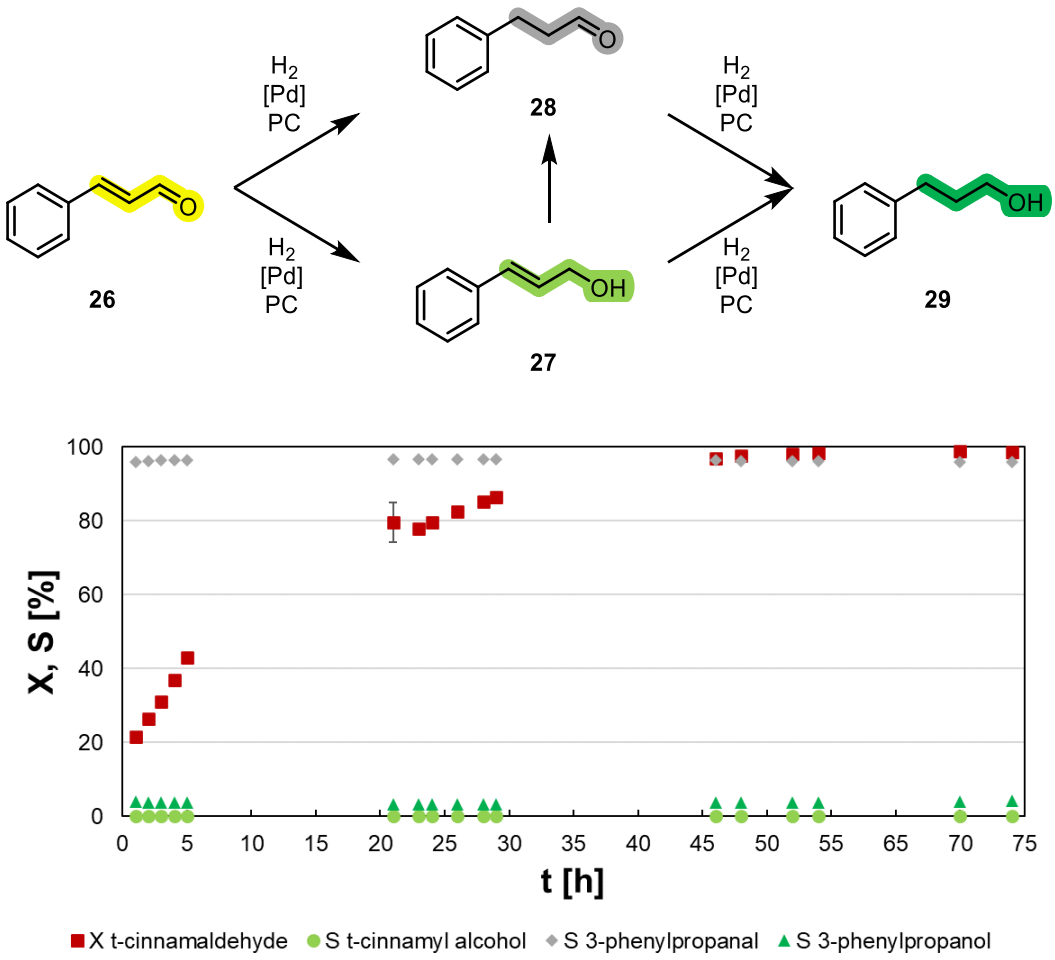


Figure 40: Long-term selective partial hydrogenation of **26**. Conditions: $n_{substrate}$= 50 mmol, S:C= 10,000:1, T= 100 °C, $f_{stirrer}$ = 3,500 rpm, $p_{H2}$= 50 bar, $w_{Pd,PC}$= 11 ppm, semibatch. Data merged from two single experiments.

As a second example of α,β-unsaturated aldehydes, the aliphatic 2-octene-1-al (**30**) is investigated at the same reaction conditions as a comparison. In contrast to the aromatic substrate **26**, selective hydrogenation of **30** proceeds more rapidly with a $TOF_{20,H2}$ of 26,600 $h^{-1}$ and an even increased selectivity towards the saturated aldehyde of more than 99% throughout the whole reaction (Figure 41).

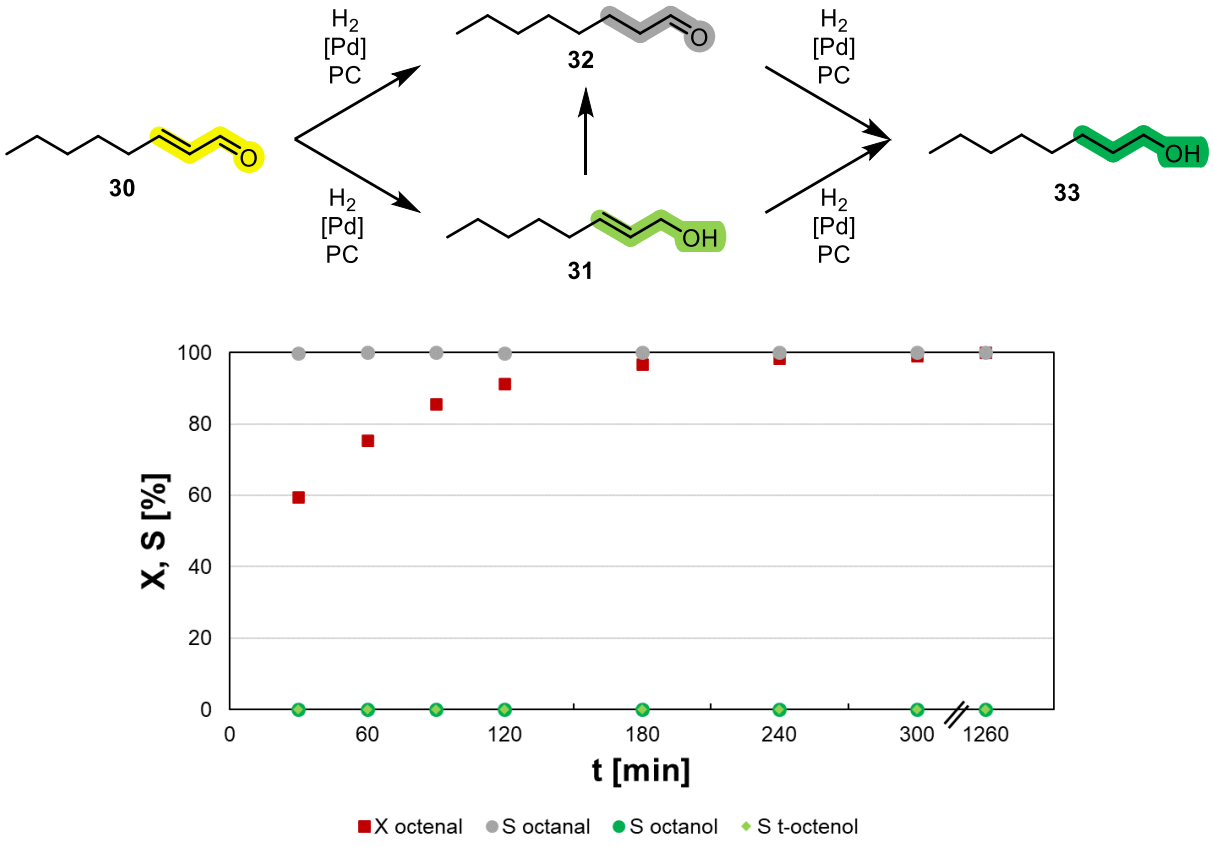


Figure 41: Selective partial hydrogenation of **30** at 50 bar $H_2$. Conditions: $n_{substrate}$= 50 mmol, S:C= 10,000:1, T= 100 °C, $f_{stirrer}$ = 3,500 rpm, $p_{H2}$= 50 bar, $w_{Pd,PC}$= 11 ppm, semibatch.

Apparently, selectivity in the hydrogenation of α,β-unsaturated aldehydes is always thermodynamically controlled, as the resulting product is always the thermodynamically more favored one. That can be attributed to favored adsorption of the C=C bond onto Pd compared to the C=O bond – being characteristic for most metal surfaces –, which consequently favors C=C hydrogenation[6]. An energy barrier seems to exist either during adsorption or during reaction that prevents further hydrogenation towards the alcohol. Further experiments would be necessary to identify the exact nature of this energy barrier. Concluding, it was shown that the nature of the substituents strongly influences reactivity and, to a minor extent, selectivity. Overall, the investigated catalyst system is capable of the highly selective synthesis of saturated aldehydes from α,β-unsaturated substrates. This can, in certain cases, be an alternative to hydroformylation, like in the synthesis of **28**, where hydroformylation of styrene typically yields the branched product[210].

### 6.3.3 Cyclic Non-Conjugated Polyenes

Cyclic nonconjugated polyenes like the industrially relevant 1,5,9-cyclododecatriene (1,5,9-CDT, **39**) are of further interest in the selective partial hydrogenation. Cyclododecene (CDE, **40**) may be used as a polymer precursor for the production of 12-laurolactam and dodecanedioic acid used in polyamide synthesis, replacing the commonly used cyclododecane (CDA, **41**), to enable an environmentally more benign synthesis route, avoiding unselective partial oxidation of CDA[206].

In a first step, 1,5-cyclooctadiene (1,5-COD, **34**) is used as a simpler model substance with the same structural motifs and double bond distance (Scheme 14), applying the same conditions as for the α,β-unsaturated aldehydes.

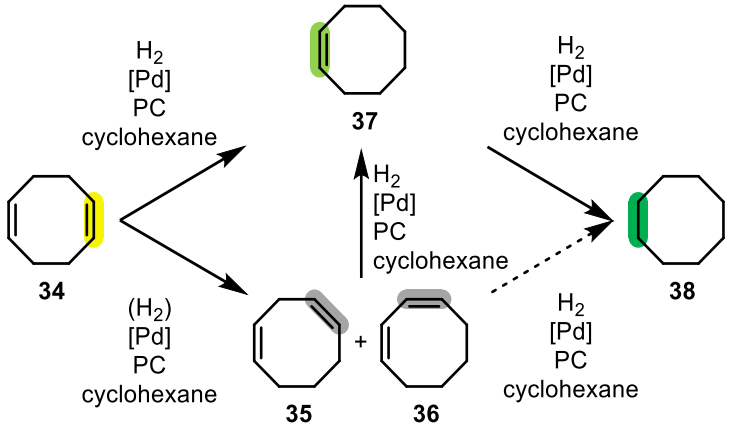


Scheme 14: Reaction network for the selective partial hydrogenation of 1,5-Cyclooctadiene.

Although the reaction initially proceeds very fast with a $TOF_{20,H2}$ of 65,000 $h^{-1}$, it drastically slows down toward the end at a rather constant selectivity of 91% at 97% conversion after 60 minutes. Isomerization towards **35** is observable; however, no conjugated isomer (**36**) was detected. It is therefore unclear whether a pre-conjugation prior to hydrogenation is necessary, in contrast to linear molecules with isolated double bonds discussed in chapter 5.3.3.2.

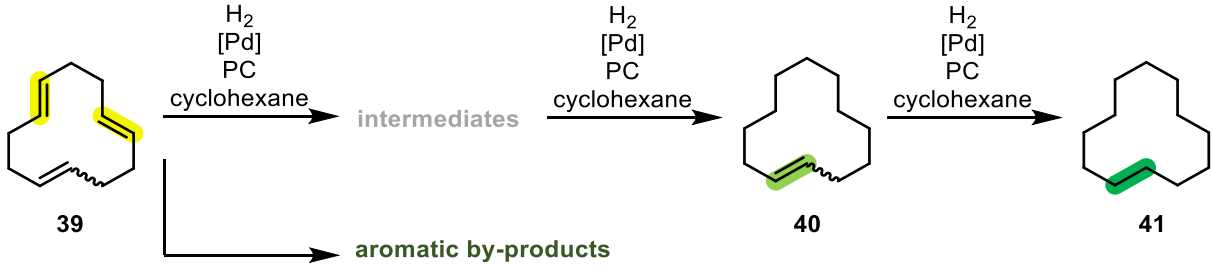


Scheme 15: Reaction network for the selective partial hydrogenation of 1,5,9-cyclododecatriene.

Applying the same conditions for the selective partial hydrogenation of **39** (Scheme 15) results in 8% selectivity at stagnant 40% conversion at prolonged reaction times (Figure 42, left). Most of the loss in selectivity does not result from the formation of the byproduct **41**, but from the formation of intermediates that are not hydrogenated further to the desired product **40**. These intermediates may include isomerized **39** or cyclododecadiene (CDD) isomers. An unexpected fast reaction progress within the first minutes is again observable. This behavior cannot be altered either by a decrease of the S:C ratio or an increase in temperature, which even results in less conversion (Figure 42, middle and right), probably due to temperature-induced changes in particle properties.

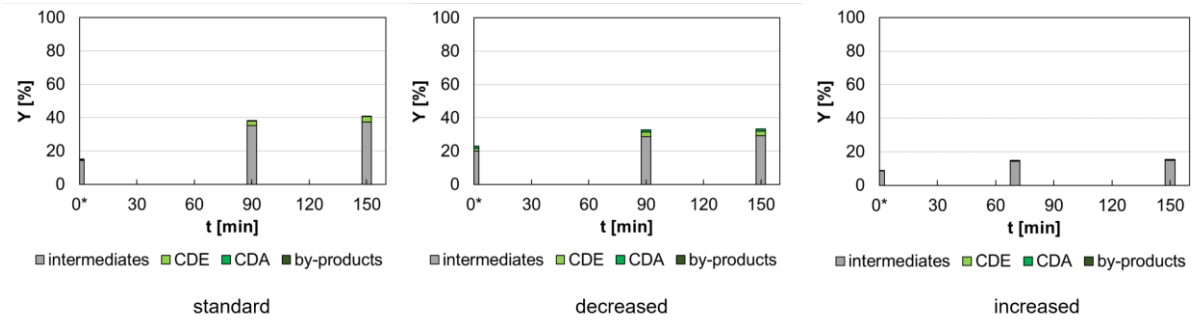


Figure 42: Selective partial hydrogenation of **39**. General conditions: $f_{stirrer}$ = 3,500 rpm, $p_{H2}$= 50 bar, $w_{Pd,PC}$= 11 ppm, $V_{total}$=55 mL, semibatch. 0*: sample withdrawal immediately after reaction start
standard: $n_{substrate}$= 50 mmol, S:C= 10,000:1, T= 100 °C, $V_{cyclohexane}$= 6 mL
decreased S:C: $n_{substrate}$= 5 mmol, S:C= 1,000:1, T= 100 °C, $V_{cyclohexane}$= 14.1 mL
increased T: $n_{substrate}$= 50 mmol, S:C= 10,000:1; T= 150 °C, $V_{cyclohexane}$= 6 mL.

Obviously, an activity problem for the chosen catalyst system with this certain substrate is observable that cannot be circumvented by high temperatures, high pressure, or high Pd loading. In general, the parallel orientation of the double bonds in **34** favors simple and simultaneous bond formation with the Pd surface, which is not possible for non-conjugated **39** and CDD isomers, except for c,c-1,5-CDD.[91] This suggests inherent lower activity and selectivity for **39**.

The literature benchmark system for liquid phase hydrogenation is Pd on activated carbon (Pd/C) and requires a temperature of 160 °C and a maximum pressure of ca. 2 bar, but several (aromatic) byproducts are known to form that were not observable for laser-ablated Pd nanoparticles[211],[212]. The low pressure is applied to decrease the reaction rate. This results in a greater surface coverage with CDT and CDD, since these molecules adsorb preferentially (due to the adsorption of two double bonds of one molecule), which in turn hinders the adsorption of the target product **40** for further conversion.[91] A direct benchmark experiment with the laser-ablated Pd nanoparticles at the stated literature conditions is not meaningful due to the demonstrated activity barrier at 150 °C and 50 bar. Instead, Pd/C was applied at own and literature conditions for verification purposes (Figure 43).

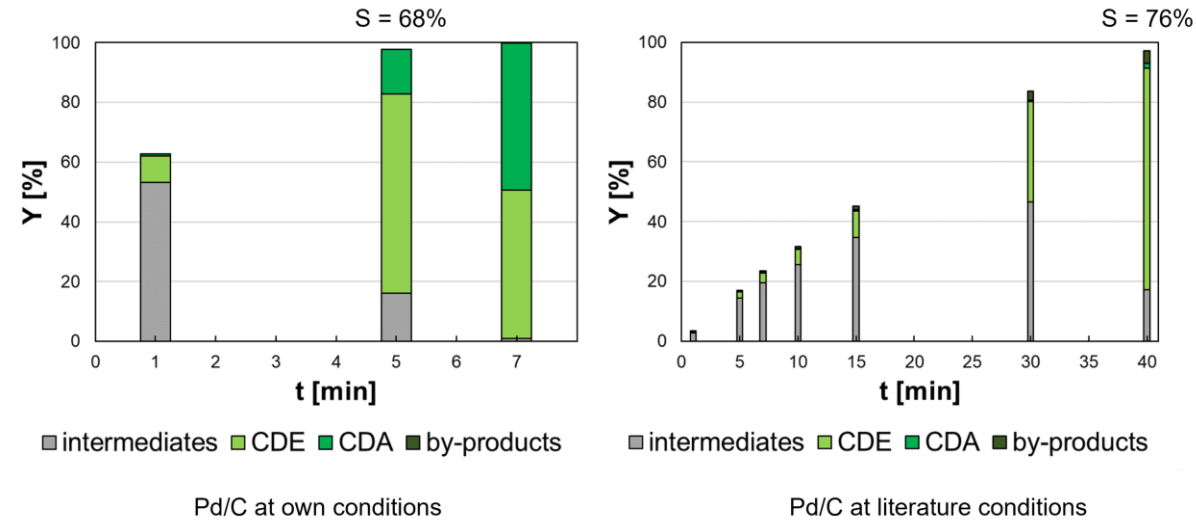


Figure 43: Selective partial hydrogenation of **39** with Pd/C.General conditions: $n_{substrate}$= 301 mmol, $f_{stirrer}$ = 3,500 rpm, $V_{total}$= 55 mL, semibatch
own conditions: T= 160 °C, $p_{H2}$= 2 bar, S:C= 6,800:1
literature conditions: T= 100 °C, $p_{H2}$= 50 bar, S:C= 1,000:1.

Under own conditions, the reaction proceeds rapidly and produces high amounts of undesired CDA. Under literature conditions, selectivity can be drastically increased, although undesired byproducts are observable for the first time. This strongly indicates that **39** shows not only literature-known difficulties, but also additional challenges specific to laser-ablated Pd nanoparticles. In connection with the results from **34**, the necessity of preconjugation cannot be excluded. However, literature confirms the Horiuti-Polanyi mechanism for supported Pd for this substrate[206]. Another option is the fast formation of sterically more hindered isomers or intermediates like cyclododecadienes or conjugated species that prevent sufficient adsorption on active Pd sites and thus disable further conversion. The effect of self-poisoning of conjugated dienes is literature-known for Pd particles and is expected to also appear for non-conjugated ones, but less pronounced[91]. The identification of the exact nature of the intermediates requires further research.

According to these results, the Pd NPs in the present form are insufficient for the hydrogenation of **39** and would need to be modified for better reaction performance: The presence of PC is expected to show lower impact on reactivity, since this is no problem in all other biphasic reactions with apolar substrates. Thus, the results indicate that a support might be necessary, assuming a comparable size distribution of the Pd particles on activated carbon.

### 6.3.4 Terpenes

To enable further functionalizations of renewable substrates and as a further substrate class of activated alkenes, a selection of polyunsaturated terpenes is subjected to selective partial hydrogenation. At first, β-myrcene (**14**), an acyclic monoterpene with conjugated double bonds, was investigated in a biphasic approach under FAME hydrogenation conditions. **14** can be derived from β-pinene (**43**) via pyrolysis; the isomer α-pinene (**42**) is also valuable for the production of dihydromyrcene (**45**) via intermediate hydrogenation (Scheme 16)[103].

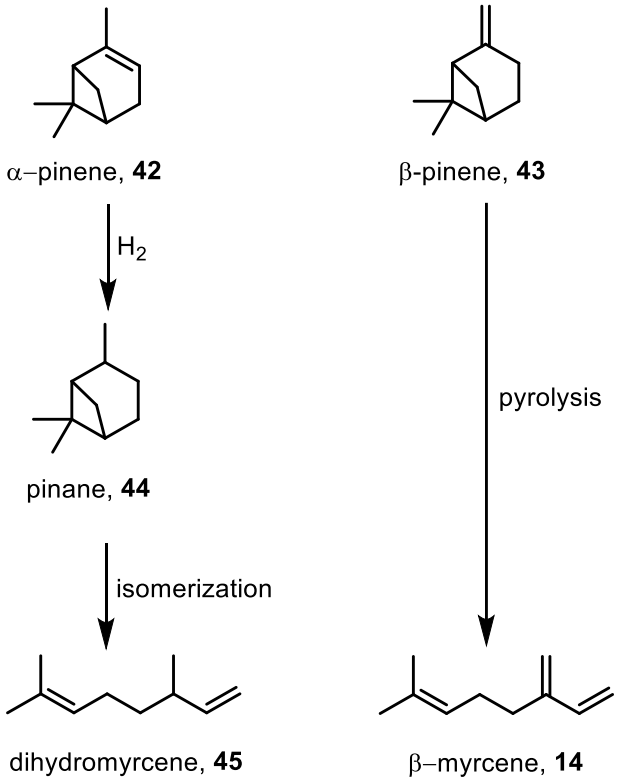


Scheme 16: Routes to **14** and **45** starting from pinenes[103],[213].

The selective partial hydrogenation of **14** was considerably fast, with stagnant hydrogen consumption after ca. 60 min (see also Figure 44, left). Hydrogen uptake for this reaction is characterized by a sigmoidal behavior (as already shown in chapter 5.3.3.2 for particles from the autoreductive approach); thus, TOF cannot be determined exactly. As an approximation, a $TOF_{20,H2}$ of ca. 67,000 $h^{-1}$ can be calculated for the whole first 20% of conversion, including the sigmoidal behavior. Accordingly, this value underestimates the actual TOF at the distinct point of 20% conversion that can be found in the part with linear hydrogen consumption.

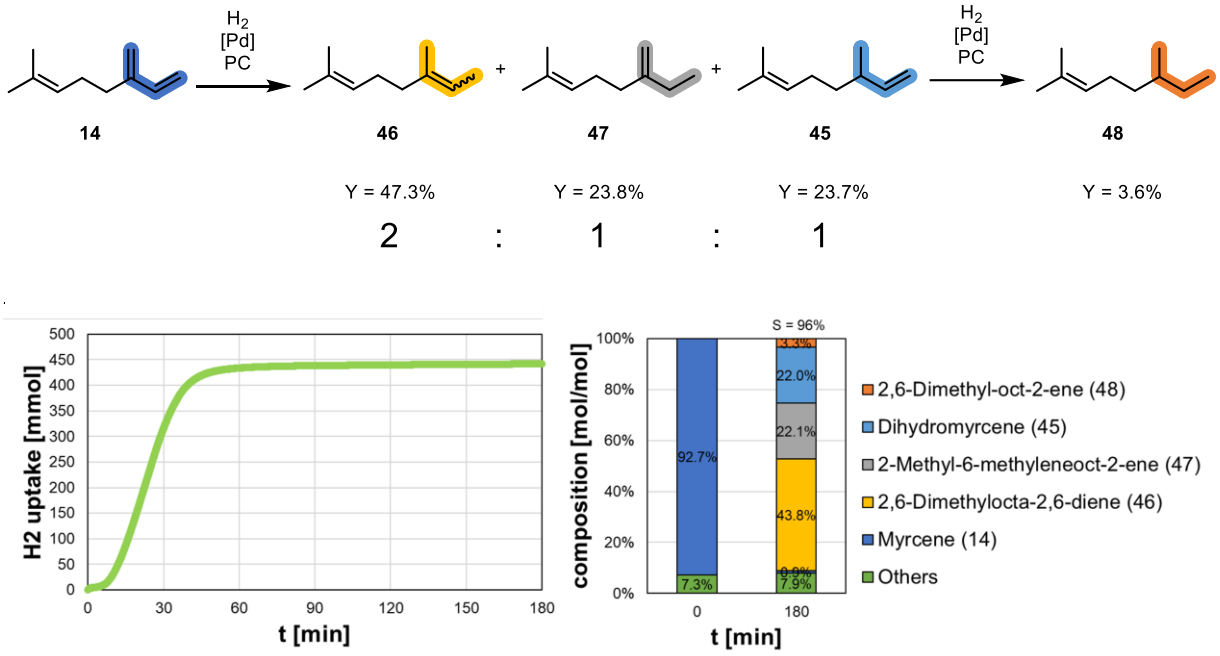


Figure 44: Hydrogen uptake and product composition of the selective partial hydrogenation of **14**. Conditions: $n_{substrate\ mixture}$= 479 mmol, $V_{total}$= 100 mL, S:C= 100,000:1, T= 50 °C, $f_{stirrer}$ = 3,400 rpm, $p_{H2}$= 10 bar, $w_{Pd,PC}$= 24 ppm, semibatch.

The reaction stops at a conversion of **14** of >99%, with only 3.6% yield of the overhydrogenated species **48**. All other products comprise only one hydrogenated double bond. The isolated internal double bond does not get hydrogenated at all, possibly because it is, in general, less reactive in hydrogenation[214]. The observed product distribution strongly indicates a $\eta^3$-mechanism (thus involving a Pd-allyl species): both conjugated double bonds may be hydrogenated at roughly the same rate, because they are equally accessible. Concerning all possible transition states and similar reaction rates/probabilities explains the observed characteristic product distribution of 2:1:1 (internal:terminal:terminal). Literature confirms this by the fact that the reaction stops, although residues of the substrate are still present, as the catalyst may form stable allylic compounds that prevent further reactions.[215],[216]

In this biphasic hydrogenation, the Pd content in the product phase is within the limit of quantification of the ICP-OES of 1 ppm (w/w) and thus negligible. This is surprising, as stable Pd-myrcene compounds are expected to be more soluble in the apolar product phase than in the catalyst phase. Therefore, other effects might also come into play, like stronger binding substances from the unidentified residues, changes in particle morphology during the reaction with resulting changes in reactivity, or only partial coverage with unreacted substrate due to very low solubility of the phases in each other. The latter would lead to sufficient particle stabilization in the catalyst phase. The elucidation of the exact reason is challenging and demands further work.

To further verify the hypothesis of the proposed reaction mechanism, commercially available dihydromyrcene (**45**), which is also one product in the selective partial hydrogenation of **14** by laser-ablated Pd in PC (refer to Figure 44), is investigated in hydrogenation under the same conditions. In contrast to the product mixture obtained by selective partial hydrogenation of **14**, **45** can be further

converted, mostly getting hydrogenated and in parts also isomerized towards **49** (Figure 45). Full hydrogenation towards the saturated 2,6-dimethyloctane still does not occur in relevant amounts. Pd contamination of the product phase is similar to β-myrcene at the limit of quantification of 1 ppm. This reaction takes far longer than the hydrogenation of the conjugated system, but still reaches a $TOF_{20}$ of 32,000 $h^{-1}$ due to the low catalyst loading. Accordingly, the reaction of this non-conjugated substrate is by a factor of at least 2 slower than for the very similar, conjugated substrate under similar conditions. This is in line with the results from chapter 5.3.3.2 for particles from the autoreductive approach, although the difference in activity is even more pronounced within different FAMEs there. Obviously, a different mechanism compared to the hydrogenation of **14** must occur for **45**, probably a hydride mechanism. At the same time, the hydrogenation of **45** in the absence of residues of **14** supports the $\eta^3$-mechanism for conjugated double bonds, since they cannot compete for Pd and thus, follow-up reactions may occur.

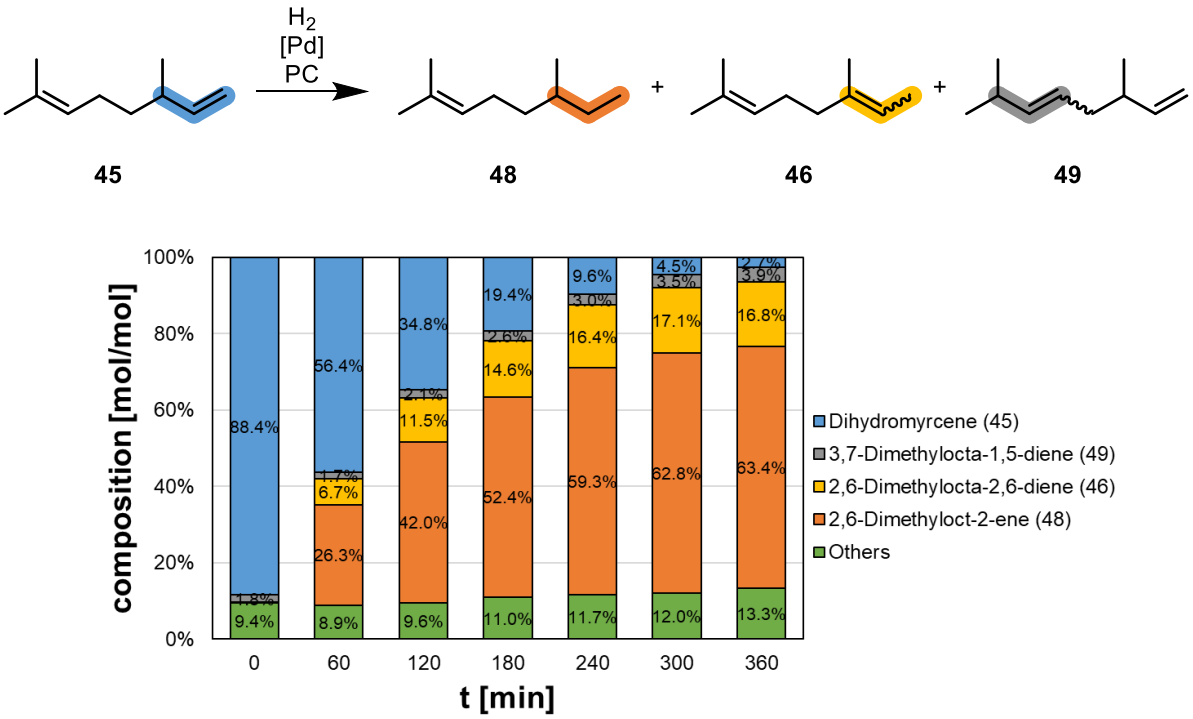


Figure 45: Reaction network and product composition of the selective partial hydrogenation of **45**. Conditions: $n_{substrate\ mixture}$= 456 mmol, $V_{total}$= 100 mL, S:C= 100,000:1, T= 50 °C, $f_{stirrer}$ = 3,400 rpm, $p_{H2}$= 10 bar, $w_{Pd,PC}$= 24 ppm, semibatch.

β-Farnesene (**50**) was investigated as a further terpene in selective partial hydrogenation. It contains the same structural motif as **14**, which consequently results in a 2:1:1 product composition too (internal:terminal:terminal, Figure 46) after selective partial hydrogenation with comparable Pd leaching. As expected, the reaction again terminates at full conversion of the conjugated system, showing 98.5% selectivity towards mono-hydrogenated products.

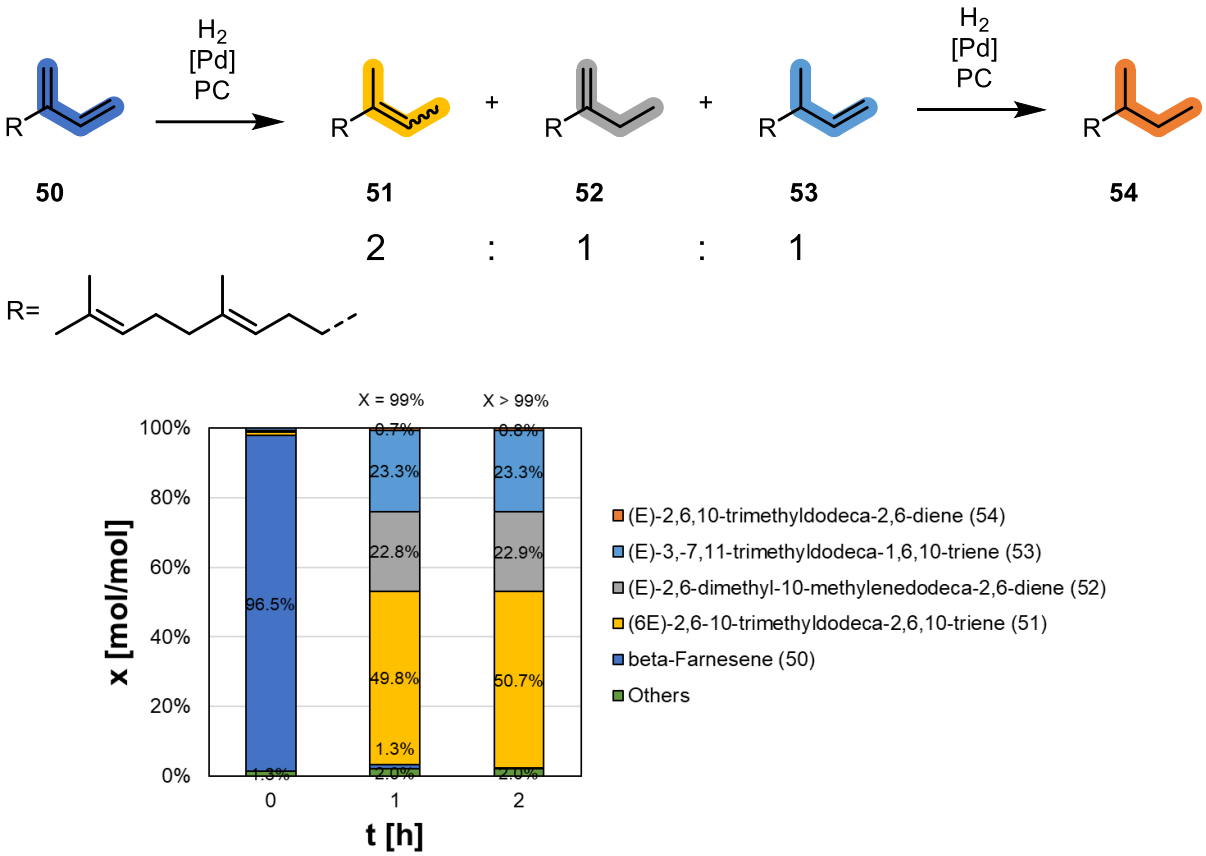


Figure 46: Reaction network and product composition of the selective partial hydrogenation of **50**. Conditions: $n_{substrate}$= 50 mmol, $V_{cyclohexane}$= 26.5 mL, S:C= 100,000:1, T= 50 °C, $f_{stirrer}$ = 3,500 rpm, $p_{H2}$= 10 bar, $w_{Pd,PC}$= 24 ppm, semibatch.

A crude farnesene mixture containing at least 33 unknown additional components can also be hydrogenated to a limited extent. Although many of the resulting products remain as unclear as their corresponding educts, $^1$H-NMR studies reveal the complete hydrogenation of conjugated double bonds within one hour (c.f. Figure S 7), while Pd leaching is comparable to the other reactions.

Limonene (**55**) was chosen as an example for cyclic terpenes, containing one endo- and one exocyclic double bond, serving as a typical model substance[91]. Typically, the exocyclic double bond is preferentially hydrogenated[91]. The results shown above indicate a strongly disfavored hydrogenation of double bonds with a degree of substitution of more than 2. The exocyclic, terminal double bond of limonene should therefore be hydrogenated preferentially[217]. Figure 47 shows that this is indeed the case, although isomerization of this double bond towards the ring or isomerization of the remaining double bond within the ring appears nearly equally, leading to full selectivity towards menthenes **58** and **59** after 26% conversion of **55** and its isomers **56** and **57**. Although S:C was already decreased from 100,000:1 to 10,000:1, any reaction appears at a reduced rate, resulting in a $TOF_{20}$ (regarding pure **55**) of 3,300 $h^{-1}$. In comparison to **45**, which also contains a terminal and a trisubstituted double bond, either the cyclic nature of **55** seems to inhibit its reactivity; or the fact that the terminal double bond is disubstituted instead of monosubstituted (in **45**) causes this phenomenon.

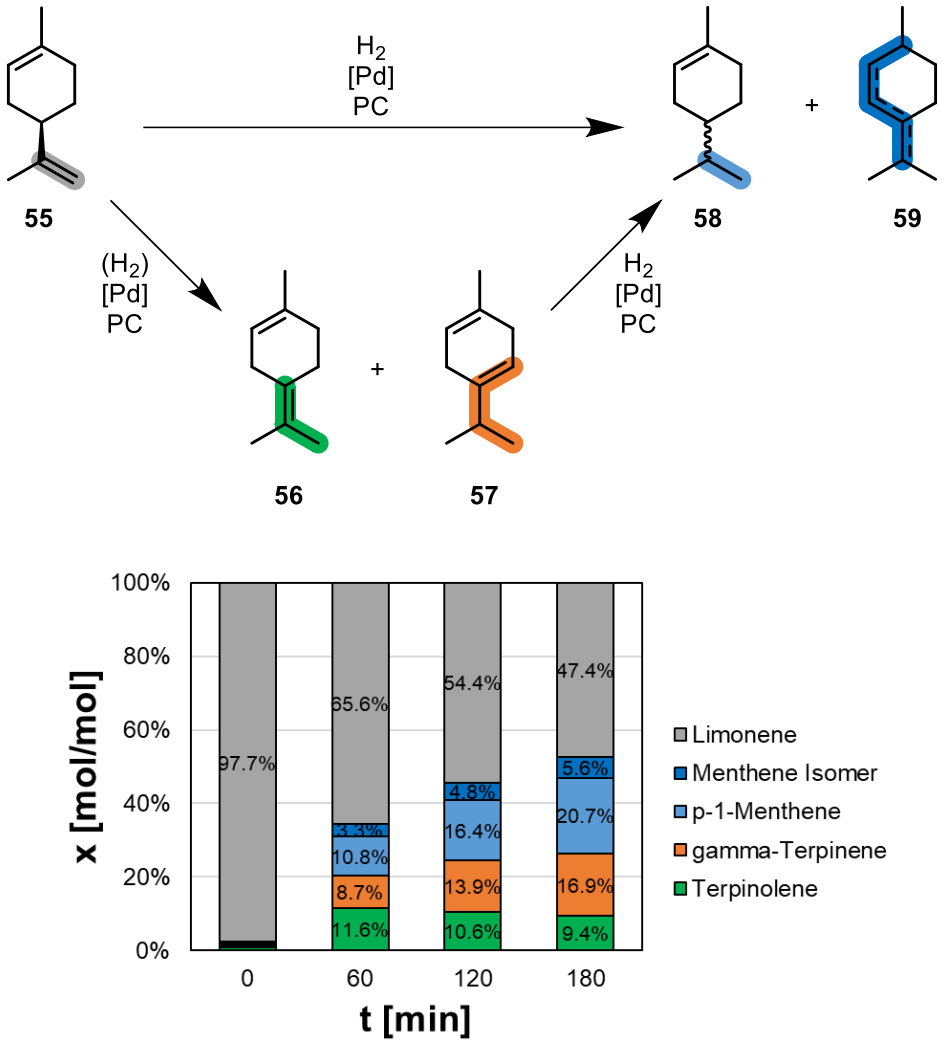


Figure 47: Reaction network and product composition of the selective partial hydrogenation of **55**. Conditions: $n_{substrate}$= 105 mmol, $V_{total}$= 55 mL, S:C= 10,000:1, T= 50 °C, $f_{stirrer}$ = 3,500 rpm, $p_{H2}$= 10 bar, $w_{Pd,PC}$= 24 ppm, semibatch.

### 6.3.5 Hydroformylation of Selectively Hydrogenated Terpenes

In chapter 2.2.2.2, the formation of stable η³-allyl complexes has been presented as the major issue in hydroformylation of terpenes containing conjugated double bonds, as well as of other polyunsaturated compounds. This major hurdle can be overcome by either a huge excess of $PPh_3$ ligand at high pressures, the use of dppe under specifically optimized conditions, or previous partial hydrogenation. Moreover, bulky phosphite ligands like tris(2,4-di-tert-butylphenyl)phosphite (**62**) promise high reactivities even for highly substituted substrates and natural compounds. As one solution to the described challenge is selective partial hydrogenation, the hydroformylation of formerly conjugated terpenes after selective hydrogenation was chosen to show the applicability of the obtained hydrogenation products in further functionalizations. The aliphatic product aldehydes are expected to be valuable fragrance compounds (Scheme 17)[103].

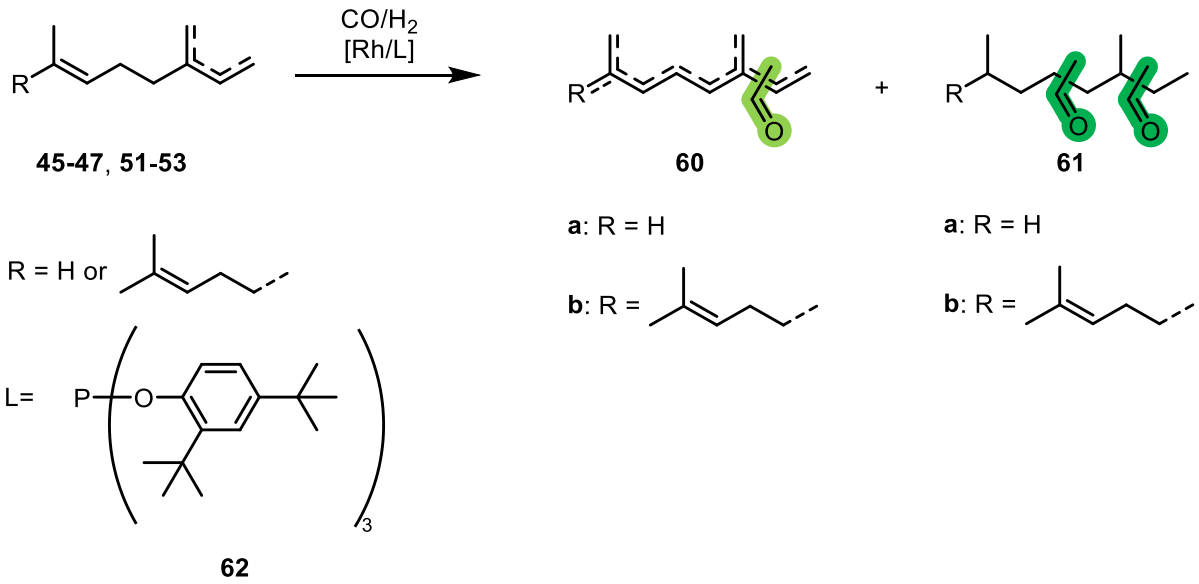


Scheme 17: Hydroformylation of partially hydrogenated β-myrcene or dihydromyrcene to mono- and dialdehydes.

Rh was chosen as the catalyst metal, with the ligand being the bulky phosphite **62**. Consequently, $Rh(acac)(CO)_2$ was used as a typical laboratory rhodium precursor. **45** serves as benchmark substrate, because it is commercially available. Initial reaction conditions were adapted from literature, from general conditions for this or closely related ligands, as well as from hydroformylation of other terpenes[50],[102],[116],[218].

β-Myrcene (**14**) and β-farnesene (**50**) expectedly show no product formation, but sometimes minor dimer formation due to catalyst deactivation caused by the presence of the conjugated double bonds. In contrast, conducting hydroformylation with the selectively hydrogenated acyclic terpenes (mainly resulting in **45-47** and **51-53**) under the same conditions yields mono- and dialdehydes with a rapid reaction within the first hour, followed by a reduced reaction rate (Figure 48).

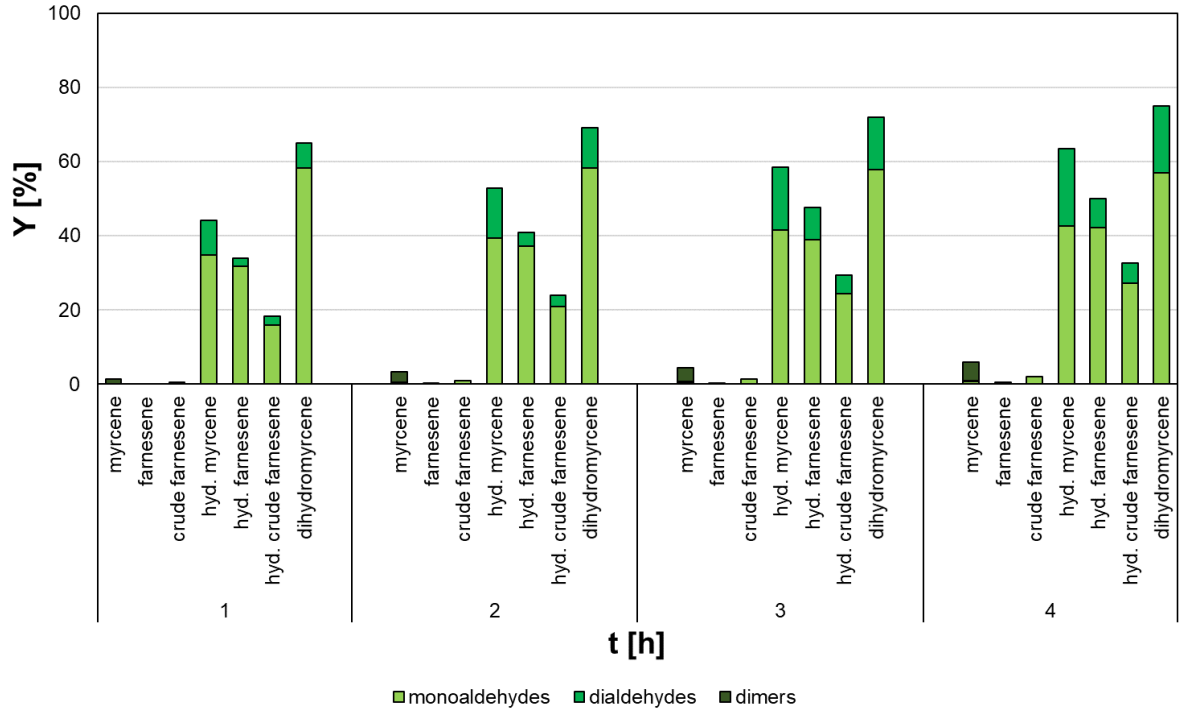


Figure 48: Product composition of the hydroformylation of unhydrogenated substrates and product mixtures of the selective partial hydrogenation of **14** and **50**, crude farnesene mixture and commercial **45**. Conditions: $n_{substrate}$= 34-40 mmol, T= 120 °C, $f_{stirrer}$ = 3,500 rpm, $p_{syngas}$= 45 bar, CO:$H_2$= 1:1, $c_{Rh,total}$= 0.8-0.89 mmol $L^{-1}$; S:C=1,000 ; P:Rh= 10; $c_{substrate,toluene}$= 1 mol $L^{-1}$; precursor= Rh(acac)$(CO)_2$; ligand= tris(2,4-di-tert-butylphenyl)phosphite, $t_{preforming}$=1 h, semibatch.

The comparison of the selectively hydrogenated products from **14** and **50** elucidates very similar yields for monoaldehydes of ca. 40%. The comparison of selectively hydrogenated **14** with commercial **45** gives slightly higher yields for **45**. This can be deduced to a higher amount of sterically easier accessible double bonds in **45** than in the product mixture of the selective partial hydrogenation of **14**. Especially in the latter case, the preferential conversion of isomers with any terminal double bond compared to internal ones is clearly visible in the measurements. Insights into the isomerization pattern in the case of **45** moreover reveal a fast depletion of terminal species towards isomerized species, mainly **46**.

For comparison, in the literature hydroformylation of **45** for the application as fragrance compounds, full conversion of **45** with a selectivity of at least 70% towards the linear monoaldehyde is achieved in a monophasic and a biphasic approach with different ligands and varying conditions, but in a comparable time[111],[114]. It has to be stated that unoptimized conditions were used in the present work, which demand optimization of reaction parameters to achieve quantitative aldehyde yields. In combination with the structure-related insights, the optimization study needs to enhance the isomerization of internal double bonds into terminal positions with a subsequent rapid hydroformylation. A ligand change might be necessary for this: For example, Biphephos was identified as a potent ligand for tandem isomerization-hydroformylation towards linear products, but the exploitation of its full potential required temperatures higher than 120 °C, which was applied here[219]. Although Biphephos is a bidentate ligand and has a rigid backbone, it is also a bulky phosphite ligand like **62**; hence, improvements in yield might also be possible with **62**, enabled by parameter screening.

Even the hydroformylation of the hydrogenated crude farnesene mixture enables higher aldehyde yields than without hydrogenation, attributable to the absence of conjugated double bonds. Hence, the selective partial hydrogenation enables the further functionalization of terpenes, like in hydroformylation, by eliminating conjugated double bonds. Thus, the combination of selective partial hydrogenation with subsequent hydroformylation is a highly valuable tool for the production of value-added chemicals from renewable resources without competition with food uses.

## 6.4 Conclusions

In this chapter, a highly active and selective hydrogenation catalyst system obtained by PLAL of Pd in PC is introduced. This innovative and easy-to-prepare system was shown not to require any further stabilizers or additives. The catalyst system is capable of selectively hydrogenating different substrate classes at high S:C ratios of more than 7,000 at Pd concentrations in the catalyst phase of 24 ppm and less in mono- or biphasic systems at mild conditions. The biphasic approach offers opportunities for the workup of the reaction mixture, aiming at a simplified catalyst reuse and product purification that need to be evaluated in future work.

Various alkynes with different structural motifs and industrial relevance were hydrogenated at room temperature with turnover frequencies at 20% conversion or less of up to 88,000 $h^{-1}$ and excellent trans/cis ratios of less than 0.09. While N-containing additives show no significant effect on selectivity, they slow down the reaction. Accordingly, they show no benefit and can be completely avoided. Different substituents in the vicinity of the triple bond seem to play a key role in alkyne hydrogenation, most probably by electronic effects. The catalyst system outperforms a typical Lindlar catalyst under comparable conditions by one magnitude in activity at improved selectivity.

In the hydrogenation of α,β-unsaturated aldehydes, laser-ablated Pd in PC showed a thermodynamically determined selectivity towards the saturated aldehydes. The aromatic substrate t-cinnamaldehyde is converted completely with a $TOF_{20}$ of around 2,500 $h^{-1}$, while the aliphatic t-2-octene-1-al gets fully converted much faster with a $TOF_{20,H2}$ of 26,600 $h^{-1}$ and a constant remarkably excellent selectivity of >99%.

Conjugated double bonds are preferentially hydrogenated as observed for some acyclic terpenes, most probably following a $\eta^3$-mechanism. Subsequently, the reaction terminates at nearly full conversion with selectivities towards mono-hydrogenated species of more than 96%. Only in the absence of conjugated double bonds, further hydrogenation is possible at reduced rates. Isolated double bonds, especially higher substituted ones, are more isomerized than hydrogenated.

Remarkably, product contamination with Pd in the case of biphasic reaction systems was always within the limit of quantification of the ICP-OES of 1 ppm. Therefore, the chosen catalyst system comprising laser-ablated Pd nanoparticles in PC is a versatile, robust, and highly selective hydrogenation catalyst and a lead-free alternative outperforming the Lindlar catalyst in environmental, manufacturing aspects,

and reaction performance. The Pd NPs show a high preference for conjugated systems and are of relevance for industrially applied substrates.

The subsequent hydroformylation of the selectively hydrogenated acyclic terpenes with a bulky phosphite ligand was shown for the first time. Under unoptimized reaction conditions, aldehyde yields of more than 60% were achieved, while unhydrogenated substrates showed only minor conversion. Furthermore, it was shown that the elimination of conjugated double bonds from a crude farnesene mixture with several unknown compounds enables those technical substrates for further value addition. Thus, several renewable materials are made available for further sustainable chemistry or direct use. This approach is the first example of an advanced reaction sequence, but an intermediate workup is still required. Nevertheless, these investigations lead in the direction of potential further reaction sequences for process intensification.

Further research should focus on investigations at the Pd catalyst surface to elucidate structure-effect relationships for a better understanding of the reaction mechanisms during partial hydrogenation and reaction rates of the individual substrates, especially in the case of conjugated dienes. For hydroformylation, the optimization of reaction parameters for increased aldehyde yield needs to be carried out, possibly in combination with a more selective synthesis of certain desirable product isomers.

# 7 Application of Laser-Ablated Pd Nanoparticles in Suzuki Cross-Coupling Reactions

**Author contributions:** The concept and ideas for this project were provided by me. PLAL was performed together with T. Fromme. TEM images were recorded by J. Jakobi. T. Holzberger performed microwave reactions as part of his apprenticeship under my supervision. M. Hubmann performed initial tests as part of his bachelor's thesis under my supervision. Further experiments, overall analyses, visualization, and writing were performed by me. T. Seidensticker acquired funding and supervised this project.

## 7.1 Introduction

The investigation of Suzuki couplings with both supported and unsupported Pd nanocatalysts is a vital research area and offers valuable applications for fine chemistry and pharmaceuticals, as already described in chapter 2.2.3.2[123]. In the previous chapters, the investigated Pd nanoparticles were shown to be highly active catalysts, while especially the laser-ablated NPs proved to be very versatile. In order to expand the application range of laser-ablated nanoparticles, the Suzuki coupling is selected for investigation as a representative example of a Pd-based catalytic reaction. Here, laser ablation is intended to serve as a reproducible complementary manufacturing method to expand the toolkit for the synthesis of Suzuki coupling catalysts and as an intensified nanoparticle synthesis method. As has been stated in chapter 2.2.3.2, numerous synthesis and stabilizing strategies of Pd nanoparticles for coupling reactions were invented and investigated. Many of the truly colloidal approaches use iodides as substrates mainly or exclusively, while broader substrate scopes are only rarely investigated[26],[121],[172],[195],[220]–[233]. Especially in light of the previous chapter that employed laser-ablated Pd NPs in PC, investigations by Lux demand a closer look. Here, Pd nanoparticles, generated via the autoreductive approach in PC, were used in a Suzuki coupling of 4'-bromoacetophenone with phenylboronic acid, achieving a yield of 63% at most after 24 h at 150 °C and a catalyst loading of 0.5 mol% Pd[172]. Furthermore, Reetz and coworkers synthesized Pd colloids (sometimes additionally stabilized) by several bottom-up and top-down approaches in PC, DMF, or dimethylacetamide (DMA). However, the PC-stabilized particles were applied only for Heck reactions and mainly stabilized particles in DMF and DMA were used instead for Suzuki couplings, for which they achieved high yields.[220],[221],[234] Apart from the "homeopathic Pd" approach mentioned in chapter 2.2.3.2, these two examples are the only candidates for truly ligand-free conditions without further stabilizers.

The choice of both the appropriate solvent and reaction conditions is crucial. Therefore, this chapter investigates several questions in a proof of concept: Are laser-ablated Pd NP capable of catalyzing Suzuki cross-couplings? Which solvent should be chosen for this task? Which base performs best? Can the reaction time be reduced without loss in yield? After the establishment of the basic catalytic system, several substrates are screened for their applicability, and light will be shed on the underlying catalytic mechanism.

## 7.2 Experimental

PLAL of Pd in pure BuOH with subsequent laser fragmentation of the obtained primary particles was performed twice in the setup described in chapter 5.2 with a Nd:YAG-laser (IS400-1-L, Edgewave) at a power output of 50 W, a wavelength of 532 nm, and a repetition rate of 5 kHz. Again, the Pd concentration (in ppm, w/w) of the obtained solutions was measured using ICP-OES prior to first use as described in chapter 4.3.

Experiments on Suzuki couplings were performed under reflux or microwave conditions. The catalyst solution was sonicated for at least 3 min. prior to use. Eventually, 1-butanol was removed in vacuo to reach the desired Pd content. For experiments under reflux, the solid substrates were weighed into an argon-flushed round-bottom flask. Subsequently, all liquids were introduced via Eppendorf pipettes. The flask was shaken, and a cross-shaped magnetic stirrer bar was added; then it was installed at the reflux condenser. Experiments under argon atmosphere were carried out using standard Schlenk techniques and included the use of an additional stopper for the reflux condenser that allowed flushing with argon. The flask was heated under stirring using a heating plate, and the reaction started after the desired temperature was reached. For experiments with mercury, 4 h of reaction time were allowed; after that, 2,000 eq mercury were added through a side neck that also allowed sampling prior to mercury addition. For the adsorption test with alumina, 1.5 g of alumina was stirred for 4 h together with the catalyst solution, filtered through a glass frit and a syringe filter, before the required amount of filtrate was introduced into a fresh vessel with a fresh stirrer bar for the reaction in the standard manner in the microwave reactor. In a second run, the whole alumina with adsorbed Pd was used as catalyst in the standard manner, again in a fresh vessel and with a fresh stirrer bar.

Reaction solutions in the microwave vessel were prepared in the same way as for reflux in a corresponding microwave flask of a CEM Discover 2.0. After the addition of all substances, argon was again used to flush the vessel that was sealed afterwards and transferred into the microwave reactor. Here, the reaction was carried out at 130 °C for 2.5 h under stirring. For quantitative poisoning experiments, stock solutions of $PPh_3$ or octanethiol in BuOH were prepared, in the case of $PPh_3$ according to standard Schlenk techniques.

Samples were analyzed using a calibrated GC-FID. For detailed information on sample preparation and analysis, see chapter 11.4.2.

## 7.3 Results and Discussion

### 7.3.1 Selection of a Solvent

For solvent selection, criteria apart from pure solubility, such as safety, cost, environmental compatibility, physicochemical properties, and the remaining amount in the product, are essential[235]. In the present case, appropriate stabilization of the NPs is also a major requirement. Typical solvents for Suzuki couplings include water-miscible alcohols, ketones, ethers, and carboxylic acid amides, as well as

dioxane, DMF, or aromatic compounds[236]. Furthermore, ionic liquids (ILs) and fluorinated solvents have already been employed for Suzuki reactions with colloidal nanoparticles[226],[237]. Various solvents have been evaluated regarding the aforementioned criteria, with a resulting recommendation of short-chain alcohols[235],[238].

It is crucial that the solvent can at least dissolve all involved educt compounds, including the Pd catalyst (and its stabilizer or ligand if needed), the base, and both substrates. Especially for inorganic bases, this may necessitate the addition of water. In this work, the system is designed to be as simple as possible, utilizing solvent-stabilized Pd nanoparticles produced by laser ablation, and should require neither additional stabilizers nor ligands. It should moreover allow for a precise adjustment of the catalyst concentration before the reaction and a good separability after the reaction. Ideally, it should also be a "green" solvent.

As a consequence, two major options appear (c.f. Figure 49). The first one is the utilization of apolar substances like toluene, to provide good solubility for organic compounds. As a downside, these compounds offer only poor stabilization for solvent-stabilized nanoparticles[22]. The other option is the use of very polar compounds such as ethanol or water. They enable good separability, but may lack effective stabilization, depending on the exact nature of the solvent[22]. However, organic solvents show limited solubility of inorganic bases with cations up to period 4 in the periodic system of elements. On the contrary, most bases are well water-soluble, but PLAL in water can lead to significant oxidation[27]. As a consequence, a trade-off between these two extremes must be made and can be found in 1-butanol.

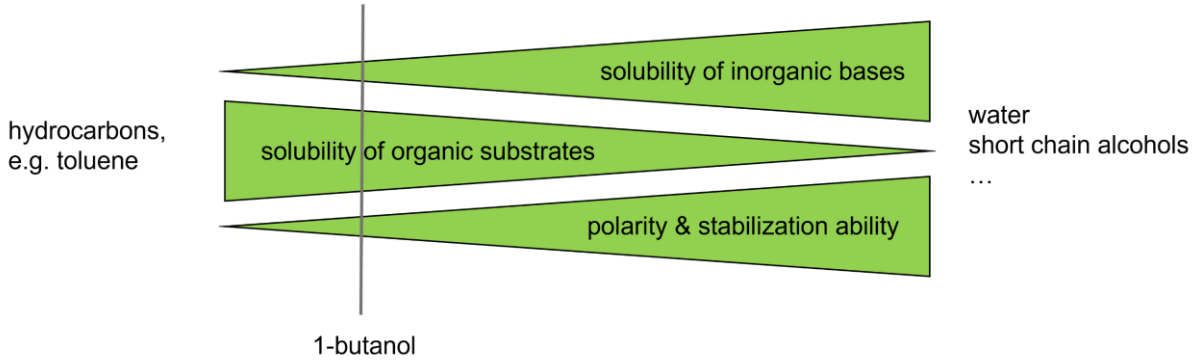


Figure 49: Options for solvent selection for Suzuki couplings.

1-Butanol (BuOH in the following) is environmentally friendly, may be produced from renewable resources, and can thus be classified as "green" solvent[238][171]. It is miscible with nearly all organic solvents and is partially miscible with water[171]. Also, it can be evaporated without major effort, allowing simple product purification as well as adjusting catalyst concentration in case the Pd concentration is originally too low, as long as Pd remains stabilized. While BuOH is a promising solvent from these aspects and fulfills the criteria for beneficial solvents, only two reports featuring BuOH as a solvent in Suzuki coupling were found, both focusing on coupling reactions with heteroaryl halides[239],[240].

Consequently, BuOH was chosen as the solvent for the following investigations. The particles obtained by PLAL in pure BuOH were analyzed by TEM and possess a mean diameter of 3.8 ± 1.6 nm (see also Figure 27). The concentrations were found to be 30 ppm and 48 ppm as measured by ICP-OES, depending on the laser operation time. The obtained catalyst solutions are not as stable as Pd in PC and thus can only be used for a shorter amount of time, since the already present agglomerates begin to grow and aggregate (c.f. Figure 50). These solutions are not catalytically active anymore, even after ultrasonication.

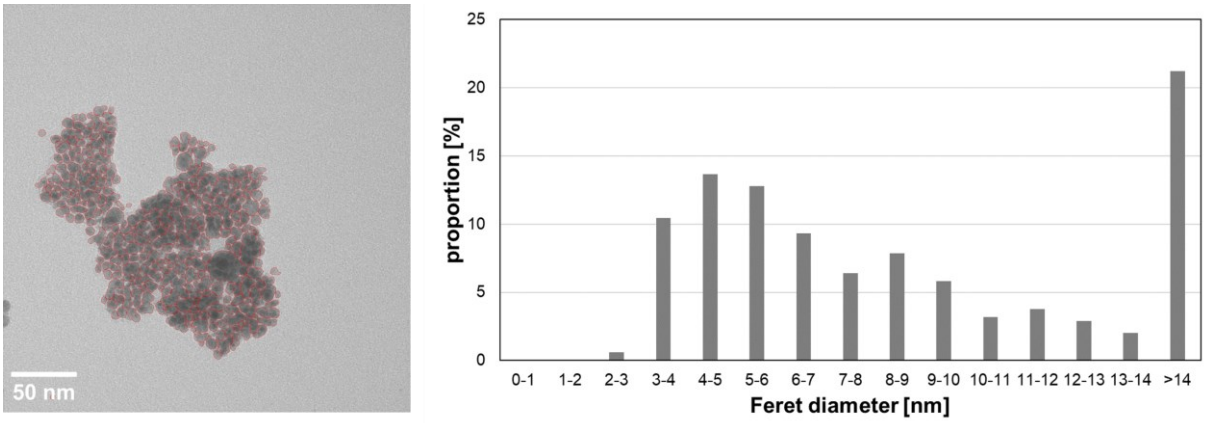


Figure 50: TEM images of laser-ablated Pd in BuOH after longer shelf-life and resulting particle size distribution, obtained by the count of the particles with red surrounding.

## 7.3.2 Establishing Reaction Conditions

To find suitable reaction conditions, the reaction of 4'-bromoacetophenone **64a** with phenylboronic acid **63** was chosen, since this system performs well with several other catalyst species[121],[195],[220],[225],[228]. First, a base screening was performed with 40 ppm Pd in BuOH (as a trade-off between stability and solvent amount) under reflux conditions at 80°C, resulting in a catalyst loading of 0.32 mol% (equivalent to a S:C ratio of 313; Scheme 18) for the 1 mmol batch.

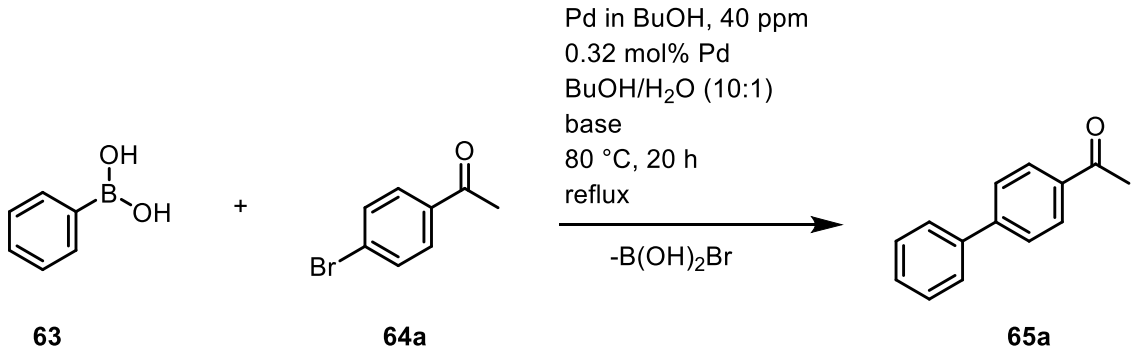


Scheme 18: Reaction scheme for the base screening.

Here, the solubility of the inorganic bases in BuOH was too low, so water was added in a volumetric ratio of 10:1 (BuOH:water) to increase the polarity. Related experiments confirm these conditions as a

reasonable compromise between substrate solubility, dilution, particle concentration, stabilization, and catalytic activity in terms of the S:C ratio.

Under the chosen reaction conditions, a monophasic system forms, while after cooling, a small second phase begins to appear, which contains mainly water. Furthermore, the base starts to precipitate, and Pd deposits form on the glass wall. Nevertheless, with an appropriate base, full conversion of the substrate can be achieved within the reaction time of 20 h, as evident from Table 10.

Table 10: Yields of **65a** in the base screening of **64a** with **63**. Conditions: $n_{substrate}$= 1 mmol, $n_{boronic\ acid}$ = 1.5 mmol , $n_{base}$= 2 mmol, S:C= 313:1, T= 80 °C, $V_{BuOH}/V_{water}$ = 10, $w_{Pd,BuOH}$= 40 ppm, t= 20 h, reflux. a: averaged from two single runs.

| base | Y [%] |
|---|---|
| **$K_2CO_3$** | >99 |
| **$Na_2CO_3$** | >99 |
| **$Cs_2CO_3$** | 78 |
| **KOH** | 61 |
| **NaOAc** | 64 |
| **$NaHCO_3$** | 53[a] |
| **NaOH** | 48 |
| **$NEt_3$** | 3 |

Carbonates are shown to perform best, with $K_2CO_3$ resulting in the highest reactivity, along with $Na_2CO_3$. For further reactions, $K_2CO_3$ was chosen as the base because of its superior solubility under the given reaction conditions. With $K_2CO_3$, even a second catalytic run is possible: after addition of fresh substrates to a spent reaction mixture, the reaction proceeds with only slightly decreased yield of 94% after 20 hours. This is remarkable, because even after the first run, black deposits were observable on the glass wall, resulting in a continuous decrease of the Pd content in solution as confirmed by ICP-OES analyses: the Pd content of the solution after the first run was 7 ppm (full stability should result in 33 ppm), which decreased to 2 ppm after the second run. This observation raises the question of the true catalytic species, which will be answered below.

These results confirm the principal applicability of solvent-stabilized, laser-ablated Pd nanoparticles in BuOH for Suzuki coupling reactions. However, the long reaction times pose a drawback. This fact, in combination with the non-inert conditions applied until now, results in the formation of the by-products phenol and biphenyl through slow oxidation of the excess of phenylboronic acid **63** by oxygen from air according to Scheme 19.

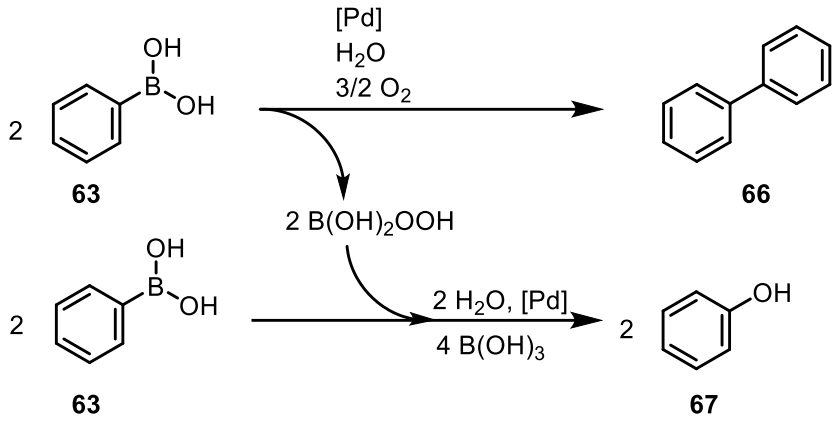


Scheme 19: Homocoupling of **63** with oxygen and subsequent phenol formation[241].

Related experiments confirm that the reaction time of 24 h cannot be substantially lowered under reflux conditions. Therefore, the process needs to be intensified through a different measure. As a result, microwave irradiation was chosen for drastic enhancements in productivity and activity. In pre-experiments, optimal reaction conditions for the microwave reactor were determined, once for the already applied substrate **64a** (giving quantitative yields) and for comparison also with **64b**, a more challenging substrate. The obtained yield of **65b** was 9% in reflux and 14% in the microwave reactor after only one eighth of the reaction time, showcasing that comparable or even better results can be achieved under microwave conditions. Furthermore, the reaction is conducted in closed vessels in the microwave that can be inertized with argon prior to the reaction, minimizing the formation of by-products. This approach accelerates reaction rates by a kinetic method without changing the reaction mixture and is therefore part of process intensification, located at the phase level.

### 7.3.3 Substrate Screening

After successful implementation of this process-intensification measurement, a substrate scope was carried out, investigating the influence of leaving groups and different substituents of the aryl halide (Scheme 20). The catalyst system tolerates several substituents, although the arylbromides are severely less active than their iodide counterparts. This is observable from the poor yields of the bromides (with the only exception being the originally applied **64a**), and especially the difference in the yield applying the phenol derivatives **64d** and **64g** and toluene derivatives **64e** and **64h**. The superior reactivity of the iodides over their bromide analogues is expected from the literature, since the iodide is the better leaving group[13]. A clear trend regarding the reactivity of structural motifs for aryl bromides is becoming apparent. The electronic effects of the different substituents seem to play a significant role: all arylbromides with electron-donating substituents perform poorly, while the only electron-deficient arylbromide **64a** can be converted quantitatively. To substantiate this hypothesis, further experiments with arylbromides containing electron-withdrawing substituents would be necessary. Nevertheless, similar results were observed for arylbromides in the “homeopathic Pd” approach by de Vries and co-workers[121]. Mechanistically, the approximation of the aromatic ring towards the $Pd^0$ is discussed as a

prerequisite to the subsequent oxidative addition of the arylhalide[242]. For electron-deficient aromatic systems, the subsequent oxidative addition to the $Pd^0$ might thus be favored due to the more electrophilic character of these substrates against electron-rich systems. Literature confirms aryl iodides and aryl bromides with electron-withdrawing groups as especially suited for ligand-free cross-couplings[29]. In summary, the obtained results are in alignment with the literature, but the observable effect is severe for this specific catalyst system.

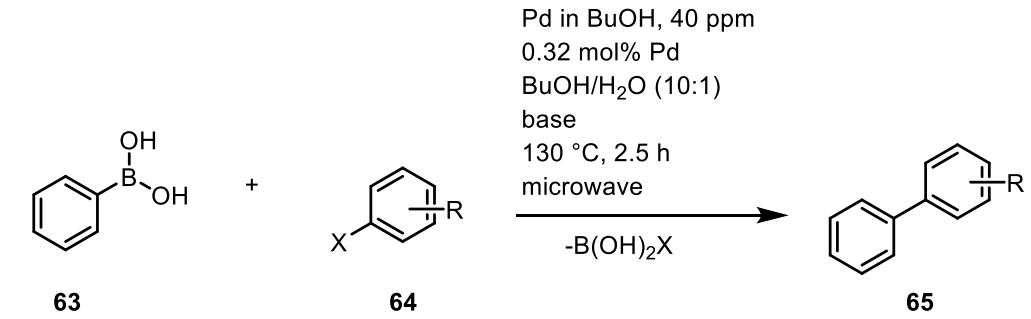


**63** **64** **65**

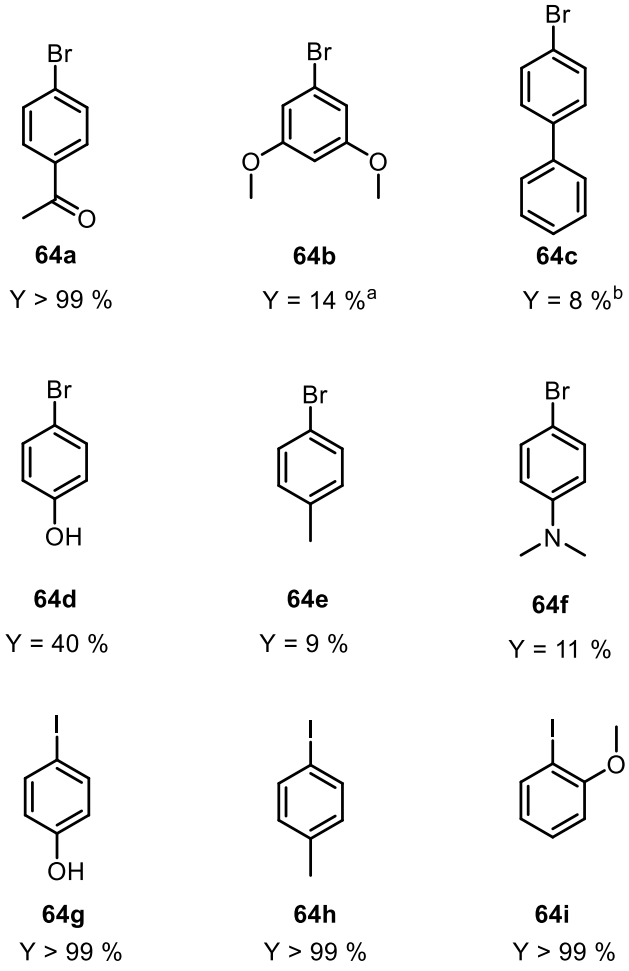


**64a** Y > 99 %

**64b** Y = 14 %[a]

**64c** Y = 8 %[b]

**64d** Y = 40 %

**64e** Y = 9 %

**64f** Y = 11 %

**64g** Y > 99 %

**64h** Y > 99 %

**64i** Y > 99 %

Scheme 20: Substrate scope of the Suzuki coupling with **63**. Conditions: $n_{substrate}$= 1 mmol, $n_{boronic\ acid}$ = 1.5 mmol , $n_{base}$= 2 mmol, S:C= 313:1, T= 130 °C, $V_{BuOH}/V_{water}$ = 10, $w_{Pd,BuOH}$= 40 ppm, t= 2.5 h, microwave. a: confirmed by both GC-FID and $^1$H-NMR; b: additional homocoupling of the substrate to give p-terphenyl observed.

In comparison with other literature on Suzuki couplings under reflux conditions with aryl bromides and colloidal Pd NPs, the presented approach occupies an intermediate position in terms of yields, activity and applicability: Especially dendrimer-stabilized Pd NPs and the homeopathic system can convert similar substrates with lower Pd loadings of 0.06 mol% to 0.02 mol% in the same time frame or less (for comparison: 0.32 mol% are used in this work)[121],[195],[225]. Several other Pd NPs also enabled good to excellent yields for aryl bromides with varying reaction times and catalyst loadings, and thus are only hardly comparable[226],[228],[230]–[232]. Still, it has to be kept in mind that the microwave approach is compared with reflux conditions. For the comparison of the conversion of iodides with other colloidal approaches from literature, the investigated catalyst system can indeed compete with them and often outperforms them[26],[222],[223],[227]. Especially the interplay of short reaction times due to microwave irradiation in combination with the low Pd loading of 0.32 mol% is beneficial. In any case, the presented system outperforms autoreductive Pd NPs in PC in terms of catalyst loading and achievable yield, even at lower temperatures[172].

### 7.3.4 Investigation of the Catalytic Species

In an attempt to answer the question about the nature of the true catalytic species, a combination of several tests was performed for the reaction of **64a** with **63**. At first, quantitative poisoning tests were carried out with 1-octanethiol in the microwave reactor. As the amount of active Pd species may be changing in the case of dynamic catalysis, no definite number of equivalents of poison can be estimated, although typical values are in the range of 0.1-0.2 eq for truly heterogeneous catalysts[31],[117]. Therefore, two different thiol:Pd ratios were tested: after the addition of 1 eq of octanethiol, no catalytic activity was observable. Even after the addition of only 0.2 eq, a reduction of the activity to 54% yield in the same reaction time was observable. Since this yield is still considerably high, neither a true heterogeneous nor a true homogenous pathway is confirmed. Similar results are obtained after the addition of $PPh_3$: here, the addition of 0.1 eq $PPh_3$ gives 81% yield, which is very similar to the yield of 84% obtained for 0.2 eq $PPh_3$. Even after the addition of 0.5 eq $PPh_3$, 70% yield remains. Accordingly, less than 0.5 eq of $PPh_3$ is not able to suppress the reaction. Since an often used active species for Suzuki couplings is $Pd(PPh_3)_2$, opposing effects come into play during quantitative poisoning with $PPh_3$: while some proportion of the $PPh_3$ might indeed poison heterogeneous Pd particles, another proportion might be able to enhance the reaction rate of possible single Pd atoms in solution by formation of active catalyst complexes. It was confirmed in the Suzuki coupling of the challenging substrate **64b** with **63** using in situ synthesized $Pd(PPh_3)_4$ under inert reflux conditions at 100 °C that the yield can be increased from 28% for the laser-ablated NPs to 68% for the homogeneous system. Thus, the result of $PPh_3$ poisoning test is ambiguous and does not allow for precise statements on the character of the active species.

A qualitative poisoning test under reflux conditions with 2,000 eq mercury (as proposed by literature[32]) that was introduced at a reaction time of 4 hours under vigorous stirring does not allow for a subsequent increase in yield, although the initially obtained yield after 4 h was less than expected from pre-experiments. Nevertheless, control reactions confirmed the known reactivity of the catalyst solution. From this experiment, it can only be concluded that indeed a $Pd^0$ intermediate is apparent during the

reaction, but no statement can be made regarding the location or any further chemical environment of this intermediate species[117].

As a last test, an adsorption test on alumina was performed. For this test, the catalyst solution was stirred for 4 h with alumina, after which a subsequent filtration through a glass frit was carried out. The filtrate and the alumina residue were both used for catalytic tests in the microwave reactor, which enabled a quantitative yield. An ICP-OES measurement of the filtrate confirmed less than 1 ppm in solution, which is below the limit of quantification. Hence, filtration/adsorption was shown to be effective, at least for large particles. Of course, very small particles in the size of clusters or even single atoms may not be effectively filtered off; thus, this test clearly points towards sub-nanoparticle or homogeneous catalysis.

When considering all the different applied tests, it shows that for the applied Suzuki coupling with laser-ablated Pd nanoparticles, neither a true homogeneous nor a true heterogeneous pathway is plausible. Instead, the often applicable mechanism described by de Vries[120],[121] (Figure 51) can explain all results and thus is highly likely to proceed. In this mechanism, the NPs serve as a reservoir for leaching Pd single atoms that undergo the catalytic cycle ligand-free in the medium. The particles tend to form inactive Pd black that was also visible at the glass walls of the reaction vessels, while only a very small amount of remaining soluble Pd is sufficient for catalytic activity. The sensitivity of the activity to long storage times can also be explained by this mechanism. It furthermore allows to explain the superior performance of preformed $Pd(PPh_3)_4$: here, all Pd atoms are directly catalytically accessible, thus the total amount of active Pd is higher and the time delay for leaching of active species is omitted.

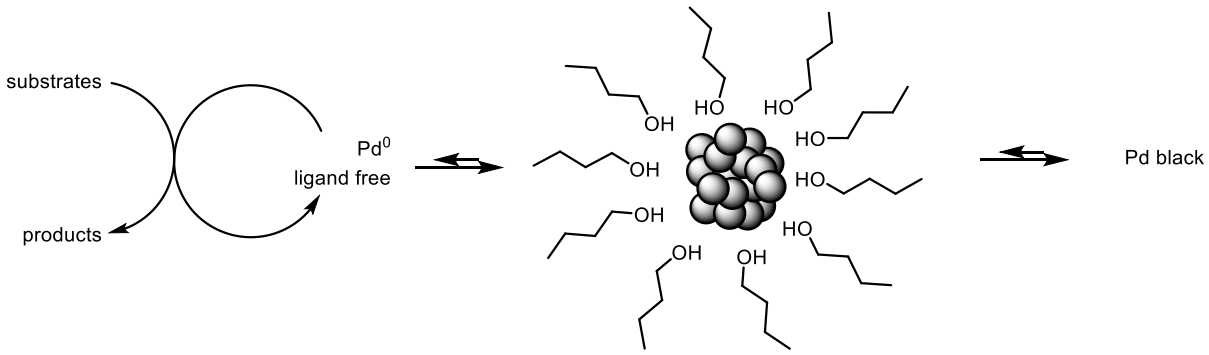


Figure 51: Formation of catalytically active species in the Suzuki coupling with laser-ablated Pd nanoparticles in BuOH, with the particles serving as a reservoir for leaching Pd single atoms, adapted from de Vries[121].

In comparison to all reactions from previous chapters, this behavior is unique. Although corresponding tests were not performed for the other reactions, literature-known heterogeneous hydrogenation mechanisms and literature-known structure-specific activity relationships match all observations and thus do not suggest that the hydrogenations proceed via soluble Pd single atoms. Furthermore, the hydrogenation activity and selectivity of the other catalyst solutions are not affected by prolonged storage. However, for a final statement, comparable tests would need to be performed for each catalytic system.

## 7.4 Conclusions

In this chapter, the Suzuki coupling with solvent-stabilized, ligand-free, laser-ablated Pd NP in the rarely applied “green” solvent BuOH was shown for the first time. With these findings, the toolbox for the production of Suzuki coupling catalysts is extended by laser-ablated Pd NPs in a green solvent without the need for any further stabilizers. At the same time, the applicability of laser-ablated Pd NPs is expanded by another reaction.

Reaction conditions were optimized for the model substrate 4’-bromoacetophenone. The choice of a carbonate base like $K_2CO_3$ enables quantitative yield. The incomplete solubility of the inorganic bases in BuOH necessitates the addition of small amounts of water. To increase productivity, the reaction was transferred into a microwave reactor, allowing to reduce the reaction time from 20 hours to 2.5 hours while achieving comparable yields. This measure contributes to process intensification on the phase level.

In a subsequent substrate scope, strong dependencies were not only observable in terms of the halide on the achievable yield. Rather, within the arylbromides, all substrates with electron-donating substituents are only converted poorly, whereas the only substrate with electron-withdrawing substituents was converted quantitatively. This is attributable to electron density in the aromatic ring, affecting the initial oxidative addition to the catalyst. Further research might strengthen this finding in a broadened substrate scope, including other substrates with electron-withdrawing substituents in combination with a Hammett-plot. Furthermore, the applicability of boronic acids other than the simple phenylboronic acid can be investigated. While the catalyst system cannot compete with certain specialized literature-known colloidal systems, comparison with further literature is hardly feasible due to strongly varying reaction conditions. Nevertheless, laser-ablated Pd NPs present an improvement over the autoreductive Pd NPs in PC investigated by Lux and show excellent conversion of iodides at comparatively low Pd loadings[172].

Ultimately, several tests elucidated that very likely the nanoparticles themselves are not directly taking part in the catalytic cycle. Rather, they serve as a reservoir for leaching Pd single atoms that enable product formation.

# 8 Combining Partial Hydrogenation of Soybean-Derived Biodiesel and Methoxycarbonylation Using a Single Palladium Source

This chapter was published as

F. Lehmann, H. W. Wegener, N. Brede, T. Seidensticker, “Combining Partial Hydrogenation of Soybean-Derived Biodiesel and Methoxycarbonylation Using a Single Palladium Source”, *Eur. J. Lipid Sci. Technol.* **2025**, *127*, e70073, DOI: 10.1002/ejlt.70073.

Citation style and numbering, as well as Figure and Table numbering, were changed to a sequential mode to fit the document style.

**Author contributions:** The concept, ideas and most of the experiments for this project were provided by H.W. Wegener and me. N. Brede contributed isomerization experiments in the Supporting Information as part of his master’s thesis under the supervision of H.W. Wegener. Manuscript preparation including formal analyses, writing, and visualization was performed by me. T. Seidensticker acquired funding, supervised this project, and reviewed and edited the manuscript.

## 8.1 Abstract

Valorization of soybean-derived biodiesel through an integrated tandem one-pot approach was examined. Recent studies have indicated the necessity of pretreating unsaturated fatty acid methyl esters (FAMEs) to remove polyunsaturated FAME (PU-FAME), due to their inhibitory effect on various homogeneous catalyzed reactions. The first step in the process under investigation involves the selective partial hydrogenation of PU-FAME towards monounsaturated FAME (MU-FAME), catalyzed by palladium nanoparticles in methanol. This is followed by the Pd/1,2-bis[(di-tert-butylphosphino)methyl]benzene (1,2-DTBPMB)-catalyzed isomerizing methoxycarbonylation (iMC) of MU-FAME, resulting in a linear $C_{19}$-diester. Utilizing the protonated derivative of the 1,2-DTBPMB ligand for the iMC, the Pd nanoparticles employed in the hydrogenation step function as a catalyst precursor. The combination of both reactions in a tandem one-pot approach would eliminate the need for a work-up, thereby streamlining the process. However, the process is hindered by several challenges arising from the contrary optimal operating conditions for both reactions, such as the selection of solvent, the amount of catalyst, and the presence of the accompanying gas in the reaction mixture. These aspects have been thoroughly examined in this study, leading to the development of an optimized reaction workflow. Utilizing this method, the partial hydrogenation of soybean FAME is achieved with conversions of 95%–98%, followed by the in situ formation of the homogeneous catalyst and the iMC, yielding a linear $C_{19}$-diester with a selectivity of 98%.

*Practical Applications:* This study proposes a novel integrated tandem one-pot approach for the selective partial hydrogenation of vegetable FAME to MU-FAME, followed by the homogeneously catalyzed iMC.

The integration of Pd nanoparticles as both a catalyst for hydrogenation and as a precursor for the formation of a homogeneous catalyst utilized in iMC ensures the efficient utilization of the metal throughout the whole reaction sequence. The method integrates the necessary pretreatment with sequential functionalization under optimized conditions.

## 8.2 Introduction

With the growing demand for climate-neutral productions and products, bio-based plastics offer a promising avenue for incorporating renewable resources into everyday consumables. Notably, unsaturated fatty acid methyl esters (FAME) hold significant potential due to their aliphatic chain structure, which resembles polyethylene[243].

In related studies, several homogeneously catalyzed functionalization reactions and their capability to transform FAME into polymer precursors have been studied[12]. For instance, the isomerizing methoxycarbonylation (iMC) of methyl oleate enables direct access to linear diesters through a complete atom economic reaction[244].

However, recent studies have demonstrated that natural polyunsaturated FAME (PU-FAME) exhibit significant inhibition of the reaction, necessitating their removal to ensure efficient conversion of monounsaturated FAME (MU-FAME)[12],[97]. To achieve high conversions it was shown that selective partial hydrogenation of FAME derived from cheap oils like soybean and canola enables the use of those substrates of former highly unsaturated oleochemicals in functionalization reactions like the iMC or hydroformylation[12]. The whole presented process was a two-step approach.

One highly promising but underrated catalyst system for the selective partial hydrogenation of fatty acids and derivatives is already literature-known: Colloidal Pd nanoparticles stabilized in different organic solvents were used that superseded the need for further stabilizing agents or supports. Propylene carbonate (PC) as a stabilizing solvent showed high activities and selectivities at full conversion under mild conditions[68],[70]. Later, a simplified synthesis route to solvent-stabilized Pd nanoparticles was published, confirming PC as one of the solvents of choice[22].

In principle, numerous catalyst systems for the selective hydrogenation of fatty acid derivatives are known, resulting from attempts to produce and upgrade biodiesel for combustion purposes. In general, the highest hydrogenation activity is achievable by applying Pd-based catalysts, although Pd also shows the highest isomerization activity compared to other metals[62],[67].

The iMC of MU-FAME is a well-investigated process applying the well-known Pd/1,2-bis[(di-tert-butylphosphino)methyl]benzene (1,2-DTBPMB) catalyst and its isomerization activity to produce linear α,ω-diesters[96],[99],[100],[245],[246]. Mecking et al. were able to show that the protonated version of the usually applied ligand 1,2-DTBPMB, 1,2-DTBPMB$(OTf)_2H_2$, is capable of disintegrating Pd bulk metal with different surface morphologies and sizes of several tens of nanometers in order to form homogeneous Pd complexes active in the iMC of technical grade methyl oleate[95].

Following these findings, Pd seems to be the ideal metal for combining selective partial hydrogenation of FAME with followup iMC. As this is until now a two-step approach including workup of the biphasic reaction mixture of the hydrogenation step, we envisioned a one-pot assisted tandem reaction starting from in situ synthesis of Pd nanoparticles, selective partial hydrogenation followed by addition of protonated ligand and iMC of the hydrogenation product mixture to simplify the reaction system (Scheme 21). This comes with the additional benefit that fresh precious Pd must not be used for each step individually, but the same amount is rather used twice. In this work, the general compatibility ofthe two reactions, possible hurdles, and strategies to overcome those will be examined.

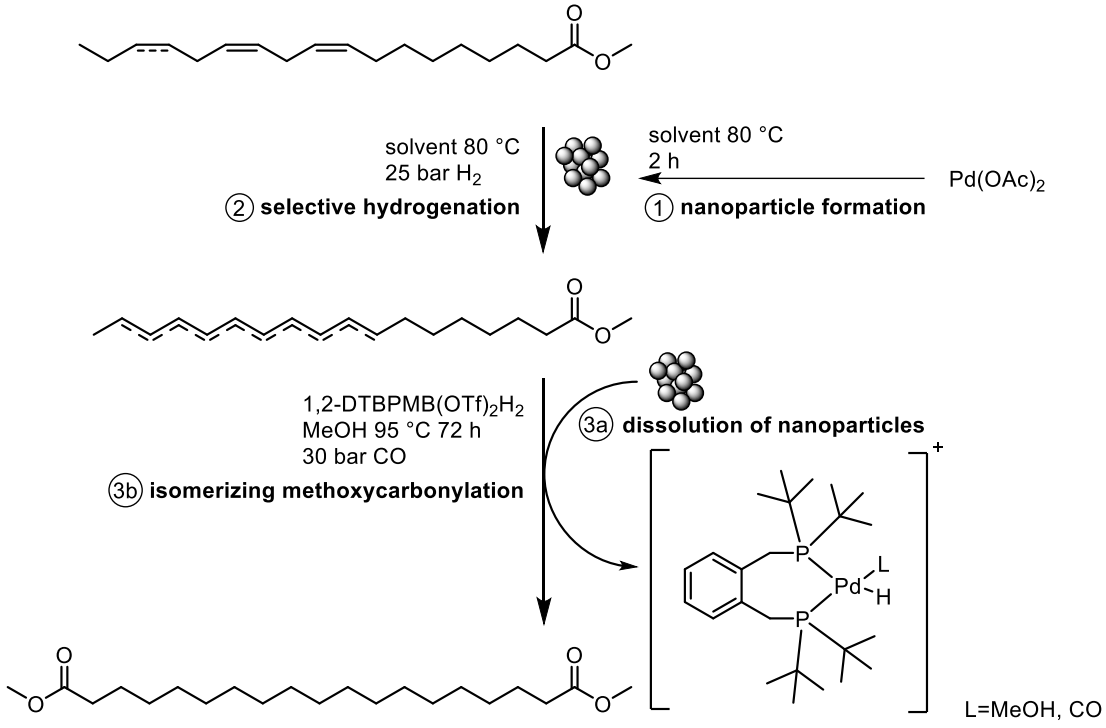


Scheme 21: Envisioned tandem catalysis route of selective FAME hydrogenation followed by isomerizing methoxycarbonylation. Numbers in circles represent individual reactions in the experimental procedure.

Waste oils would pose a desirable resource with regard to multiple material usages but may contain several potentially undesired byproducts and potential catalyst poisons like other heavy metals or insolubles[247]. Impacts of reaction conditions on a clean and defined substrate are of fundamental interest. Consequently, as an established, inexpensive, and abundant substrate, FAME derived from soybean oil will be investigated. As it is industrially prepared from grown plants without former usage, it is not assumed to contain potentially disturbing residues. This readily available substrate contains high amounts of PU-FAME with 53% C18:2 and even ca. 8% C18:3, thereby being a highly unsuitable substrate for sole iMC. By the envisioned process, valorization of this promising substrate shall be improved.

## 8.3 Materials and Methods

All tandem reactions and iMCs were handled using standard Schlenk techniques; sole hydrogenation experiments were conducted without degassing in accordance with the literature[68],[70]. The protonated ligand was prepared according to known methods[248]. MeOH was dried over $Na_2SO_4$ and degassed for 30 min in an ultrasonic bath under constant argon flow prior to use. All substrates were freshly purified from peroxides using neutral alumina and then degassed for 30 min in an ultrasonic bath under constant argon flow. Reactions with standard mixing behavior were conducted in a 75-mL stainless steel pressure reactor with a cross-shaped stirring bar; reactions with enhanced mixing behavior were conducted in a 125-mL stainless steel reactor with an overhead gas injection stirrer. Both reactors were equipped with dropping funnels. In a typical (tandem) catalysis experiment, $Pd(OAc)_2$ was weighed into the vessel, and the reactor was sealed. It was cautiously purged with argon, and a vacuum was applied afterwards for a total of three cycles. A volume of 20 mL MeOH was added via a syringe in argon counterflow, then 9 bar argon was applied, and heating to 80 °C started under constant stirring at 1100 rpm. At the desired temperature, preforming was started for 2 h. Afterwards, the reactor was cooled down to room temperature in an ice bath, vented, and the substrate was introduced via a syringe in argon counterflow into the dropping funnel. Hydrogen was added to the desired pressure, and the temperature was set again to 80 °C. After reaching reaction temperature, the substrate was added, and the hydrogenation started. After the desired reaction time, stirring was stopped, and the reactor was cooled to room temperature in an ice bath. Hydrogen was removed by cautious purging with argon at least three times. For reactions with enhanced mixing, additional steps were performed for hydrogen degassing prior to iMC: 10 bar of argon were applied, and the solution was stirred for 30 min under argon. After this, vacuum was applied for 15 min under heating with a setpoint of 40 °C to remove as much hydrogen as possible. Subsequently, the reactor was cooled down to room temperature. A volume of 20 mL dried and degassed MeOH was refilled under argon counterflow. In all cases, protonated ligand was weighed into an inertized Schlenk flask, dissolved in 10 mL of dried and degassed MeOH, and introduced into the reactor via syringe in argon counterflow. CO pressure was applied, and the reactor was heated under stirring to the desired temperature. A schematic workflow, including all relevant steps, is depicted in Figure 52.

The formation of the Pd complex at the boiling temperature of MeOH was performed in a Schlenk flask in a similar manner without argon overpressure and without the hydrogenation step until CO would have been applied. Instead, the mixture was heated up to 80 °C again under reflux with argon. Photos were taken at given time stamps.

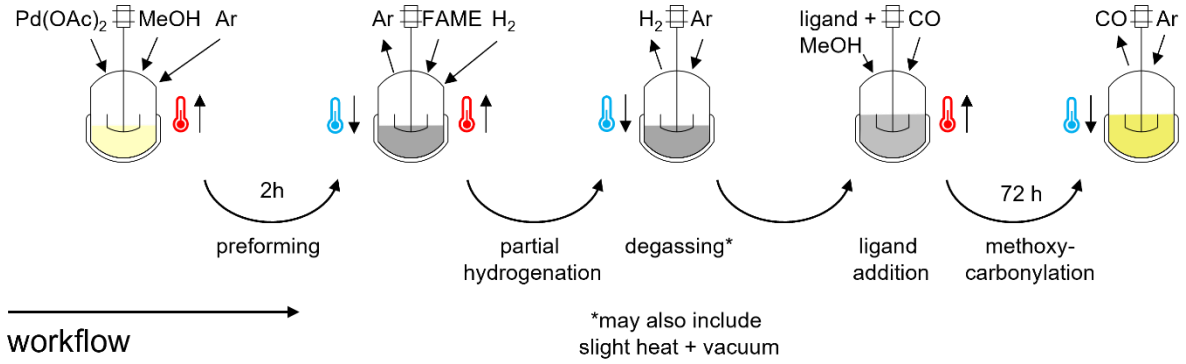


Figure 52: Schematic workflow of the whole reaction sequence

Samples were diluted and analyzed on a 90-m DBFastFAME GC column (hydrogenation) or 30-m HP-5 GC column (methoxycarbonylation) with flame ionization detector (FID). For hydrogenation, C16:0 served as an internal standard; for methoxycarbonylation, heptadecanoic acid methyl ester (for FAME samples) or dodecane (for $C_{11}$-ME) was added. Further details on analysis methods can be found in chapter 11.5.

## 8.4 Result and Discussion

The envisaged reaction route comprises two different main types of reaction, starting with the selective hydrogenation of PU-FAME from soybean oil having a high content of polyunsaturated compounds (>60%) using Pd nanoparticles. The major challenge in the whole reaction route is to find conditions suitable for both main reactions. Figure 53 lists typical conditions for each reaction step, their compatibility, and their impact on the reaction performance or workflow. It becomes obvious that both reactions need very different reaction conditions, especially regarding solvent as well as Pd loading, showing only a small overlap at this critical point. As the envisioned route is an assisted tandem catalysis approach, differences in pressure, temperature, and reaction time for each individual step are independent of each other and thus not critical.

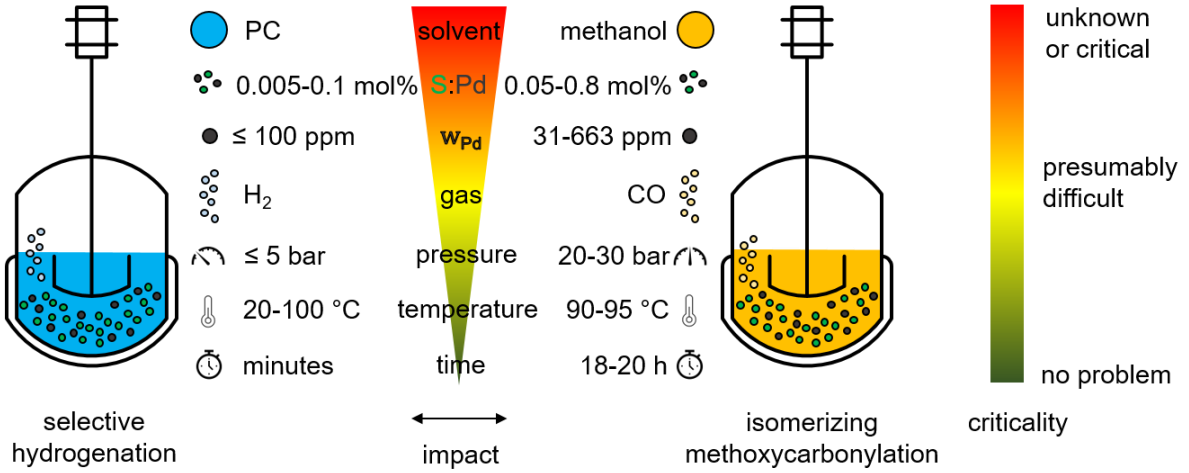


Figure 53: Typical reaction conditions for the selective FAME hydrogenation with Pd nanoparticles (left) and the isomerizing methoxycarbonylation of fatty acid derivatives (right) combined with their impact on each other and the corresponding criticality[12],[68],[70],[94],[95],[97]–[100],[249]

### 8.4.1 Influence of Solvent: PC in Methoxycarbonylation

As, according to literature, PC is highly desirable in the hydrogenation step[68], preliminary tests of methoxycarbonylation with and without PC were performed to evaluate the effect of the presence of PC in methoxycarbonylation. According to the literature review in Figure 53, this is the first and most critical issue to be analyzed. Therefore, methyl-10-undecenoate ($C_{11}$-ME), a renewable substrate derived from castor oil and commercially available, was chosen as established monounsaturated model substrate (cf., Section 11.5.3). $C_{11}$-ME is particularly suitable for this initial test, as the objective MU-FAME is structurally very similar: It also contains one double bond, a long carbon chain, and one already existing methyl ester group. Although the position of the double bond is more internal for the partially hydrogenated FAME, this is negligible, because the applied catalyst system for the methoxycarbonylation is highly active in isomerization. Furthermore, methanolysis is the rate limiting step that preferentially occurs for the terminal double bond[99]. Beneficially, $C_{11}$-ME comes without residues of any further polyunsaturated species that would affect the catalyst performance.

Previously used standard reaction conditions for methoxycarbonylation were applied, comprising a substrate:Pd loading of 1000:1[94],[97],[98],[249]. This results in a rather high Pd loading for hydrogenation[70], nevertheless being in the small overlapping area of applicable conditions. For simplicity reasons, the applied catalyst was derived from $Pd_2(dba)_3$ to purely study the influence of additional PC.

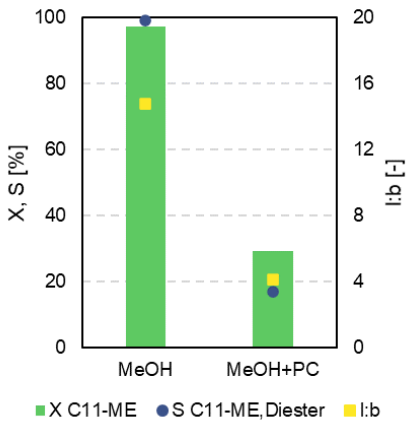


Figure 54: Results of the methoxycarbonylation of $C_{11}$-ME with and without the addition of PC in the reaction starting directly from $Pd_2(dba)_3$ and protonated ligand. Reaction conditions: S:Pd = 1000:1, L:Pd = 17.5, $p_{CO}$ = 30 bar, $T$= 95 °C, $V_{total}$ ca. 70 mL, $\omega$ = 1100 rpm, cross-shaped stirring bar, $t$ = 10 h, $n_{C11\text{-}ME,MeOH}$ =33.8 mmol, $n_{C11\text{-}ME,MeOH+PC}$ = 15.4 mmol.

It can be clearly seen in Figure 54 that the required amount of PC drastically inhibits the methoxycarbonylation of $C_{11}$-ME: Conversion drops from 98% in the benchmark experiment, which is in line with the literature, to 29%[98],[249]. Moreover, increased amounts of branched products are formed when conducting the reaction with additional PC, which can be seen in the loss in selectivity to diester products to only about 16.7% and the sharply decreased l:b-ratio of only 4.1. This also means that the main portion of the converted $C_{11}$-ME is simply isomerized and does not undergo methoxycarbonylation. Methanolysis is known to be the rate limiting step[99], explaining that dilution of MeOH results in a reduced reaction rate. At the same time, isomerization and reversible CO insertion are not influenced by MeOH shortage, resulting in pronounced isomerization compared to methoxycarbonylation. The higher amount of isomerized educt may lead to MeOH insertion not at the chain end, resulting in a lower l:b-ratio. Obviously, the presence of PC in methoxycarbonylation must be avoided, resulting also in the need to be replaced in the prior hydrogenation step.

### 8.4.2 Influence of Solvent: MeOH in Hydrogenation

As a consequence, the use of MeOH in the selective hydrogenation of the highly unsaturated soybean FAME was evaluated since it needs to be present in high excess in methoxycarbonylation, acting as a solvent and reagent at the same time. This was done in order to avoid the addition of other potentially inhibiting solvents. The catalyst loading was held constant, like in methoxycarbonylation (substrate:Pd (S:Pd) = 1000:1; 0.1 mol%), resulting in a rather high Pd content of 114 ppm (w/w) in MeOH regarding hydrogenation. According to Figure 53, this lies within the small area of possibly applicable conditions for both reactions, although Pd mass loading is slightly out of its typical boundaries.

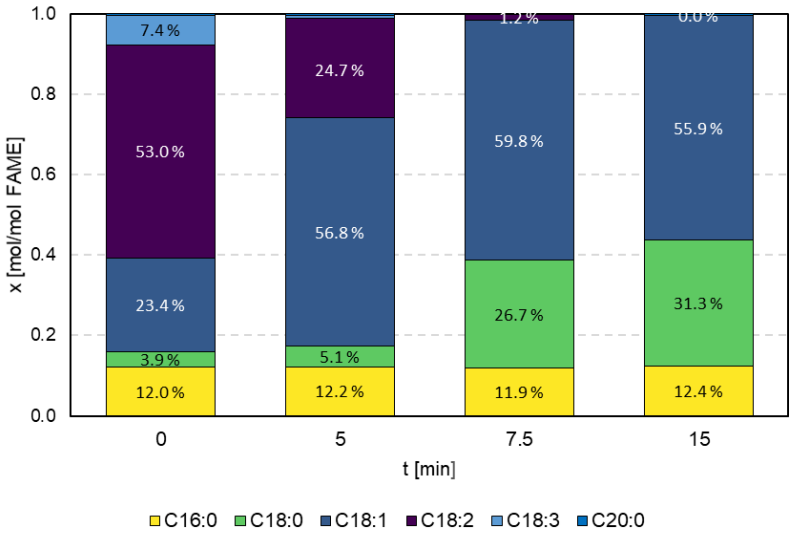


Figure 55: Reaction progress of hydrogenation of soybean FAME with Pd nanoparticles in MeOH. Reaction conditions: S:Pd = 1000:1, $p_{H2}$ = 25 bar; $T$ = 80°C, $V_{MeOH}$ = 20 mL, $n_{FAME}$ = 16.9 mmol, $w_{Pd,MeOH}$ = 114 ppm, $\omega$ = 1100 rpm, cross-shaped stirring bar, $t_{Preforming}$ = 2 h. Composition determined after venting and cooling down.

Figure 55 shows the high amount of polyunsaturated species present in the initial substrate FAME mixture, summing up to more than 60%. It can be seen that the hydrogenation takes place very fast in the first 7.5 min, converting more than 61% of excess double bonds even within 5 min. After 7.5 min, 98% conversion is achieved. Drastic overhydrogenation to C18:0 is observable, resulting in nearly 66% selectivity. Further increase in reaction time results mainly in further increase of undesirable saturated species, lowering selectivity further to ca. 59%. Obviously, finding the “best” reaction time is an optimization problem that needs to balance overhydrogenation against residues of polyunsaturated species. To maximize the content of reactive C18:1 species at nearly full conversion, a 7.5-min reaction time in hydrogenation was chosen. This enables the use of potentially 60% of a former nonapplicable substrate for further utilization in the methoxycarbonylation.

### 8.4.3 Dissolution of Nanoparticles

Having shown that the partial hydrogenation of FAME with unsupported Pd nanoparticles in MeOH is taking place sufficiently, the basis is laid to further focus on the viability of conducting the subsequent iMC. The main prerequisite is the dissolution of the formed nanoparticles by the protonated ligand. To follow this process, an experiment was conducted under reflux in a glass flask, allowing the observation of the macroscopic behavior (Figure 56).

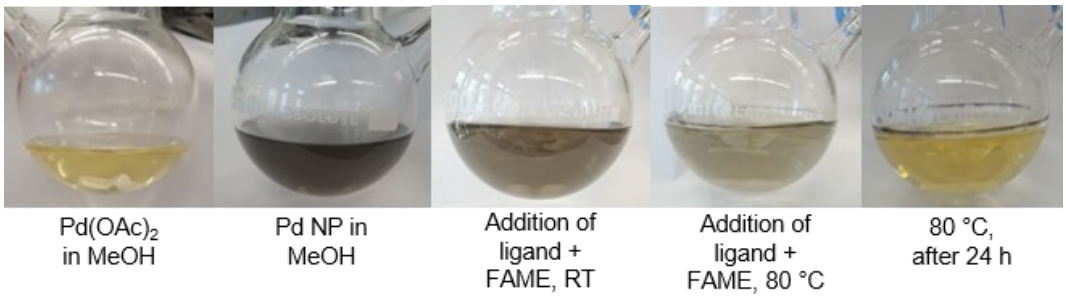


Figure 56: Evolution of the catalyst system throughout the reaction course. Reaction conditions: S:Pd = 1000:1, reflux, $T$ = 80°C, $V_{MeOH}$ = 20 + 10 mL, $n_{FAME}$ = 16.9 mmol; L:Pd = 6, $t_{Preforming}$ = 2 h, $t_{complexation+reaction}$ = 24 h.

First, the precursor $Pd(OAc)_2$ dissolves in MeOH. After preforming under reflux, the black nanoparticle solution is formed. Upon cooling to RT and addition of (unhydrogenated) FAME and dissolved 1,2-DTBPMB$(OTf)_2H_2$ (in MeOH), the solution becomes lighter, which is even more pronounced upon heating, resulting in a yellow solution after 24 h. Already at boiling temperature, a black deposit forms at the phase boundary, rising in amount in the course of the preforming. The obtained solution is showing an expected yellow color, and slight isomerization after 24 h is observable. To achieve full isomerization within the given time using a properly formed catalyst, the temperature would need to be higher than the boiling temperature of MeOH applicable here (see Figure S 15). This implies that the catalyst is formed in principle, although not to the full extent. Performing the same experiment under 5 bar of Ar atmosphere in the pressure reactor at the desired temperature of 95 °C results in 75% of Pd in solution (determined by inductively coupled plasma optical emission spectrometry) and full isomerization of the substrate with known isomerization patterns like expected[97]. This leads to the conclusion that without $H_2$ or CO treatment, the desired catalyst can form from the in situ generated nanoparticles as expected, although rather severe deposition and thus loss of Pd must be taken into account.

### 8.4.4 Influence of Gas on the Individual Reaction Step

To show that the formation of the Pd complex from nanoparticles is also possible under CO atmosphere, $C_{11}$-ME was again applied as simplified model substance; L:Pd was chosen to be 6 as it was done by Mecking et al. for their 30 nm nanoparticles in order to obtain maximum yield[95]. In a second run, the nanoparticle solution was exposed to $H_2$ atmosphere for 8 min and the atmosphere released. The reactor was then flushed with argon five times before $C_{11}$-ME and the ligand were added.

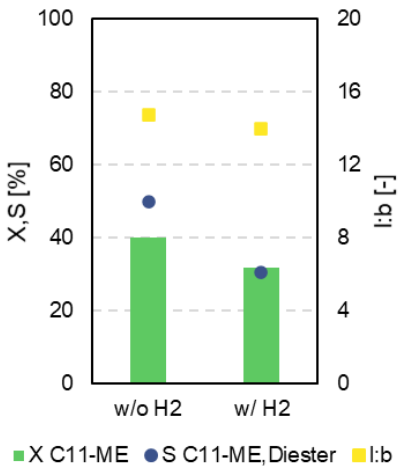


Figure 57: Results of the methoxycarbonylation of $C_{11}$-ME with and without exposure to hydrogen. General reaction conditions: S:Pd = 1000:1, L:Pd = 6, $p_{CO}$ = 25 bar, $T_{methoxycarbonylation}$ = 95°C, $V_{MeOH}$ = 30 mL, $n_{C11\text{-}ME}$ = 16.9 mmol, $\omega$ = 1100 rpm, cross-shaped stirring bar, $t_{Preforming}$ = 2 h; (a) $t_{methoxycarbonylation}$ = 48 h; (b) $t_{methoxycarbonylation}$ = 44 h, $t_{stirring,H2}$ = 8 min, $T_{stirring,H2}$ = 80°C, $p_{H2}$ = 25 bar.

Conversion drops from 40% to 32% for the pretreatment with hydrogen (Figure 57). Although the l:b-ratio remains roughly constant, the selectivity to diesters drops drastically, emphasizing the formation of increased amounts of $C_{11}$-ME isomers. It becomes clear that the pretreatment with hydrogen of the reaction solution of methoxycarbonylation has a negative effect on both conversion and selectivity to diesters. It seems that trace amounts of hydrogen that are not being removed during venting, for example, due to the high solubility in short-chain alcohols like MeOH[175], interact with noncomplexated Pd species. It is known that bulk Pd adsorbs hydrogen at its surface and acts like a sponge for hydrogen by forming Pd hydride (storing up to 0.7 mol $H_2$ per mol Pd at standard conditions) that may theoretically lead to isomerization or hydrogenation via the Horiuti–Polanyi mechanism[71],[83],[250]. At low partial pressures of hydrogen, isomerization is favored over hydrogenation[42],[75]. Therefore, it can be concluded that the hydrogen-lean gas phase, in combination with hydrogen-saturated nanoparticles and solvent present in the initial period following ligand addition, would likely cause isomerization reactions of the substrate with a high degree of probability. Indeed, no hydrogenation product is observable. Moreover, the saturation of Pd with hydrogen might result in a decreased complexation rate with the protonated ligand. This phenomenon would result in a decrease in methoxycarbonylation, attributable to a reduced quantity of Pd complex in solution, concomitant with pronounced isomerization due to the nanoparticles. As the active catalyst is able to convert isomerized substrates into the desired product, the comparable l:b-ratio can be explained, because methanolysis is the rate-determining step in sole iMC[99].

Even small residual amounts of CO from previously conducted reactions that remain in secondary piping due to improper gas change and purging completely suppress any hydrogenation reaction. It is literature-known that CO is a catalyst poison for many different types of catalysts[6],[47]. Accordingly, it deactivates the nanoparticulate hydrogenation catalyst used here, although it is indispensable for the subsequent methoxycarbonylation. This observation underscores the importance of meticulous gas purging routines for both reaction steps to ensure safety and efficacy. It is evident that for each of the

two reaction steps, the gas of the other reaction is at least disadvantageous and must be removed to the greatest extent possible.

### 8.4.5 Combining Both Reaction Steps

The demonstration of the feasibility of conducting methoxycarbonylation subsequent to exposure to hydrogen, in principle, is noteworthy. However, the execution of the complete tandem catalysis with the intricate FAME mixture results in a mere 1% conversion of FAME after a 72-h reaction period with L:Pd= 6 (all other conditions equal to those of Figure 59, left). This outcome underscores the necessity for a comprehensive adjustment of the reaction conditions. To counteract the negative influence of hydrogen on the dissolution of the nanoparticles by the ligand, the amount of ligand was increased to literature adjacent previously known conditions for methoxycarbonylation starting from $Pd_2(dba)_3$ of L:Pd=17.5 [97],[98],[249]. This leads, in combination with prolonged degassing of hydrogen under argon flow, to 37% conversion in methoxycarbonylation with 98% selectivity to the linear diester (Figure 59, left). The two-step approach described in literature is attributed to yielding a roughly doubled yield at half catalyst loading under otherwise mostly comparable conditions[12]. Hence, limitations in the presented one-pot system seem to be present.

A reuse of the catalyst solution of the reaction with standard mixing in a subsequent selective hydrogenation of fresh FAME does not lead to any conversion and is thereby not successful. Again, this might originate from the contact of both complexated and deposited Pd with CO during methoxycarbonylation that is expected to poison the solid Pd particles and eventually prevent formation of nanoparticles under the reducing atmosphere. Further research might shed light on underlying processes regarding poisoning mechanisms and resulting reactivation of the catalyst system.

### 8.4.6 Influence of Mass Transport

It might be argued that one limitation of the presented one-pot system is the availability of carbon monoxide in the liquid phase. In this work, a stirring bar used to be the agitator until now, whereas the literature's two-step approach used an overheadstirred reactor[12]. Accordingly, yield could be enhanced through the implementation of an advanced mixing technique, with the objective of increasing the availability of carbon monoxide in the liquid phase. To this end, the configuration of the reactor system was modified to an overhead stirred reactor, which was operated at an elevated rotational speed and equipped with a gas inlet stirrer. This improvement leads to shortened reaction times in the hydrogenation step, enabling the reaction to be shortened by at least three, eventually even 5.5 min (see Figure S 16), affecting also the composition of the obtained hydrogenation product as can be seen in Figure 58: The desired C18:1 fraction is increased by about 10%, reducing the amount of overhydrogenated product by 12%. This corresponds to 84% selectivity at 95% conversion in hydrogenation, meaning an even higher utilization of the applied substrate. The fraction of nonhydrogenated PU-FAMEs is increased by 2%, although sufficient reaction time was allowed. Commercial high oleic FAME contains C18:2 in comparable amounts (also Figure 58) and has been used successfully in the work by Mecking et al.[95]. For comparison, the product composition using PC

instead of MeOH is also displayed here. As this is a biphasic reaction, mass transport limitations are significant, leading to only reduced conversions applying standard mixing (see Figure S 14). Applying enhanced mixing, Pd in PC yields very similar results compared to Pd in MeOH at typical conditions for this system.

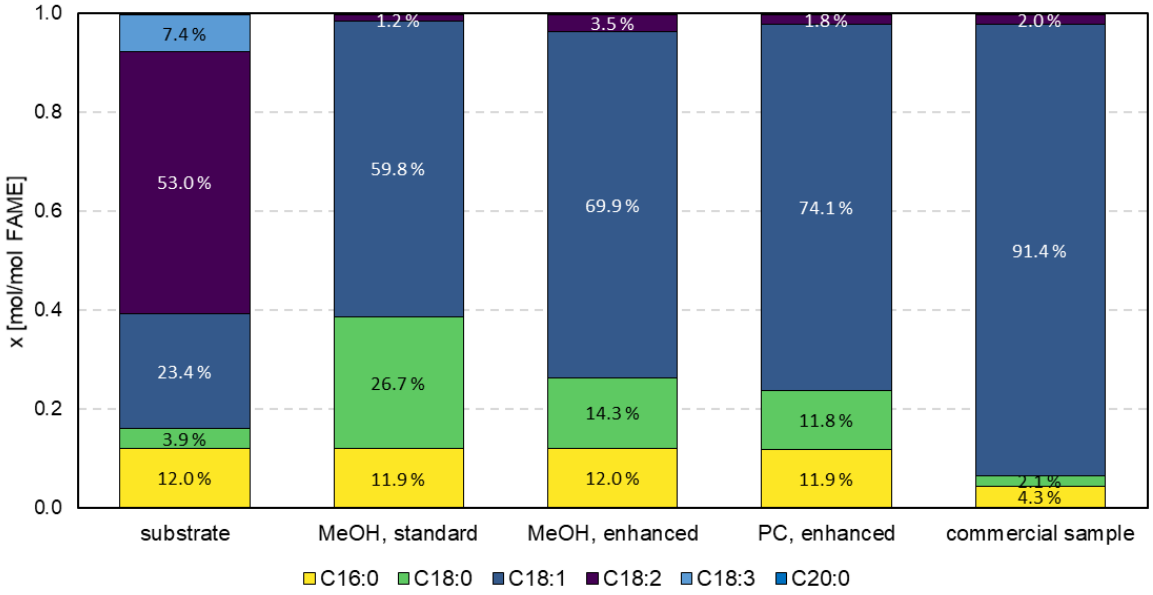


Figure 58: Composition of soybean FAME before and after hydrogenation with Pd nanoparticles in MeOH and PC and comparison with a commercial sample. Reaction conditions: S:Pd = 1000:1, $V_{solvent}$ = 20 mL, $n_{FAME}$ = 16.9 mmol, $\omega$ = 1100 rpm, $t_{Preforming}$ = 2 h,
MeOH, standard: cross-shaped stirring bar, $p_{H2}$ = 25 bar; $T$ = 80°C, $w_{Pd,MeOH}$ = 114 ppm, $t_{hydrogenation}$ = 7.5 min,
MeOH,enhanced: overhead stirrer, $p_{H2}$ = 25 bar; $T$ = 80°C, $w_{Pd,MeOH}$ = 114 ppm, $t_{hydrogenation}$ = 4.5 min,
PC, enhanced: overhead stirrer, $p_{H2}$ = 5 bar; $T$ = 35°C, $w_{Pd,PC}$ = 74.4 ppm, $t_{hydrogenation}$ = 15 min,
commercial sample: product “Dakolub MB9001” by Dako, obtained from grown specialised sunflowers.

## 8.4.7 Influence of Unsaturated Species

Although stirring has an obvious influence on the hydrogenation step, the subsequent iMC is not improved much, even though degassing of hydrogen was further optimized (see section 8.3). Using an equivalent amount of high-purity methyl oleate (purity 98.9%) in iMC instead of the hydrogenated product mixture yields, in the same reaction time, 91% conversion (Figure 59). The high-purity substrate has been exposed to hydrogen as well to allow for saturation but was not in contact with the nanoparticle solution to avoid possible hydrogenation or isomerization.

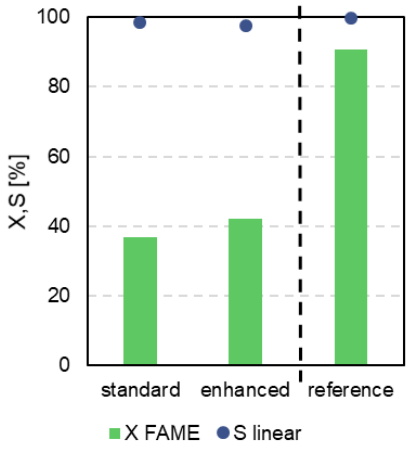


Figure 59: Results of the methoxycarbonylation of soybean FAME in tandem catalysis. General reaction conditions: S:Pd = 1000:1, L:Pd = 17.5, $p_{CO}$ = 30 bar, $T_{methoxycarbonylation}$ = 95 °C, $V_{MeOH}$ = 30 mL, $\omega_{hydrogenation}$ = 1100 rpm, $t_{Preforming}$ = 2 h, $t_{methoxycarbonylation}$ = 72 h
standard: $\omega_{methoxycarbonylation}$ = 1100 rpm, cross-shaped stirring bar, $n_{FAME}$ = 16.9 mmol,
enhanced: $\omega_{methoxycarbonylation}$ = 3500 rpm, overhead stirrer, $n_{FAME}$ = 16.9 mmol,
reference: $\omega_{methoxycarbonylation}$ = 3500 rpm, overhead stirrer, $n_{FAME}$ = 11.8 mmol, $t_{stirring,H2}$ = 4.5 min, $T_{stirring,H2}$ = 80°C, $p_{H2}$ = 25 bar.

It is evident that mass transport does not constitute the rate-limiting step in the methoxycarbonylation of the selectively hydrogenated FAME mixture. Rather, investigation of the hydrogenation product and the unreacted FAME after 72 h of methoxycarbonylation in comparison with isomerized conjugated methyl linoleate (iCML) revealed the presence of several conjugated species that formed only in methoxycarbonylation from non-hydrogenated residues of C18:2 (Figure S 17). These conjugated species, in turn, are known for catalyst inhibition via the formation of rather stable Pd allyl species, explaining reduced conversion by decelerated reaction rates[97],[99]. As already shown, the dissolution of the nanoparticles is incomplete, and therefore, the amount of active catalyst complex is reduced from the beginning; hence, this contributes to overall slower reaction rates for all methoxycarbonylations displayed in Figure 59. Moreover, the incomplete complexation of the former nanoparticles with protonated ligand prevents the formation of new catalytically active species for methoxycarbonylation in order to replace the deactivated ones. This shows that in principle the tandem catalysis approach is working but is hindered to a certain extent when applying real-world substrates.

## 8.5 Conclusion

In this study, we demonstrate for the first time the feasibility of integrating a monophasic tandem one-pot approach with selective hydrogenation of a standard, inexpensive polyunsaturated FAME from soybean oil via palladium nanoparticles in methanol and iMC of the obtained products. This approach eliminates the need for a workup step after hydrogenation and utilizes a single reactor with a constant Pd loading, thereby streamlining the process. This enables the direct use of a commercially available feedstock for the production of polymer precursors. Nevertheless, contradictions difficult to reconcile exist and can be circumvented only in parts:

- On the one hand, PC is advantageous in selective hydrogenation but drastically inhibits methoxycarbonylation. On the other hand, MeOH is a less preferred solvent in selective

hydrogenation, leading to incomplete hydrogenation already at increased overhydrogenation to unuseful saturated species.

- CO used in methoxycarbonylation is a severe catalyst poison for hydrogenation; the presence of trace amounts ofhydrogen in turn is at least disadvantageous for methoxycarbonylation. This gives need to thorough gas phase change after each reaction, which is complicated by the fact that hydrogen gets probably integrated into the nanoparticles and is also soluble in the used solvent MeOH.
- Formed nanoparticles may deposit at the reactor wall and are incompletely complexated by 1,2-DTBPMB$(OTf)_2H_2$, whereas at the same time, conjugated C18:2 species are generated due to slight incomplete hydrogenation in MeOH. This leads to deactivation of the methoxycarbonylation catalyst by forming allyl species, whereas the Pd complex is insufficiently (re)generated by dissolution of the nanoparticles.

Nevertheless, applying an optimized workflow allows for the use of this tandem one-pot approach properly, achieving nearly complete hydrogenation of the soybean FAME with complete removal of triple unsaturated species, generating a product mixture with amounts of polyunsaturated species comparable to commercially available products. Overall, 37% - 42% conversion of the obtained C18:1 FAME in the following iMC with a very high selectivity to the linear product of 98% is thereby made possible.

Subsequent research on detailed molecular poisoning mechanisms and reactivation possibilities of the spent catalyst solution would be beneficial in order to recycle the valuable catalyst metal. Further investigations might include a diversified substrate basis to other inexpensive oils or preferentially even waste streams that would potentially come with several new challenges. By doing so, the influence of traces impurities of those technical substrates could be highlighted. Although the chosen solvents consider literature-known optimal solvents for each single reaction step, a broader solvent screening might be of interest.

## 8.6 Acknowledgments

The authors thank the networking program “Sustainable Chemical Synthesis 2.0” (SusChemSys 2.0) for the support and fruitful discussions across disciplines.

Finally, we are very thankful to the German Federal Ministry of Agriculture, Food and Regional Identity (Bundesministerium für Landwirtschaft, Ernährung und Heimat), represented by the FNR (Fachagentur Nachwachsende Rohstoffe) for financial support of the young research group “Renewlysis” (project number 2219NR355).

Open access funding enabled and organized by Projekt DEAL.

# 9 Integrating Gas Permeation with Gas-Consuming Reactions in Slug-Flow Capillaries: Continuous and Selective Hydrogenation of Biodiesel

Reprinted with permission from

F. Lehmann, N. von Vietinghoff, P. Pey, K. S. Wulle, T. Seidensticker, N. von Vietinghoff, “Integrating Gas Permeation with Gas-Consuming Reactions in Slug-Flow Capillaries: Continuous and Selective Hydrogenation of Biodiesel”, *ACS Sustainable Chem. Eng.* **2025**, *13*, 20242–20252, DOI: 10.1021/acssuschemeng.5c09302.  Accessible via https://pubs.acs.org/articlesonrequest/AOR-TTFEFUMYBAMM6TEGS5RR

Citation style and numbering, as well as Figure and Table numbering, were changed to a sequential mode to fit the document style.

**Author contributions:** The concept and ideas for this project were provided by N. von Vietinghoff and me equally. P. Pey and K.S. Wulle performed the experiments as part of their bachelor’s theses and P. Pey’s internship under the supervision of N. von Vietinghoff and me. Manuscript preparation including formal analyses, writing, and visualization, was performed by me; N. von Vietinghoff reviewed and edited the manuscript. T. Seidensticker acquired funding, supervised this project, and reviewed and edited the manuscript.

## 9.1 Abstract

The catalytic and selective hydrogenation of biodiesel is employed here as a model reaction to demonstrate, for the first time, the integration of gas permeation with a gas-consuming process in a capillary slug-flow. In such systems, gas consumption during the reaction leads to bubble shrinkage and ultimately destabilizes the flow regime, which counteracts the benefits of intensified mass transport and mixing. By continuously replenishing hydrogen through the permeable capillary wall, a stable slug flow under reactive conditions can be maintained. Compared to batch operation, the model reaction illustrates more than a 9-fold increase in reaction rate while preserving high selectivity. This proof-of-concept highlights how permeation enables continuous operation of reactive slug-flow systems without a loss of stability. Beyond the chosen example of biodiesel upgrading, the approach establishes a generalizable method for conducting gas-limited multiphase reactions in a continuous flow. The concept combines reactor engineering and catalysis to support sustainable process intensification and opens new opportunities for multiphase transformations requiring precise gas management.

## 9.2 Introduction

Multiphase reactions often face mass transport limitations.[133] To address these issues, reactor design is crucial for achieving optimal mixing of the phases.[133] One solution for laboratory experiments involving immiscible liquid phases and/or an additional gas phase is to use a capillary reactor setup. This approach is especially beneficial when a regular flow pattern with elongated, well-mixed bubbles or drops, known as slugs, is formed. This results in a well-defined residence time, enhanced mixing, and a high surface-to-volume ratio, leading to efficient mass and energy transfer within each phase or segment and across the phase interface. Ultimately, this reduces mass transfer limitations and boosts overall reaction rates.[131],[132],[141] However, for reactions with gaseous components, a common challenge is the low solubility of gases in liquids, which often requires an additional gas slug.[140] The total amount of gas available is limited due to density differences between gas and liquid, resulting in rapid gas consumption and an imbalance between the required and available amounts of gas, especially with highly concentrated substrates.[141] Additionally, high dilution with inert solvents reduces the space-time yield and economic viability. Gas slug consumption also affects the residence time, as shrinking gas slugs decrease the total flow rate, resulting in longer residence times. This can be problematic for reaction networks involving follow-up reactions and should be avoided. A promising method for continuous gas replenishment involves gas permeation through fluorinated capillary materials, which has been successfully demonstrated in slug flow without reactions by us. However, there are only a few examples of reactions in capillary reactors with gas permeation.[141],[251],[252]

Several model reactions may be considered for g/l multiphase reactions, with selective hydrogenation being one of them. For example, selective partial hydrogenation of oleochemicals produces monounsaturated compounds from polyunsaturated ones (Scheme 22). For this purpose, many catalysts have been developed, typically tested in batch.[62] Among them, solvent-stabilized Pd nanoparticles in propylene carbonate proved to be highly promising candidates.[62],[68]–[70] These catalytic systems appear to be rather fast, with reaction times as short as a few minutes, requiring high mass transport rates. At the same time, the consecutive reaction toward saturated C18:0 needs to be prevented to facilitate the further use of the desired C18:1 species in subsequent reactions. Hence, selective partial hydrogenation with solvent-stabilized Pd nanoparticles acts as an ideal model reaction for a multiphase capillary operation with additional gas permeation. Until now, this reaction has only been carried out in batch operation.[12],[50],[62],[68]–[70] The relatively polar solvent propylene carbonate (PC) was found to be a highly beneficial solvent for reaction performance and stabilization of the chosen catalyst[22],[68]. This sustainable system employs a fully atom-economical reaction that utilizes renewable carbon sources in a catalytic reaction with a benign solvent. The capillary approach, with its small dimensions and limited volume, is furthermore an inherently safe process.[8]

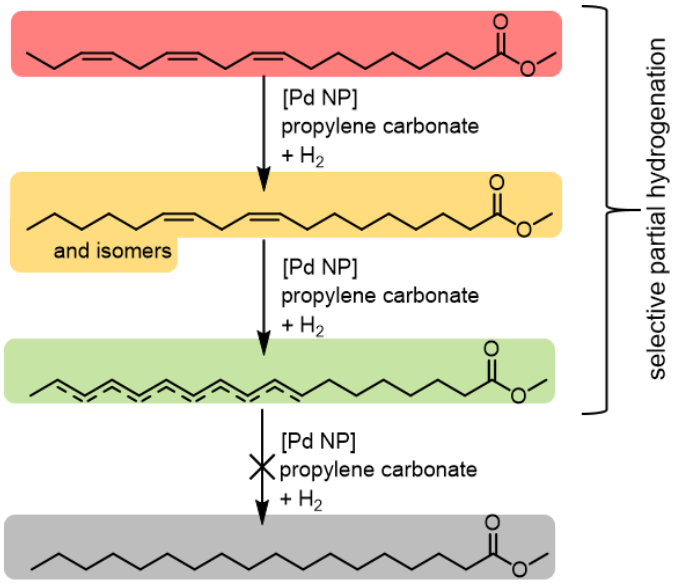


Scheme 22: Reaction Scheme of the Studied Selective Partial Hydrogenation of Soybean Fatty Acid Methyl Esters

In this work, we aim to integrate the concept of gas permeation in a capillary slug flow with a gas-consuming catalytic reaction. Using the selective partial hydrogenation of FAMEs as an exemplary case, our objective is to demonstrate that continuous gas replenishment can compensate for gas consumption, thereby stabilizing the flow regime and enabling continuous operation. The feasibility and meaningfulness of the general reactor concept and the influence of gas supply will be evaluated, and a comparison of different operation modes (batch reaction; initial presence of gas slugs; see Figure 60) will be performed. By integrating a permeation-controlled gas supply with a catalytically demanding model reaction, we aim to establish a reactor concept that combines high selectivity with the benefits of intensified mass transport. Beyond this case study, the approach is intended as a transferable strategy for a broad range of gas−liquid multiphase reactions.

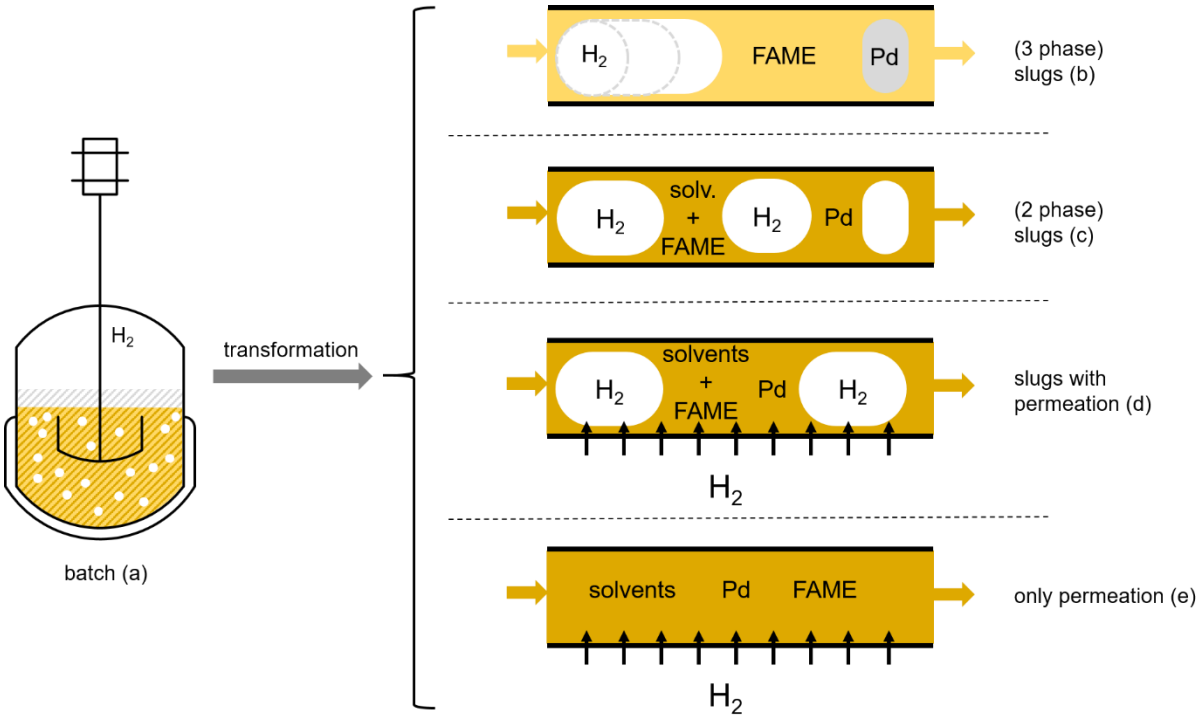


Figure 60: Schematic and enlarged (not to scale) possibilities of investigated reactor concepts.
(a) Batch reaction with one or two liquid phases and one gas phase.
(b) Reaction in capillary with three phases, shrinking gas slugs and without additional solvent.
(c) Reaction in capillary with two phases, shrinking gas slugs, and additional solvent.
(d) Reaction in capillary with two phases, additional solvent, and gas replenishment by permeation leading to gas slugs with roughly constant size.
(e) Reaction in capillary with one phase, additional solvent, and permeation, without additional gas slugs.

## 9.3 Experimental Section

All chemicals were received from commercial suppliers and used without further purification. The colloidal Pd nanoparticles were produced according to known methods with a resulting Pd loading of 24 ppm (w/w).[12] The catalyst solution was mostly further diluted with an inert solvent. Hydrogenations in the 1 mm inner diameter FEP capillary reactor were performed in a previously described setup after minor modifications.[141] A simplified version of the setup is shown in Figure 61. Full schematic flowsheets for different pressure ranges can be found in the Supporting Information (Figure S 18).

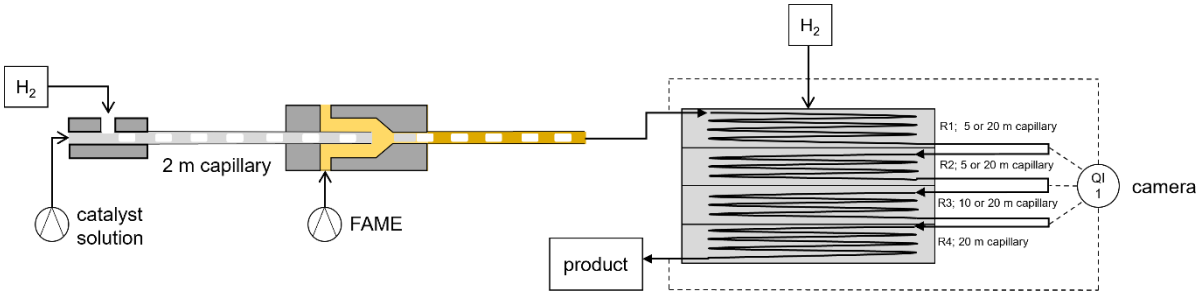


Figure 61: Simplified flowsheet of the reactor setup for operation with slugs and permeation.

Substrate and diluted catalyst solution were placed in separate vessels and introduced into the reactor by using syringe pumps. First, the catalyst solution was contacted with hydrogen introduced by a mass flow controller in a T-junction to allow a certain saturation of the catalyst phase with hydrogen and preforming of the catalyst. Typically, the hydrogen flow rate is equal to the total liquid flow rate. Afterward, the substrate was added using a coaxial contactor[138] that allows for manipulating slug lengths in order to obtain as equal lengths ofgas and liquid slugs as possible. The resulting flow was transferred to the preheated and pressurized reaction zone. Samples were withdrawn at distinct points. After each reactor segment and before entering the first section, the capillary passes a photo station with a high-speed camera that allows for gathering information about flow behavior and slug lengths at exemplary reactor lengths.

Inside the metal jacket, the capillary is coiled in loops, and hydrogen overpressure for experiments with permeation was applied as stated. In experiments without permeation, the free space was filled with thermal oil and pressurized with nitrogen to prevent capillary damage as well as mass transport, especially of hydrogen, across the material to the outside of the capillary. Samples were taken at steady state, which was reached after several theoretical residence times (at least 3). Blind experiments ensured resilient results.

All obtained samples were diluted with methyl tert-butyl ether (MTBE) or cyclohexane to a constant concentration of analytes and were measured on a GC-FID with a DB-FastFAME GC column for quantitative analysis.

Conversion refers to the conversion of excess double bonds that exist in C18:2 and C18:3 species (one for C18:2 and two for C18:3). Selectivity considers the depletion of already existing C18:2 by the formation of C18:1 and the depletion of C18:3 to form the necessary intermediate C18:2, as shown in Formula (2), and was rounded to significant digits. Further details are given in SI.

$$S = \frac{x_{C18:1} - x_{C18:1;0} + x_{C18:3;0} - x_{C18:3}}{x_{C18:2;0} - x_{C18:2} + 2 \cdot (x_{C18:3;0} - x_{C18:3})} \tag{2}$$

For the calculation ofthe residence time, $\tau$, the average total volume flow must be calculated. The consumption of hydrogen in each reactor segment is taken into account via optical measurements of the length of the gas bubbles passing through the photo station after each segment ($l_{p,i}$), weighted with the fraction of each segment contributing to the total length of the reactor $\left(\frac{l_{segment,i}}{l}\right)$. Under the assumption of a constant liquid flow rate, the average volume flow is calculated using Formula (3).

$$\bar{\dot{V}} = \dot{V}_L + \dot{V}_G \cdot \sum_{i=1}^{4} \left( \frac{l_{p,i}}{l_{p,0m}} \cdot \frac{l_{segment,i}}{l} \right) \tag{3}$$

## 9.4 Results and Discussion

### 9.4.1 Prerequisite: Flow Stability

The widely investigated selective partial hydrogenation toward the monounsaturated species (Scheme 22) was conducted in this work at conditions based on literature, including a temperature of 80 °C, a high substrate-to-catalyst ratio (S:C) of 50,000:1 (total molar amount of substrate mixture: total molar amount of Pd), and a pressure above 10 bar.[12] A soybean-derived FAME mixture containing up to 60% polyunsaturated species was used as the substrate (for the exact composition, see Figure 62)

An attempt to transfer the known batch reactor conditions to the flow setup without an intermediate gas feed (Figure 60b) reveals several challenges: The necessary particle-stabilizing solvent PC is not miscible with FAME, leading to a three-phase flow with significantly different volume flows for each phase, which causes unstable flow patterns. Even with balanced volume flow ratios of 1:1:1, undesired parallel flow may occur, indicating that a minimum flow rate (at least >0.9 mL $min^{-1}$) must always be maintained for three-phase flow (see SI, Figure S 20).

To circumvent these instability issues, we used an additional solvent to combine both liquid phases into one single liquid phase (Figure 60c). The substrate is diluted, ultimately resulting in a reduced total hydrogen consumption. Moreover, this flow pattern makes it easier to implement gas permeation for ensuring a sufficient gas supply throughout the entire reactor length (Figure 60d). This would also allow for a reduced usage of any additional solvent if the permeation fluxes are high enough to allow increased substrate concentrations. Accordingly, a solvent was chosen and evaluated first, and the effect of permeation was applied afterward.

### 9.4.2 Solvent Selection and Identification of Operating Conditions Without Permeation

Isopropanol (IPA) was identified as a suitable solvent. Several other solvents were also investigated, but discarded for several reasons (see SI). In these pre-experiments, an operation window for pure slug flow without permeation (Figure 60c) was determined, with total flow rates ranging from ca. 1.2 to at least 4.5 mL $min^{-1}$. 2.0 to 3.0 mL $min^{-1}$were revealed to be the best compromise between flow stability and productivity (see Figure S 22). Same volumetric flow rates for the resulting liquid and the gas phase are still applied for stability reasons.

In this operation mode, the concept of continuous gas replenishment in slug-flow directly translates into a remarkable improvement in productivity compared with batch operation. At a total volume flow of 3.0 mL $min^{-1}$, 82% of the excess double bonds are already converted, leaving only about 12% polyunsaturated species (Figure 62). Importantly, this high conversion is achieved while maintaining the excellent selectivity known from batch operation with added IPA. The advantage of the continuous approach becomes even clearer when benchmarked against batch: under comparable conditions, only 20% of the excess double bonds are converted in the same reaction time. Thus, the capillary system

combines fast conversion with sustained selectivity, resulting in a space-time yield (STY) for C18:1 of 0.236 g $h^{-1}$ $mL^{-1}$ already in this initial experiment. These results provide the first direct evidence that the integration of permeation-stabilized slug-flow enables both continuous operation and a step-change in performance over conventional batch processing.

Moreover, we demonstrated that the specifically chosen solvent system not only ensures high reaction performance but also enables an exceptionally straightforward catalyst-product separation. Upon the simple evaporation of IPA, the palladium concentration in the product phase was below the detection limit of 1 ppm (measured by ICP-OES). This result effectively overcomes one of the major challenges in catalysis, namely, metal leaching into the product, and paves the way for efficient catalyst recycling.

The chosen conditions with incomplete conversion enable us to optimize the system and study the influence of certain operational parameters in detail, serving as a benchmark for all capillary experiments conducted in this work. After identifying suitable operating conditions in the given setup and setting a benchmark for further experiments, consumption of the introduced gas bubbles still turns out to be significant; see Figure 63 left. Hence, residence time is strongly influenced, and the implementation of additional gas feed via permeation (Figure 60d) is performed next to refill the gas slugs.

### 9.4.3 Implementation of Gas Permeation

Initially, the sole gas addition by permeation is investigated at otherwise constant conditions. Hydrogen bubbles are still fed from the beginning; the additionally permeating gas is intended only to refill the otherwise shrinking gas bubbles (c.f. Figure 60d).

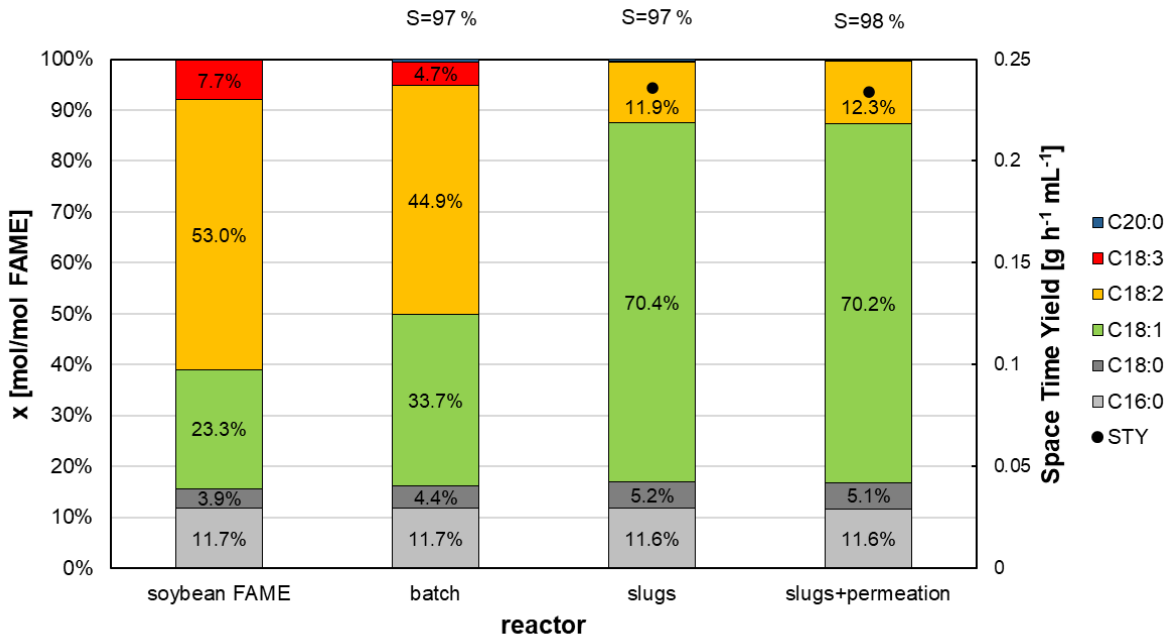


Figure 62: Composition of samples of the selective partial hydrogenation of soybean FAME with additional IPA in different reactors or modes. Reaction conditions: S:C = 50,000:1, T= 80 °C, solvent= IPA, $w_{Pd,PC}$= 24 ppm
batch: $p_{H2}$= 11.5 bar, t= 15.2 min, ω= 3500 rpm, PC:solvent= 1:17.12 mL $mL^{-1}$
slugs: $\dot{V}_{cat.}$= 1.20 mL $min^{-1}$, $\dot{V}_{H_2,T}$= 1.50 mL $min^{-1}$, $\dot{V}_{FAME}$= 0.30 mL $min^{-1}$, τ= 15.5 min, l= 40 m, $p_{H2,back}$= 11 bara,

PC:solvent= 1:17,24 mL mL$^{-1}$
slugs+permeation: $\dot{V}_{cat.}$= 1.20 mL min$^{-1}$, $\dot{V}_{H_2,T}$= 1.50 mL min$^{-1}$, $\dot{V}_{FAME}$= 0.30 mL min$^{-1}$, τ= 14.2 min, l= 40 m, $p_{H2,back}$= 11 bara, PC:solvent= 1:17,24 mL mL$^{-1}$, $\Delta p_{Perm.}$= 1.2 bar.

The slug flow with permeation achieves a C18:1 content of 70.2%, which is similar to that without permeation (Figure 62); hence, the STY remains constant. Permeation of hydrogen into the capillary results in a more regular flow pattern over the entire reactor length: especially at the end of the reactor, the slug flow is still intact, with gas bubbles retaining half of their original size (Figure 63). Additionally, the hydrogen permeation reduces the residence time from 15.5 to 14.2 min. The coefficient of variation (CV) for the slug lengths at each axial position fluctuates constantly between 0.05 and 0.1 for the operation with permeation, indicating equally sized slugs within each position, in contrast to the operation without permeation, where a drastic increase by a factor of more than 3 is observable toward the end of the reactor for both liquid and gas phase (Figure 72, left), pronouncing worse flow stability.

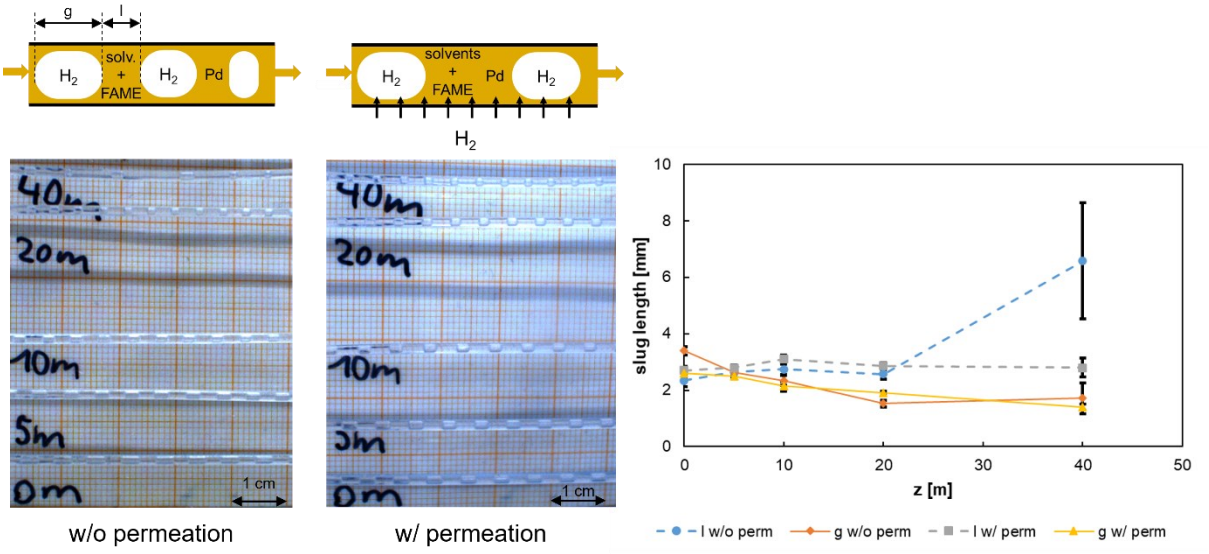


Figure 63: Flow patterns and slug lengths at different axial positions obtained during selective partial hydrogenation of soybean FAME with additional IPA. Lines are shown for visualization purposes only. On average, 9 complete slugs were measured at each axial position, if applicable. Reaction conditions: S:C=50,000:1, T= 80 °C, solvent= IPA, l= 40 m, $w_{Pd,PC}$= 24 ppm, $\dot{V}_{cat.}$= 1.20 mL min$^{-1}$, $\dot{V}_{H_2,T}$= 1.50 mL min$^{-1}$, $\dot{V}_{FAME}$= 0.30 mL min$^{-1}$, $p_{H2,back}$= 11 bara, PC:solvent= 1:17.24 mL mL$^{-1}$
slugs (c.f. Figure 60c): τ= 15.5 min,
slugs+permeation (c.f. Figure 60d): τ= 14.2 min, l= 40 m, $\Delta p_{Perm.}$= 1.2 bar.

For stability reasons, the lengths of the gas phase must at least equal the inner diameter of the capillary (1 mm) to maintain a slug flow. Otherwise, several gas segments will coalesce. In this case, longer gas slugs will occur, separated by longer or irregularly sized liquid slugs. Accordingly, the length of the liquid slugs together with the length of the gas slugs must be considered for the evaluation of stability. However, correlations for the transition of any flow regimes are still missing.[136] Figure 63 shows that the lengths of the gas bubbles decrease toward the end of the reactor, a similar trend observed for both reactions with and without permeation. In contrast, the length of the liquid slugs without permeation drastically increases, and deviations in length become significant, indicating unstable flow. Conversely, permeation can maintain the liquid slug size and thus the entire flow pattern constant. This fulfills the initially set objective of refilling the gas bubbles and accordingly allowing a continuous operation at a stable flow pattern.

With these experiments, the expected reduction of mass transport limitations in the capillary mode with gas slugs is evidenced. Moreover, residence time is reduced, and the flow pattern stabilizes without the cost of losses in conversion or selectivity.

### 9.4.4 Comparison of Reactor Operation Modes

As an alternative operation mode, it is also possible to waive the feed of hydrogen in the T-junction at the reactor inlet and to apply it solely via permeation (c.f. . Figure 60e), although irregular gas bubble formation may occur if the permeation rate exceeds reaction rates.[141] It is therefore necessary to estimate the permeation flux for each experiment: according to literature, the amount of permeating gas is dependent on temperature, material constants, and permeation pressure difference and hence theoretically predictable (see SI)[141],[253]. Under the chosen conditions, spontaneous gas bubble formation never occurred. Thus, the actual hydrogen supply by permeation was found to be at least 2.25 times as large as calculated for operation without slugs and even around 3.8 times as large for operation with slugs, measured indirectly by substrate conversion at distinct points. Higher permeation fluxes than calculated have also been found earlier for slug flow without reaction and were attributed to more nonideal conditions of the setup as well as varying FEP properties regarding different ratios of ethylene/propylene and degree of crystallinity.[141] Additionally, different concentration gradients within the liquid may be considered in this case: for the monophasic reactions without additional gas slugs, a laminar flow is prevalent. Hydrogen diffusion from the wall to the bulk liquid is superimposed by the parabolic velocity profile of the liquid, leading to strongly differing radial hydrogen concentrations within the liquid with high concentrations at the wall and thus a relatively small permeation driving force. At operation with slugs, half of the capillary is filled with gas slugs that are separated from the wall only by a very thin liquid film. While the additional phase change between liquid (film) and gas (slugs) may cause another mass transport resistance, no radial concentration gradient inside the gas slug is present, leading in total to a higher permeation driving force than that for a rather saturated liquid without gas slugs.

This allows to reduce the experimentally adjusted permeation pressure differences that are obtained from theoretical correlations. Obviously, the underlying model must be reevaluated for permeation with reactions in capillaries (depending on whether slugs are introduced or not), since the model was designed for short permeators and turns out to be valid only for slug flow without reactions.[141],[253] To quantify the acceleration of reaction rates and assess the role of hydrogen slugs in the permeation-assisted approach, a pseudokinetic model was established. Overall kinetic rate constants were fitted to experimental hydrogenation data at varying residence times under otherwise identical conditions. The used approach considers a consecutive reaction network and lumping of several different isomers of the same saturation but differentiates between C18:1 cis and trans species (Figure 64). Furthermore, mass transport mechanisms as well as adsorption to the catalyst surface are combined by kinetic constants of pseudo-first order. Hydrogen is applied in excess in most of the cases and is therefore also included in the pseudo-first-order approach like it is typically also done in literature[52],[74]. Details on the model equations are provided in SI. Resulting pseudokinetic rate constants can be found in Table 11.

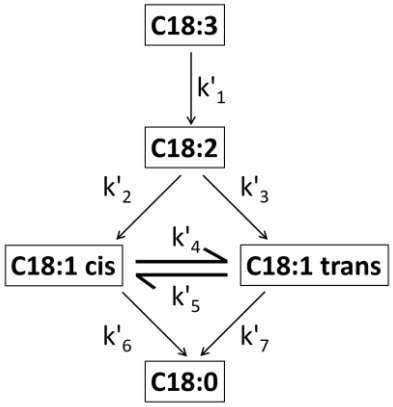


Figure 64: Reaction network used for the pseudokinetic modeling.

Table 11: Obtained Pseudokinetic Rate Constants for the Reaction Network from Figure 64 for Different Operation Modes from Figure 60

| | **batch (Figure 60a)** | **slug + permeation (Figure 60d)** | **permeation (Figure 60e)** |
|---|---|---|---|
| $\mathbf{k_1'}$ **[s$^{-1}$]** | $5.338 \cdot 10^{-4}$ | $5.830 \cdot 10^{-3}$ | $3.256 \cdot 10^{-3}$ |
| $\mathbf{k_2'}$ **[s$^{-1}$]** | $1.727 \cdot 10^{-4}$ | $2.184 \cdot 10^{-3}$ | $1.129 \cdot 10^{-3}$ |
| $\mathbf{k_3'}$ **[s$^{-1}$]** | $6.627 \cdot 10^{-5}$ | $1.120 \cdot 10^{-8}$ | $5.528 \cdot 10^{-12}$ |
| $\mathbf{k_4'}$ **[s$^{-1}$]** | $1.196 \cdot 10^{-9}$ | $8.147 \cdot 10^{-4}$ | $6.203 \cdot 10^{-4}$ |
| $\mathbf{k_5'}$ **[s$^{-1}$]** | $1.032 \cdot 10^{-4}$ | $3.011 \cdot 10^{-3}$ | $2.271 \cdot 10^{-3}$ |
| $\mathbf{k_6'}$ **[s$^{-1}$]** | $1.028 \cdot 10^{-5}$ | $4.129 \cdot 10^{-5}$ | $1.859 \cdot 10^{-12}$ |
| $\mathbf{k_7'}$ **[s$^{-1}$]** | $4.552 \cdot 10^{-14}$ | $1.633 \cdot 10^{-10}$ | $1.694 \cdot 10^{-4}$ |

The results for both investigated operation modes (with and without hydrogen slugs) are summarized in Figure 65 and clearly demonstrate the outstanding performance of the capillary system compared with batch operation. The formation rate of C18:1 from C18:2 is increased by a factor of at least 4.7 in the permeation mode without gas slugs and by more than 9.1 in the presence of permeated gas and segmented slugs.

An equivalent measure, the turnover frequency at 20% conversion ($TOF_{20}$), highlights this effect even more strikingly: while the batch experiment achieves a $TOF_{20}$ of 27,000 h$^{-1}$, the capillary approach boosts this value by a factor of 5 to 135,000 h$^{-1}$ without slugs and by almost an order of magnitude to 257,000 h$^{-1}$ in permeated slug-flow operation. This dramatic increase underscores the decisive role of the permeation-stabilized slug-flow in intensifying multiphase catalysis.

The latter mode (Figure 60d) is therefore highly favored, most likely due to the additional mass transfer enhancement by Taylor vortices within the gas slugs combined with continuous hydrogen replenishment. Especially at the reactor entrance, sufficiently large slugs are required to ensure stable segmentation even under high initial hydrogen consumption rates, thereby preventing their premature disappearance.

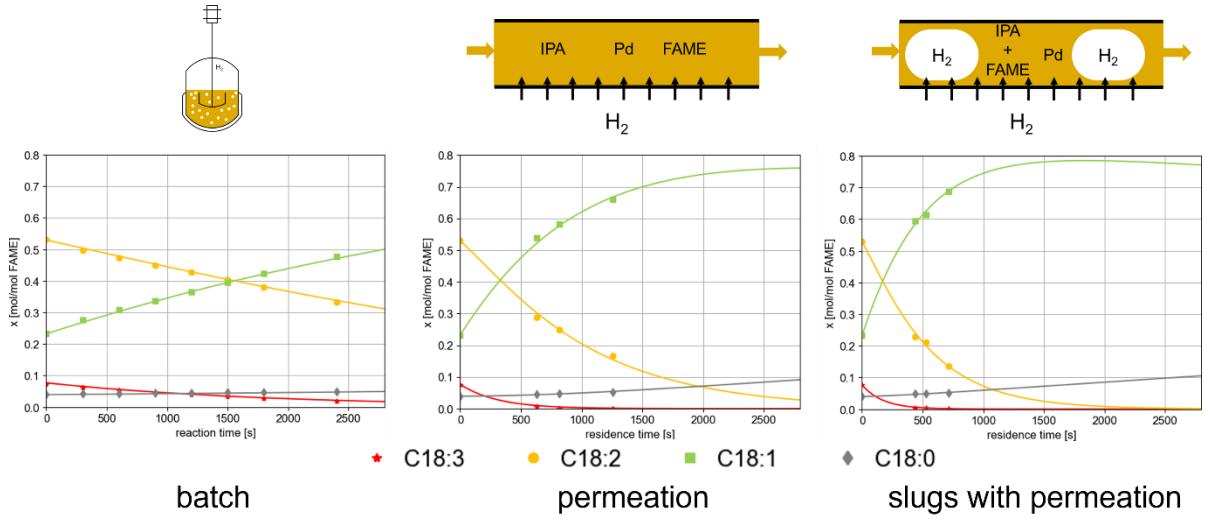


Figure 65: Modeled (solid lines; extrapolating for residence times larger than the highest one) vs measured compositions of samples of the selective partial hydrogenation of soybean FAME in different reactors and with different operational modes at constant conditions. Reaction conditions for all experiments: S:C=50,000:1, T= 80 °C, solvent= IPA, PC:solvent= 1:17.02-17.12 mL mL$^{-1}$, $w_{Pd,PC}$= 24 ppm
batch: $p_{H2}$= 11.5 bar, $V_l$=56.9 ml, ω= 3500 rpm with baffles and gas injection stirrer
permeation: $\dot{V}_{H_2,T}$= 0 mL min$^{-1}$, $\dot{V}_{total}$= 1.5-3 mL min$^{-1}$, $p_{H2,back}$= 11 bara, $\Delta p_{Perm.}$= 5.33-8.51 bar, τ= 10.5-20.9 min, l= 40 m
slugs + permeation: $\dot{V}_{total}$= 3-4.57 mL min$^{-1}$, $p_{H2,back}$= 11 bara, $\Delta p_{Perm.}$= 1.16-1.71 bar, τ= 7.3-11.9 min, l= 40 m.

### 9.4.5 Influences on Permeation

After showing the applicability of the permeation concept for the given reaction system and validating its positive effect on reaction rate enhancement, further investigations on influences on the permeation are conducted. The focus was set on the key parameters pressure, temperature, and capillary length (since length influences residence time at constant volume flows and especially permeation area). Increasing the temperature or pressure enlarges the hydrogen solubility and enhances diffusion in both the capillary material and liquid slugs, thus supplying more hydrogen in the liquid phase. Additionally, an increased temperature results in higher reaction rates according to Arrhenius' law and lowers viscosity, additionally enhancing mass transport and reducing overall pressure drop. Accordingly, variations in temperature are investigated first (Figure 66).

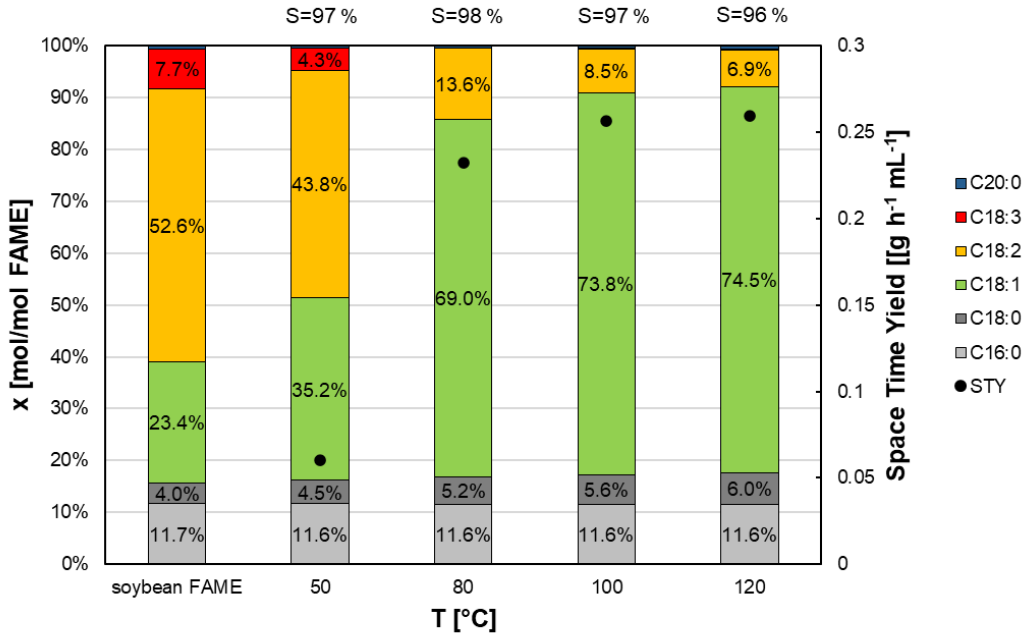


Figure 66: Composition of samples of the selective partial hydrogenation of soybean FAME in the capillary reactor with additional IPA. Reaction conditions: S:C= 50,000:1, T as stated, $p_{H2,back}$= 11 bara, l= 40 m, $w_{Pd,PC}$= 24 ppm, solvent= IPA, PC:solvent= 1:17.13 mL mL$^{-1}$,$\dot{V}_{cat.}$= 1.20 mL min$^{-1}$; $\dot{V}_{H_2,T}$= 1.50 mL min$^{-1}$; $\dot{V}_{FAME}$= 0.30 mL min$^{-1}$
T= 50 °C: $\Delta p_{Perm.}$= 0.99 bar, $\tau$= 10.2 min
T= 80 °C: $\Delta p_{Perm.}$= 1.16 bar, $\tau$= 11.9 min
T= 100 °C: $\Delta p_{Perm.}$= 1.24 bar, $\tau$= 11.7 min
T= 120 °C: $\Delta p_{Perm.}$= 1.4 bar, $\tau$= 10.8 min.

A temperature of 50 °C results in a conversion of 24% at a typical selectivity of 97% and STY of 0.06 g h$^{-1}$ mL$^{-1}$. As expected, the reaction rates accelerate at 80 °C in a comparable residence time. STY can be further improved by 10% by raising the temperature from 80 to 100 °C. When considering the last step from 100 to 120 °C, STY remains nearly constant, while at the same time, selectivity starts to decrease. Temperatures higher than 80-100 °C seem therefore not advisable for the given setup and volume flows, since the intrinsic and invariant catalyst activity and thus the given liquid volume flow appear to be the limiting factor. At all applied temperatures, gas bubbles in a regular pattern and of rather constant or even increasing size exist over the entire reactor length.

The residence time is determined by numerous parameters such as the volumetric flow rates, the length of the reactor, and, in this special case, also the reaction rate. The influence of the capillary length is further investigated, as a longer capillary results not only in a higher pressure drop but also in higher permeation fluxes as the surface area is enlarged. First, the length and volumetric flow rate are increased at the same time. In slug flow, mass transport rate via the g/l interphase is roughly linearly dependent from vertex circulation frequency[135], which in turn is enlarged for higher flow rates. Therefore, at least gas replenishment and the hydrogen supply in the liquid phase should be increased by the combination of both adjustments. However, at otherwise standard conditions of S:C of 50,000:1 and 80 °C, only minor changes in the composition after the reaction are observable for varying velocities while maintaining the same residence time (Figure S 26), indicating no limitations resulting from possible resistances in the g/l- and l-mass transport (mixing of and diffusion within the liquid slugs). Additionally,

variation of the back pressure between 11 and 16 bara does not influence the product composition significantly (Figure S 27). Hence, hydrogen concentration in the liquid phase is no limiting effect either.

Taking these results into account, extending the capillary length enables a substantial reduction of the substrate-to-catalyst (S:C) ratio to 100,000:1 at standard total flow rates, owing to the increased residence time. At this condition, operation with an 80 m capillary yields an even more favorable product composition compared to the benchmark experiment (Figure 67). Importantly, the space-time yield is further enhanced by about 13%, reaching 0.266 g $h^{-1}$ $mL^{-1}$. In the STY calculation, the higher FAME throughput is balanced by the larger reactor volume, such that the extended S:C ratio of 100,000:1 effectively halves the catalyst demand for producing the same amount of product mixture. At the same time, the concentration of the desired C18:1 species is further enriched. These findings clearly demonstrate that increasing the capillary length and thereby enlarging the S:C ratio is highly advantageous, combining more efficient catalyst utilization with improved product composition and enhanced process productivity.

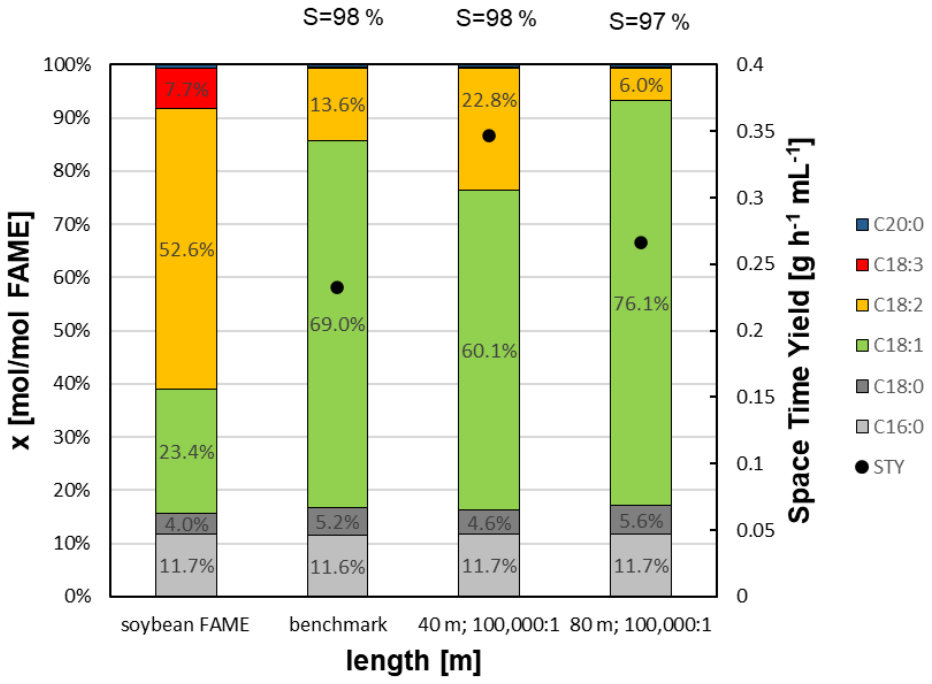


Figure 67: Composition of samples of the selective partial hydrogenation of soybean FAME in the capillary reactor with additional IPA. Reaction conditions: T= 80 °C, $p_{H2,back}$= 11 bara, $w_{Pd,PC}$= 24 ppm, solvent= IPA, $\dot{V}_{H_2,T}$= 1.50 mL $min^{-1}$; benchmark: S:C= 50,000:1, l= 40 m, $\dot{V}_{cat.}$= 1.20 mL $min^{-1}$, $\dot{V}_{FAME}$= 0.30 mL $min^{-1}$, PC:solvent= 1:17.13 mL $mL^{-1}$, $\Delta p_{Perm.}$= 1.16 bar, τ= 11.9 min
l=40 m: S:C= 100,000:1, PC:solvent= 1:12.6 mL $mL^{-1}$, $\dot{V}_{cat.}$= 0.90 mL $min^{-1}$, $\dot{V}_{FAME}$= 0.60 mL $min^{-1}$ $\Delta p_{Perm.}$= 3.45 bar, τ= 12.2 min
l=80 m: S:C= 100,000:1, PC:solvent= 1:12.6 mL $mL^{-1}$, $\dot{V}_{cat.}$= 0.90 mL $min^{-1}$, $\dot{V}_{FAME}$= 0.60 mL $min^{-1}$, $\Delta p_{Perm.}$= 1.57 bar, τ= 28.9 min.

Overall, 80 °C was confirmed as the beneficial reaction temperature for the chosen model reaction, although permeation also works for higher temperatures in principle. The reaction is not limited by g/l- and l-mass transport anymore, and hydrogen solubility in the liquid phase is sufficient, proving 11 bara of back pressure to be adequate and allowing a further reduction of catalyst usage.

### 9.4.6 Reducing the Solvent Amount

In previous sections, most of the experiments were conducted at a rather high dilution. One reason is the limited hydrogen availability in the liquid and gas phases combined with a high hydrogen demand for higher concentrated reagents. In contrast to pure slug flow, permeation offers the possibility to compensate for the converted hydrogen amount, thereby potentially allowing a reduced solvent usage. To study the influence of the solvent amount in order to increase STY, the standard proportion of FAME in the total liquid phase of $\varphi_{FAME}$= 0.2 mL mL$^{-1}$ is gradually increased, keeping the total liquid flow, gas flow, and S:C ratio constant (Figure 68).

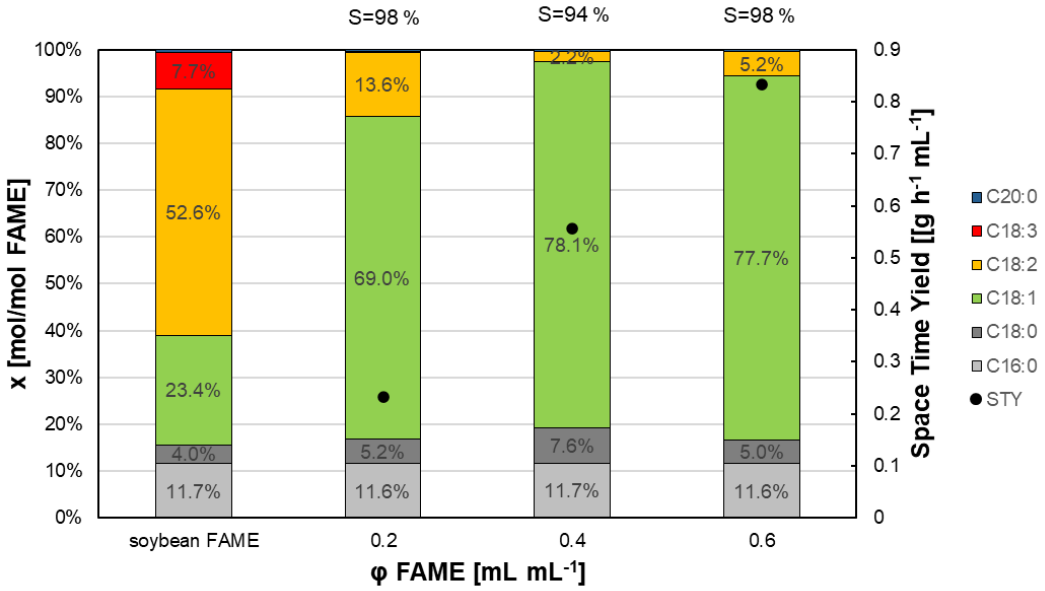


Figure 68: Product composition of the selective partial hydrogenation of soybean FAME in the capillary reactor with varying IPA content. Reaction conditions: S:C= 50,000:1, T=80 °C, $p_{H2,back}$= 11 bara, l= 40 m, $w_{Pd,PC}$= 24 ppm, solvent= IPA, $\varphi_{FAME}$= 0.2 mL mL$^{-1}$: $\dot{V}_{cat.}$= 1.20 mL min$^{-1}$; $\dot{V}_{H_2,T}$= 1.50 mL min$^{-1}$; $\dot{V}_{FAME}$= 0.30 mL min$^{-1}$, PC:solvent= 1:17.13 mL mL$^{-1}$, $\Delta p_{Perm.}$= 1.16 bar, τ= 11.9 min
$\varphi_{FAME}$= 0.4 mL mL$^{-1}$: $\dot{V}_{cat.}$= 0.90 mL min$^{-1}$; $\dot{V}_{H_2,T}$= 1.50 mL min$^{-1}$; $\dot{V}_{FAME}$= 0.60 mL min$^{-1}$, PC:solvent= 1:5.8 mL mL$^{-1}$, $\Delta p_{Perm.}$= 3.65 bar, τ= 18.8 min
$\varphi_{FAME}$= 0.6 mL mL$^{-1}$: $\dot{V}_{cat.}$= 0.60 mL min$^{-1}$; $\dot{V}_{H_2,T}$= 1.50 mL min$^{-1}$; $\dot{V}_{FAME}$= 0.90 mL min$^{-1}$, PC:solvent= 1:2.02 mL mL$^{-1}$, $\Delta p_{Perm.}$= 6.35 bar, τ= 19.8 min, full conversion is restricted by limited hydrogen supply.

The results show that the STY increases with increasing FAME concentration, reaching an STY of up to 0.83 g h$^{-1}$ mL$^{-1}$. This is mainly due to higher FAME volume flows resulting from lower solvent proportions. Simultaneously, residence time also increases due to complete bubble loss. This effect contributes to the observation of incomplete conversion for the highest FAME concentration, even though the longest residence time was achieved. That indicates that permeation did not provide sufficient hydrogen for this high substrate concentration in the investigated setup. A complete abandonment of IPA ($\varphi_{FAME}$= 0 mL mL$^{-1}$, not shown in Figure 68) is accordingly not meaningful; very small catalyst slugs of inconsistent size form, and the flow pattern becomes highly unstable, leading to only 42% conversion.

Applying a proportion of $\varphi_{FAME}$= 0.4 mL mL$^{-1}$ enables 97% conversion of the excess double bonds in the capillary reactor. Although both higher concentrated experiments show comparable amounts of

C18:1 and STY is highest for the lowest solvent amount, $\varphi_{FAME}$= 0.4 mL mL$^{-1}$ is favorable if the product will be used for further chemical conversions due to lower amounts of interfering polyunsaturated species, marking this concentration as optimum unless a higher permeation flux can be established.

### 9.4.7 Influences of Dilution and Permeation on Gas Slugs and Residence Time

The results presented so far implicitly highlight the strong interdependence among dilution, apparent reaction rate, and permeation fluxes, all of which ultimately govern the effective residence time. The dynamic balance between permeation-driven gas replenishment and catalytic conversion directly determines the evolution of gas slug lengths along the reactor. At higher reaction rates or elevated FAME concentrations, gas uptake by permeation becomes more demanding, underscoring the critical role of the liquid-phase composition. In this way, dilution not only defines the reaction environment but also modulates the gas phase behavior and thereby indirectly shapes the residence time. The latter, in turn, controls the final product distribution as long as hydrogen is present in excess. Figure 69 schematically illustrates how typical liquid-phase compositions influence these key parameters, emphasizing the tight interplay between transport phenomena and catalytic performance in the permeation-assisted slug-flow operation.

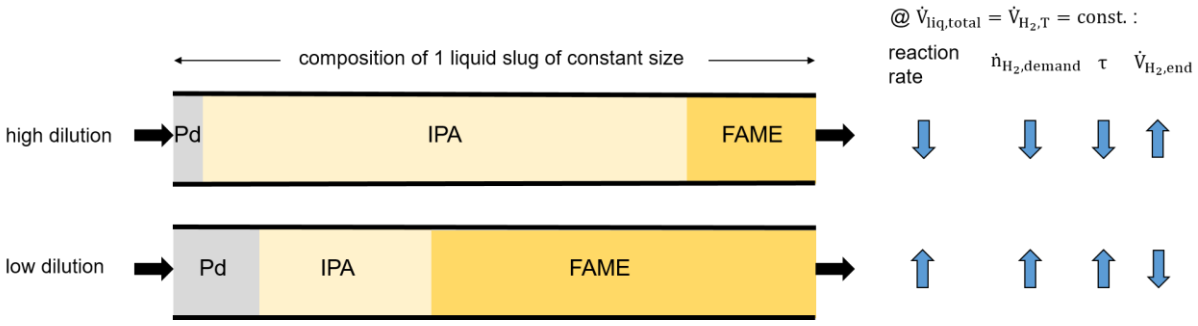


Figure 69: Sketch of the effects of substrate dilution on operational parameters.

Figure 70 (magnified version: Figure S 28) addresses the impact of the solvent amount (and accordingly the concentration of FAME in the liquid phase) on the residence time at typically applied equal liquid and gaseous inlet volume flows. The lower red curve corresponds to a constant ideal gas bubble size, and the upper red curve corresponds to instantaneous bubble disappearance. The gray areas mark operational constraints of the setup; thus, the feasible operational window lies within the white area and below the upper red line.

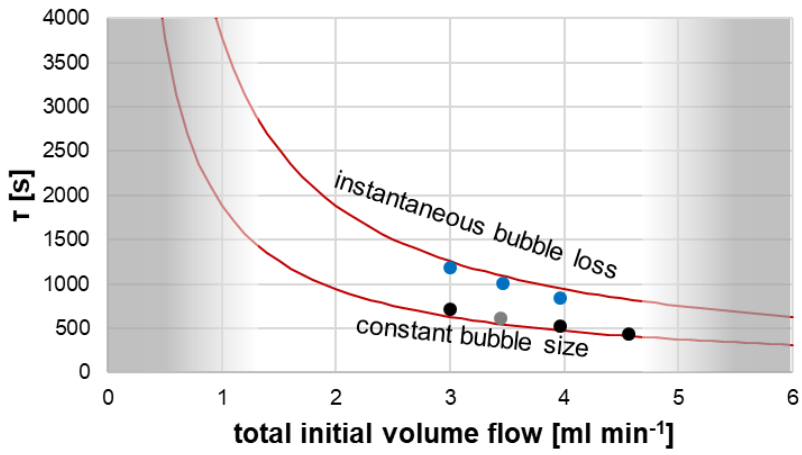


Figure 70: Obtained residence times of the selective partial hydrogenation of soybean FAME in the capillary reactor with varying IPA contents and at different volume flows (blue: low dilution; black/ gray: high dilution). Reaction conditions: S:C= 50,000:1 (gray point: 69,570:1), T=80 °C, $p_{H2,back}$= 11 bara, l= 40 m, $w_{Pd,PC}$= 24 ppm, solvent= IPA, $\dot{V}_{H_2,T} = \dot{V}_{liq,total}$
black/gray points: PC:solvent= 1:17.13 mL mL$^{-1}$ (gray point: 1:14.64), $\Delta p_{Perm.}$= 1.16-1.71 bar, $\dot{V}_{total}$= 3-4.57 mL min$^{-1}$,
blue points: PC:solvent= 1:2.02 mL mL$^{-1}$, $\Delta p_{Perm.}$= 6.35-8.27 bar, $\dot{V}_{total}$= 3-3.96 mL min$^{-1}$, full conversion and spontaneous bubble formation are restricted by limited hydrogen supply.
Red lines: constant bubble size resp. instantaneous bubble disappearance;
gray areas: operational limits of the system.

For high IPA concentrations (and hence high dilution; mostly presented until now), the converted hydrogen can be compensated, showing more than 60% of the initial slug length at the end of the reactor. The drastic reduction of IPA by a factor of 8.5 (c.f. Figure 69) leads to fast gas consumption, resulting in prolonged residence times and fewer gas slugs (see also Figure 71). Correspondingly, the CV of the liquid slugs for the first two measurements starts to vary by drastic shrinkage by ca. 1/3, whereas the CV of the gas slugs roughly doubles (Figure 72, right). Here, even the enlarged permeation pressure difference is not able to replenish hydrogen appropriately. In general, this would present a major drawback, favoring consecutive or side reactions of the obtained products. However, for this specific catalyst system, side reactions do not exist and the follow-up overhydrogenation toward the undesired C18:0 species is concurrently limited due to the low hydrogen availability. The limited hydrogen supply underlines that IPA cannot be fully omitted and simultaneously demands for higher permeation fluxes.

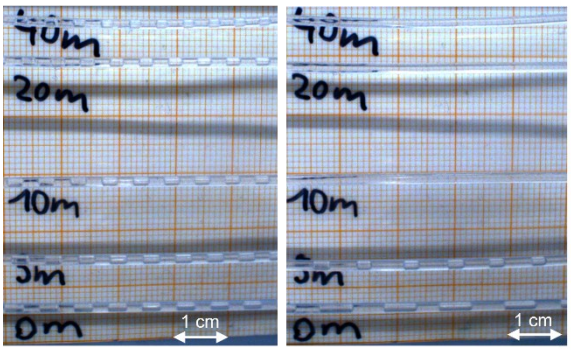


high dilution low dilution

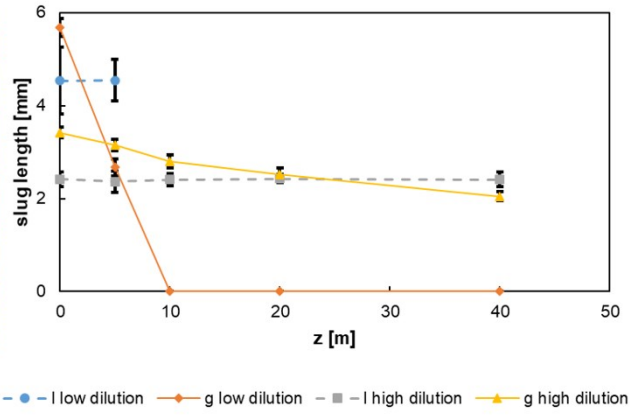


Figure 71: Images of the flow pattern and corresponding slug lengths at different axial positions obtained during the selective partial hydrogenation of soybean FAME in the capillary reactor with permeation and varying IPA content. Lines are shown for

visualization purposes only. On average, 9 complete slugs were measured at each axial position, if applicable. Reaction conditions: S:C= 50,000:1, T=80 °C, $p_{H2,back}$= 11 bara, l= 40 m, $w_{Pd,PC}$= 24 ppm, solvent= IPA
high dilution: PC:solvent= 1:17.13 mL mL$^{-1}$, $\dot{V}_{cat.}$= 1.20 mL min$^{-1}$; $\dot{V}_{H_2,T}$= 1.50 mL min$^{-1}$; $\dot{V}_{FAME}$= 0.30 mL min$^{-1}$, $\Delta p_{Perm.}$= 1.16 bar, $\tau$= 11.9 min
low dilution: PC:solvent= 1:2.02 mL mL$^{-1}$, $\dot{V}_{cat.}$= 0.60 mL min$^{-1}$; $\dot{V}_{H_2,T}$= 1.50 mL min$^{-1}$; $\dot{V}_{FAME}$= 0.90 mL min$^{-1}$, $\Delta p_{Perm.}$= 6.35 bar, $\tau$= 19.8 min. Full conversion and spontaneous bubble formation are restricted by limited hydrogen supply.

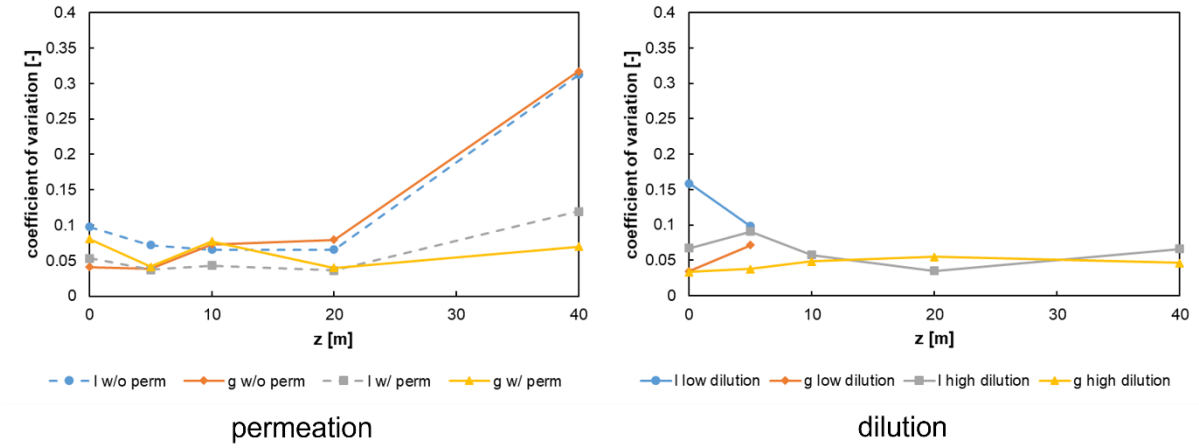


Figure 72: Axial profile of the coefficients of variation for slugs during selective partial hydrogenation of soybean FAME with additional IPA. Lines are shown for visualization purposes only. On average, 9 complete slugs were measured at each axial position, if applicable. Left: comparison for slug flow with and without permeation. For conditions, see Figure 63. Right: comparison for slug flow with permeation with varying dilution. For conditions, see Figure 71.

## 9.5 Conclusion

The catalytic and selective hydrogenation of biodiesel was employed as a model reaction to demonstrate, for the first time, the integration of gas permeation into a reactive slug flow. Continuous replenishment of hydrogen through the capillary wall compensates for bubble shrinkage during the reaction and stabilizes the slug-flow regime. This ensures that the characteristic advantages of capillary operation – enhanced mixing, intensified gas-liquid mass transport, and narrow residence time distributions – are preserved under reactive conditions.

Using soybean-derived FAME as substrate, the system achieved more than a 9-fold increase in the rate of formation of the desired C18:1 product from C18:2 compared to batch operation under similar conditions, directly underlining the limitations of batch setups and the transport benefits of slug-flow with permeation. The resulting $TOF_{20}$ equivalent figure reaches a remarkable value of 257,000 h$^{-1}$. Selectivities of up to 98% were obtained with space−time yields (STYs) of approximately 0.23 g h$^{-1}$ mL$^{-1}$ at high dilution. Increasing the substrate concentration raised the STY to about 0.56 g h$^{-1}$ mL$^{-1}$ at an optimum FAME fraction of 0.4 mL mL$^{-1}$, while the extent of overhydrogenation remained low under typical flow conditions. At these conditions, no mass transport limitations in gas-liquid exchange or liquid mixing were observed, and hydrogen solubility did not limit the overall performance.

Slug-flow with permeation consistently proved to be more efficient than laminar flow without gas segments. Nevertheless, the precise quantification of permeated gas remains challenging due to error-

prone literature values of permeation coefficients, indicating that further work is required to refine predictive models.

Overall, this study establishes permeation as a powerful tool to enable the continuous operation of gas-consuming reactions in capillary slug-flow reactors. The demonstrated biodiesel hydrogenation highlights both the catalytic selectivity achievable with renewable feedstocks and the engineering advantages of the permeation-stabilized flow. The methodology is broadly applicable beyond this model reaction, offering new perspectives for the sustainable process intensification. Future work should focus on developing quantitative kinetic−transport models and extending the concept to tandem or cascade reactions, in which permeation-controlled gas addition and removal could provide localized control and further broaden the versatility of permeable capillary reactors.

## 9.6 Acknowledgments

The authors thank the networking program “Sustainable Chemical Synthesis 2.0” (SusChemSys 2.0) for the support and fruitful discussions across disciplines. Finally, we are very thankful to the German Federal Ministry of Agriculture, Food and Regional Identity (Bundesministerium für Landwirtschaft, Ernährung und Heimat), represented by the FNR (Fachagentur Nachwachsende Rohstoffe) for financial support of the young research group ″Renewlysis″ (project number 2219NR355).

# 10 Summary and Outlook

This thesis showcases the broad applicability of colloidal Pd nanoparticles in all four levels of process intensification and demonstrates, for the first time, a holistic, application-oriented catalyst and process development with this highly active catalyst class. In doing so, a selection of process intensification measurements on all four hierarchical levels is applied for a variety of catalytic reactions, summarized in Figure 73.

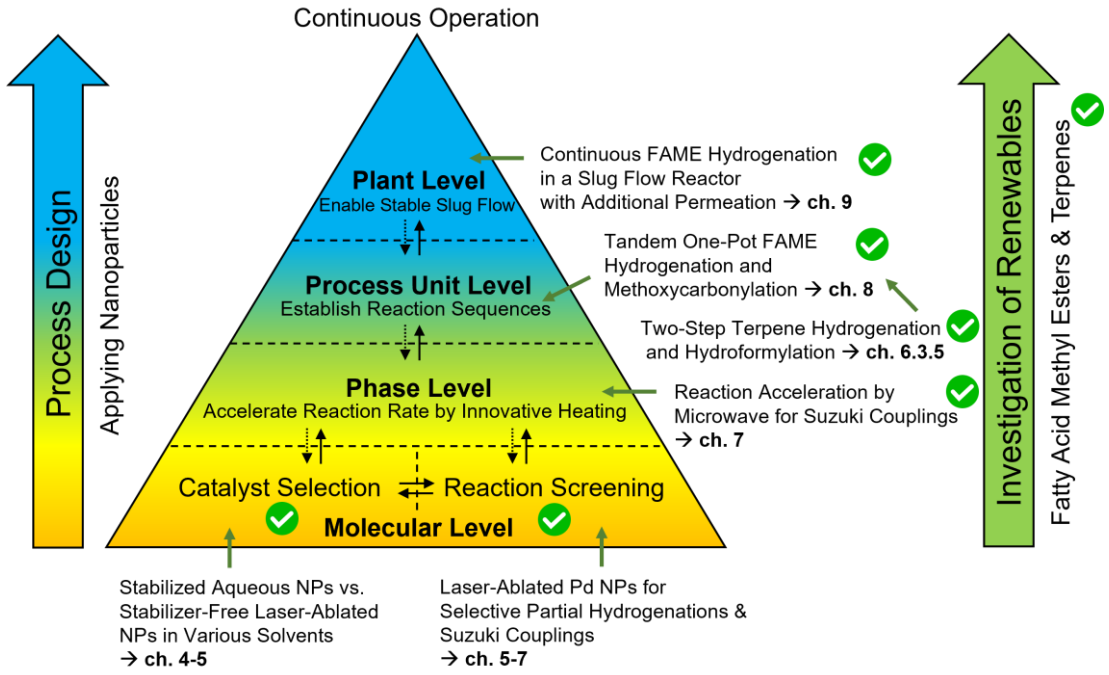


Figure 73: Summary of all main aspects of this work towards an intensified utilization of catalytically active nanoparticles.

The molecular level was remarkably divided into catalyst selection and reaction screening. Starting with the selection of a suitable catalyst, top-down and bottom-up synthesis procedures for catalytically active colloidal nanoparticles were presented and evaluated for a more complete overview. Aqueous, differently stabilized colloidal Pd nanoparticles of various sizes and shapes were shown to be suitable for the selective partial hydrogenation of two different alkynes at an unmatched pressure of 50 bar, once in a monophasic approach and once in a biphasic approach. A strong size dependence was found, with the most active nanoparticles being spherical particles of ca. 5 nm diameter, regardless of their stabilizer. These particles exhibit turnover frequencies up to 183,000 $h^{-1}$. However, mass transport limitations were observable for the biphasic approach, leading to reduced turnover frequencies. The comparison of transmission electron microscopy images of the particles before and after the reaction was extensively performed for the first time and shows for all larger particles significant aggregation, while size and shape of the primary particles remain intact. This often leads to precipitation of these types of nanoparticles after catalysis, especially in the biphasic reaction. The conclusion can be made that the particle size of 5 nm is favorable for catalytic applications, but water is not a preferred stabilizer for catalytic applications. Furthermore, the wet-chemical approach requires a long synthesis procedure including workup steps.

Therefore, to drastically improve the synthesis route to particles with a comparable particle size and to compare the wet-chemical bottom-up approach with a physical top-down approach, solvent-stabilized nanoparticles with average sizes of 5 nm were, in a second step, produced by pulsed laser ablation in liquids. Variations of metals and solvents were tested in the selective partial hydrogenation of polyunsaturated fatty acid methyl esters towards the monounsaturated compounds to identify the optimal combination. During these tests, Pd in the rather “green” solvent propylene carbonate was found to be the best compromise in terms of activity, selectivity, and availability for this reaction. Further tests and a typically not performed comparison with literature data reveal this system as one of the most selective ones, even for high conversions of the polyunsaturated species (with a selectivity of more than 95% until 90% conversion), showing comparatively low amounts of trans-configured species. At the same time, this system shows superior robustness against varying reaction conditions. The Horiuti-Polanyi mechanism is able to explain all observed phenomena, as evidenced by nanoparticles with similar characteristics from the literature-known autoreductive approach. However, further experiments are demanded to verify a truly heterogeneous reaction pathway for hydrogenation.

The highly promising catalyst system of colloidal laser-ablated Pd nanoparticles in propylene carbonate was subsequently subjected to a reaction screening located at the molecular level of process intensification to generate first insights into potentially useful reactions beyond alkene hydrogenation. The selective partial hydrogenation of various substrate classes was investigated first, ranging from several alkynes to α,β-unsaturated aldehydes, cyclic non-conjugated polyenes, and several terpenes, including conjugated examples. Substrate:catalyst ratios higher than 7,000 and Pd concentrations of 24 ppm and less in the catalyst phase were applied in both mono- or biphasic reaction systems, enabling a very low Pd usage due to high activities. The biphasic approach offers opportunities for a subsequent catalyst reuse and product purification. Alkynes and conjugated dienes were shown to react in a very short time frame of ca. 2 h and less with high selectivities, whereas α,β-unsaturated aldehydes and non-conjugated terpenes react far more slowly, showing a superior thermodynamic selectivity behaviour. For cyclic non-conjugated polyenes, a strong dependence on steric properties seems to prevail. Overall, Pd in propylene carbonate was found to be a versatile, robust, and highly selective alternative to the conventional Lindlar catalyst, also in terms of environmental and manufacturing aspects. The hydrogenation of conjugated systems most likely proceeds via a $\eta^3$-mechanism, resulting in a sharply defined product composition. For the biphasic systems, product contamination with Pd was within the limit of quantification of the ICP-OES of 1 ppm. Accordingly, pulsed laser ablation in liquids allows a fast and reproducible synthesis of highly active and selective catalysts and can thus be considered as a measure for intensification of the synthesis itself. Laser-ablated nanoparticles in stabilizing solvents like propylene carbonate have been tested in the literature for catalytic gas/liquid reactions only once before, examining a different substrate class and solvent[11]. Therefore, these investigations broadly extend the applicability of these types of particles.

On the transition to the phase level for further expansion of the catalytic applicabilities of laser-ablated nanoparticles, Suzuki coupling reactions with colloidal laser-ablated Pd in the “green” solvent 1-butanol were carried out in reflux and in a microwave reactor. Here, microwave irradiation enabled the drastic

reduction of the reaction time to one-eighth compared to conventional reflux conditions, maintaining similar product yields. Accordingly, the application of microwave irradiation with solvent-stabilized Pd nanoparticles for reaction rate enhancement is a measure located on the phase level. In a subsequent substrate scope under microwave conditions, yield was found to strongly depend on the halide and, within the same halide, on the electronic properties of the substrate. In accordance with the literature, those with electron-donating substituents only gave poor yields. However, further substrates with electron-withdrawing substituents should be investigated to strengthen this finding. For the investigated Suzuki couplings, a dynamic catalytic reaction mechanism was elucidated via several complementary test reactions. In this case, Pd nanoparticles only serve as a reservoir for leaching Pd species that are the true catalytic species, which is a well-known phenomenon in the literature. During this process, deactivation by agglomeration and aggregation is a strong competitive reaction to the desired C-C coupling by leaching Pd species. Accordingly, the kinetically stabilized catalyst nanoparticle is more susceptible to deactivation/destabilization during Suzuki couplings as well as storage than the solutions in propylene carbonate for the hydrogenation reactions. These findings allow a more thoughtful catalyst handling for any similar coupling reactions and might be transferred to similar nanoparticulate coupling catalysts.

Advancing the application of nanoparticles, a subsequent hydroformylation of nanocatalytically partially hydrogenated terpenes was carried out for the first time, applying a bulky phosphite and Rh as the catalyst metal for hydroformylation. Under initially chosen, unoptimized reaction conditions, product aldehyde yields up to ca. 40% were achievable within one hour of reaction. Non-hydrogenated terpenes with conjugated double bonds were found to be nearly completely inactive, as expected. This strongly necessitates selective partial hydrogenation for the utilization of polyunsaturated terpenes for fragrance applications and might be transferable to other conversions of such polyunsaturated terpenes with homogeneous catalysts. Further research should focus on the optimization of hydroformylation reaction conditions, including a ligand screening, in order to reduce the amount of product isomers and to achieve higher total aldehyde yields. This is intended to meet industrial requirements and enable the utilization of this reaction sequence on larger scales. These first-principle investigations lead in the direction of further, intensified reaction sequences with nanoparticles.

On the process unit level, such a reaction sequence was thoroughly investigated: Based on initially generated knowledge from the selective partial fatty acid methyl ester hydrogenation with colloidal Pd nanoparticles, an integrated two-step reaction sequence comprising a selective partial fatty acid methyl ester hydrogenation with a subsequent isomerizing methoxycarbonylation was established for the first time for colloidal Pd nanoparticles. For this tandem reaction system, a one-pot procedure was developed to avoid intermediate workup and to enable dual use of the precious catalyst metal Pd. Accordingly, this approach is a representative of process intensification at the process unit level. In this streamlined process, special attention must be paid to accurate gas change, among other things. The solvents of each individual reaction step were partly found to negatively influence the other reaction of the sequence. Pure methanol was identified to be a viable compromise; however, polyunsaturated compounds remain after hydrogenation, which negatively influence the subsequent isomerizing

methoxycarbonylation. Nevertheless, applying the optimized workflow enables excellent 98% selectivity towards the linear diester at ca. 40% conversion of monounsaturated fatty acid methyl esters obtained from the first reaction step. In order to enable the utilization of the whole applied amount of Pd for the second reaction step, further attention should be paid to deactivation mechanisms during gas change and ligand addition. Moreover, recycling of the spent catalyst solution is of major interest for the highest possible resource utilization and cost efficiency, which can be investigated in future work. Catalyst recycling is also a valuable future development task for all other presented hydrogenations and the hydroformylation step. For this purpose, the stabilization ability of propylene carbonate seems highly advantageous, especially for the biphasic approaches. However, experiments in this regard still need to be performed.

Ultimately, the selective partial fatty acid methyl ester hydrogenation was conducted in a capillary reactor. Here, the focus was set not only on pure process intensification by enhanced mixing behavior due to slug flow, but also on the replenishment of the consumed reaction gas via permeation through the capillary material, which has mostly been shown only without a simultaneous reaction before. In this setup, the fluorinated ethylene-propylene capillary reactor is operated as a catalytic membrane reactor of the distributor type[124],[125], being a striking example for process intensification on the topmost plant scale, enabling the application of nanoparticles in a first continuous and even intensified process. The multifunctional process unit represents the incorporation of a mass transfer unit into a reactor unit. With this approach, it was shown for the first time that gas replenishment by permeation compensates for bubble shrinkage in a reactive capillary slug flow, preserving the beneficial slug flow properties over the whole reactor length. This reactor operation mode facilitates drastic rate enhancements at a comparable selectivity: The reaction rate of the formation of C18:1 from C18:2 with slug flow and permeation was found to be more than 9-fold as high as for a conventional batch reactor with baffles at high stirring rates. Furthermore, operation with gas slugs was found to be more efficient than a laminar liquid flow without gas slugs. Further optimization enabled a space-time-yield up to 560 $kg\ h^{-1}\ m^{-3}$, and shows concentration limits of the substrate, necessitating further improvements of the permeation flux for highly concentrated or pure substrates. These findings offer new opportunities for various other reactions in multiphase gas/liquid capillary slug flow, with targeted gas replenishment or removal that should be addressed in future work. At the same time, quantitative models that combine reaction kinetics, mass transport phenomena, and hydrodynamics need to be developed to enable a knowledge-based design and operation of this highly promising continuous laboratory reactor type.

All presented investigations are valuable building blocks to stringently develop and utilize new, highly efficient catalyst materials like the applied nanoparticle systems in an extended, holistic approach, based on an engineering perspective. This approach pursues and facilitates the aim of innovative, integrated, intensified, and sustainable chemical processes for a successful transformation towards an environmentally more benign chemical industry. The repeated use of renewable substrates on several different levels of this research also emphasizes their potential for bio-based building blocks of the future.

# 11 Appendix

## 11.1 Supporting Information for Chapter 4

### 11.1.1 Chemicals and Reagents

2-methyl-3-butyn-2-ol (Thermo Scientific, 99.5%), 2-methyl-3-butene-2-ol (TCI, 98.5%), 2-methyl-2-butanol (Thermo Scientific, 99.9%), tert.-butanol (Carl Roth, 99.9%), 1-octyne (abcr, Thermo Scientific, >99%), 1-octene (Acros Organics, 99.7%), 2-octenes (AlfaAesar, 99.8%), n-octane (TCI, >99.5%), o-xylene (Acros Organics, 99.5%), cyclohexane (Hanke+Seidel, ≥99.7%), dodecane (ABCR, 99%), hydrogen gas (Messer, 99.999%), argon gas (Messer, 99.996%), Lindlar catalyst (Sigma-Aldrich, 4.5 wt% Pd), chloroform-d (Deutero, ≥99.8%), disodium tetrachloropalladate (Carbolution, 98%), glutathione (Sigma-Aldrich, 98%), sodium borohydrate (Sigma-Aldrich, 98%), potassium bromide (Carl Roth, 99.5%), ascorbic acid (Carl Roth, 99%), polyvinylpyrrolidone ($PVP_{55}$, 55 kDa, Sigma-Aldrich), polyvinylpyrrolidone ($PVP_{40}$, 40 kDa, Fluka), and glucose (Baker, 97%) were used as obtained. Deionized water was freshly prepared with an ELGA Purelab instrument.

### 11.1.2 Analysis of Reaction Mixtures with GC-FID, GC-MS-EI and NMR

Hydrogenations of **1** were analyzed by GC-FID with an Agilent 7890B instrument, equipped with a HP-Innowax column (30 m, 0.25 mm, 0.25 µm) with $N_2$ as carrier gas. 200 mg of the water-containing samples were mixed with 15 mg tert.-butanol as external standard in a GC vial with microinserts. The pure reaction mixture from the Lindlar catalyst experiment was diluted with water to reach the same mass of water and analytes.

Table S 1: Heating profile of GC-FID for the analysis of hydrogenation products of **1**

| | **Rate / K min$^{-1}$** | **Temperature / °C** | **Holding time / min** |
|---|---|---|---|
| **$T_{Start}$** | - | 50 | 2 |
| **Ramp 1** | 30 | 90 | 2 |
| **Ramp 2** | 20 | 150 | 4 |
| **Ramp 3** | 7 | 210 | 2 |
| **Ramp 4** | 50 | 250 | 3 |

65 mg of the organic phase of the hydrogenation of **2** were diluted with 285 mg cyclohexane and mixed with 15 mg o-xylene as external standard. For quantification, these mixtures were measured on an Agilent 7890B instrument with a HP-5 GC column (30 m, 0.32 mm, 0.25 µm) and FID with $N_2$ as carrier gas. t-3-octene and n-octane elute at the same retention time. To exclude the formation of t-3-octene, additional GC-MS-EI measurements were conducted on the same device with the same temperature profile on a HP-5 (30 m, 0.25 mm, 0.25 µm) GC-MS column with He as carrier gas in order to search for characteristic fragments of the respective compounds.

$^{1}H$ and $^{13}C$ NMR spectra were recorded on Bruker NMR instruments (Avance III HD or Avance NEO series) with frequencies of 400, 500 or 600 MHz to exclude the formation of 3-octenes. Thereby, it was confirmed that t-3-octene was formed only in traces or (in most cases) not at all. Due to the very low solubilities of substrate and all commercially available products in water, only the organic phase was measured and used for all further calculations.

Table S 2: Heating profile of the GC-FID and GC-MS-EI for the analysis of hydrogenations of **2**

| | **Rate / K min$^{-1}$** | **Temperature / °C** | **Holding time / min** |
|---|---|---|---|
| **$T_{Start}$** | - | 50 | 2 |
| **Ramp 1** | 1 | 60 | 0 |
| **Ramp 2** | 40 | 250 | 2 |

## 11.1.3 Calculation of Reaction Indicators

Conversion and selectivity for both hydrogenation types were determined after calibration of the instruments with reference samples. The response factors of the dimers were estimated as average of the response factors of all monomers for **1** and as average of all alkenes for **2**. Conversion accounts for all converted substrate molecules; selectivity is only calculated towards the desired alkene. Thus, dimer formation and overhydrogenation to the alkane lower selectivity. In particular, the isomerization of **5** to **7** also lowers the selectivity.

The pressure reactor setup used allowed logging of the evolution of temperature and gas consumption. This was used for further analysis of the experiments: Initial turnover frequencies were calculated by the profile of consumed hydrogen detected by the mass flow controller (MFC). To correct measurement errors, $H_2$ consumption until the first sample withdrawal was calculated from GC measurements applying the ideal gas law. The measured consumption values (by MFC) were adjusted to this calculated value. For nearly all reactions, a roughly linear progression at the beginning of each experiment was observed. Therefore, a linear regression of consumption over time for the first 10 mmol (224 mLn) of consumed $H_2$ (corresponding to $X_{substrate} \leq 0.2$) was performed. This regression value was used to calculate the initial TOF by equation (4). All values were rounded to significant digits.

$$TOF = \frac{\partial \frac{n_{H2}}{n_{Pd}}}{\partial t}\bigg|_{10\ mmol\ H2} \xrightarrow{linear\ regression} TOF = \frac{1}{n_{Pd}} \cdot \left(\frac{\Delta n_{H2}}{\Delta t}\bigg|_{10\ mmol\ H2}\right)_{regression} \quad (4)$$

It has to be stated that some of the reactions permitted a linear regression in the initial phase but showed accelerating behaviour towards the end of the reaction. Therefore, both TOF and $t_{T,max}$ are always given.

## 11.1.4 Further Procedures for Hydrogenation Reactions

The palladium content of all concentrated nanoparticle solutions was determined by ICP-OES prior to the hydrogenation reactions to determine adjust the palladium concentration to the desired value.

After each high-pressure reaction, the vessels and stirrers used were first cleaned with acetone and laboratory wipe and subsequently with brushes and scrubbing milk under water to remove any visible palladium deposit. Each substrate was hydrogenated in a separate reactor to allow maximum comparison of the different particles. Blind reactions without palladium were conducted prior to the whole set of catalytic experimemts and again thereafter. While at the beginning only negligible blind activity was visible, it rose to roughly 23% *X* per 30 min for **1** and 13% *X* in the first hour for **2**. On the other hand, we found that an equivalent amount (the same as attached to the nanoparticles) of free dissolved GSH reduced the blind activity to 4% in 30 min.

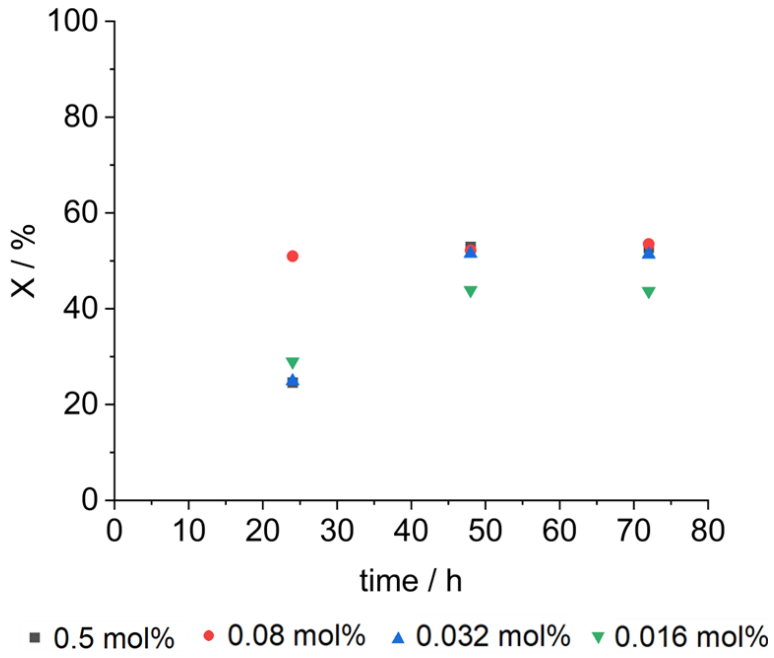


Figure S 1: Hydrogenation of **1** at 1 atm $H_2$. *X*,*t*-plot of the hydrogenation of **1** with GSH-coated ultrasmall palladium nanoparticles (2 nm) at different catalyst loadings. Further conditions: $n_{substrate}$ = 25 mmol (10 mmol for 0.5 mol%), $p_{H2}$ = 1 atm, $f_{stirrer}$ = 1,400 rpm, *T* = RT, $t_{preforming}$ = 10 min, semibatch conditions.

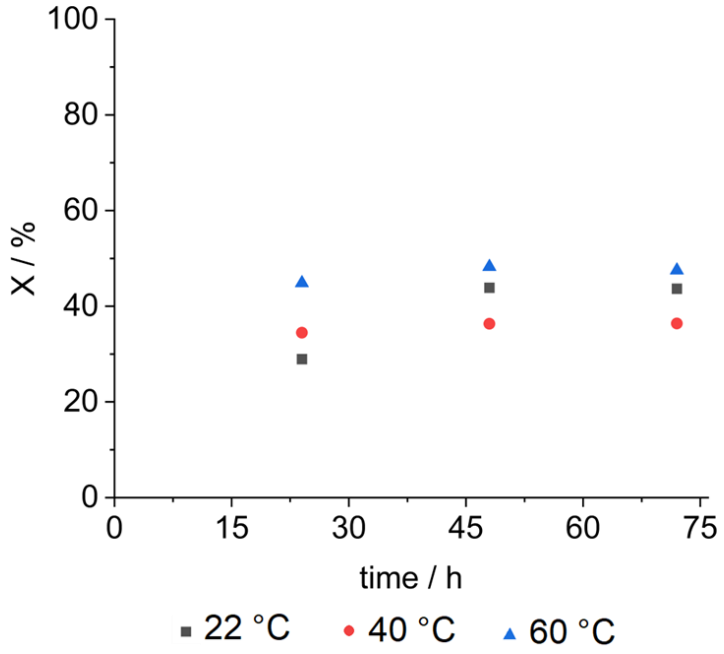


Figure S 2: Hydrogenation of **1** at 1 atm $H_2$. *X*,*t*-plot of the hydrogenation of **1** w with GSH-coated ultrasmall palladium nanoparticles (2 nm) at different temperatures. Further conditions: $n_{substrate}$ = 25 mmol, $p_{H2}$ = 1 atm, $f_{stirrer}$ = 1,400 rpm, $c_{Pd}$ = 0.016 mol%, $w_{Pd,H2O}$ = 16 ppm, $t_{preforming}$ = 10 min, semibatch conditions.

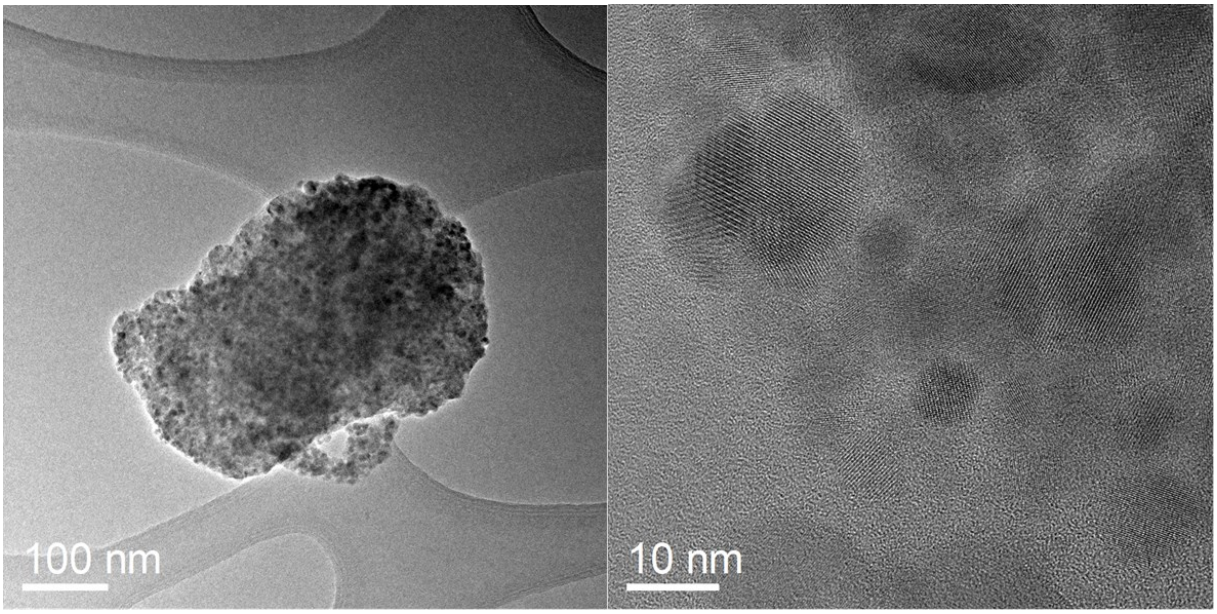


Figure S 3: Hydrogenation of **1** at 1 atm $H_2$. HRTEM images of the recovered particles after hydrogenation of **1** with GSH-coated ultrasmall palladium nanoparticles (2 nm) under hydrogen at 1 atm. Conditions: $n_{substrate}$ = 25 mmol, $p_{H2}$ = 1 atm, $f_{stirrer}$ = 1,400 rpm, $c_{Pd}$ = 0.016 mol%, *T* = RT, $w_{Pd,H2O}$ = 16 ppm, $t_{preforming}$ = 10 min, semibatch conditions.

Hydrogen solubility in water is rather low in comparison to organic solvents.[254] At 1 atm, hydrogen supply by solubility in the liquid phase is assumed to be insufficient, leading to an increased competition of hydrogen with the polar substrate **1** and the stabilizer GSH, causing increased coordination of the alkynol. **1** might be a weak stabilizer, thus aggregates of nanoparticles can form. The surface area available for catalysis is thereby reduced, which in turn leads to incomplete conversion.

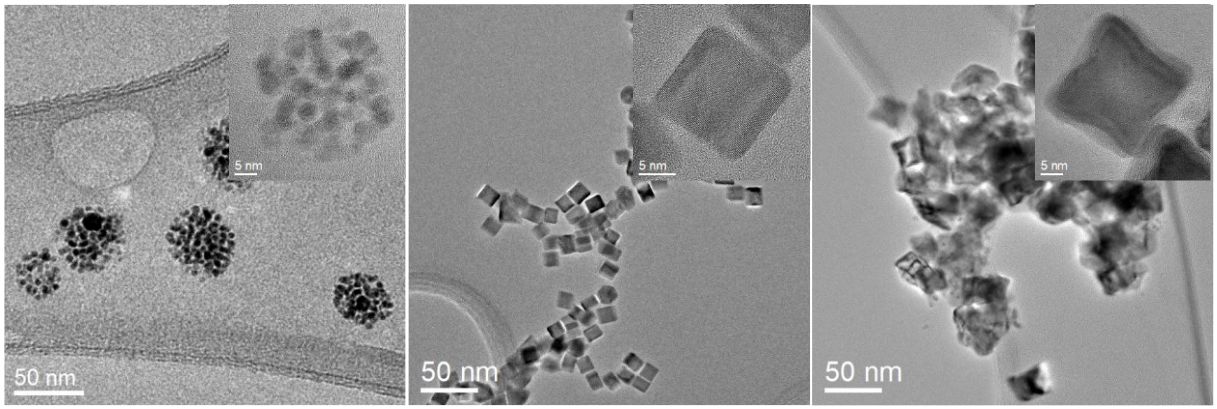


Figure S 4: Hydrogenation of **1** with palladium nanoparticles at 50 bar. TEM images of larger PVP-coated spherical palladium nanoparticles (5 nm) (**left**), of smaller palladium nanocubes (18 nm) (**center**), and larger palladium nanocubes (28 nm) (**right**) after hydrogenation of **1** at 50 bar hydrogen pressure. Conditions: $n_{substrate}$ = 50 mmol, $p_{H2}$ = 50 bar, $f_{stirrer}$ = 1,500 rpm, $c_{Pd}$ = 0.016 mol-%, $T_{start}$ = RT, $w_{Pd,H2O}$ = 16 ppm, $V_{total}$ = 58.1 mL, $t_{preforming}$ = 10 min, semibatch conditions.

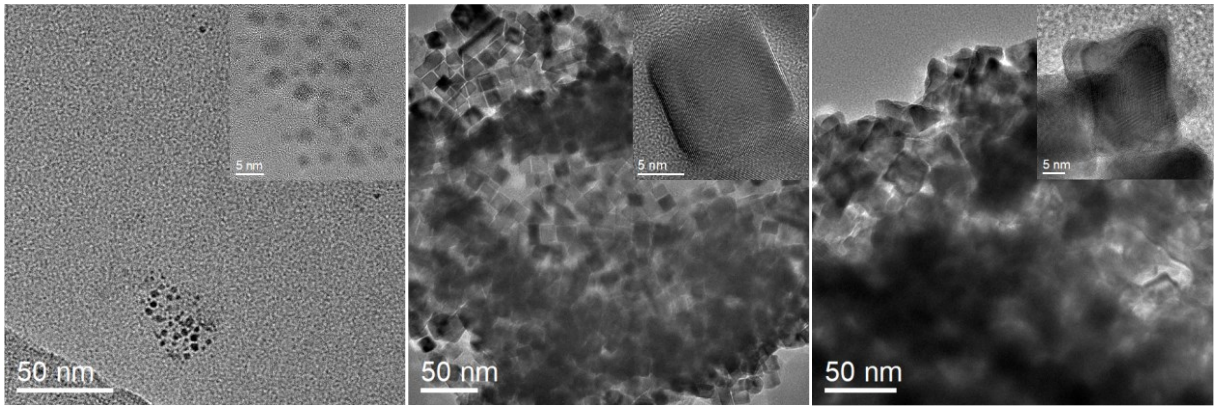


Figure S 5: Biphasic hydrogenation of **2** with palladium nanoparticles at 50 bar. TEM-images of larger PVP-coated spherical palladium nanoparticles (5 nm) (**left**), of smaller palladium nanocubes (18 nm) (**center**), and of larger palladium nanocubes (28 nm) (**right**) after biphasic hydrogenation of **2** at 50 bar hydrogen pressure. Conditions: $n_{substrate}$ = 50 mmol, $p_{H2}$ = 50 bar, $f_{stirrer}$ = 1,500 rpm, $c_{Pd}$ = 0.016 mol%, $T_{start}$ = RT, $w_{Pd,H2O}$ = 16 ppm, $V_{total}$ = 60.6 mL, $t_{preforming}$ = 10 min, semibatch conditions.

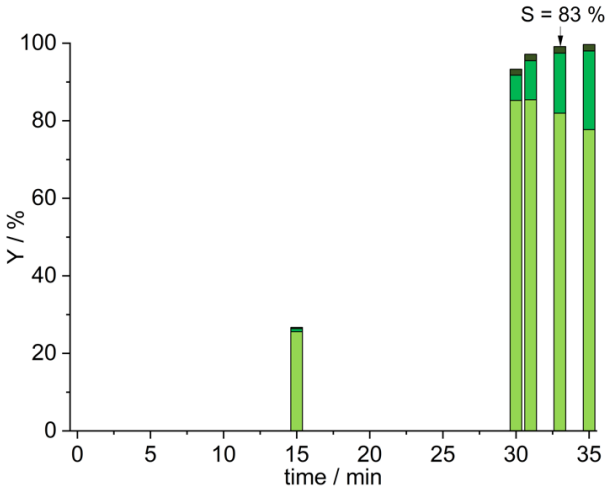


Figure S 6: *Y*,*t*-plot of the hydrogenation of **1** at 50 bar hydrogen pressure with a commercial Lindlar catalyst. Conditions: $n_{substrate}$ = 500 mmol, $p_{H2}$= 50 bar, $f_{stirrer}$ = 1,500 rpm, $c_{Pd}$ = 0.016 mol%, $T_{start}$ = RT, $V_{total}$ = 48.9 mL, semibatch conditions.

## 11.2 Further Experimental Details for Chapter 5

### 11.2.1 Chemicals Used

Table S 3: Chemicals used in chapter 5

| Substance | Manufacturer | Purity [%] |
|---|---|---|
| **Palladium** | Saxonia | 99.99 |
| **Copper** | Evek | 99.99 |
| **Iridium** | Evochem | 99.9 |
| **Platinum** | AlfaAesar | 99.99 |
| **$Pd(OAc)_2$** | Umicore | ≥99 |
| **Propylene carbonate** | VWR | 99 |
| **1-butanol** | VWR | 99.9 |
| **Ethylene glycol** | ThermoFisher | ≥99 |
| **Glycerol** | Henkel | 99 |
| **Glycerol carbonate** | Huntsman | 98.5 |
| **Dimethylformamide** | Carl Roth | >99.9 |
| **Methanol** | VWR | ≥99.9 |
| **Hydrogen** | Messer | 99.999 |
| **Argon** | Messer | 99.996 |
| **Helium** | Messer | 99.996 |
| **β-Myrcene** | ThermoFisher | 90; remainder isomers |
| **Soybean-FAME** | IG Chemicals | - |
| **Crude FAME mixture** | Inkemia | - |
| **Methyl oleate** | Sigma-Aldrich | 98.9 |
| **Conjugated ethyl linoleate** | WeightWorld | 83.8 |
| **Linoleic acid** | Sigma-Aldrich | 97 |
| **$NaHCO_3$** | VWR | >99.9 |
| **$Na_2SO_4$** | ThermoFisher | ≥99 |
| **Pentane** | Carl Roth | >99 |
| **Sulfuric acid** | Chem-Lab | 95-97 |
| **Methyl-tert-butyl ether** | abcr, Carl Roth | 99 |
| **Cyclohexane** | Hanke+Seidel | 99.7 |
| **Ethanol** | VWR | 99 |
| **Dodecane** | TCI | 99 |
| **Deionized water** | with ELGA PURELAB flex 3 | - |
| **Nitric acid** | ThermoFisher | 70 |

For the synthesis of CML (**13**), conjugated ethyl linoleate and linoleic acid were transesterified with an excess of MeOH at 90 °C under reflux overnight using ca. 5 mol% sulfuric acid. Afterwards, MeOH was

removed in vacuo. The residue was dissolved in pentane and neutralized with 2.5 ml saturated $NaHCO_3$ solution twice, followed by washing with deionized water. The organic phase was separated, dried with $Na_2SO_4$, and filtered. Pentane was removed in vacuo. iCML (**12**) was prepared from **13** according to known methods[97] and purified from residues of Pd via repeated percolation through alumina with pentane after removal of MeOH in vacuo.

## 11.2.2 Details on Sample Analysis

Methyl-tert-butyl ether (MTBE) was used to dilute most of the samples; otherwise, cyclohexane was used. Reaction mixtures were diluted to reach 100 mg analyte in 800 mg of solvent; reference samples were diluted with pure dried MTBE to the same concentration. The samples were measured on an Agilent 8860 GC-FID device equipped with a DB-FastFAME column (90 m, 0.25 mm, 0.25 µm) using He as carrier gas.

Table S 4: Heating profile of the GC device for the analysis of FAME samples

| | Rate [°C min$^{-1}$] | Temperature [°C] | Holding time [min] |
|---|---|---|---|
| $T_{Start}$ | | 70 | 0 |
| **Ramp 1** | 15 | 150 | 1 |
| **Ramp 2** | 50 | 175 | 1 |
| **Ramp 3** | 5 | 178 | 0 |
| **Ramp 4** | 1 | 180 | 1 |
| **Ramp 5** | 3 | 192 | 1 |
| **Ramp 6** | 1 | 202 | 1 |
| **Ramp 7** | 3 | 210 | 3 |
| **Ramp 8** | 10 | 230 | 1 |

Hydrogenations of β-myrcene were analyzed on an Agilent Intuvo 9000 with a HP-5 GC column (30 m, 0.32 mm, 0.25 µm) and FID with $N_2$ as carrier gas. For GC-FID, samples of the product phase were diluted with cyclohexane or ethanol to reach 800 mg of solvent and 100 mg of substance. 25 mg of dodecane was added but not used as an external standard. Instead, response factors were expected to vary to a negligible extent and were thus assumed to be constant. Accordingly, evaluation was done by area percent. Hydrogenation products of the hydrogenation of β-myrcene were determined by MS-EI analysis and comparison with literature data. NMR studies confirmed product identification.[214]–[216]

Table S 5: Heating profile of the GC device for the analysis of β-myrcene hydrogenation

| | Rate [°C min$^{-1}$] | Temperature [°C] | Holding time [min] |
|---|---|---|---|
| $T_{Start}$ | - | 50 | 1 |
| **Ramp 1** | 10 | 65 | 2 |
| **Ramp 2** | 5 | 90 | 0 |
| **Ramp 3** | 10 | 110 | 0 |
| **Ramp 4** | 20 | 250 | 5 |

### 11.2.3 Calculation of Reaction Performance Indicators for FAME Hydrogenation

Calculation of X and S: A constant response factor for all compounds was approximated since all possible isomers are structurally very similar, supported by correction factors known from literature[255]. Accordingly, sample composition was obtained directly from GC areas. Conversion takes into account only the conversion of excess double bonds contained in C18:2 and C18:3 species as observable by Equation (5):

$$X = \frac{x_{C18:2;0} - x_{C18:2} + 2 \cdot (x_{C18:3;0} - x_{C18:3})}{x_{C18:2;0} + 2 \cdot x_{C18:3;0}} \quad (5)$$

Selectivity is defined via the produced amount of C18:1 and the amount of hydrogenated C18:3 according to Formula (6).

$$S = \frac{x_{C18:1} - x_{C18:1;0} + x_{C18:3;0} - x_{C18:3}}{x_{C18:2;0} - x_{C18:2} + 2 \cdot (x_{C18:3;0} - x_{C18:3})} \quad (6)$$

Calculation of normalized hydrogen consumption: Hydrogen consumption for Figure 34 was calculated from the molar amount of the substrate $n_{Substrate}$, the amount of consumed hydrogen according to GC measurements $n_{H2,GC}$, the maximum hydrogen uptake from the mass flow controller $V_{measured,max}$ and the time dependent measured hydrogen uptake $V_{measured}$ according to Formula (7).

$$V_{norm} = \frac{V_{measured}}{V_{measured,max}} \cdot \frac{n_{H2,GC}}{n_{Substrate}} \quad (7)$$

Calculation of turnover frequency: The turnover frequency at 20% targeted hydrogen consumption ($TOF_{20,H2}$) was calculated from the hydrogen uptake, as described in chapter 11.1.3 for 5 mmol (112 mLn) of consumed $H_2$ (corresponding to $X_{substrate} \leq 0.2$). This regression value was used to calculate $TOF_{20,H2}$ by equation (4). All values were rounded to significant digits.

# 11.3 Further Experimental Details for Chapter 6

## 11.3.1 Chemicals Used

Table S 6: Chemicals used in chapter 6

| Substance | Manufacturer | Purity [%] |
|---|---|---|
| **Palladium** | Saxonia | 99.99 |
| **Propylene carbonate** | VWR | 99 |
| **Hydrogen** | Messer | 99.999 |
| **Argon** | Messer | 99.996 |
| **Helium** | Messer | 99.996 |
| **Synthesis gas ($CO:H_2$=1:1)** | Messer | 99.997 |
| **$Al_2O_3$** | Thermo Scientific | 99.7 |
| **Thermal oil (silicone oil)** | Carl Roth | - |
| **Cyclohexane** | Hanke+Seidel | 99.7 |
| **Ethyl acetate** | Hanke+Seidel | 99.7 |
| **2-butyne-1,4-diol** | Acros Organics | 99 |
| **2-butene-1,4-diol** | abcr | >97 |
| **butane-1,4-diol** | Carl Roth | >99.8 |
| **Tetrahydrofurane** | Carl Roth | >99.8 |
| **Phenylacetylene** | TCI | 99.7 |
| **Styrene** | Acros Organics | 99.9 |
| **Ethyl benzene** | TCI | >99 |
| **Lindlar catalyst** | Sigma Aldrich | 4.5 w-% Pd |
| **Piperazine** | Acros Organics | ≥99 |
| **TMEDA** | AlfaAesar | 99.9 |
| **Piperidine** | Sigma Aldrich | ≥99 |
| **Chloroform-d** | Deutero | 99.8 |
| **Toluene** | ThermoFisher | 99.8 |
| **1-Octyne** | abcr | 99.6 |
| **2-Octyne** | TCI | 99.6 |
| **3-Octyne** | TCI | 99.3 |
| **4-Octyne** | TCI | 99.4 |
| **1-Octene** | Acros Organics | 99.7 |
| **2-Octenes** | AlfaAesar | 99.8 |
| **t-3-Octene** | TCI | 99.0 |
| **t-4-Octene** | AlfaAesar | 98 |
| **n-Octane** | TCI | 99.7 |
| **o-Xylene** | Acros Organics | 99.5 |

| | | |
|---|---|---|
| **2-Methyl-3-butyne-2-ol** | ThermoScientific | 99.5 |
| **2-Methyl-3-butene-2-ol** | TCI | 98.5 |
| **2-Methyl-2-butanol** | ThermoScientific | 99.9 |
| **Pentane-1-ol** | Sigma-Aldrich | 99.8 |
| **t-Cinnamaldehyde** | ThermoScientific | 99.6 |
| **t-Cinnamyl alcohol** | ThermoScientific | 99.1 |
| **3-Phenylpropane-1-ol** | ThermoScientific | 99.2 |
| **3-Phenylpropane-1-al** | ThermoScientific | 98.5 |
| **t-2-Octene-1-al** | Sigma-Aldrich | 96.7 |
| **t-2-Octene-1-ol** | TCI | 96.7 |
| **Octane-1-al** | Acros Organics | 99.6 |
| **Octane-1-ol** | abcr | 99 |
| **β-Myrcene** | ThermoFisher | 90; remainder isomers |
| **β-Farnesene** | DSM | 98.2 |
| **Dihydromyrcene** | Symrise | 88; remainder isomers |
| **Crude farnesene mixture** | Sigma-Aldrich | - |
| **Ethanol** | VWR | 99 |
| **Dodecane** | TCI | 99 |
| **(+)-Limonene** | Acros Organics | 98.4 |
| **p-Cymene** | Acros Organics | >99 |
| **Rh(acac)(CO)2** | Umicore | 99 |
| **Silica** | Thermo Fisher | 95 |
| **Tris(2,4-di-tert-butylphenyl)phosphite** | TCI | 98 |

## 11.3.2 Details on Sample Analysis

All samples were analyzed using GC-FID for quantitative evaluation. Further $^{1}H$ and $^{13}C$ NMR spectra were recorded on Bruker NMR instruments (Avance III HD or Avance NEO series) with frequencies of 400 to 700 MHz to support the findings from GC-FID or GC-MS-EI.

Reactions of **15**, **1**, **26**, **30**, and **39** were measured on an Agilent 7890B GC device equipped with a HP-Innowax GC column (30 m, 0.25 mm, 0.25 µm) and FID with $N_2$ as carrier gas. 350 mg reaction solution were measured without further dilution after the addition of 15 mg THF as external standard for **15**. For the hydrogenation of **1**, the standard was changed to 1-pentanol. For the hydrogenation of **26** and **30**, toluene was used as standard. For **39**, 25 mg toluene was added as external standard to 156 mg product phase (yielding 100 mg analytes for experiments with S:C of 10,000:1) and 744 mg ethanol. The device was calibrated for all commercially available substances. The unknown substance in the hydrogenation of **15** was assigned the same response factor as **16**. Dimers in hydrogenation of **1** were calculated with

a mean response factor of all other substances, as they are very similar. In the hydrogenation of **39**, aromatic byproducts were assigned the same response factor as **39**; for the unknown intermediates, a weighted average between **39** and **40** was used.

Table S 7: Heating profile of the GC device for the analysis of **15**, **1**, and **39**.

| | Rate [°C min$^{-1}$] | Temperature [°C] | Holding time [min] |
|---|---|---|---|
| $T_{Start}$ | - | 50 | 2 |
| **Ramp 1** | 30 | 90 | 2 |
| **Ramp 2** | 20 | 150 | 4 |
| **Ramp 3** | 7 | 210 | 2 |
| **Ramp 4** | 50 | 250 | 3 |

Table S 8: Heating profile of the GC device for the analysis of **26** and **30**.

| | Rate [°C min$^{-1}$] | Temperature [°C] | Holding time [min] |
|---|---|---|---|
| $T_{Start}$ | - | 50 | 2 |
| **Ramp 1** | 30 | 90 | 2 |
| **Ramp 2** | 20 | 150 | 4 |
| **Ramp 3** | 15 | 210 | 2 |
| **Ramp 4** | 50 | 250 | 7 |

Due to the very low solubilities of **2**, **21-23** and all commercially available products in PC, only the organic phase of the hydrogenations of **2**, **21-23** was measured and used for all further calculations. For the analysis, 350 mg of the organic phase were mixed with 15 mg o-xylene as external standard and measured on an Agilent 7890B instrument with a HP-5 GC column (30 m, 0.32 mm, 0.25 µm) and FID with $N_2$ as carrier gas. GC-MS-EI measurements were conducted on the same device with the same temperature profile on a HP-5 (30 m, 0.25 mm, 0.25 µm) GC-MS column with He as carrier gas to search for characteristic fragments of non-available products or to distinguish between t-3-octene and octane, as they elute at the same retention time. The GC was calibrated for all commercially available substrates and products. Dimers were calculated with a response factor obtained as median of all calibrated octenes.

Table S 9: Heating profile of the GC device for the analysis of **2** and **21-23**.

| | Rate [°C min$^{-1}$] | Temperature [°C] | Holding time [min] |
|---|---|---|---|
| $T_{Start}$ | - | 50 | 2 |
| **Ramp 1** | 1 | 60 | 0 |
| **Ramp 2** | 40 | 250 | 2 |

Samples of the hydrogenation of **18** and **34** were measured on an Agilent Intuvo 9000 with a HP-5 GC column (30 m, 0.32 mm, 0.25 µm) and FID with $N_2$ as carrier gas. For **18**, 15 mg toluene were added to 350 mg reaction mixture. For **34**, 25 mg toluene were added to 100 mg of the product phase and diluted with 800 mg ethanol. All substances were calibrated, except for 1,4-COD. Here, the response factor for 1,5-COD and 1,3-COD was averaged. The absence of 1,3-COD was cross-checked with $^1$H-NMR spectroscopy.

Table S 10: Heating profile of the GC device for the analysis of **18** and **34**.

| | Rate [°C min$^{-1}$] | Temperature [°C] | Holding time [min] |
|---|---|---|---|
| $T_{Start}$ | - | 50 | 1 |
| **Ramp 1** | 10 | 65 | 2 |
| **Ramp 2** | 5 | 90 | 0 |
| **Ramp 3** | 10 | 110 | 0 |
| **Ramp 4** | 40 | 250 | 2 |

Hydrogenations of **14**, **45**, and **55** were analyzed on an Agilent Intuvo 9000 with a HP-5 GC column (30 m, 0.32 mm, 0.25 µm) and FID with $N_2$ as carrier gas. Samples of **50** and crude farnesene was measured on an Agilent 7890B GC system with a HP-5 GC column (30 m, 0.32 mm, 0.25 µm) and FID with $N_2$ as carrier gas. GC-MS-EI measurements were conducted on the same device with each corresponding temperature profile on a HP-5 (30 m, 0.25 mm, 0.25 µm) GC-MS column with He as carrier gas to identify reaction products. For GC-FID, samples of the product phase were diluted with cyclohexane or ethanol to reach 800 mg of solvent and 100 mg of substance. 25 mg of dodecane was added but not used as external standard. Instead, response factors were expected to vary to a negligible extent and were thus assumed to be constant. Accordingly, evaluation was done by area percent.

Hydrogenation products of the hydrogenation of β-myrcene were determined by MS-EI analysis and comparison with literature data. NMR studies confirmed product identification.[214]–[216] The hydrogenation of **50** yields the same peak pattern in GC-FID like for **14**. Detailed literature on possible products is scarce, but for known products, the obtained results are in line[256]. Literature finds similar product compositions[257] and GC-MS-EI results in generally corresponding m/z. Thus, the general assignment of the double bond position was transferred from **14** to **50**.

Hydrogenation products of **55** were identified by GC-MS-EI with reference to Thomas et al..[258],[259] The formation of p-cymene was excluded by the addition of a reference substance. The formation of menthene with an exocyclic double bond can be excluded from the MS data, but the exact location of the remaining double bond cannot be elucidated from the obtained data. The general reaction pathway via the shown products is confirmed by Bogel-Lukasik et al.[260].

Table S 11: Heating profile of the GC device for the analysis of reactions with **14**, **45**, and **55**.

| | Rate [°C min$^{-1}$] | Temperature [°C] | Holding time [min] |
|---|---|---|---|
| $T_{Start}$ | - | 50 | 1 |
| **Ramp 1** | 10 | 65 | 2 |
| **Ramp 2** | 5 | 90 | 0 |
| **Ramp 3** | 10 | 110 | 0 |
| **Ramp 4** | 20 | 250 | 5 |

Table S 12: Heating profile of the GC device for the analysis of **50** and crude farnesene.

| | Rate [°C min$^{-1}$] | Temperature [°C] | Holding time [min] |
|---|---|---|---|
| $T_{Start}$ | - | 50 | 1 |
| **Ramp 1** | 10 | 65 | 2 |
| **Ramp 2** | 20 | 100 | 5 |
| **Ramp 3** | 1 | 130 | 0 |
| **Ramp 4** | 30 | 300 | 5 |

The hydroformylation products of myrcene derivatives and farnesene derivatives were measured on an Agilent 7890B GC system with a HP-5 GC column (30 m, 0.32 mm, 0.25 µm) and FID with $N_2$ as carrier gas. GC-MS-EI measurements were conducted on the same device with each corresponding temperature profile on a HP-5 (30 m, 0.25 mm, 0.25 µm) GC-MS column with He as carrier gas for product identification. Samples were diluted with toluene to reach 50 mg of analytes in a total amount of 400 mg mixture and then mixed with 12.5 mg dodecane as external standard. Myrcene mono- and dialdehydes and farnesen monoaldehydes were isolated for identification and calibration by flash chromatography on a silica column using a gradient of ethylacetate and cyclohexane as solvent (c.f. Table S 14) and subsequent solvent evaporation at 50 °C and 35 mbar. All isomers of one species were lumped and calculated as one species with a constant response factor. Further $^{1}H$ and $^{13}C$ NMR analyses, as well as GC-MS-EI measurements of the isolated products, were performed. The obtained quantity for the myrcene monoaldehyde was not sufficient for calibration; thus, an average of the response factors of myrcene and dialdehydes was used. Dimers were assigned the same response factor as monomers. The response factor of farnesene dialdehydes was extrapolated from monoaldehydes and farnesene, as their amount did not allow isolation.

Table S 13: Heating profile of the GC device for the analysis of **60** and **61**.

| | Rate [°C min$^{-1}$] | Temperature [°C] | Holding time [min] |
|---|---|---|---|
| $T_{Start}$ | - | 35 | 12 |
| **Ramp 1** | 8 | 180 | 0 |
| **Ramp 2** | 20 | 245 | 5 |

Table S 14: Solvent gradient of the flash chromatography for the purification of all product aldehydes (**60** and **61**), starting with pure cyclohexane and adding EtOAc at the given rate. Total flow rate 30 mL $min^{-1}$.

| | **Rate [% $min^{-1}$]** | **Final proportion EtOAc [%]** | **Holding time [min]** |
|---|---|---|---|
| **Start** | 0 | 0 | 3 |
| **Ramp 1** | 1 | 2 | 2 |
| **Ramp 2** | 0.75 | 5 | 2 |
| **Ramp 3** | 95 | 100 | 3 |

Calculation of turnover frequencies: All turnover frequencies refer to ca. 20 % substrate conversion and were calculated either by hydrogen uptake or from GC data in cases where sufficient hydrogen uptake data were not available. The hydrogen method to calculate $TOF_{20,H2}$ was performed as described in chapter 11.1.3 for an amount of consumed $H_2$ corresponding to $X_{substrate} \leq 0.2$. This regression value was used to calculate the $TOF_{20,H2}$ like in equation (4). In cases where GC data was used ($TOF_{20}$), the time to reach 20% conversion was interpolated between the two closest data points. All TOF values were rounded to significant digits. In cases where hydrogen uptake was not available and too less or data points too far from 20 % conversion exist, the calculation of the TOF was not conducted.

## 11.3.3 Additional Results

### *11.3.3.1 Selective Partial Hydrogenation of the Crude Farnesene Mixture*

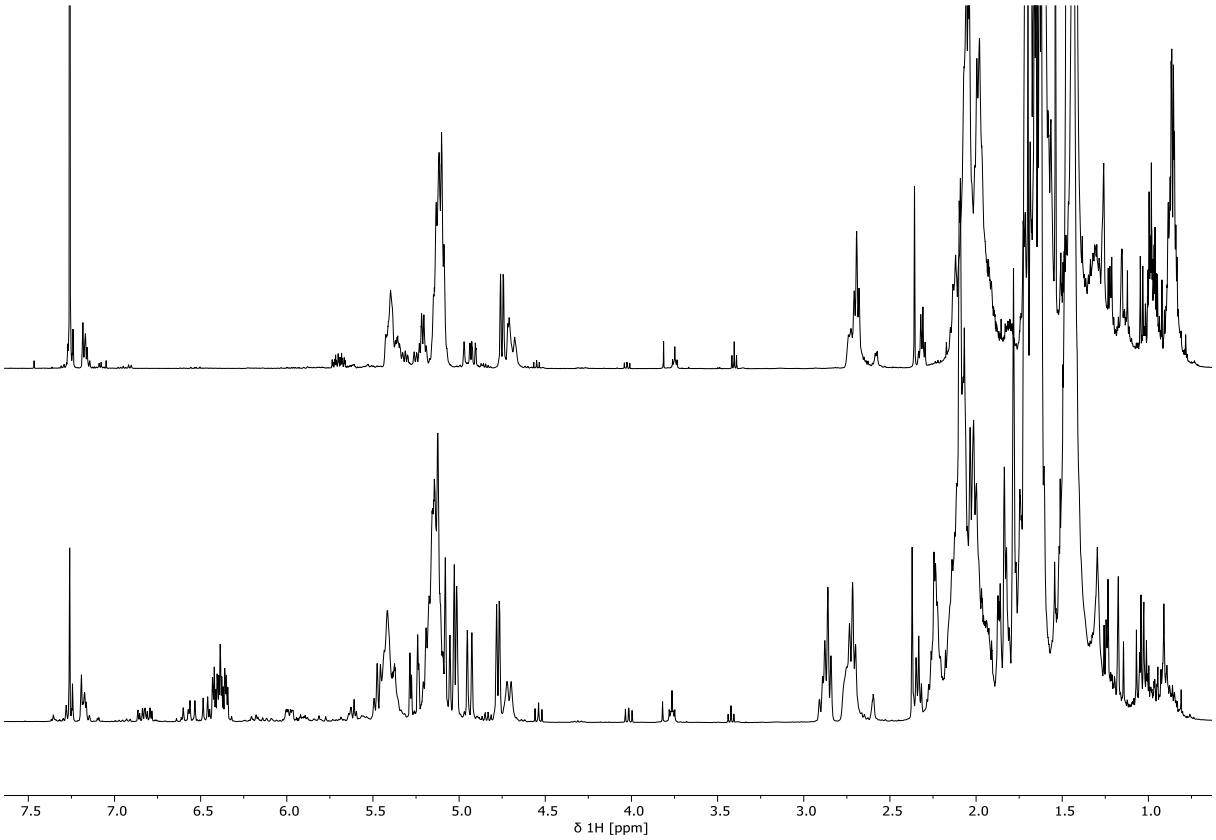


Figure S 7: **Bottom**: $^{1}$H-NMR ($CDCl_3$, 400 MHz) of the crude farnesene mixture; **Top**: $^{1}$H-NMR ($CDCl_3$, 500 MHz) after 1h of selective partial hydrogenation. Signals between 5.75 ppm and 7 ppm (corresponding to conjugated species) disappear. Conditions: $n_{substrate}$= 50 mmol, $V_{cyclohexane}$= 26.2 mL, S:C= 100,000:1, T= 50 °C, $f_{stirrer}$ = 3,500 rpm, $p_{H2}$= 10 bar, $w_{Pd,PC}$= 24 ppm, semibatch.

### *11.3.3.2 Characterization of Product Aldehyde Mixtures*

**GC-MS-EI** for **60a**: calculated for $[M]^+$: 168.2; found: 168.2

**GC-MS-EI** for **61a**: calculated for $[M]^+$: 198.2; found: 198.2

**GC-MS-EI** for dimers of **14**: calculated for $[M]^+$: 272.3; found: 272.3

**GC-MS-EI** for **60b**: calculated for $[M]^+$: 236.2; found: 236.2

**GC-MS-EI** for **61b**: calculated for $[M\text{-}H_2O]^+$: 248.2; found: 248.2

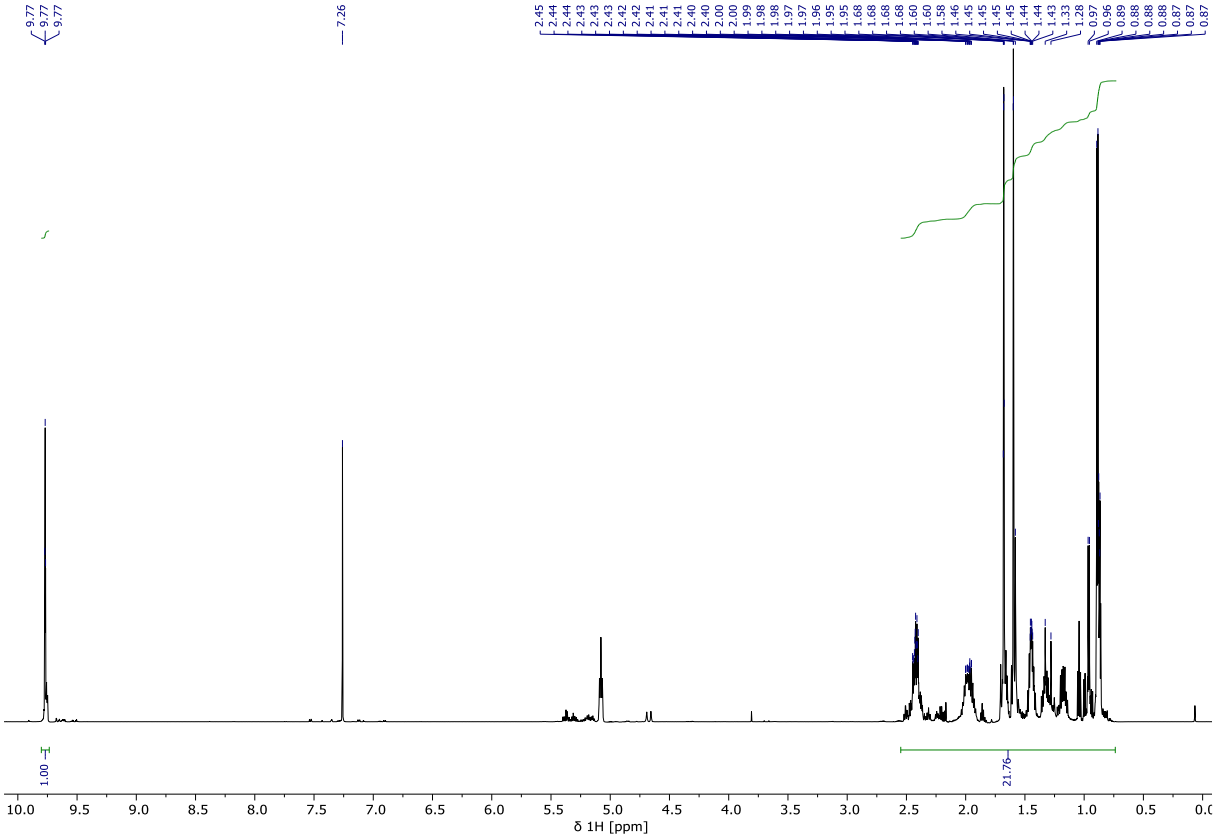


Figure S 8: $^{1}$H-NMR ($CDCl_3$, 600 MHz) of monoaldehydes **60a**.

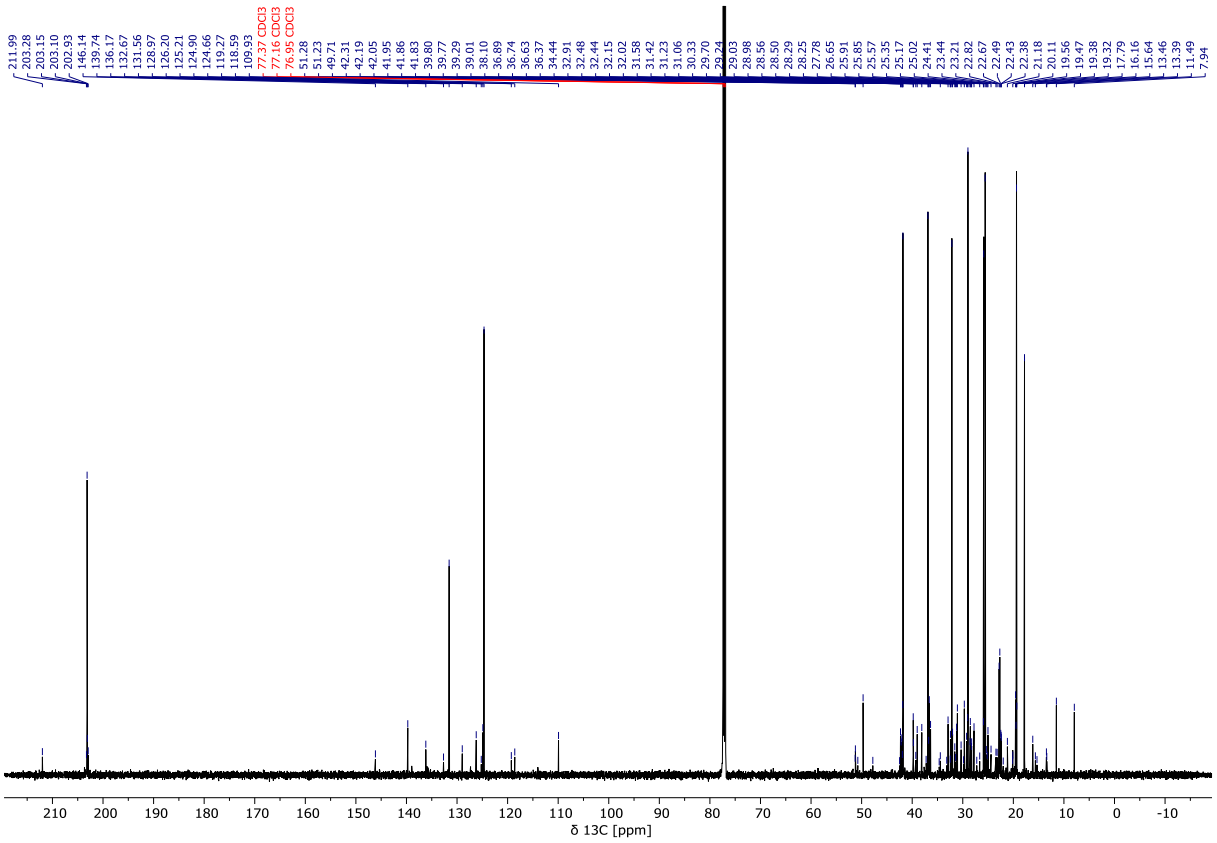


Figure S 9: $^{13}C\{^{1}H\}$-NMR ($CDCl_3$, 151 MHz) of monoaldehydes **60a**.

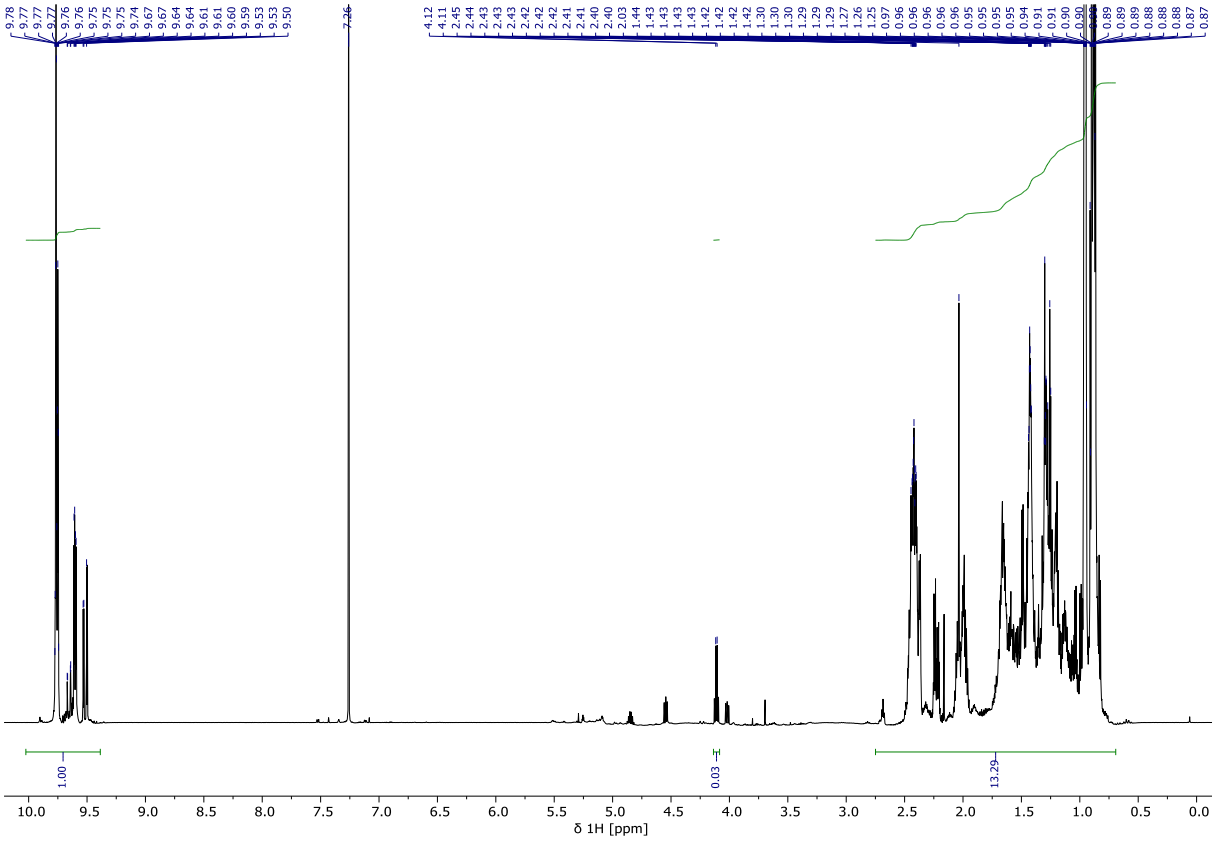


Figure S 10: $^{1}$H-NMR ($CDCl_3$, 600 MHz) of dialdehydes **61a**.

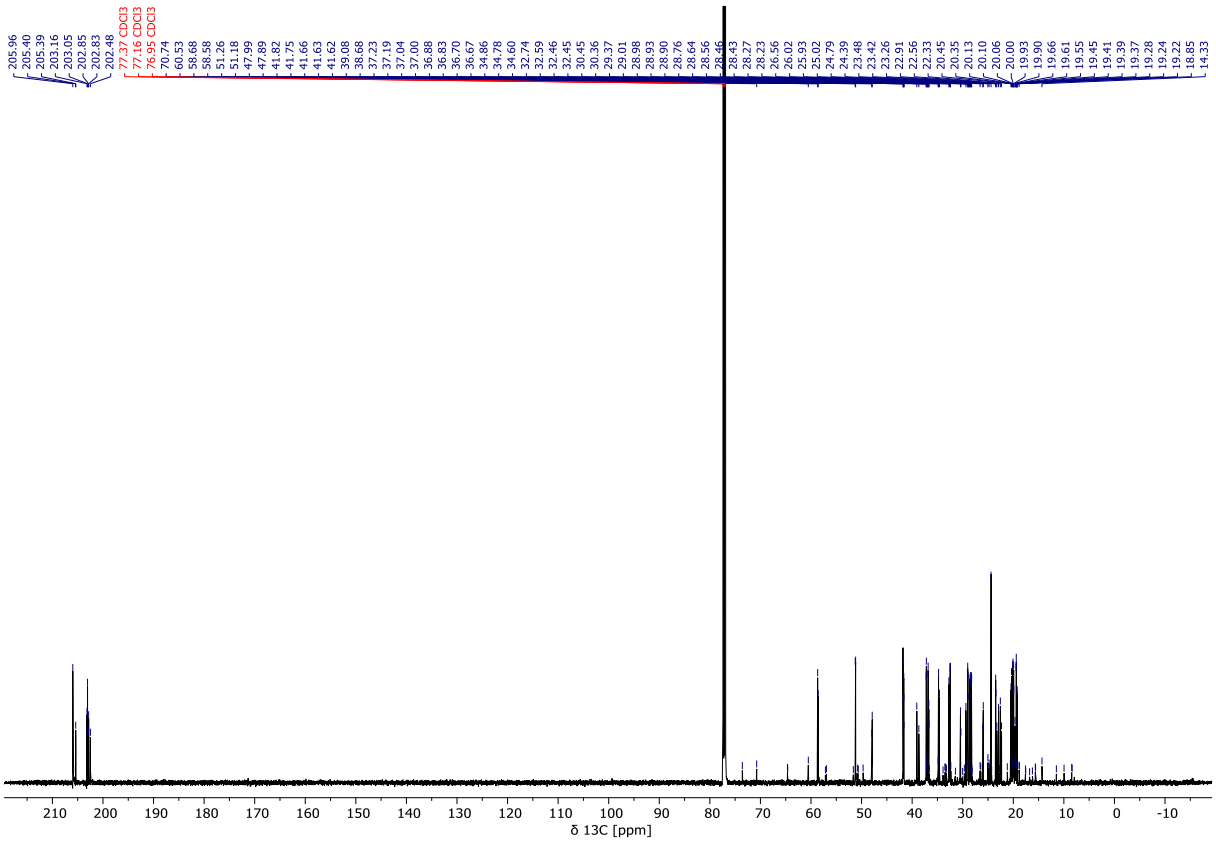


Figure S 11: $^{13}C\{^{1}H\}$-NMR ($CDCl_3$, 151 MHz) of dialdehydes **61a**.

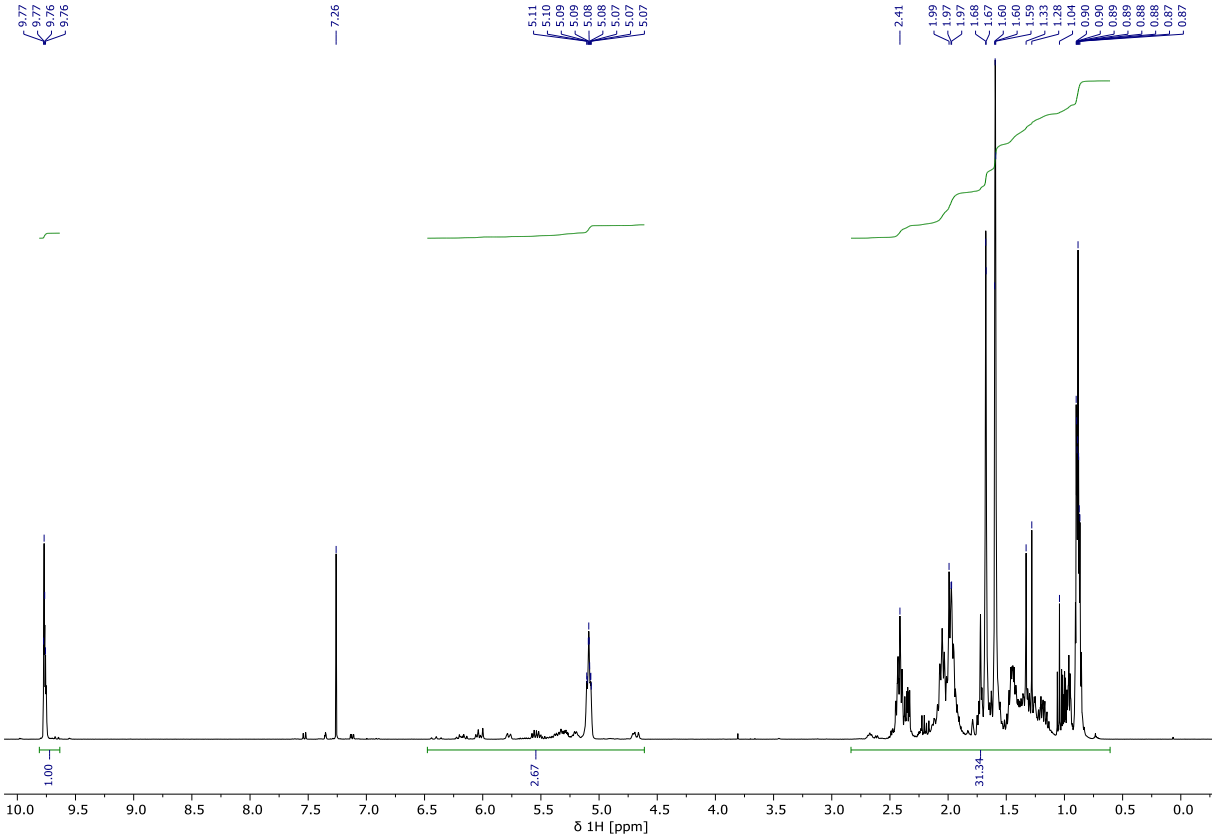


Figure S 12: $^{1}$H-NMR ($CDCl_3$, 400 MHz) of monoaldehydes **60b**.

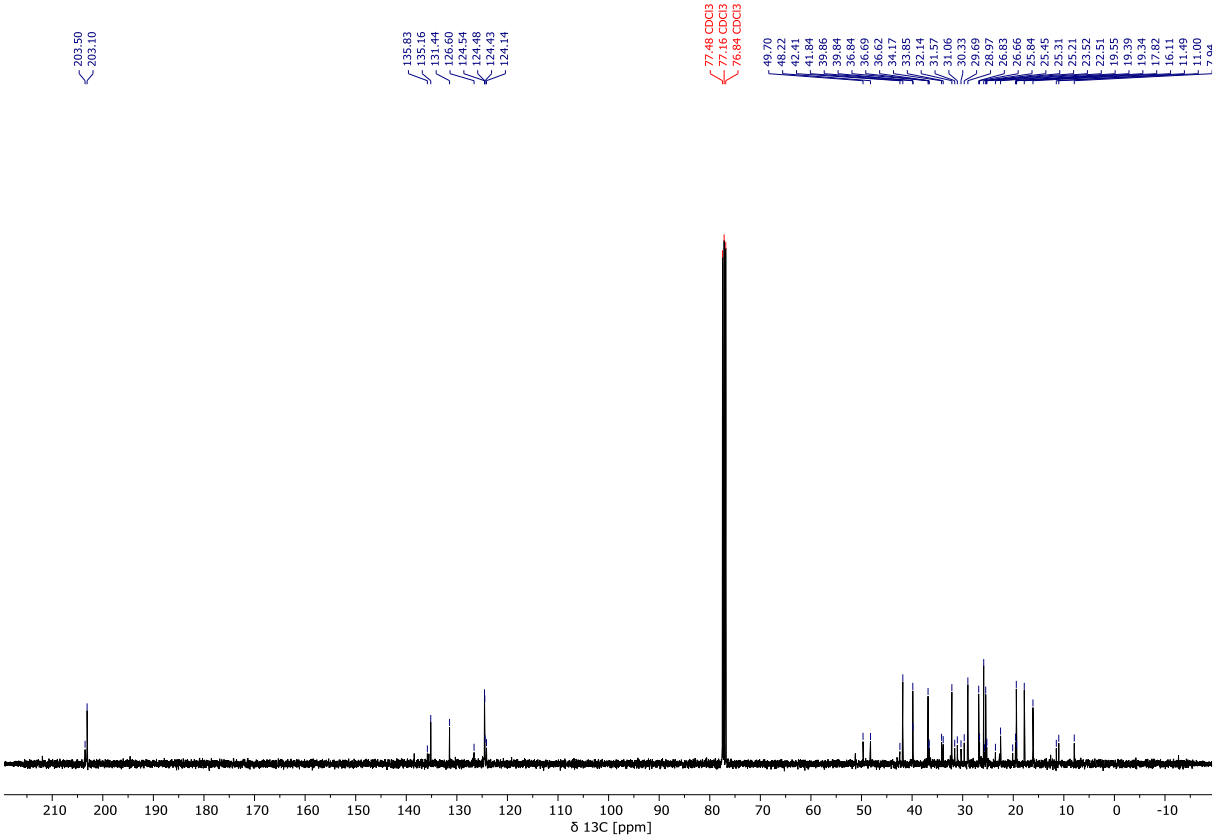


Figure S 13: $^{13}$C{$^{1}$H}-NMR ($CDCl_3$, 100 MHz) of monoaldehydes **60b**.

## 11.4 Further Experimental Details for Chapter 7

### 11.4.1 Chemicals Used

Table S 15: Chemicals used in chapter 7

| Substance | Manufacturer | Purity [%] |
|---|---|---|
| **Palladium** | Saxonia | 99.99 |
| **1-Butanol** | VWR | 99.9 |
| **$Pd(PPh_3)_4$** | ThermoFisher | 99 |
| **$PdCl_2(PPh_3)_2$** | Sigma Aldrich | 98 |
| **Argon** | Messer | 99.996 |
| **Silica** | Thermo Fisher | 95 |
| **$Al_2O_3$** | Thermo Scientific | 99.7 |
| **Cyclohexane** | Hanke+Seidel | 99.7 |
| **Ethyl acetate** | Hanke+Seidel | 99.7 |
| **Toluene** | ThermoFisher | 99.8 |
| **Deionized water** | with ELGA PURELAB flex 3 | - |
| **Mercury** | donated by AK Strohmann | - |
| **1-Octanethiol** | Abcr | 98 |
| **$PPh_3$** | Abcr | 99 |
| **$K_2CO_3$** | Acros | ≥99 |
| **$Na_2CO_3$** | Riedel-de Haën | ≥99.5 |
| **$Cs_2CO_3$** | Evonik | - |
| **KOH** | Carl Roth | ≥85 |
| **NaOAc** | Carl Roth | ≥98.5 |
| **$NaHCO_3$** | Merck | >99 |
| **NaOH** | ThermoFisher | ≥97 |
| **$NEt_3$** | Acros | 99.9 |
| **$H_3PO_4$** | Acros | 85 |
| **HCl** | ThermoFisher | 37 |
| **Phenylboronic acid** | TCI | >99 |
| **4'-Bromoacetophenone** | TCI | >98 |
| **1-Bromo-3,5-dimethoxybenzene** | TCI | 99.7 |
| **p-Bromobiphenyl** | TCI | >98 |
| **p-Bromophenol** | TCI | >99.2 |
| **p-Bromotoluene** | TCI | 99.7 |
| **p-Bromo-N,N-dimethylaniline** | TCI | 99.9 |
| **p-Iodophenol** | TCI | 99.4 |

| | | |
|---|---|---|
| **p-Iodotoluene** | TCI | 99.8 |
| **2-Iodoanisole** | Thermo Fisher | 99.5 |
| **p-Acetylbiphenyl** | TCI | 99.8 |
| **p-Terphenyl** | TCI | 99.8 |
| **p-Hydroxybiphenyl** | TCI | 99.6 |
| **p-Methylbiphenyl** | TCI | 99.5 |
| **o-Methoxybiphenyl** | TCI | 99.1 |
| **Chloroform-d** | Deutero | 99.8 |
| **Ethylene glycol** | ThermoFisher | ≥99 |
| **1,4-Dioxane** | ThermoFisher | ≥99 |
| **Methanol** | VWR | ≥99.9 |
| **Dichloromethane** | Sigma-Aldrich | ≥99.8 |

## 11.4.2 Details on Sample Analysis

All samples were analyzed on an Agilent Intuvo 9000 with a HP-5 GC column (30 m, 0.32 mm, 0.25 µm) and FID with $N_2$ as carrier gas after neutralization with 0.1M HCl and derivatization of **63** according to the following procedure: An aliquot of the organic product phase was taken, of which solids were removed by means of a syringe filter. 800 mg of the sample were used without further dilution. 25 mg toluene were added as standard, and 85 mg of ethylene glycol for derivatization of the phenylboronic acid. Afterwards, the vial was shaken to ensure proper mixing. The pH value of the resulting solution was tested, and 1 M HCl was used for neutralization when needed. All educts and products were calibrated. For this, commercially available samples were used. **65b** and **65f** needed to be synthesized according to the procedures in chapter 11.4.3.

Table S 16: Heating profile of the GC device for the analysis of all coupling reactions

| | **Rate [°C min$^{-1}$]** | **Temperature [°C]** | **Holding time [min]** |
|---|---|---|---|
| **$T_{Start}$** | | 50 | 1 |
| **Ramp 1** | 3 | 65 | 1 |
| **Ramp 2** | 40 | 170 | 0 |
| **Ramp 3** | 20 | 300 | 3 |

## 11.4.3 Preparation of Reference Samples

**65b** was synthesized based on a procedure by Bréard et al[261]: 435 mg (2 mmol) of **64b** was mixed with 365 mg (3 mmol) of **63**, 829 mg (6 mmol) of $K_2CO_3$, 70 mg (0.1 mmol) of $PdCl_2(PPh_3)_2$, and 14.5 ml degassed solvent (dioxane:water, 43:5) under inert conditions. The reaction was conducted for 3 h at 100°C. Afterwards, a saturated aqueous solution of $NaHCO_3$ was added, and the organic products were

extracted with 20 mL EtOAc three times. This mixture was dried with $Na_2SO_4$, and all solvents were evaporated afterwards. The crude product was purified with flash chromatography with a gradient of EtOAc and cyclohexane (c.f. Table S 17). $^1$H-NMR, $^{13}$C-NMR, and MS-EI data are in agreement with literature.

For the synthesis of **65f**, 864,7 mg (7.5 mmol) of $H_3PO_4$ was reacted with 1485.1 mg (22.5 mmol) KOH in 9.5 mL deionized water. Subsequently, 500 mg (2.5 mmol) of **64c** was mixed with 457 mg (3.75 mmol) of **63**. Thereafter, the reaction was degassed for 25 minutes in an ultrasonic bath. Subsequently, 144.4 mg (0.125 mmol) of $Pd(PPh_3)_4$ and 10 ml degassed MeOH were added under inert conditions based on different literature[262],[263]. This reaction mixture was stirred for 20 h at 85 °C. Afterwards, it was washed three times with $CH_2Cl_2$ and the solvent was removed from the filtrate at 50 °C without vacuum, and the product was purified using flash chromatography with a gradient of EtOAc and cyclohexane (c.f. Table S 17). $^1$H-NMR, $^{13}$C-NMR, and MS-EI data are in agreement with literature.

Table S 17: Solvent gradient of the flash chromatography for the purification of **65b** and **65f**, starting with pure cyclohexane and adding EtOAc at the given rate. Total flow rate 30 mL min$^{-1}$.

| | **Rate [% min$^{-1}$]** | **Final proportion EtOAc [%]** | **Holding time [min]** |
|---|---|---|---|
| **Start** | 0 | 0 | 3 |
| **Ramp 1** | 5 | 5 | 4 |
| **Ramp 2** | 45 | 50 | 2 |
| **Ramp 3** | 50 | 100 | 2 |

# 11.5 Supporting Information for Chapter 8

## 11.5.1 General Methods and Reagents

Table S 18: Chemicals used in this work.

| Substance | Manufacturer | Purity [%] |
|---|---|---|
| **Methyl undecanoate** | AlfaAesar | 99 |
| **10-Methyl undecenoate** | Carl Roth | >96 |
| **Conjugated ethyl linoleate** | WeightWorld | 83.8 |
| **Palladium acetate** | Umicore | ≥99 |
| **$Pd_2(dba)_3$** | Fisher Scientific | 97 |
| **Propylene carbonate** | VWR | 99 |
| **Methanol** | VWR | ≥99.8 |
| **1,2-DTBPMB** | Donation by Digital Specialty Chemicals | - |
| **Trifluoromethanesulfonic acid** | TCI | >98 |
| **Methanesulfonic acid** | Carl Roth | 99.5 |
| **Hydrogen** | Messer | 99.999 |
| **Argon** | Messer | 99.996 |
| **CO** | Messer | 98 |
| **Soybean methyl ester** | IG Chemicals | - |
| **Methyl oleate, pure** | Sigma-Aldrich | 98.9 |
| **Methyl oleate, commercial** | Dako | 91.2 |
| **Linoleic acid** | Sigma-Aldrich | 97 |
| **Heptadecanoic acid** | TCI | >98 |
| **Dodecane** | TCI | ≥99 |
| **$Al_2O_3$** | Thermo Scientific | 99.7 |
| **Sodium sulfate** | Fisher Scientific | ≥99 |
| **2-propanol** | Hanke+Seidel | 99.7 |
| **$NaHCO_3$** | VWR | >99.9 |
| **Pentane** | Carl Roth | >99 |
| **Sulfuric acid** | Chem-Lab | 95-97 |
| **Deionized water** | With ELGA PURELAB flex 3 | - |
| **Diethylether** | Honeywell | 99.8 |
| **Methyl-tert-butyl ether** | abcr | 99 |
| **Mole sieve 3 Å** | Thermo Scientific | - |
| **Toluene** | Thermo Scientific | 99.8 |

### 11.5.1.1 General Procedures

Transesterification: Conjugated linoleic acid, ethyl linoleate or heptadecanoic acid were transesterified with excess MeOH at 90 °C under reflux over night applying ca. 5 mol % sulfuric acid. Afterwards, MeOH was evaporated under reduced pressure. The residue was dissolved in pentane and neutralized with 2.5 ml saturated $NaHCO_3$ solution twice followed by washing with deionized water. The organic phase was separated, dried with $Na_2SO_4$ and filtered. Pentane was removed under reduced pressure.

Preparation of iCML: iCML was prepared from CML according to previously published methods[97].

Temperature dependence of the isomerization of methyl linoleate (ML): In a glovebox, $Pd_2(dba)_3$ and 1,2-DTBPMB were weighed into an inertized Schlenk flask with stirring bar under Argon atmosphere. 30 ml dried and degassed MeOH was introduced via a syringe and the solution stirred over night. Prior to the transfer into the reactor, methanesulfonic acid was added via a syringe. ML was purified from peroxides using $Al_2O_3$ and degassed in an ultrasonic bath under Argon flow. The catalyst solution was transferred into the inertized 75 ml reactor using a syringe in Argon counterflow. ML was introduced into the dropping funnel under Argon counterflow. The reactor was pressurized with 6 bar Argon, heated to the desired temperature and the substrate added at reaction temperature. After the reaction period, the reactor was cooled down in an ice bath, opened and samples for analysis taken.

### 11.5.1.2 Calculation of Reaction Indicators

Calculation of X and S of the hydrogenation: Since all possible isomers are structurally very similar, a constant response factor for all compounds was assumed. This is supported by correction factors known from literature[255]. Conversion is defined as conversion of excess double bonds contained in C18:2 and C18:3 species:

$$X = \frac{x_{C18:2;0} - x_{C18:2} + 2 \cdot (x_{C18:3;0} - x_{C18:3})}{x_{C18:2;0} + 2 \cdot x_{C18:3;0}} \quad (8)$$

The combined selectivity is defined via the formed amount of desired product and amount of hydrogenated C18:3, thereby taking into account the formation of the intermediate C18:2 (that is also an educt).

$$S = \frac{x_{C18:1} - x_{C18:1;0} + x_{C18:3;0} - x_{C18:3}}{x_{C18:2;0} - x_{C18:2} + 2 \cdot (x_{C18:3;0} - x_{C18:3})} \quad (9)$$

Calculation of X and S of the methoxycarbonylation of FAME: Conversion is calculated from calibrated GC-FID peak areas and includes the formation of l and b diesters from the crude FAME mixture. Selectivity is calculated via the total amount of diester obtained from the crude reaction mixture.

Calculation of X and S of the methoxycarbonylation of $C_{11}$-ME: Conversion is calculated from calibrated GC-FID peak areas and includes the formation of l and b diesters as well as isomerization of $C_{11}$-ME to

monoesters with internal double bonds. Accordingly, selectivity is calculated via the total amount of diester obtained from terminal $C_{11}$-ME.

## 11.5.2 Analytics

GC analysis of hydrogenation mixtures: MTBE was dried over mole sieve and used to dilute the samples. Reaction mixtures were diluted to reach 100 mg analyte in 800 mg of solvent, reference samples were diluted with pure dried MTBE to the same concentration. The samples were measured on a Agilent 8860 GC device equipped with a DB-FastFAME column (90 m, 0.25 mm, 0.25 µm) and FID using He as carrier gas.

Table S 19: heating profile for the analysis of the hydrogenation mixtures using GC-FID.

| | Rate [°C min$^{-1}$] | Temperature [°C] | Holding time [min] |
|---|---|---|---|
| $T_{Start}$ | | 50 | 0 |
| **Ramp 1** | 50 | 175 | 1 |
| **Ramp 2** | 5 | 185 | 1 |
| **Ramp 3** | 0.1 | 188 | 5 |
| **Ramp 4** | 25 | 235 | 15 |

GC analysis of methoxycarbonylation of FAME: 475 mg of the reaction solution were diluted with 500 mg toluene or warm 2-propanol and 25 mg of heptadecanoic acid methyl ester were added as internal standard. The samples were measured on a Agilent 7890A with a HP-5 GC column (30 m, 0.32 mm, 0.25 µm) and FID using $N_2$ as carrier gas.

Table S 20: heating profile for the analysis of methoxycarbonylation of FAME using GC-FID.

| | Rate [°C min$^{-1}$] | Temperature [°C] | Holding time [min] |
|---|---|---|---|
| $T_{Start}$ | | 40 | 1 |
| **Ramp 1** | 40 | 285 | 1 |
| **Ramp 2** | 10 | 300 | 3 |
| **Ramp 3** | 40 | 325 | 0 |

GC analysis of methoxycarbonylation of $C_{11}$-ME: 500 mg of the reaction solution were diluted with 500 mg 2-propanol and 25 mg of dodecane were added as internal standard. The samples were measured on a Agilent 7890A device with a HP-5 GC column (30 m, 0.32 mm, 0.25 µm) or a Agilent 7890B device with a HP-5 GC column (30 m, 0.32 mm, 0.25 µm) and FID using $N_2$ as carrier gas.

Table S 21: heating profile for the analysis of methoxycarbonylation of $C_{11}$-ME using GC-FID.

| | Rate [°C min$^{-1}$] | Temperature [°C] | Holding time [min] |
|---|---|---|---|
| **$T_{Start}$** | | 40 | 1 |
| **Ramp 1** | 40 | 220 | 1 |
| **Ramp 2** | 40 | 320 | 3 |

## 11.5.3 Additional Results

PC in methoxycarbonylation: As the Pd loading in PC used in the hydrogenation step is preferentially 100 ppm and below, PC was needed to be added in high amounts. In this case, a ca. double amount of PC compared to MeOH (V/V) was chosen. The liquid level inside the reactor was roughly held constant in both cases to ensure comparable mixing and mass transport behavior. The reaction is monophasic in both cases, enabling the methoxycarbonylation to perform without any further mass transport resistance introduced by possible biphasic behavior.

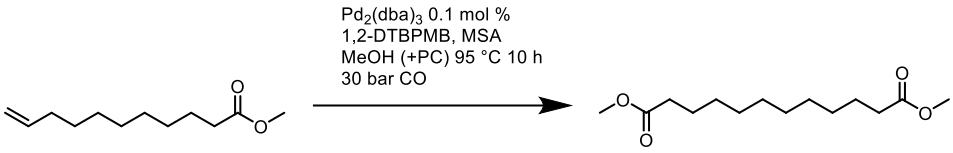


Scheme S 1: methoxycarbonylation of $C_{11}$-ME.

FAME hydrogenation with PC:

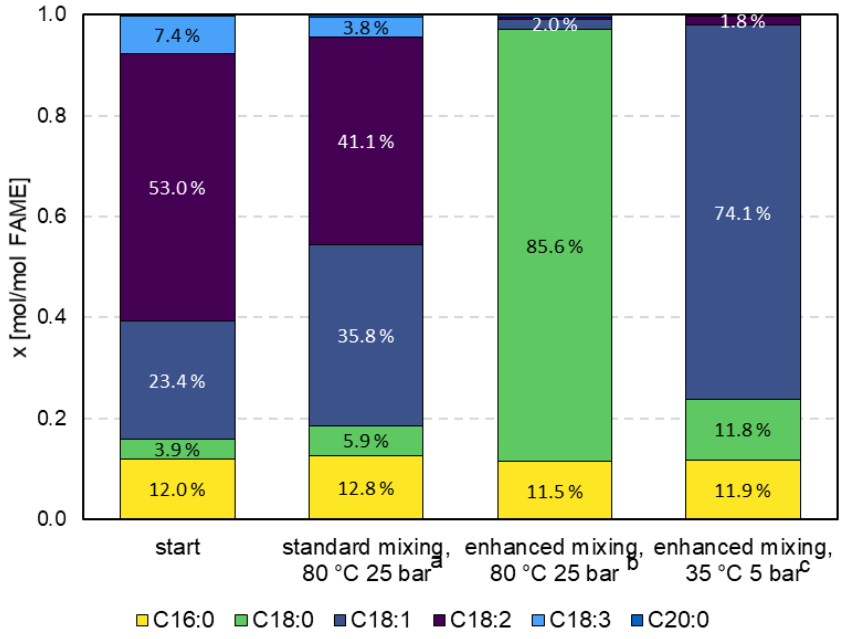


Figure S 14: Composition after hydrogenation of soybean FAME with Pd nanoparticles in PC. Reaction conditions: S:Pd= 1,000:1, $V_{PC}$= 20 ml, $n_{FAME}$= 16.9 mmol, ω= 1100 rpm, $t_{Preforming}$= 2 h, $w_{PdPC}$= 74.4 ppm, a: $t_{hydrogenation}$= 7.5 min, b: $t_{hydrogenation}$= 4.5 min, c: $t_{hydrogenation}$= 15 min, conditions obtained from literature[68],[70]

Temperature dependence of the isomerization of methyl linoleate (ML):

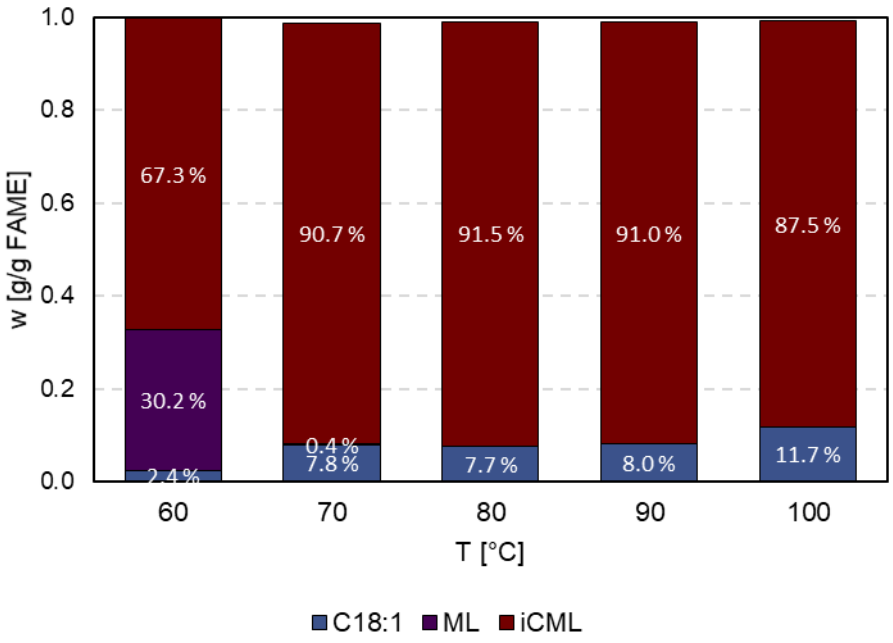


Figure S 15: Composition after isomerization of ML. Reaction conditions: S:Pd= 1,000:1, $V_{MeOH}$= 30 ml, $n_{ML}$= 16.9 mmol, ω= 1100 rpm, $p_{Ar}$= 6 bar, L:Pd= 17.5; MSA:L= 2, t= 24 h.

Full isomerization to conjugated species within 24h was observed only at 80 °C and above. At 60 °C, conversion dropped to 70°%. Transfer hydrogenation to C18:1 species started only at temperatures higher than 60 °C. Thus, the incomplete conversion to conjugated species at the boiling temperature of MeOH (64 °C) can be explained, even pronounced by the incomplete dissolution of the nanoparticles.

Evolution of the pressure in hydrogenation with enhanced mixing:

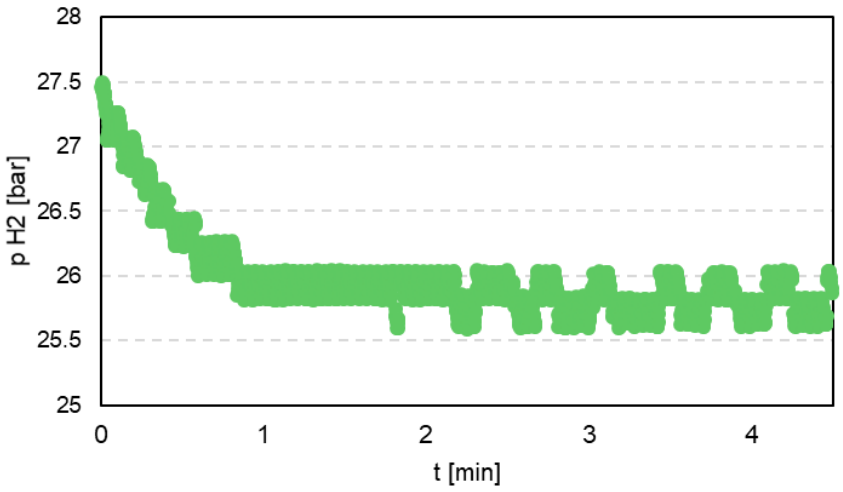


Figure S 16: Evolution of the pressure in the hydrogenation of soybean FAME with Pd nanoparticles in MeOH with enhanced mixing. Reaction conditions: S:Pd= 1,000:1, $p_{H2}$= 25 bar; T= 80 °C, $V_{MeOH}$= 20 ml, $n_{FAME}$= 16.9 mmol, $w_{Pd,MeOH}$= 114 ppm, ω= 1100 rpm, $t_{Preforming}$= 2 h.

Formation of conjugated species from residues of unhydrogenated C18:2:

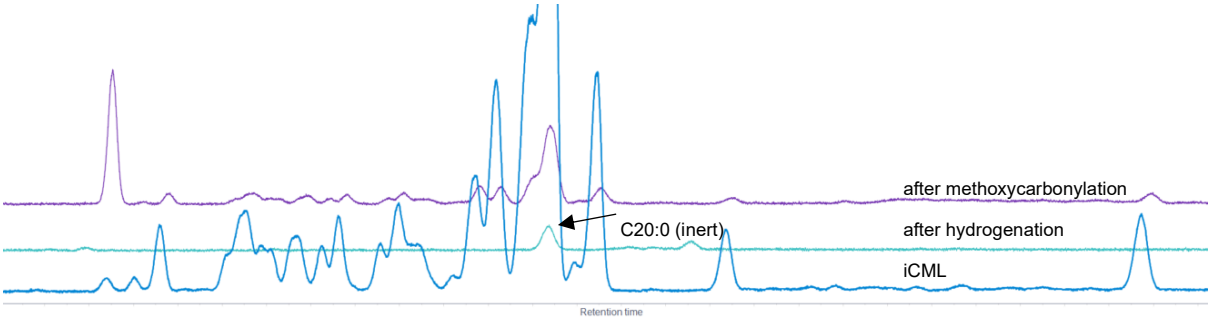


Figure S 17: Excerpt of the conjugated C18:2 area of the chromatograms of FAME in tandem catalysis. Reaction conditions: S:Pd= 1,000:1, L:Pd= 17.5, $p_{CO}$= 30 bar, $T_{methoxycarbonylation}$= 95 °C, $V_{MeOH}$= 30 ml, $\omega_{hydrogenation}$= 1100 rpm, $t_{Preforming}$= 2 h, $t_{methoxycarbonylation}$= 72 h, $\omega_{methoxycarbonylation}$= 3500 rpm, overhead stirrer, $n_{FAME}$= 16.9 mmol.

# 11.6 Supporting Information for Chapter 9

## 11.6.1 General Methods, Reagents and Setup

Capillary reactor

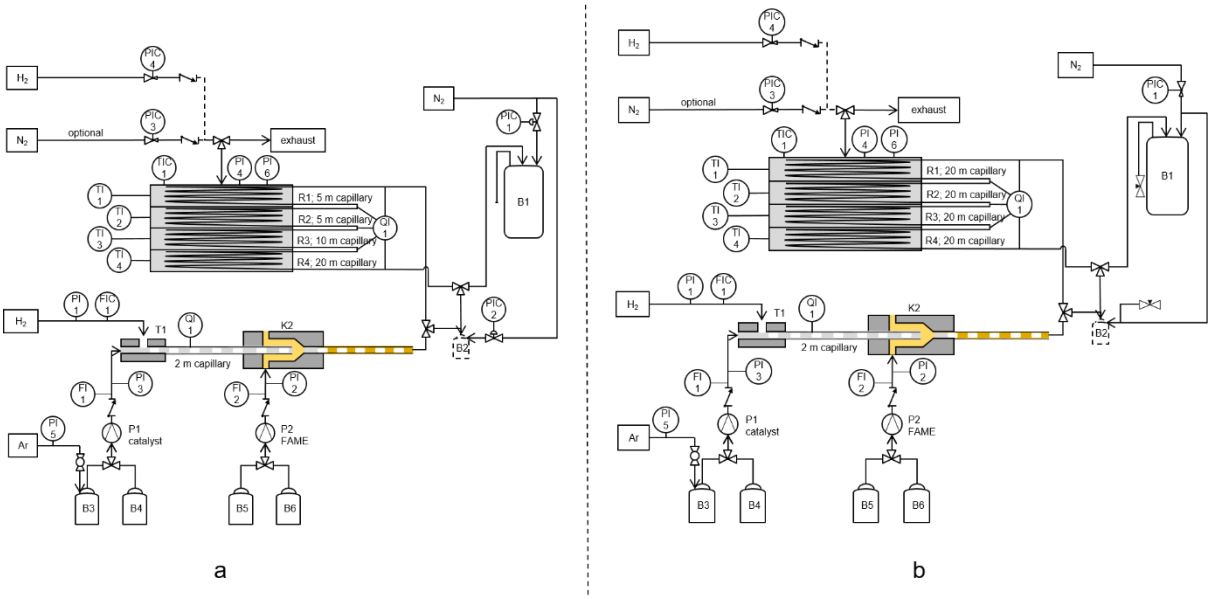


Figure S 18: Flowsheets of the capillary reactor for pressures up to 10 barg (a) or higher pressure resp. higher reactor lengths (b). R1-4: reactor segments with coiled capillary; K2: coaxial contactor; T1: T-junction; P1: syringe pump for catalyst; P2: syringe pump for FAME, FIC1: mass flow controller; PI1-4: digital pressure indicator; PI5, PI6: manometer; PIC1: pressure controller (digital for a, analog for b); PIC2: digital pressure controller; PIC3, PIC4: pressure regulator; FI1, FI2: digital flow indicator; TI1-4: digital temperature indicator; TIC1: temperature controller; B1: product vessel; B2: sample vessel; B3: substrate container catalyst; B5: substrate container FAME; B4, B6: container for rinsing solvent; QI1: high-speed camera; $H_2$, Ar, $N_2$: pipes for displayed gases.

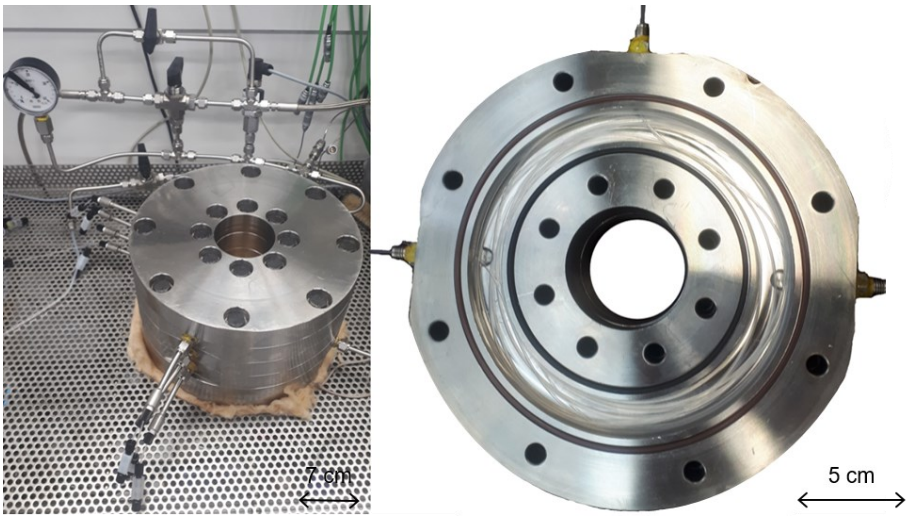


Figure S 19: Photographies of the whole main reactor without insulation and heating bands (left) and one open segment with 5 m capillary inside (right)

Table S 22: Devices used for the capillary reactor.

| device | code in flowsheet | type | manufacturer |
|---|---|---|---|
| **Data acquisition** | - | TCP 750-891 | wago |
| **Digital pressure indicator** | PI1-4 | A-10 | WIKA |
| **3-way valve** | - | UP V-101T | IDEX H&S |
| **Pressure regulator** | PIC1 (high pressure) | FM51 | spectron |
| **Digital pressure controller** | PIC2 (and PIC1 for low pressure) | R414003373 | Aventics |
| **Pressure regulator** | PIC3 | KPR1JRA411A20000 | Swagelok |
| **Pressure regulator** | PIC4 | FM51 | spectron |
| **FEP-capillary** | - | KAP FEP (1mm ID, 1/16“ AD) | TechLab |
| **flangeless ferrule** | - | UP P200 | IDEX H&S |
| **flangeless male nut** | - | UP P201 | IDEX H&S |
| **heating band** | - | HAT 22 | Horst |
| **flow indicator** | FI1-2 | SLI-2000 | Sensirion |
| **high-speed camera** | QI1 | DFK37BUX | Imagingsource |
| **LabVIEW** | - | Version 2020 | National Instruments |
| **manometer** | PI5 | 232.50 | Wika |
| **manometer** | PI6 | 111.10 | Wika |
| **digital temperature indicator** | TI1-4 | type K, l=300 mm, d=2 mm | TC Direkt |
| **mass flow controller** | FIC1 | F-200CV | Bronkhorst |
| **power supply** | - | LPS 301 | Amrel |
| **check valve** | - | CV-3000 | IDEX H&S |
| **syringe pump** | P1-2 | SyrDos_CKP | Hitec-Zang |

Hydrogen volume flows are always expressed at applied conditions, not at standard conditions.

Table S 23: Chemicals used in this work.

| Substance | Manufacturer | Purity [%] |
|---|---|---|
| **Palladium** | Saxonia | 99.99 |
| **Propylene carbonate** | VWR | 99 |
| **Hydrogen** | Messer | 99.999 |
| **Argon** | Messer | 99.996 |
| **Helium** | Messer | 99.996 |
| **Soybean methyl ester** | IG Chemicals | - |
| **2-Propanol** | Hanke+Seidel | 99.7 |
| **Methyl-tert-butyl ether** | abcr, Carl Roth | 99 |
| **Mole sieve 3 Å** | Thermo Scientific | - |
| **Cyclohexane** | Hanke+Seidel | 99.7 |
| **1-Hexanol** | Carl Roth | 99.8 |
| **1-Octanol** | Acros | 99 |
| **1-Decanol** | Sigma-Aldrich | 99 |
| **Acid Red 94** | ITW Reagents | >85 |
| **Thermal oil (silicone oil)** | Carl Roth | - |

Calculation of X and S: A constant response factor for all compounds was assumed since all possible isomers are structurally very similar, supported by correction factors known from literature[255]. Accordingly, sample composition was obtained from GC areas without calibration or internal standard. Conversion takes only into account the conversion of excess double bonds contained in C18:2 and C18:3 species (one for C18:2 and two for C18:3):

$$X = \frac{x_{C18:2;0} - x_{C18:2} + 2 \cdot (x_{C18:3;0} - x_{C18:3})}{x_{C18:2;0} + 2 \cdot x_{C18:3;0}} \quad (10)$$

Selectivity is defined *via* the formed amount of C18:1 and amount of hydrogenated C18:3. This also takes the formation of the intermediate C18:2 (that is also an educt) into account. For severe overhydrogenation, selectivity gets negative, reflecting depletion of the desired product C18:1.

$$S = \frac{x_{C18:1} - x_{C18:1;0} + x_{C18:3;0} - x_{C18:3}}{x_{C18:2;0} - x_{C18:2} + 2 \cdot (x_{C18:3;0} - x_{C18:3})} \quad (11)$$

Calculation of $\tau$ and STY: For the calculation of the residence time $\tau$, the average total volume flow must be calculated. The consumption of hydrogen in each reactor segment is taken into account *via* optical measurements of the length of the gas bubbles passing through the photo station after each segment ($l_{p,i}$), weighted with the fraction of each segment contributing to the total length of the reactor $\left(\frac{l_{segment,i}}{l}\right)$.

Under the assumption of a constant liquid flow rate, the average volume flow is calculated using Formula (12).

$$\bar{\dot{V}} = \dot{V}_L + \dot{V}_G \cdot \sum_{i=1}^{4} \left( \frac{l_{p,i}}{l_{p,0m}} \cdot \frac{l_{segment,i}}{l} \right) \quad (12)$$

Space-time-yield STY is calculated *via* the amount of produced desired product according to Formula (13).

$$STY = \frac{\left(x_{C18:1,0} - x_{C18:1}\right) \cdot \dot{n}_{FAME} \cdot M_{C18:1}}{V_R} \quad (13)$$

Calculation and evaluation of permeation fluxes:

The permeation flux $q_i$ of component i through a polymer of material j with a thickness of s (in mm) and a surface area A (in cm³) is correlated with the temperature-dependent permeation coefficient $\varepsilon_{i,j}$ and permeation pressure difference $\Delta p_{perm}$ (T in K, $\Delta p_{perm}$ in kPa). For hydrogen and FEP this yields:[141]

$$\varepsilon_{H2,FEP}(T) = 2.12 \cdot 10^{-4} \cdot e^{-\frac{3.12 \cdot 10^3}{T}} \quad (14)$$

$$q_{H2} = \varepsilon_{H2,FEP}(T) \cdot \frac{A}{s} \cdot \Delta p_{perm} \quad (15)$$

The resulting flux (in mL $s^{-1}$) is valid at 20 °C and 1 bar and needs to be transferred to the desired conditions applying ideal gas law.

Comparing the obtained results of the experiments with sole permeation with their consumed amount of hydrogen resulting from the FAME compositions and flowrates leads to deviations of the factor 2.25, meaning that the real permeation fluxes must be substantially higher than those calculated with Formula (15). For cases of reactions with slugs and permeation at drastically reduced IPA content, this value is still not sufficient as evident from GC measurements and must rather be a factor of ca. 3.8. The solubility of hydrogen within the liquid was neglected as a first approach due to a lack of reliable data and due to strongly minor soluble amounts compared to the hydrogen content of a gas phase. The reactor pressure at the inlet and the outlet was measured and averaged, assuming a linear pressure drop along the reactor. Thus, the exact permeation flux in each experiment is – although most of the experiments were conducted with a constantly low PC:solvent ratio like applied for the evaluation experiments – uncertain and only permeation pressure differences are given.

Determination of slug lengths:

Slug lengths were determined manually for a freezed frame of the recorded video of the flow in steady state. For the determination of residence times, up to 3 bubbles were measured and averaged. The software Fiji was used for a more detailed analysis of slug lengths: approx. 9 complete slugs were measured using the straight line tool from cap to cap. From that, average value and standard deviation were calculated.

Estimation of $TOF_{20}$:

$TOF_{20}$-equivalent figures are obtained from the fitted values of the presented model and refer to 20 % conversion of the excess double bonds. The turnover number at 20 % conversion was divided by the associated time and the resulting value rounded to significant digits.

Investigation of Pd leaching:

After hydrogenation, samples were collected and the solvent removed in vacuo. For 1-hexanol, sufficient removal was confirmed by $^{1}$H-NMR analysis. Product and catalyst (Pd with PC) form a biphasic system that is fully separated via two centrifugation cycles for 3 min at 1000 $min^{-1}$. Each phase is further analyzed in ICP-OES (AnalytikJena Plasma Quant PQ9000 Elite) to obtain its Pd concentration.

Hydrogenation in batch reactors:

A 120 ml stainless steel reactor with a substrate container, baffles and gas injection stirrer was inertized using argon and vacuum in alternation for in total three cycles. The catalyst solution and solvent were introduced *via* a syringe in argon counterflow into the vessel. The substrate was introduced into the substrate container in argon counterflow *via* a syringe. Afterwards, the reactor was heated, pressurized and stirring was started. The substrate was additionally preheated. At constant conditions, the substrate was added and the reaction started. Samples were withdrawn, degassed using argon and cooled in an ice bath at the same time.

## 11.6.2 Analytics

GC analysis of hydrogenation mixtures: MTBE was dried over mole sieve and used to dilute most of the samples; otherwise, cyclohexane was used. Reaction mixtures were diluted to reach 100 mg analyte in 800 mg of solvent; reference samples were diluted with pure dried MTBE to the same concentration. The samples were measured on a Agilent 8860 GC device equipped with a DB-FastFAME column (90 m, 0.25 mm, 0.25 µm) and FID using He as carrier gas.

The standard deviation of the GC measurements was calculated using the amount of C16:0 in every measured sample including samples that are not shown in the graphs (like from start-up behavior), and was quantified to be 0.092 mol $mol^{-1}$. Mean standard error was calculated to 0.0048 mol $mol^{-1}$.

Table S 24: Heating profile for the analysis of the hydrogenation mixtures using GC-FID.

| | Rate [°C $min^{-1}$] | Temperature [°C] | Holding time [min] |
|---|---|---|---|
| $T_{Start}$ | | 70 | 0 |
| **Ramp 1** | 15 | 150 | 1 |
| **Ramp 2** | 50 | 175 | 1 |
| **Ramp 3** | 5 | 178 | 0 |
| **Ramp 4** | 1 | 180 | 1 |
| **Ramp 5** | 3 | 192 | 1 |
| **Ramp 6** | 1 | 202 | 1 |
| **Ramp 7** | 3 | 210 | 3 |
| **Ramp 8** | 10 | 230 | 1 |

## 11.6.3 Additional Results

Investigation of flow behaviour without additional solvent:

Setup constraints limit maximum pressure to less than 20 bar, thus 10 barg back pressure were used for standard experiments, based on literature[12]. The low catalyst loading results in a very small catalyst phase slug, although Pd concentration in PC is within the ppm range. At the same time, the high amount of substrate results in enlarged substrate slugs. The phase ratios were calculated for a Pd concentration of 12 ppm (w/w) in PC and S:C of 100,000:1 as a worst-case estimation for maximum versatility in reaction conditions. This results in volumetric phase ratios of 1:4.5:22.8 (catalyst : FAME : $H_2$, including ca. 10 % excess of hydrogen). For the pure flow behavior experiments, these were conducted without additional Pd to purely study the influence of constant phase ratios. PC was colored pink with Acid Red 94 for better distinguishability. Applying this typical ratio in the flow setup without reaction, the large gas bubbles disintegrate into several smaller ones that segregate catalyst from substrate and thus would inhibit the reaction (Figure S 20).

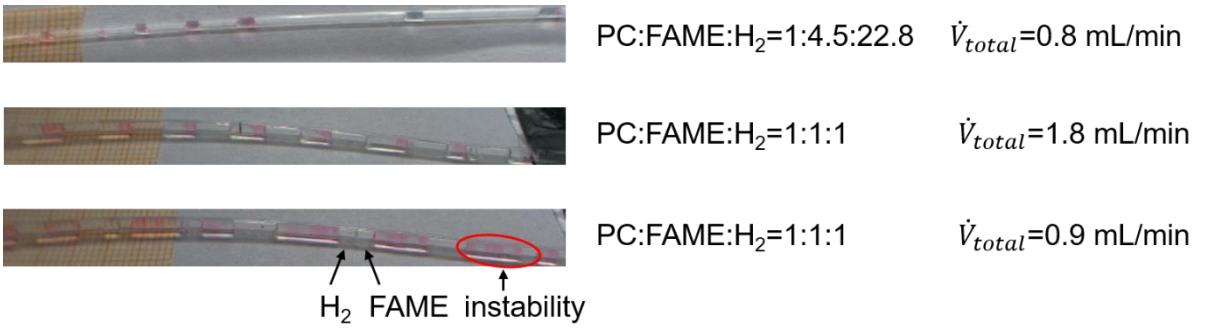


Figure S 20: Images of flow patterns after 5 m in the reactor for different phase ratios and volume flows without reaction. PC was coloured pink for better distinguishability. Volumetric phase ratios are given as catalyst : FAME : $H_2$. Scale: length of one small square = 1 mm

Further investigated solvents

Initially, MTBE was chosen as solvent due to its low viscosity, high vapor pressure (enabling easy separability afterwards) and a good solubility of catalyst and substrate phase. Dissolution of Pd to ca. 0.81 ppm in the liquid phase by the additional solvent comes into play as can be seen in Figure S 21 for the reaction with S:C of 100,000:1 even for 24 ppm P in PC.

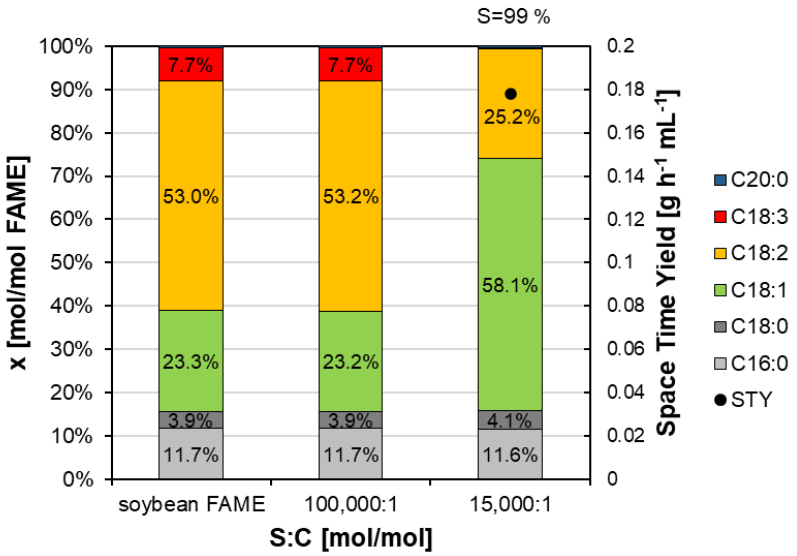


Figure S 21: Composition of samples of the selective partial hydrogenation of soybean FAME in the capillary reactor with additional MTBE. Reaction conditions: S:C as stated, T= 80 °C, $p_{H2,back}$= 11 bara, solvent= MTBE, l= 40 m, $w_{Pd,PC}$= 24 ppm
S:C= 100,000:1: PC:solvent= 1:17.24 mL mL$^{-1}$; $\dot{V}_{cat.}$= 1.20 mL min$^{-1}$; $\dot{V}_{H_2,T}$= 1.50 mL min$^{-1}$; $\dot{V}_{FAME}$= 0.30 mL min$^{-1}$; τ= 10.5 min
S:C= 15,000:1: PC:solvent= 1:4.47 mL mL$^{-1}$; $\dot{V}_{cat.}$= 1.20 mL min$^{-1}$; $\dot{V}_{H_2,T}$= 1.50 mL min$^{-1}$; $\dot{V}_{FAME}$= 0.30 mL min$^{-1}$; τ= 12.6 min

Afterwards, potentially applicable volume flows and their resulting residence times were evaluated to identify beneficial values (Figure S 22). Volume flows less than 1.2 mL min$^{-1}$ do not lead to significantly enhanced conversions and give rise to unstable flow patterns. Volume flows greater than 3 mL min$^{-1}$ are in principle applicable (although the mass flow controller limits hydrogen volume flows to ca. 2.5 mL min$^{-1}$) but are expected to give less conversion due to short residence times.

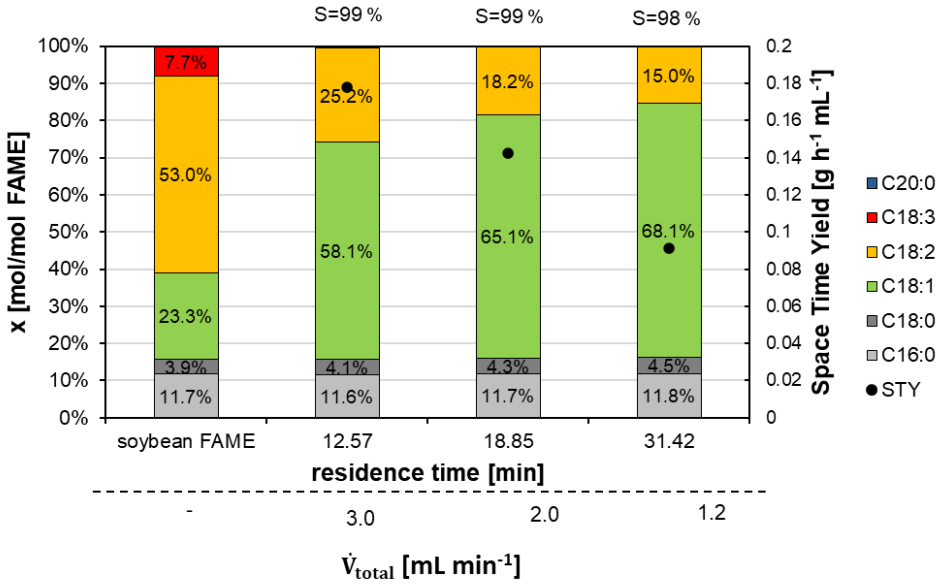


Figure S 22: Composition of samples of the selective partial hydrogenation of soybean FAME in the capillary reactor with additional MTBE. Reaction conditions: S:C= 15,000:1, T= 80 °C, $p_{H2,back}$= 11 bara, PC:solvent= 1:4.47 mL mL$^{-1}$, solvent= MTBE, l= 40 m, $w_{Pd,PC}$= 24 ppm
τ= 12.6 min: $p_{PI2}$= 11.7 bara; $\dot{V}_{cat.}$= 1.20 mL min$^{-1}$; $\dot{V}_{H_2,T}$= 1.50 mL min$^{-1}$; $\dot{V}_{FAME}$= 0.30 mL min$^{-1}$
τ= 18.8 min: $p_{PI2}$= 11.5 bara; $\dot{V}_{cat.}$= 0.80 mL min$^{-1}$; $\dot{V}_{H_2,T}$= 1.00 mL min$^{-1}$; $\dot{V}_{FAME}$= 0.20 mL min$^{-1}$
τ= 31.4 min: $p_{PI2}$= 11.4 bara; $\dot{V}_{cat.}$= 0.48 mL min$^{-1}$; $\dot{V}_{H_2,T}$= 0.60 mL min$^{-1}$; $\dot{V}_{FAME}$= 0.12 mL min$^{-1}$

The major drawback of the use of MTBE is a nanoparticle-destabilizing behavior, even pronounced at elevated temperatures, that results in deposition of Pd at the capillary material, leading to an activation of the material even without Pd feeding. The destabilizing behavior results in a peak performance at 80 °C for MTBE (Figure S 23).

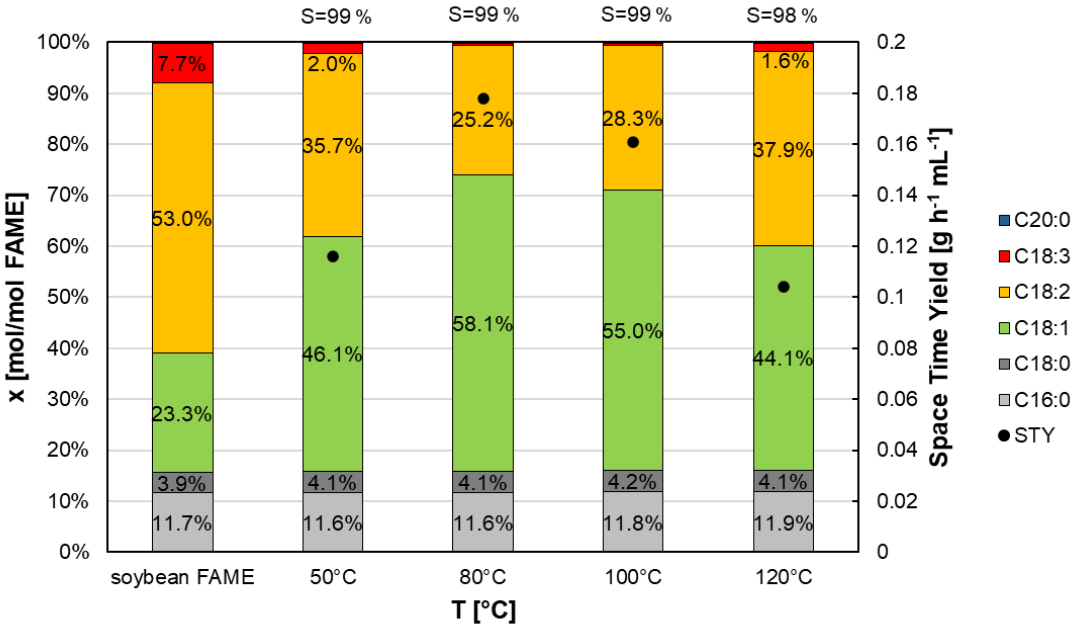


Figure S 23: Composition of samples of the selective partial hydrogenation of soybean FAME in the capillary reactor with additional MTBE. Reaction conditions: S:C= 15,000:1, T as stated, $p_{H2,back}$= 11 bara, PC:solvent= 1:4.47 mL mL$^{-1}$, solvent= MTBE, l= 40 m, $w_{Pd,PC}$= 24 ppm, $\dot{V}_{cat.}$= 1.20 mL min$^{-1}$; $\dot{V}_{H_2,T}$= 1.50 mL min$^{-1}$; $\dot{V}_{FAME}$= 0.30 mL min$^{-1}$

T= 50°C: $p_{PI2}$= 11.8 bara, $\tau$= 12.7 min
T= 80°C: $p_{PI2}$= 11.7 bara, $\tau$= 12.6 min
T= 100°C: $p_{PI2}$= 11.5 bara, $\tau$= 12.0 min
T= 120°C: $p_{PI2}$= 11.5 bara, $\tau$= 11.4 min

Further investigated solvents as an alternative to MTBE include 1-octanol, 1-decanol, 1-hexanol and 2-propanol. Octanol and decanol form two liquid phases at room temperature and show high viscosities and were therefore excluded. The use of hexanol results in spontaneously occurring flow instabilities due to still increased viscosity. Furthermore, an emulsion is formed when mixed with PC which only gets monophasic after the addition of FAME. Adversely, 2-propanol showed a promising mixing and flow behavior and was therefore further investigated.

Table S 25 gives an overview of the Pd concentrations after hydrogenation in the capillary reactor and removal of the low-boiling solvents. Note that resolution of the device is only possible in 1 ppm steps and that Pd loss during workup (evaporation and centrifugation) by deposition or accumulation at the phase interface is highly possible. A combination of all mentioned factors may explain unclosed mass balances (at least for IPA), since Pd deposition inside the reactor during the use of IPA was not observable.

Table S 25: Found Pd concentrations in each phase after hydrogenation and evaporation of the respective solvent

| solvent | $w_{Pd,FAME}$ [ppm] | $w_{Pd,PC}$ [ppm] |
|---|---|---|
| **IPA** | 1 | 9 |
| **MTBE** | 2 | 8 |
| **1-hexanol** | 1 | 12 |

Lower S:C for hydrogenation with additional IPA

Further decrease of S:C towards 15,000:1 results in strong overhydrogenation towards the undesired C18:0 with a reduced selectivity of 82 %.

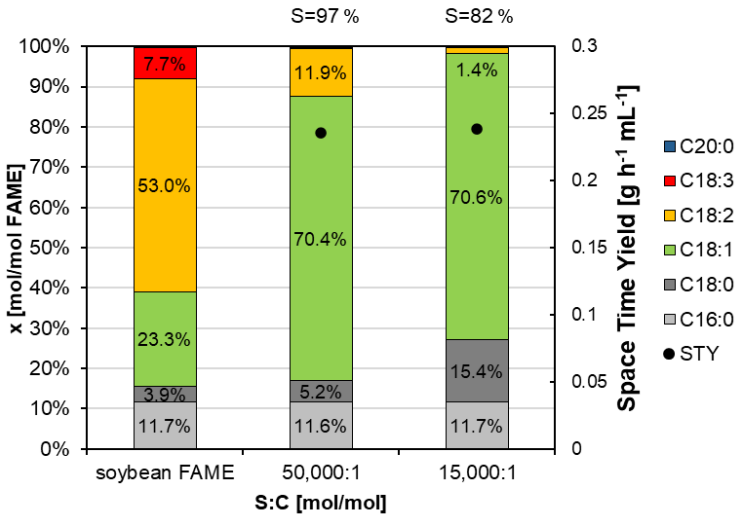


Figure S 24: Composition of samples of the selective partial hydrogenation of soybean FAME in the capillary reactor with additional IPA. Reaction conditions: S:C as stated, T= 80 °C, $p_{H2,back}$= 11 bara, l= 40 m, $w_{Pd,PC}$= 24 ppm, solvent= IPA, $\dot{V}_{cat.}$= 1.20 mL min$^{-1}$; $\dot{V}_{H_2,T}$= 1.50 mL min$^{-1}$; $\dot{V}_{FAME}$= 0.30 mL min$^{-1}$
S:C= 50,000:1: PC:solvent= 1:17.24 mL mL$^{-1}$, τ= 15.5 min
S:C= 15,000:1: PC:solvent= 1:4.47 mL mL$^{-1}$, τ= 19.7 min

Reaction modelling

The used approach considers lumping of several different species. Furthermore, mass transport mechanisms as well as adsorption to the catalyst surface are combined by kinetic constants of pseudo-first order. Hydrogen is applied in excess in most of the cases and therefore also included in the pseudo-first-order approach like it is typically also done in literature[52],[74]. As has been shown, g/l-mass transport resistances show no limitation at least for the slug with permeation approach. The resulting reaction network is presented in Figure S 25 and the resulting differential equation system in Formula (16). The differential equation system is obtained at a constant molar amount or molar flow regarding the FAME in the reactor, thus accumulation terms are obsolete. Furthermore, constant liquid properties like density and viscosity are assumed, since relevant changes in the structural motif of the molecules are minimal. The capillary reactor was operated in stationary mode, and ideal plug flow behaviour was assumed, enabled by the slug flow. The use of the equations of the batch reactor for the capillary reactor was enabled by the transferability between time and coordinate of ideal batch resp. flow reactors, as only the composition at the outlet of the capillary reactor is relevant here instead of an axial profile. Different residence times were enabled by adjustment of the volume flows.

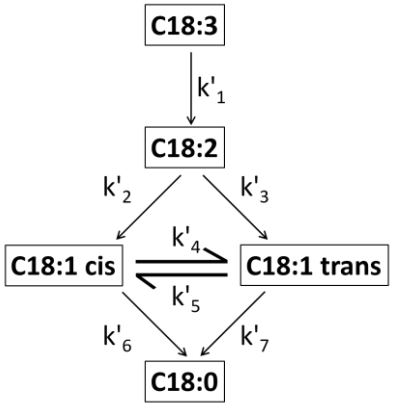


Figure S 25: Reaction network used for the pseudokinetic modelling

$$\begin{pmatrix} \frac{\partial x_{C18:3}}{\partial t} \\ \frac{\partial x_{C18:2}}{\partial t} \\ \frac{\partial x_{C18:1,cis}}{\partial t} \\ \frac{\partial x_{C18:1,trans}}{\partial t} \\ \frac{\partial x_{C18:0}}{\partial t} \end{pmatrix} = \begin{pmatrix} -k'_1 & 0 & 0 & 0 & 0 \\ k'_1 & -(k'_2+k'_3) & 0 & 0 & 0 \\ 0 & k'_2 & -(k'_4+k'_6) & k'_5 & 0 \\ 0 & k'_3 & k'_4 & -(k'_5+k'_7) & 0 \\ 0 & 0 & k'_6 & k'_7 & 0 \end{pmatrix} \begin{pmatrix} x_{C18:3} \\ x_{C18:2} \\ x_{C18:1,cis} \\ x_{C18:1,trans} \\ x_{C18:0} \end{pmatrix} \quad (16)$$

The pseudokinetic constants were fitted to measured data by a self-written Python program utilizing the Levenberg-Marquardt algorithm. Results of this fitting for the kinetic constants can be found in Table S 26, derived x,t-diagrams in Figure 65.

Table S 26: Obtained pseudokinetic constants

| | **Slug+permeation** | **Permeation** | **Batch** |
|---|---|---|---|
| $\mathbf{k'_1}$ **[s$^{-1}$]** | 5.830E-03 | 3.256E-03 | 5.338E-04 |
| $\mathbf{k'_2}$ **[s$^{-1}$]** | 2.184E-03 | 1.129E-03 | 1.727E-04 |
| $\mathbf{k'_3}$ **[s$^{-1}$]** | 1.120E-08 | 5.528E-12 | 6.627E-05 |
| $\mathbf{k'_4}$ **[s$^{-1}$]** | 8.147E-04 | 6.203E-04 | 1.196E-09 |
| $\mathbf{k'_5}$ **[s$^{-1}$]** | 3.011E-03 | 2.271E-03 | 1.032E-04 |
| $\mathbf{k'_6}$ **[s$^{-1}$]** | 4.129E-05 | 1.859E-12 | 1.028E-05 |
| $\mathbf{k'_7}$ **[s$^{-1}$]** | 1.633E-10 | 1.694E-04 | 4.552E-14 |

## Influence of capillary length

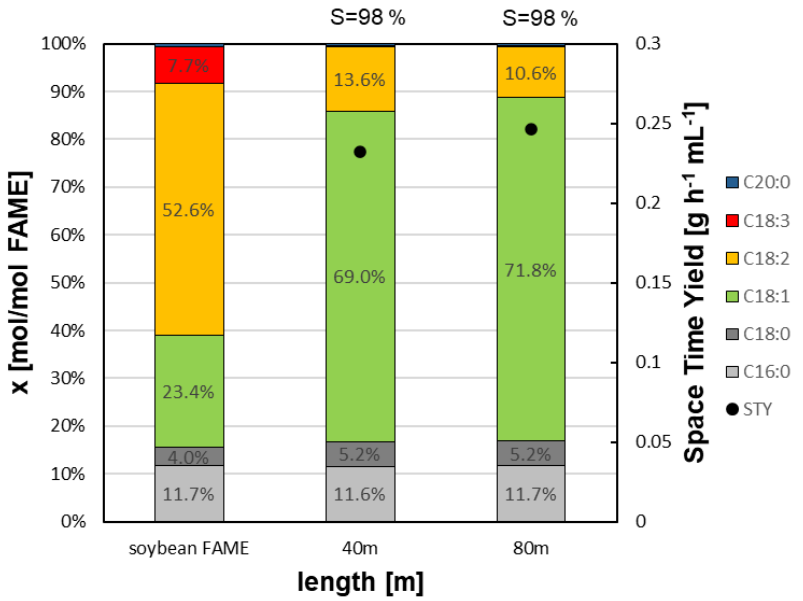


Figure S 26: Composition of samples of the selective partial hydrogenation of soybean FAME in the capillary reactor with additional IPA. Reaction conditions: S:C= 50,000:1, T= 80 °C, $p_{H2,back}$= 11 bara, l as stated, $w_{Pd,PC}$= 24 ppm, solvent= IPA, PC:solvent= 1:17.13 mL mL$^{-1}$,-
l=40 m: $\Delta p_{Perm.}$= 1.16 bar, $\tau$= 11.9 min, $\dot{V}_{cat.}$= 1.20 mL min$^{-1}$; $\dot{V}_{H_2,T}$= 1.50 mL min$^{-1}$; $\dot{V}_{FAME}$= 0.30 mL min$^{-1}$
l=80 m: $\Delta p_{Perm.}$= 1.41 bar, $\tau$= 14.2 min, $\dot{V}_{cat.}$= 2.40 mL min$^{-1}$; $\dot{V}_{H_2,T}$= 2.00 mL min$^{-1}$; $\dot{V}_{FAME}$= 0.60 mL min$^{-1}$

## Variation of pressure

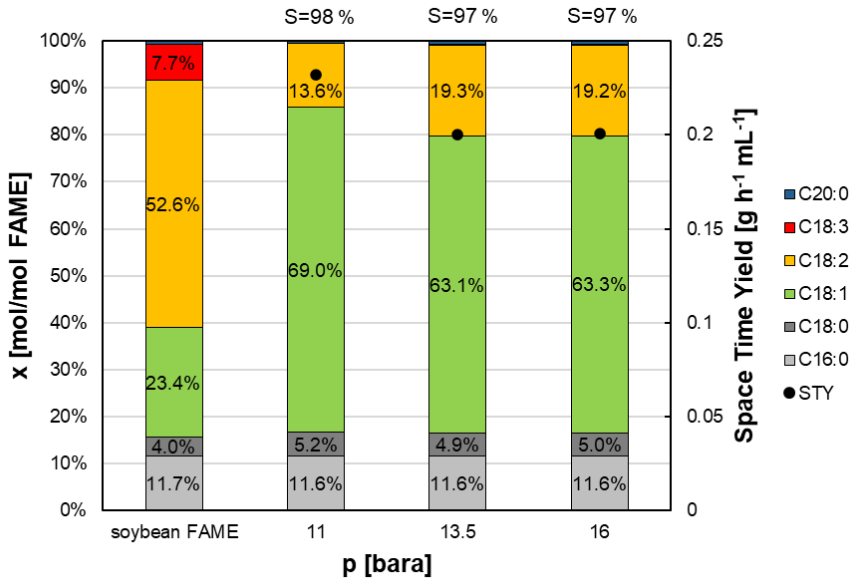


Figure S 27: Composition of samples of the selective partial hydrogenation of soybean FAME in the capillary reactor with additional IPA. Reaction conditions: S:C= 50,000:1, T= 80 °C, l= 40 m, $w_{Pd,PC}$= 24 ppm, solvent= IPA, PC:solvent= 1:17.13 mL mL$^{-1}$, $\dot{V}_{cat.}$= 1.20 mL min$^{-1}$; $\dot{V}_{H_2,T}$= 1.50 mL min$^{-1}$; $\dot{V}_{FAME}$= 0.30 mL min$^{-1}$
$p_{H2,back}$= 11 bara: $\Delta p_{Perm.}$= 1.16 bar, $\tau$= 11.9 min
$p_{H2,back}$= 13.5 bara: $\Delta p_{Perm.}$= 2.34 bar, $\tau$= 10.7 min
$p_{H2,back}$= 16 bara: $\Delta p_{Perm.}$= 3.68 bar, $\tau$= 10.6 min

The slightly elevated yield for 11 bar might result from the longer residence time.

Influence of IPA and permeation on the residence time

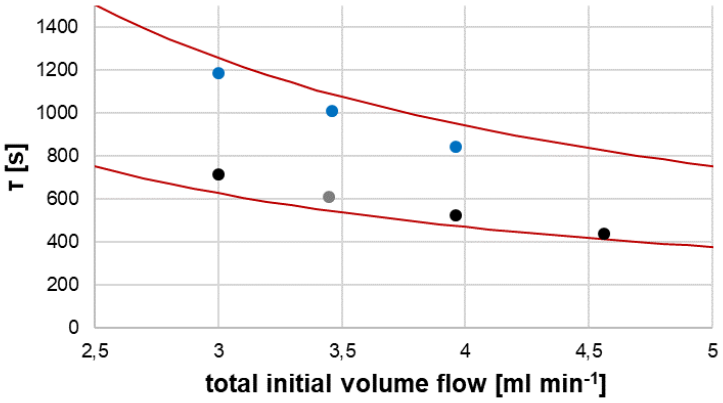


Figure S 28: Magnified version of Figure 70: Obtained residence times of the selective partial hydrogenation of soybean FAME in the capillary reactor with varying IPA content and at different volume flows. Reaction conditions: S:C= 50,000:1 (gray point: 69,570:1), T=80 °C, $p_{H2,back}$= 11 bara, l= 40 m, $w_{Pd,PC}$= 24 ppm, solvent= IPA, $\dot{V}_{H_2,T} = \dot{V}_{liq,total}$
black/gray points: PC:solvent= 1:17.13 mL mL$^{-1}$ (gray point: 1:14.64), $\Delta p_{Perm.}$= 1.16-1.71 bar, $\dot{V}_{total}$= 3-4.57 mL min$^{-1}$,
blue points: PC:solvent= 1:2.02 mL mL$^{-1}$, $\Delta p_{Perm.}$= 6.35-8.27 bar, $\dot{V}_{total}$= 3-3.96 mL min$^{-1}$, full conversion and spontaneous bubble formation are restricted by limited hydrogen supply.
Red lines: constant bubble size resp. instantaneous bubble disappearance

# 12 References


[1] Europäische Kommission, "COM(2020) 667 final. Chemikalienstrategie für Nachhaltigkeit", eur-lex.europa.eu, **2020**, last access: 19.12.2025.

[2] Europäische Kommission, "COM(2019) 640 final. Der europäische Grüne Deal", eur-lex.europa.eu, **2019**, last access: 19.12.2025.

[3] P. T. Anastas, J. B. Zimmerman, "Design Through the 12 Principles of Green Engineering", *Environ. Sci. Technol.* **2003**, *37*, 94A-101A, DOI: 10.1021/es032373g.

[4] The Royal Society, "Catalysing change: Defossilising the chemical industry. Policy Briefing", royalsociety.org/defossilising-chemicals, **2024**, last access: 05.01.2026.

[5] R. C. Forsythe, C. P. Cox, M. K. Wilsey, A. M. Müller, "Pulsed Laser in Liquids Made Nanomaterials for Catalysis", *Chem. Rev.* **2021**, *121*, 7568–7637, DOI: 10.1021/acs.chemrev.0c01069.

[6] W. Grünert, W. Kleist, M. Muhler, "Catalysis at Surfaces", De Gruyter, Berlin, Boston, **2023,** DOI: 10.1515/9783110632484-202.

[7] H. Freund, K. Sundmacher, "Process Intensification, 1. Fundamentals and Molecular Level" in *Ullmann's Encyclopedia of Industrial Chemistry*, Wiley, Weinheim, **2003,** DOI: 10.1002/14356007.o22_o02.

[8] P. T. Anastas, J. C. Warner, "Green Chemistry - Theory and Practice", Oxford University Press, Oxford, **1998**.

[9] A. Roucoux, K. Philippot, "New Trends in the Design of Metal Nanoparticles and Derived Nanomaterials for Catalysis" in *Nanoparticles in Catalysis*. *Advances in Synthesis and Applications,* (Eds.: K. Philippot, A. Roucoux), Wiley-VCH, Weinheim, **2021**.

[10] S. Reichenberger, G. Marzun, M. Muhler, S. Barcikowski, "Perspective of Surfactant‐Free Colloidal Nanoparticles in Heterogeneous Catalysis", *ChemCatChem* **2019**, *11*, 4489–4518, DOI: 10.1002/cctc.201900666.

[11] C.-B. Hwang, Y.-S. Fu, Y.-L. Lu, S.-W. Jang, P.-T. Chou, C. Wang, S. J. Yu, "Synthesis, Characterization, and Highly Efficient Catalytic Reactivity of Suspended Palladium Nanoparticles", *J. Catal.* **2000**, *195*, 336–341, DOI: 10.1006/jcat.2000.2992.

[12] T. F. H. Roth, A. Kühl, M. L. Spiekermann, H. W. Wegener, T. Seidensticker, "Biodiesel as a Sustainable Platform Chemical Enabled by Selective Partial Hydrogenation: Compounds Outplace Combustion?!", *ChemSusChem* **2024**, e202400036, DOI: 10.1002/cssc.202400036.

[13] A. Behr, T. Seidensticker, D. Vogt, "Applied Homogeneous Catalysis. A Tool for Sustainable Chemistry", Wiley, Newark, **2025,** DOI: 10.1002/9783527853205.

[14] A. Roucoux, J. Schulz, H. Patin, "Reduced transition metal colloids: a novel family of reusable catalysts?", *Chem. Rev.* **2002**, *102*, 3757–3778, DOI: 10.1021/cr010350j.

[15] A. Z. Moshfegh, "Nanoparticle catalysts", *J. Phys. D: Appl. Phys.* **2009**, *42*, 233001–233030, DOI: 10.1088/0022-3727/42/23/233001.

[16] V. Polshettiwar, T. Asefa, "Introduction to Nanocatalysis" in *Nanocatalysis*. *Synthesis and applications,* (Eds.: V. Polshettiwar, T. Asefa), John Wiley & Sons Inc, Hoboken New Jersey, **2013**.

[17] M. Kumari, B. Parshad, J. S. Yadav, S. Kumar, "Functionalized Nanomaterials for Catalytic Application: Trends and Developments" in *Functionalized Nanomaterials for Catalytic Application,* (Eds.: C. M. Hussain, S. K. Shukla, B. Mangla), John Wiley & Sons Incorporated, Hoboken, New Jersey, **2021**.

[18] M. Kim, S. Osone, T. Kim, H. Higashi, T. Seto, "Synthesis of Nanoparticles by Laser Ablation: A Review", *KONA Powder Part. J.* **2017**, *34*, 80–90, DOI: 10.14356/kona.2017009.

[19] J. D. Aiken, III, R. G. Finke, "A review of modern transition-metal nanoclusters: their synthesis, characterization, and applications in catalysis", *J. Mol. Catal. A: Chem.* **1999**, *145*, 1–44, DOI: 10.1016/S1381-1169(99)00098-9.

[20] S. Barcikowski, V. Amendola, G. Marzun, C. Rehbock, S. Reichenberger, D. Zhang, B. Gökce, "Handbook of Laser Synthesis of Colloids", DuEPublico: Duisburg-Essen Publications Online, University of Duisburg-Essen, Germany, **2016,** DOI: 10.17185/duepublico/41087.

[21] T. Tadros, "General Principles of Colloid Stability and the Role of Surface Forces" in *Colloid Stability*. *The Role of Surface Forces*, *Vol. 1,* (Ed.: T. F. Tadros), Wiley-VCH, Weinheim, **2007**.

[22] A. Behr, A. Lux, "Ein einfacher Syntheseweg zu Lösungsmittel-stabilisierten Metallnanopartikeln und ihre Anwendung in der Hydrierung", *Chem. Ing. Tech.* **2014**, *86*, 1933–1940, DOI: 10.1002/cite.201400057.

[23] W. Huang, Q. Hua, T. Cao, "Influence and Removal of Capping Ligands on Catalytic Colloidal Nanoparticles", *Catal. Lett.* **2014**, *144*, 1355–1369, DOI: 10.1007/s10562-014-1306-5.

[24] J. Zhang, M. Chaker, D. Ma, "Pulsed laser ablation based synthesis of colloidal metal nanoparticles for catalytic applications", *J. Colloid Interface Sci.* **2017**, *489*, 138–149, DOI: 10.1016/j.jcis.2016.07.050.

[25] H. Hirai, N. Toshima, "Polymer-attached catalysts" in *Tailored Metal Catalysts*, *Vol. 7,* (Ed.: Y. Iwasawa), Reidel, Dordrecht, **1986**.

[26] R. Narayanan, M. A. El-Sayed, "Effect of catalysis on the stability of metallic nanoparticles: Suzuki reaction catalyzed by PVP-palladium nanoparticles", *J. Am. Chem. Soc.* **2003**, *125*, 8340–8347, DOI: 10.1021/ja035044x.

[27] A. A. Nastulyavichus, S. I. Kudryashov, A. M. Emelyanenko, L. B. Boinovich, "Laser Generation of Colloidal Nanoparticles in Liquids: Key Processes of Laser Dispersion and Main Characteristics of Nanoparticles", *Colloid J.* **2023**, *85*, 233–250, DOI: 10.1134/S1061933X23600136.

[28] S. Mecking, U. Schlotterbeck, "Coupling Reactions" in *Multiphase Homogeneous Catalysis,* (Eds.: B. Cornils, W. A. Herrmann, I. T. Horváth, W. Leitner, S. Mecking, H. Olivier-Bourbigou, D. Vogt), Wiley-VCH, Weinheim, **2005**.

[29] L. M. Rossi, N. J. S. Costa, J. Limberger, A. L. Monteiro, "Nanocatalysts for the Suzuki coupling reactions" in *Nanocatalysis*. *Synthesis and applications,* (Eds.: V. Polshettiwar, T. Asefa), John Wiley & Sons Inc, Hoboken New Jersey, **2013**.

[30] J. A. Widegren, R. G. Finke, "A review of the problem of distinguishing true homogeneous catalysis from soluble or other metal-particle heterogeneous catalysis under reducing conditions", *J. Mol. Catal. A: Chem.* **2003**, *198*, 317–341, DOI: 10.1016/S1381-1169(02)00728-8.

[31] A. S. Galushko, A. S. Kashin, D. B. Eremin, M. V. Polynski, E. O. Pentsak, V. M. Chernyshev, V. P. Ananikov, "Introduction to Dynamic Catalysis and the Interface Between Molecular and Heterogeneous Catalysts" in *Nanoparticles in Catalysis*. *Advances in Synthesis and Applications,* (Eds.: K. Philippot, A. Roucoux), Wiley-VCH, Weinheim, **2021**.

[32] V. M. Chernyshev, A. V. Astakhov, I. E. Chikunov, R. V. Tyurin, D. B. Eremin, G. S. Ranny, V. N. Khrustalev, V. P. Ananikov, "Pd and Pt Catalyst Poisoning in the Study of Reaction Mechanisms: What Does the Mercury Test Mean for Catalysis?", *ACS Catal.* **2019**, *9*, 2984–2995, DOI: 10.1021/acscatal.8b03683.

[33] L. Staiger, "Nanometallurgy in Solution: Synthesis Strategies for Nano-Sized Materials and Investigation on their Catalytic Performance in the Alkyne Semi-Hydrogenation", *Dissertation*, Technische Universität München, München, **2022**.

[34] J. Xian, Q. Hua, Z. Jiang, Y. Ma, W. Huang, "Size-dependent interaction of the poly(N-vinyl-2-pyrrolidone) capping ligand with Pd nanocrystals", *Langmuir* **2012**, *28*, 6736–6741, DOI: 10.1021/la300786w.

[35] K. Lee, M. Kim, H. Kim, "Catalytic nanoparticles being facet-controlled", *J. Mater. Chem.* **2010**, *20*, 3791–3798, DOI: 10.1039/b921857b.

[36] T. Tano, K. Esumi, K. Meguro, "Preparation of organopalladium sols by thermal decomposition of palladium acetate", *J. Colloid Interface Sci.* **1989**, *133*, 530–533, DOI: 10.1016/S0021-9797(89)80069-4.

[37] C. A. Schaumberg, "Mechanismen der Laserablation zur Synthese nanoskopischer Kolloide", *Dissertation*, Humboldt-Universität zu Berlin, Berlin, **2016**.

[38] J. Zhang, J. Claverie, M. Chaker, D. Ma, "Colloidal Metal Nanoparticles Prepared by Laser Ablation and their Applications", *ChemPhysChem* **2017**, *18*, 986–1006, DOI: 10.1002/cphc.201601220.

[39] A. Nastulyavichus, S. Kudryashov, A. Ionin, Y. Yushina, A. Semenova, S. Gonchukov, "Focusing effects during ultrashort-pulse laser ablative generation of colloidal nanoparticles for

antibacterial applications", *Laser Phys. Lett.* **2022**, *19*, 65601–65605, DOI: 10.1088/1612-202X/ac642e.

[40] D. Zhang, C. Zhang, J. Liu, Q. Chen, X. Zhu, C. Liang, "Carbon-Encapsulated Metal/Metal Carbide/Metal Oxide Core–Shell Nanostructures Generated by Laser Ablation of Metals in Organic Solvents", *ACS Appl. Nano Mater.* **2019**, *2*, 28–39, DOI: 10.1021/acsanm.8b01541.

[41] T. Fromme, S. Reichenberger, K. M. Tibbetts, S. Barcikowski, "Laser synthesis of nanoparticles in organic solvents - products, reactions, and perspectives", *Beilstein J. Nanotechnol.* **2024**, *15*, 638–663, DOI: 10.3762/bjnano.15.54.

[42] C. M. Lok, "Structure and performance of selective hydrogenation catalysts" in *Hydrogenation*. *Catalysts and Processes,* (Ed.: S. D. Jackson), De Gruyter, **2018,** DOI: 10.1515/9783110545210-001.

[43] N. Cherkasov, D. Y. Murzin, C. R. A. Catlow, A. Chutia, "Selectivity of the Lindlar catalyst in alkyne semi-hydrogenation: a direct liquid-phase adsorption study", *Catal. Sci. Technol.* **2021**, *11*, 6205–6216, DOI: 10.1039/D1CY01016F.

[44] X. Chen, C. Shi, C. Liang, "Highly selective catalysts for the hydrogenation of alkynols: A review", *Chin. J. Catal.* **2021**, *42*, 2105–2121, DOI: 10.1016/S1872-2067(20)63773-1.

[45] J. Ballesteros-Soberanas, J. A. Carrasco, A. Leyva-Pérez, "Parts-Per-Million of Soluble Pd0 Catalyze the Semi-Hydrogenation Reaction of Alkynes to Alkenes", *J. Org. Chem.* **2023**, *88*, 18–26, DOI: 10.1021/acs.joc.2c00616.

[46] A. A. Shesterkina, A. A. Strekalova, E. V. Shuvalova, G. I. Kapustin, O. P. Tkachenko, L. M. Kustov, "CuO-Fe2O3 Nanoparticles Supported on SiO2 and Al2O3 for Selective Hydrogenation of 2-Methyl-3-Butyn-2-ol", *Catalysts* **2021**, *11*, 625–635, DOI: 10.3390/catal11050625.

[47] H. F. Rase, "Handbook of Commercial Catalysts. Heterogeneous Catalysts", CRC Press, Boca Raton, **2000**.

[48] A. Behr, A. J. Vorholt, "Homogeneous Catalysis with Renewables" in *Catalysis by Metal Complexes,* (Eds.: D. J. Cole-Hamilton, P. W. N. M. van Leeuwen), Springer, Berlin, Heidelberg, **2017,** DOI: 10.1007/978-3-319-54161-7.

[49] R. Kusy, K. Grela, "Renaissance in Alkyne Semihydrogenation: Mechanism, Selectivity, Functional Group Tolerance, and Applications in Organic Synthesis", *Chem. Rev.* **2025**, *125*, 4397–4527, DOI: 10.1021/acs.chemrev.4c00001.

[50] T. F. H. Roth, M. L. Spiekermann, D. Lütkenhaus, F. Niefer, D. Vogt, T. Seidensticker, "The effect of polyunsaturation – insights into the hydroformylation of oleochemicals", *Catal. Sci. Technol.* **2024**, *14*, 5551–5558, DOI: 10.1039/D4CY00839A.

[51] R.-W. Albach, M. Jautelat (Bayer AG), "Verfahren zur Herstellung von Sechsring-Carbocyclen", DE 198 07 995 A 1, **1998**.

[52] H. Patterson, "The Hydrogenation Reaction" in *Hydrogenation of fats and oils*. *Theory and practice,* (Eds.: G. R. List, J. W. King), AOCS Press, Urbana, **2011,** DOI: 10.1016/B978-1-893997-93-6.50007-5.

[53] J. A. Delgado, O. Benkirane, C. Claver, D. Curulla-Ferré, C. Godard, "Advances in the preparation of highly selective nanocatalysts for the semi-hydrogenation of alkynes using colloidal approaches", *Dalton Trans.* **2017**, *46*, 12381–12403, DOI: 10.1039/c7dt01607g.

[54] J. Chung, C. Kim, H. Jeong, T. Yu, D. H. Binh, J. Jang, J. Lee, B. M. Kim, B. Lim, "Selective semihydrogenation of alkynes on shape-controlled palladium nanocrystals", *Chem. - Asian J.* **2013**, *8*, 919–925, DOI: 10.1002/asia.201201166.

[55] N. Semagina, A. Renken, D. Laub, L. Kiwi-Minsker, "Synthesis of monodispersed palladium nanoparticles to study structure sensitivity of solvent-free selective hydrogenation of 2-methyl-3-butyn-2-ol", *J. Catal.* **2007**, *246*, 308–314, DOI: 10.1016/j.jcat.2006.12.011.

[56] M. Crespo-Quesada, A. Yarulin, M. Jin, Y. Xia, L. Kiwi-Minsker, "Structure sensitivity of alkynol hydrogenation on shape- and size-controlled palladium nanocrystals: which sites are most active and selective?", *J. Am. Chem. Soc.* **2011**, *133*, 12787–12794, DOI: 10.1021/ja204557m.

[57] A. Yarulin, I. Yuranov, F. Cárdenas-Lizana, P. Abdulkin, L. Kiwi-Minsker, "Size-Effect of Pd-(Poly(N-vinyl-2-pyrrolidone)) Nanocatalysts on Selective Hydrogenation of Alkynols with Different Alkyl Chains", *J. Phys. Chem. C* **2013**, *117*, 13424–13434, DOI: 10.1021/jp402258s.

[58] L. Nikoshvili, E. Shimanskaya, A. Bykov, I. Yuranov, L. Kiwi-Minsker, E. Sulman, "Selective hydrogenation of 2-methyl-3-butyn-2-ol over Pd-nanoparticles stabilized in hypercrosslinked polystyrene: Solvent effect", *Catal. Today* **2015**, *241*, 179–188, DOI: 10.1016/j.cattod.2014.01.045.

[59] J. J. Brunet, P. Caubere, "Activation of reducing agents. Sodium hydride containing complex reducing agents. 20. Pdc, a new, very selective heterogeneous hydrogenation catalyst", *J. Org. Chem.* **1984**, *49*, 4058–4060.

[60] A. Behr, T. Seidensticker, "Einführung in die Chemie nachwachsender Rohstoffe. Vorkommen, Konversion, Verwendung", Springer, Berlin, Heidelberg, **2018**.

[61] H. Iida, D. Itoh, S. Minowa, A. Yanagisawa, A. Igarashi, "Hydrogenation of soybean oil over various platinum catalysts: Effects of support materials on trans fatty acid levels", *Catal. Commun.* **2015**, *62*, 1–5, DOI: 10.1016/j.catcom.2014.12.025.

[62] M. L. Spiekermann, T. Seidensticker, "Catalytic processes for the selective hydrogenation of fats and oils: reevaluating a mature technology for feedstock diversification", *Catal. Sci. Technol.* **2024**, *14*, 4390–4419, DOI: 10.1039/D4CY00488D.

[63] A. Psalidas, E. Emmanouilidou, N. C. Kokkinos, "Catalytic Upgrading of Biodiesel by Partial Hydrogenation of Its FAME Composition: A Systematic Review", *Energies* **2024**, *17*, 561–581, DOI: 10.3390/en17030561.

[64] N. Numwong, A. Luengnaruemitchai, N. Chollacoop, Y. Yoshimura, "Partial hydrogenation of polyunsaturated fatty acid methyl esters over Pd/activated carbon: Effect of type of reactor", *Chem. Eng. J.* **2012**, *210*, 173–181, DOI: 10.1016/j.cej.2012.08.034.

[65] M. Kondratiuk, M. L. Spiekermann, T. Seidensticker, L. J. Gooßen, "Sustainable Diesel from Rapeseed Oil Esters by Sequential Semi-Hydrogenation, Double Bond Isomerization, and Metathesis", *Chem. Eur. J.* **2025**, e202500523, DOI: 10.1002/chem.202500523.

[66] A. Behr, "Anwendungsmöglichkeiten der homogenen Übergangsmetallkatalyse in der Fettchemie", *Fat Sci. Technol.* **1990**, *92*, 375–388, DOI: 10.1002/lipi.19900921002.

[67] C. Hu, D. Creaser, S. Siahrostami, H. Grönbeck, H. Ojagh, M. Skoglundh, "Catalytic hydrogenation of C=C and C=O in unsaturated fatty acid methyl esters", *Catal. Sci. Technol.* **2014**, *4*, 2427–2444, DOI: 10.1039/C4CY00267A.

[68] A. Behr, N. Döring, S. Durowicz‐Heil, B. Ellenberg, C. Kozik, C. Lohr, H. Schmidke, "Selektive Härtung mehrfach ungesättigter Fettsäuren in der Flüssigphase", *Fat Sci. Technol.* **1993**, *95*, 2–12, DOI: 10.1002/lipi.19930950103.

[69] A. Behr, N. Döring, C. Kozik, H. Schmidtke, S. Durowicz (Henkel KGaA), "Verfahren zur Herstellung von einfach ungesättigten Fettsäuren bzw. Derivaten derselben durch katalytische Hydrierung von mehrfach ungesättigten Fettsäuren bzw. Derivaten derselben", DE 4012873 A1, **1990**.

[70] A. Behr, C. Lohr, B. Ellenberg (Henkel KGaA), "Verfahren zur Herstellung von einfach ungesättigten Fettsäuren oder deren Derivaten", DE 4109246 A1, **1991**.

[71] J. W. Veldsink, M. J. Bouma, N.-H. Schöön, A. A. C. M. Beenackers, "Heterogeneous Hydrogenation of Vegetable Oils: A Literature Review", *Catal. Rev.* **1997**, *39*, 253–318, DOI: 10.1080/01614949709353778.

[72] A. J. Dijkstra, "Kinetics and mechanism of the hydrogenation process – the state of the art", *Eur. J. Lipid Sci. Technol.* **2012**, *114*, 985–998, DOI: 10.1002/ejlt.201100405.

[73] E. Draguez de Hault, A. Demoulin, "Partial hydrogenation of polyunsaturated fatty materials", *J. Am. Oil Chem. Soc.* **1984**, *61*, 195–200, DOI: 10.1007/BF02678768.

[74] U. P. Laverdura, L. Rossi, F. Ferella, C. Courson, A. Zarli, R. Alhajyoussef, K. Gallucci, "Selective Catalytic Hydrogenation of Vegetable Oils on Lindlar Catalyst", *ACS Omega* **2020**, *5*, 22901–22913, DOI: 10.1021/acsomega.0c02280.

[75] I. Horiuti, M. Polanyi, "Exchange reactions of hydrogen on metallic catalysts", *Trans. Faraday Soc.* **1934**, *30*, 1164–1172, DOI: 10.1039/TF9343001164.

[76] W.-Y. Siau, Y. Zhang, Y. Zhao, "Stereoselective Synthesis of Z-Alkenes" in *Stereoselective Alkene Synthesis*, *Vol. 327,* (Ed.: J. Wang), Springer, Berlin, Heidelberg, **2012,** DOI: 10.1007/128_2012_315.

[77] P. T. Witte, S. Boland, F. Kirby, R. van Maanen, B. F. Bleeker, D. A. M. de Winter, J. A. Post, J. W. Geus, P. H. Berben, "NanoSelect Pd Catalysts: What Causes the High Selectivity of These Supported Colloidal Catalysts in Alkyne Semi‐Hydrogenation?", *ChemCatChem* **2013**, *5*, 582–587, DOI: 10.1002/cctc.201200460.

[78] E. Breitmaier, "Terpene", Vieweg+Teubner Verlag, Wiesbaden, **1999,** DOI: 10.1007/978-3-322-94727-7.

[79] C. V. Rode, "Catalytic Hydrogenation of 2-Butyne-1,4-diol: Activity, Selectivity and Kinetics Studies", *J. Jpn. Petrol. Inst.* **2008**, *51*, 119–133, DOI: 10.1627/jpi.51.119.

[80] J. A. Delgado, C. Godard, "Progress in the Selective Semi-hydrogenation of Alkynes by Nanocatalysis" in *Recent Advances in Nanoparticle Catalysis*, *Vol. 1,* (Eds.: P. W. van Leeuwen, C. Claver), Springer International Publishing, Cham, **2020,** DOI: 10.1007/978-3-030-45823-2_10.

[81] E. V. Rebrov, E. A. Klinger, A. Berenguer-Murcia, E. M. Sulman, J. C. Schouten, "Selective Hydrogenation of 2-Methyl-3-butyne-2-ol in a Wall-Coated Capillary Microreactor with a Pd25Zn75/TiO2 Catalyst", *Org. Process Res. Dev.* **2009**, *13*, 991–998, DOI: 10.1021/op900085b.

[82] S. Furukawa, T. Komatsu, "Selective Hydrogenation of Functionalized Alkynes to (E)-Alkenes, Using Ordered Alloys as Catalysts", *ACS Catal.* **2016**, *6*, 2121–2125, DOI: 10.1021/acscatal.5b02953.

[83] M. W. Tew, J. T. Miller, J. A. van Bokhoven, "Particle Size Effect of Hydride Formation and Surface Hydrogen Adsorption of Nanosized Palladium Catalysts: L 3 Edge vs K Edge X-ray Absorption Spectroscopy", *J. Phys. Chem. C* **2009**, *113*, 15140–15147, DOI: 10.1021/jp902542f.

[84] M. W. Tew, M. Nachtegaal, M. Janousch, T. Huthwelker, J. A. van Bokhoven, "The irreversible formation of palladium carbide during hydrogenation of 1-pentyne over silica-supported palladium nanoparticles: in situ Pd K and L3 edge XAS", *Phys. Chem. Chem. Phys.* **2012**, *14*, 5761–5768, DOI: 10.1039/c2cp24068h.

[85] D. Teschner, J. Borsodi, Z. Kis, L. Szentmiklósi, Z. Révay, A. knop-Gericke, R. Schlögl, D. Torres, P. Sautet, "Role of Hydrogen Species in Palladium-Catalyzed Alkyne Hydrogenation", *J. Phys. Chem. C* **2010**, *114*, 2293–2299, DOI: 10.1021/jp9103799.

[86] D. Teschner, J. Borsodi, A. Wootsch, Z. Révay, M. Hävecker, A. knop-Gericke, S. D. Jackson, R. Schlögl, "The roles of subsurface carbon and hydrogen in palladium-catalyzed alkyne hydrogenation", *Science* **2008**, *320*, 86–89, DOI: 10.1126/science.1155200.

[87] D. Teschner, Z. Révay, J. Borsodi, M. Hävecker, A. knop-Gericke, R. Schlögl, D. Milroy, S. D. Jackson, D. Torres, P. Sautet, "Understanding palladium hydrogenation catalysts: when the nature of the reactive molecule controls the nature of the catalyst active phase", *Angew. Chem. Int. Ed.* **2008**, *47*, 9274–9278, DOI: 10.1002/anie.200802134.

[88] D. Teschner, E. Vass, M. Hävecker, S. Zafeiratos, P. Schnörch, H. Sauer, A. knop-Gericke, R. Schlögl, M. Chamam, A. Wootsch, A. S. Canning, J. J. Gamman, S. D. Jackson, J. McGregor, L. F. Gladden, "Alkyne hydrogenation over Pd catalysts: A new paradigm", *J. Catal.* **2006**, *242*, 26–37, DOI: 10.1016/j.jcat.2006.05.030.

[89] P. T. Witte, P. H. Berben, S. Boland, E. H. Boymans, D. Vogt, J. W. Geus, J. G. Donkervoort, "BASF NanoSelect™ Technology: Innovative Supported Pd- and Pt-based Catalysts for Selective Hydrogenation Reactions", *Top. Catal.* **2012**, *55*, 505–511, DOI: 10.1007/s11244-012-9818-y.

[90] G. Vilé, N. Almora-Barrios, S. Mitchell, N. López, J. Pérez-Ramírez, "From the Lindlar catalyst to supported ligand-modified palladium nanoparticles: selectivity patterns and accessibility constraints in the continuous-flow three-phase hydrogenation of acetylenic compounds", *Chem. Eur. J.* **2014**, *20*, 5926–5937, DOI: 10.1002/chem.201304795.

[91] F. Zaccheria, N. Ravasio, "Partial Reduction of Polyenes" in *Catalytic Reduction in Organic Synthesis 1,* (Ed.: J. G. de Vries), Thieme, Stuttgart, **2018**.

[92] G. Dupont, V. Desreux, "Contribution à l'étude du beta-myrcène. Son hydrogénation catalytique", *C. R. Hebd. Seances Acad. Sci.* **1936**, 733–736.

[93] J. Vondran, M. R. L. Furst, G. R. Eastham, T. Seidensticker, D. J. Cole-Hamilton, "Magic of Alpha: The Chemistry of a Remarkable Bidentate Phosphine, 1,2-Bis(di-tert-butylphosphinomethyl)benzene", *Chem. Rev.* **2021**, *121*, 6610–6653, DOI: 10.1021/acs.chemrev.0c01254.

[94] J. Vondran, R. Moeschke, T. Deysenroth, T. Seidensticker, "Pushing Boundaries—Selective Cooling Crystallization as Tool for Selectivity Compensation and Product Purification Using a Recyclable Pd/Xantphos Catalyst in the Methoxycarbonylation of Methyl 10‐Undecenoate", *Eur. J. Lipid Sci. Technol.* **2023**, *125*, 2200126, DOI: 10.1002/ejlt.202200126.

[95] V. Goldbach, M. Krumova, S. Mecking, "Full-Range Interconversion of Nanocrystals and Bulk Metal with a Highly Selective Molecular Catalyst", *ACS Catal.* **2018**, *8*, 5515–5525, DOI: 10.1021/acscatal.8b00981.

[96] V. Goldbach, P. Roesle, S. Mecking, "Catalytic Isomerizing ω-Functionalization of Fatty Acids", *ACS Catal.* **2015**, *5*, 5951–5972, DOI: 10.1021/acscatal.5b01508.

[97] H. W. Wegener, R. Reichert, N. Brede, A. Gierse, M. L. Spiekermann, D. Vogt, T. Seidensticker, "Mechanistic Insights Into the Methoxycarbonylation of Technical Grade Oleochemicals: Catalytical and Structural Analysis of Conjugated Fatty Acid Methyl Esters", *Eur. J. Lipid Sci. Technol.* **2025,** DOI: 10.1002/ejlt.202400198.

[98] A. I. Seifert, H. W. Wegener, K. Brühl, T. Seidensticker, K. Wohlgemuth, "Polymer-Grade Bio-Monomers from Oleochemicals by Combining Homogeneous Catalysis and Selective Product Crystallization in an Integrated Process", *Processes* **2023**, *11*, 2861, DOI: 10.3390/pr11102861.

[99] P. Roesle, L. Caporaso, M. Schnitte, V. Goldbach, L. Cavallo, S. Mecking, "A comprehensive mechanistic picture of the isomerizing alkoxycarbonylation of plant oils", *J. Am. Chem. Soc.* **2014**, *136*, 16871–16881, DOI: 10.1021/ja508447d.

[100] S. K. Hess, N. S. Schunck, V. Goldbach, D. Ewe, P. G. Kroth, S. Mecking, "Valorization of Unconventional Lipids from Microalgae or Tall Oil via a Selective Dual Catalysis One-Pot Approach", *J. Am. Chem. Soc.* **2017**, *139*, 13487–13491, DOI: 10.1021/jacs.7b06957.

[101] C. Kubis, M. König, B. N. Leidecker, D. Selent, H. Schröder, M. Sawall, W. Baumann, A. Spannenberg, A. Brächer, K. Neymeyr, R. Franke, A. Börner, "Interplay between Catalyst Complexes and Dormant States: In Situ Spectroscopic Investigations on a Catalyst System for Alkene Hydroformylation", *ACS Catal.* **2023**, *13*, 5245–5263, DOI: 10.1021/acscatal.2c06320.

[102] S. Obst, K. Köhnke, T. Seidensticker, W. Leitner, A. J. Vorholt, "Development of a Highly Active Catalyst System with Tuneable Selectivity for the Hydroformylation of the Renewable 1,3‐Diene β‐Myrcene", *ChemCatChem* **2025**, *17,* DOI: 10.1002/cctc.202500553.

[103] A. Börner, R. Franke, "Hydroformylation. Fundamentals, processes, and applications in organic synthesis", Wiley-VCH, Weinheim, **2016**.

[104] R. Franke, D. Selent, A. Börner, "Applied hydroformylation", *Chem. Rev.* **2012**, *112*, 5675–5732, DOI: 10.1021/cr3001803.

[105] P. C. Kamer, J. N. Reek, P. W. van Leeuwen, "Rhodium Phosphite Catalysts" in *Rhodium Catalyzed Hydroformylation*, *Vol. 22,* (Eds.: P. W. van Leeuwen, C. Claver), Kluwer Academic Publishers, New York, Boston, Dordrecht, London, Moscow, **2000**.

[106] P. W. van Leeuwen, "Catalyst preparation and decomposition" in *Rhodium Catalyzed Hydroformylation*, *Vol. 22,* (Eds.: P. W. van Leeuwen, C. Claver), Kluwer Academic Publishers, New York, Boston, Dordrecht, London, Moscow, **2000**.

[107] P. W. N. M. van Leeuwen, C. F. Roobeek (Shell Internationale Research Maatschappij B.V.), "A process for the hydroformylation of olefins", EP 0054986 A1, **1981**.

[108] W. H. Clement, M. Orchin, "Hydroformylation of Terpenes", *Ind. Eng. Chem. Prod. Res. Dev.* **1965**, *4*, 283–286.

[109] G. Liu, M. Garland, "The competitive and non-competitive hydroformylation of conjugated dienes starting with tetrarhodium dodecacarbonyl. An in-situ high-pressure infrared spectroscopic study", *J. Organomet. Chem.* **2000**, *608*, 76–85, DOI: 10.1016/S0022-328X(00)00369-7.

[110] C. G. Vieira, J. G. Da Silva, C. A. Penna, E. N. dos Santos, E. V. Gusevskaya, "Tandem hydroformylation-acetalization of para-menthenic terpenes under non-acidic conditions", *Appl. Catal., A* **2010**, *380*, 125–132, DOI: 10.1016/j.apcata.2010.03.045.

[111] C. G. Vieira, M. C. de Freitas, K. C. B. de Oliveira, A. de Camargo Faria, E. N. dos Santos, E. V. Gusevskaya, "Synthesis of fragrance compounds from renewable resources: the aqueous

biphasic hydroformylation of acyclic terpenes", *Catal. Sci. Technol.* **2015**, *5*, 960–966, DOI: 10.1039/C4CY01020E.

[112] H. J. V. Barros, J. G. Da Silva, C. C. Guimarães, E. N. dos Santos, E. V. Gusevskaya, "Hydroformylation of Monoterpenic Polyenes: Effect of the Conjugation of Double Bonds on Reactivity", *Organometallics* **2008**, *27*, 4523–4531, DOI: 10.1021/om800451t.

[113] J. C. Chalchat, R. P. Garry, E. Lecomte, A. Michet, "Hydroformylations of some monoterpenes and sesquiterpenes from essential oils", *Flavour Fragrance J.* **1991**, *6*, 179–182, DOI: 10.1002/ffj.2730060303.

[114] C. G. Vieira, E. N. dos Santos, E. V. Gusevskaya, "Synthesis of fragrance compounds from acyclic monoterpenes: Rhodium catalyzed hydroformylation and tandem hydroformylation/acetalization of linalool and β-citronellene", *Appl. Catal., A* **2013**, *466*, 208–215, DOI: 10.1016/j.apcata.2013.06.037.

[115] E. V. Gusevskaya, J. Jiménez‐Pinto, A. Börner, "Hydroformylation in the Realm of Scents", *ChemCatChem* **2014**, *6*, 382–411, DOI: 10.1002/cctc.201300474.

[116] C. M. Foca, H. J. V. Barros, E. N. dos Santos, E. V. Gusevskaya, J. Carles Bayón, "Hydroformylation of myrcene: metal and ligand effects in the hydroformylation of conjugated dienes", *New J. Chem.* **2003**, *27*, 533–539, DOI: 10.1039/b207947j.

[117] N. T. S. Phan, M. Van Der Sluys, C. W. Jones, "On the Nature of the Active Species in Palladium Catalyzed Mizoroki–Heck and Suzuki–Miyaura Couplings – Homogeneous or Heterogeneous Catalysis, A Critical Review", *Adv. Synth. Catal.* **2006**, *348*, 609–679, DOI: 10.1002/adsc.200505473.

[118] A. Jutand, G. Lefèvre, "Transition metal-catalyzed carbon-carbon cross-coupling" in *Arene Chemistry*. *Reaction Mechanisms and Methods for Aromatic Compounds,* (Ed.: J. Mortier), John Wiley & Sons, Hoboken, New Jersey, **2016**.

[119] J. G. de Vries, A. H. M. de Vries, "The Power of High‐Throughput Experimentation in Homogeneous Catalysis Research for Fine Chemicals", *Eur. J. Org. Chem.* **2003**, 799–811, DOI: 10.1002/ejoc.200390122.

[120] J. G. de Vries, "A unifying mechanism for all high-temperature Heck reactions. The role of palladium colloids and anionic species", *Dalton Trans.* **2006**, 421–429, DOI: 10.1039/b506276b.

[121] A. Alimardanov, L. Schmieder-van de Vondervoort, A. H. M. de Vries, J. G. de Vries, "Use of “Homeopathic” Ligand-Free Palladium as Catalyst for Aryl-Aryl Coupling Reactions", *Adv. Synth. Catal.* **2004**, *346*, 1812–1817, DOI: 10.1002/adsc.200404210.

[122] J. I. Ayogu, E. A. Onoabedje, "Prospects and Applications of Palladium Nanoparticles in the Cross-coupling of (hetero)aryl Halides and Related Analogues", *ChemistryOpen* **2021**, *10*, 430–450, DOI: 10.1002/open.202000309.

[123] A. Balanta, C. Godard, C. Claver, "Pd nanoparticles for C-C coupling reactions", *Chem. Soc. Rev.* **2011**, *40*, 4973–4985, DOI: 10.1039/c1cs15195a.

[124] H. Freund, K. Sundmacher, "Process Intensification, 4. Plant Level" in *Ullmann's Encyclopedia of Industrial Chemistry*, Wiley, Weinheim, **2003,** DOI: 10.1002/14356007.o22_o05.

[125] A. Seidel-Morgenstern, "Analysis and Experimental Investigation of Catalytic Membrane Reactors" in *Integrated Chemical Processes*. *Synthesis, Operation, Analysis, and Control,* (Eds.: K. Sundmacher, A. Kienle, A. Seidel-Morgenstern), Wiley-VCH, Weinheim, **2005**.

[126] H. Freund, K. Sundmacher, "Process Intensification, 2. Phase Level" in *Ullmann's Encyclopedia of Industrial Chemistry*, Wiley, Weinheim, **2003,** DOI: 10.1002/14356007.o22_o03.

[127] H. Freund, K. Sundmacher, "Process Intensification, 3. Process Unit Level" in *Ullmann's Encyclopedia of Industrial Chemistry*, Wiley, Weinheim, **2003,** DOI: 10.1002/14356007.o22_o04.

[128] G. Emig, E. Klemm, H. Freund, "Chemische Reaktionstechnik", Springer, Berlin, Heidelberg, **2024,** DOI: 10.1007/978-3-662-68826-7.

[129] E. Dietrich, C. Mathieu, H. Delmas, J. Jenck, "Raney-nickel catalyzed hydrogenations: Gas-liquid mass transfer in gas-induced stirred slurry reactors", *Chem. Eng. Sci.* **1992**, *47*, 3597–3604, DOI: 10.1016/0009-2509(92)85075-M.

[130] V. Hessel, T. Noël, "Micro Process Technology, 1. Introduction" in *Ullmann's Encyclopedia of Industrial Chemistry*, Wiley, Weinheim, **2003,** DOI: 10.1002/14356007.q16_q01.

[131] D. Hellmann, "Fluiddynamik und Stofftransport der Gas-Flüssig-Flüssig-Pfropfenströmung in Mikrokanälen. Evaluation eines neuen Kapillarreaktorkonzepts für katalysierte Gas-Flüssig-Reaktionen", *Dissertation*, Technische Universität Dortmund, Dortmund, **2021**.

[132] J. R. Burns, C. Ramshaw, "The intensification of rapid reactions in multiphase systems using slug flow in capillaries", *Lab Chip* **2001**, *1*, 10–15, DOI: 10.1039/b102818a.

[133] M. B. Plutschack, B. Pieber, K. Gilmore, P. H. Seeberger, "The Hitchhiker's Guide to Flow Chemistry", *Chem. Rev.* **2017**, *117*, 11796–11893, DOI: 10.1021/acs.chemrev.7b00183.

[134] J. Qian, X. Li, Z. Wu, Z. Jin, B. Sunden, "A comprehensive review on liquid–liquid two-phase flow in microchannel: flow pattern and mass transfer", *Microfluid. Nanofluid.* **2019**, *23,* DOI: 10.1007/s10404-019-2280-4.

[135] B. Pinho, L. M. Williams, J. Mahin, Y. Gao, L. Torrente-Murciano, "Enhancing mixing efficiency in curved channels: A 3D study of bi-phasic Dean-Taylor flow with high spatial and temporal resolution", *Chem. Eng. J.* **2023**, *471*, 144342–144355, DOI: 10.1016/j.cej.2023.144342.

[136] A. Günther, K. F. Jensen, "Multiphase microfluidics: from flow characteristics to chemical and materials synthesis", *Lab Chip* **2006**, *6*, 1487–1503, DOI: 10.1039/b609851g.

[137] D. Gorbunov, M. Nenasheva, G. Shashkin, V. Shapovalov, P. Shvets, E. Naranov, A. Maximov, A. Guda, A. Soldatov, "Transferring hydroformylation reaction into high-pressure gas–liquid microfluidic systems: Key achievements and perspectives", *J. Ind. Eng. Chem.* **2024**, *136*, 46–72, DOI: 10.1016/j.jiec.2024.02.029.

[138] L. Arsenjuk, M. Asshoff, J. Kleinheider, D. W. Agar, "A device for continuous and flexible adjustment of liquid-liquid slug size in micro-channels", *J. Flow Chem.* **2020**, *10*, 409–422, DOI: 10.1007/s41981-019-00064-7.

[139] Q. Li, P. Angeli, "Experimental and numerical hydrodynamic studies of ionic liquid-aqueous plug flow in small channels", *Chem. Eng. J.* **2017**, *328*, 717–736, DOI: 10.1016/j.cej.2017.07.037.

[140] L. Yang, K. F. Jensen, "Mass Transport and Reactions in the Tube-in-Tube Reactor", *Org. Process Res. Dev.* **2013**, *17*, 927–933, DOI: 10.1021/op400085a.

[141] N. von Vietinghoff, A. Immken, T. Seidensticker, P. de Caro, S. Thiebaud-Roux, D. W. Agar, "Gas Introduction by Permeation into Long Fluorinated Ethylene Propylene Capillaries with Slug Flow", *Chem. Eng. Technol.* **2023**, *46*, 1047–1051, DOI: 10.1002/ceat.202200557.

[142] L. W. McKeen, "Permeability properties of plastics and elastomers", Elsevier, Amsterdam, Boston, **2017**.

[143] J. W. Arblaster, "Crystallographic Properties of Palladium. Assessment of properties from absolute zero to the melting poin", *Platinum Met. Rev.* **2012**, *56*, 181–189, DOI: 10.1595/147106712X646113.

[144] O. Wetzel, O. Prymak, K. Loza, N. Gumbiowski, M. Heggen, P. Bayer, C. Beuck, C. Weidenthaler, M. Epple, "Water-Based Synthesis of Ultrasmall Nanoparticles of Platinum Group Metal Oxides (1.8 nm)", *Inorg. Chem.* **2021**, *61*, 5133–5147, DOI: 10.1021/acs.inorgchem.2c00281.s001.

[145] N. Kost, O. Prymak, K. Loza, M. Heggen, C. Weidenthaler, M. Epple, "Oxidation state of ultrasmall dodecylamine-coated palladium nanoparticles probed by X-ray techniques", *Acta Crystallogr., Sect. A:Found. Adv.* **2024**, *80*, e462, DOI: 10.1107/S2053273324095378.

[146] S. Bhama, T. R. Sibakoti, J. B. Jasinski, F. P. Zamborini, "Highly Active, Selective, and Recyclable Water‐Soluble Glutathione‐Stabilized Pd and Pd‐Alloy Nanoparticle Catalysts in Biphasic Solvent", *ChemCatChem* **2020**, *12*, 2253–2261, DOI: 10.1002/cctc.201901968.

[147] M. Pérez-Lorenzo, "Palladium Nanoparticles as Efficient Catalysts for Suzuki Cross-Coupling Reactions", *J. Phys. Chem. Lett.* **2012**, *3*, 167–174, DOI: 10.1021/jz2013984.

[148] A. M. Trzeciak, A. W. Augustyniak, "The role of palladium nanoparticles in catalytic C–C cross-coupling reactions", *Coord. Chem. Rev.* **2019**, *384*, 1–20, DOI: 10.1016/j.ccr.2019.01.008.

[149] A. Karatzia, "Mono- and bimetallic faceted noble metal nanoparticles: Synthesis and characterization", *Dissertation*, Universität Duisburg-Essen, **2023**.

[150] M. Jin, H. Liu, H. Zhang, Z. Xie, J. Liu, Y. Xia, "Synthesis of Pd nanocrystals enclosed by {100} facets and with sizes <10 nm for application in CO oxidation", *Nano Res.* **2011**, *4*, 83–91, DOI: 10.1007/s12274-010-0051-3.

[151] A. Rostek, M. Breisch, K. Pappert, K. Loza, M. Heggen, M. Köller, C. Sengstock, M. Epple, "Comparative biological effects of spherical noble metal nanoparticles (Rh, Pd, Ag, Pt, Au) with 4–8 nm diameter", *Beilstein J. Nanotechnol.* **2018**, *9*, 2763–2774.

[152] S. Ermis, K. Kaya, F. Topuz, Y. Yagci, "In-Situ and green photosynthesis of PVP-stabilized palladium nanoparticles as efficient catalysts for the reduction of 4-nitrophenol", *Inorg. Chem. Commun.* **2023**, *152*, 110626, DOI: 10.1016/j.inoche.2023.110626.

[153] J. García-Aguilar, M. Navlani-García, Á. Berenguer-Murcia, K. Mori, Y. Kuwahara, H. Yamashita, D. Cazorla-Amorós, "Evolution of the PVP-Pd Surface Interaction in Nanoparticles through the Case Study of Formic Acid Decomposition", *Langmuir* **2016**, *32*, 12110–12118, DOI: 10.1021/acs.langmuir.6b03149.

[154] Y. Fu, H. Zhang, S. Dai, X. Zhi, J. Zhang, W. Li, "Glutathione-stabilized palladium nanozyme for colorimetric assay of silver(I) ions", *Analyst* **2015**, *140*, 6676–6683, DOI: 10.1039/c5an01103e.

[155] G. Clergeaud, R. Genç, M. Ortiz, C. K. O'Sullivan, "Liposomal nanoreactors for the synthesis of monodisperse palladium nanoparticles using glycerol", *Langmuir* **2013**, *29*, 15405–15413, DOI: 10.1021/la402892f.

[156] M. Muniz-Miranda, A. Zoppi, F. Muniz-Miranda, N. Calisi, "Palladium Oxide Nanoparticles: Preparation, Characterization and Catalytic Activity Evaluation", *Coatings* **2020**, *10*, 207, DOI: 10.3390/coatings10030207.

[157] S. Sharma, "Metal dependent catalytic hydrogenation of nitroarenes over water-soluble glutathione capped metal nanoparticles", *J. Colloid Interface Sci.* **2015**, *441*, 25–29, DOI: 10.1016/j.jcis.2014.11.030.

[158] H. Hirai, H. Chawanya, N. Toshima, "Selective hydrogenation of cyclooctadienes catalyzed by colloidal palladium in poly(N‐vinyl‐2‐pyrrolidone)", *Makromol. Chem., Rapid Commun.* **1981**, *2*, 99–103, DOI: 10.1002/marc.1981.030020120.

[159] A. Behr, H. Schmidke (Henkel KGaA), "Verfahren zur Herstellung von Olefinen", DE 4203351 A1, **1992**.

[160] C. W. A. Chan, K. Y. Tam, J. Cookson, P. Bishop, S. C. Tsang, "Palladium with interstitial carbon atoms as a catalyst for ultraselective hydrogenation in the liquid phase", *Catal. Sci. Technol.* **2011**, *1*, 1584–1592, DOI: 10.1039/c1cy00257k.

[161] C. Evangelisti, N. Panziera, A. D'Alessio, L. Bertinetti, M. Botavina, G. Vitulli, "New monodispersed palladium nanoparticles stabilized by poly-(N-vinyl-2-pyrrolidone): Preparation,

structural study and catalytic properties", *J. Catal.* **2010**, *272*, 246–252, DOI: 10.1016/j.jcat.2010.04.006.

[162] M. M. Telkar, C. V. Rode, R. V. Chaudhari, S. S. Joshi, A. M. Nalawade, "Shape-controlled preparation and catalytic activity of metal nanoparticles for hydrogenation of 2-butyne-1,4-diol and styrene oxide", *Appl. Catal., A* **2004**, *273*, 11–19, DOI: 10.1016/j.apcata.2004.05.056.

[163] N. Wolff, K. Loza, M. Heggen, T. Schaller, F. Niemeyer, P. Bayer, C. Beuck, C. L. P. Oliveira, O. Prymak, C. Weidenthaler, M. Epple, "Ultrastructure and Surface Composition of Glutathione-Terminated Ultrasmall Silver, Gold, Platinum, and Alloyed Silver–Platinum Nanoparticles (2 nm)", *Inorg. Chem.* **2023**, *62*, 17470–17485.

[164] A. Thust, J. Barthel, K. Tillmann, "FEI Titan 80-300 TEM", *J. Large-scale Res. Fac.* **2016**, *2*, A41, DOI: 10.17815/jlsrf-2-66.

[165] N. Gumbiowski, K. Loza, M. Heggen, M. Epple, "Automated analysis of transmission electron micrographs of metallic nanoparticles by machine learning", *Nanoscale Adv.* **2023**, *5*, 2318–2326, DOI: 10.1039/d2na00781a.

[166] C. A. Schneider, W. S. Rasband, K. W. Eliceiri, "NIH Image to ImageJ: 25 years of Image Analysis", *Nat. Methods* **2012**, *9*, 671–675.

[167] H. Fissan, S. Ristig, H. Kaminski, C. Asbach, M. Epple, "Comparison of different characterization methods for nanoparticle dispersions before and after aerosolization", *Anal. Methods* **2014**, *6*, 7324, DOI: 10.1039/C4AY01203H.

[168] M. R. Ibrahim, Z. A. Fataftah, P. von Ragué Schleyer, P. D. Stout, "Calculation of enthalpies of hydrogenation of hydrocarbons", *J. Comput. Chem.* **1987**, *8*, 1131–1138, DOI: 10.1002/jcc.540080810.

[169] T. Fromme, M. L. Spiekermann, F. Lehmann, S. Barcikowski, T. Seidensticker, S. Reichenberger, "Preferential enrichment and extraction of laser-synthesized nanoparticles in organic phases", *Beilstein J. Nanotechnol.* **2025**, *16*, 254–263, DOI: 10.3762/bjnano.16.20.

[170] T. Fromme, L. K. Tintrop, S. Reichenberger, T. C. Schmidt, S. Barcikowski, "Impact of Chemical and Physical Properties of Organic Solvents on the Gas and Hydrogen Formation during Laser Synthesis of Gold Nanoparticles", *ChemPhysChem* **2023**, *24*, e202300089, DOI: 10.1002/cphc.202300089.

[171] O. Clavilier, D. Foy, F. Byrne, "The solvent miscibility table updated: miscibility and potential applications of green solvents", *Green Chem.* **2025**, *27*, 12151–12159, DOI: 10.1039/D5GC02901E.

[172] A. Lux, "Katalytische Reaktionen mit Lösungsmittel-stabilisierten metallischen Nanopartikeln", *Dissertation*, Technische Universität Dortmund, Dortmund, **2012**.

[173] C. L. Young (Ed.), "Hydrogen and Deuterium" in *Solubility data series*, *5/6*, Pergamon Press, Oxford, New York, Toronto, Sydney, Paris, Frankfurt, **1981**.

[174] M. S. Shaharun, H. Mukhtar, B. K. Dutta, "Solubility of carbon monoxide and hydrogen in propylene carbonate and thermomorphic multicomponent hydroformylation solvent", *Chem. Eng. Sci.* **2008**, *63*, 3024–3035, DOI: 10.1016/j.ces.2008.02.035.

[175] E. Brunner, "Solubility of Hydrogen in Alcohols", *Ber. Bunsenges. Phys. Chem.* **1979**, *83*, 715–721, DOI: 10.1002/bbpc.19790830715.

[176] F. Zaccheria, R. Psaro, N. Ravasio, P. Bondioli, "Standardization of vegetable oils composition to be used as oleochemistry feedstock through a selective hydrogenation process", *Eur. J. Lipid Sci. Technol.* **2012**, *114*, 24–30, DOI: 10.1002/ejlt.201100044.

[177] N. Ravasio, F. Zaccheria, M. Gargano, S. Recchia, A. Fusi, N. Poli, R. Psaro, "Environmental friendly lubricants through selective hydrogenation of rapeseed oil over supported copper catalysts", *Appl. Catal., A* **2002**, *233*, 1–6, DOI: 10.1016/S0926-860X(02)00128-X.

[178] C. Batiot, B. K. Hodnett, "The role of reactant and product bond energies in determining limitations to selective catalytic oxidations", *Appl. Catal., A* **1996**, *137*, 179–191, DOI: 10.1016/0926-860X(95)00322-3.

[179] F. Zaccheria, R. Psaro, N. Ravasio, "Selective hydrogenation of alternative oils: a useful tool for the production of biofuels", *Green Chem.* **2009**, *11*, 462–465, DOI: 10.1039/b817625f.

[180] A. Bouriazos, K. Mouratidis, N. Psaroudakis, G. Papadogianakis, "Catalytic Conversions in Aqueous Media. Part 2. A Novel and Highly Efficient Biphasic Hydrogenation of Renewable Methyl Esters of Linseed and Sunflower Oils to High Quality Biodiesel Employing Rh/TPPTS Complexes", *Catal. Lett.* **2008**, *121*, 158–164, DOI: 10.1007/s10562-007-9314-3.

[181] A. Bouriazos, S. Sotiriou, P. Stathis, G. Papadogianakis, "Superior aqueous-phase catalytic hydrogenation activity of palladium modified with nitrogen-containing ligands compared with the TPPTS benchmark modifier in micellar nanoreactors", *Appl. Catal., B* **2014**, *150-151*, 345–353, DOI: 10.1016/j.apcatb.2013.12.032.

[182] A. Bouriazos, S. Sotiriou, C. Vangelis, G. Papadogianakis, "Catalytic conversions in green aqueous media: Part 4. Selective hydrogenation of polyunsaturated methyl esters of vegetable oils for upgrading biodiesel", *J. Organomet. Chem.* **2010**, *695*, 327–337, DOI: 10.1016/j.jorganchem.2009.10.045.

[183] W. Liu, L. Xu, G. Lu, H. Zhang, "Selective Partial Hydrogenation of Methyl Linoleate Using Highly Active Palladium Nanoparticles in Polyethylene Glycol", *ACS Sustainable Chem. Eng.* **2017**, *5*, 1368–1375, DOI: 10.1021/acssuschemeng.6b01823.

[184] A. Behr, H. Schmidke, "Selektive Hydrierung ungesättigter Modellverbindungen mit solvensstabilisierten Palladium‐Kolloidkatalysatoren", *Chem. Ing. Tech.* **1993**, *65*, 568–569.

[185] A. Behr, H. Schmidtke (Henkel KGaA), "Verfahren zur Herstellung von Olefinen aus acetylenisch ungesättigten Verbindungen", DE 4211126 A1, **1992**.

[186] A. Behr, V. Manz, A. Lux, A. Ernst, "Highly Selective Mono-hydrogenation of Dicyclopentadiene with Pd-nanoparticles", *Catal. Lett.* **2013**, *143*, 241–245, DOI: 10.1007/s10562-013-0960-3.

[187] H. Hirai, H. Chawanya, N. Toshima, "Colloidal palladium protected with poly(N-vinyl-2-pyrrolidone) for selective hydrogenation of cyclopentadiene", *React. Polym., Ion Exch., Sorbents* **1985**, *3*, 127–141, DOI: 10.1016/0167-6989(85)90055-8.

[188] M. Adlim, M. Abu Bakar, K. Y. Liew, J. Ismail, "Synthesis of chitosan-stabilized platinum and palladium nanoparticles and their hydrogenation activity", *J. Mol. Catal. A: Chem.* **2004**, *212*, 141–149, DOI: 10.1016/j.molcata.2003.08.012.

[189] N. Győrffy, Z. Paál, "Acrolein hydrogenation on PdPt powder catalysts prepared by colloid synthesis", *J. Mol. Catal. A: Chem.* **2008**, *295*, 24–28, DOI: 10.1016/j.molcata.2008.08.012.

[190] O. M. Wilson, M. R. Knecht, J. C. Garcia-Martinez, R. M. Crooks, "Effect of Pd nanoparticle size on the catalytic hydrogenation of allyl alcohol", *J. Am. Chem. Soc.* **2006**, *128*, 4510–4511, DOI: 10.1021/ja058217m.

[191] N. Toshima, T. Takahashi, "Colloidal Dispersions of Platinum and Palladium Clusters Embedded in the Micelles. Preparation and Application to the Catalysis for Hydrogenation of Olefins", *Bull. Chem. Soc. Jpn.* **1992**, *65*, 400–409, DOI: 10.1246/bcsj.65.400.

[192] N. Toshima, Y. Shiraishi, T. Teranishi, M. Miyake, T. Tominaga, H. Watanabe, W. Brijoux, H. Bönnemann, G. Schmid, "Various ligand-stabilized metal nanoclusters as homogeneous and heterogeneous catalysts in the liquid phase", *Appl. Organometal. Chem.* **2001**, *15*, 178–196, DOI: 10.1002/aoc.146.

[193] P. J. Collier, J. A. Iggo, R. Whyman, "Preparation and characterisation of solvent-stabilised nanoparticulate platinum and palladium and their catalytic behaviour towards the enantioselective hydrogenation of ethyl pyruvate", *J. Mol. Catal. A: Chem.* **1999**, *146*, 149–157, DOI: 10.1016/S1381-1169(99)00084-9.

[194] V. Chechik, R. M. Crooks, "Dendrimer-Encapsulated Pd Nanoparticles as Fluorous Phase-Soluble Catalysts", *J. Am. Chem. Soc.* **2000**, *122*, 1243–1244, DOI: 10.1021/ja9936870.

[195] L. Wu, B.-L. Li, Y.-Y. Huang, H.-F. Zhou, Y.-M. He, Q.-H. Fan, "Phosphine dendrimer-stabilized palladium nanoparticles, a highly active and recyclable catalyst for the Suzuki-Miyaura reaction and hydrogenation", *Org. Lett.* **2006**, *8*, 3605–3608, DOI: 10.1021/ol0614424.

[196] J.-L. Pellegatta, C. Blandy, R. Choukroun, C. Lorber, B. Chaudret, P. Lecante, E. Snoeck, "Palladium colloids from an organometallic route: redox reaction between [VCp2] and [(Pd(η3 - allyl)2Cl]2. Catalytic application to the hydrogenation of aromatic nitro compounds", *New J. Chem.* **2003**, *27*, 1528–1532, DOI: 10.1039/B303130F.

[197] N. Arul Dhas, A. Gedanken, "Sonochemical preparation and properties of nanostructured palladium metallic clusters", *J. Mater. Chem.* **1998**, *8*, 445–450, DOI: 10.1039/a706100e.

[198] J. Huang, T. Jiang, B. Han, H. Gao, Y. Chang, G. Zhao, W. Wu, "Hydrogenation of olefins using ligand-stabilized palladium nanoparticles in an ionic liquid", *Chem. Commun.* **2003**, 1654–1655, DOI: 10.1039/b302750c.

[199] Y. Niu, L. K. Yeung, R. M. Crooks, "Size-Selective Hydrogenation of Olefins by Dendrimer-Encapsulated Palladium Nanoparticles", *J. Am. Chem. Soc.* **2001**, *123*, 6840–6846, DOI: 10.1021/ja0105257.

[200] M. S. Carvalho, R. A. Lacerda, J. P. B. Leão, J. D. Scholten, B. A. D. Neto, P. A. Z. Suarez, "In situ generated palladium nanoparticles in imidazolium-based ionic liquids: a versatile medium for an efficient and selective partial biodiesel hydrogenation", *Catal. Sci. Technol.* **2011**, *1*, 480–488, DOI: 10.1039/c0cy00028k.

[201] H. Ohde, C. M. Wai, H. Kim, J. Kim, M. Ohde, "Hydrogenation of olefins in supercritical CO2 catalyzed by palladium nanoparticles in a water-in-CO2 microemulsion", *J. Am. Chem. Soc.* **2002**, *124*, 4540–4541, DOI: 10.1021/ja012232j.

[202] M. Moreno, L. N. Kissell, J. B. Jasinski, F. P. Zamborini, "Selectivity and Reactivity of Alkylamine- and Alkanethiolate-Stabilized Pd and PdAg Nanoparticles for Hydrogenation and Isomerization of Allyl Alcohol", *ACS Catal.* **2012**, *2*, 2602–2613, DOI: 10.1021/cs300361y.

[203] L. Staiger, T. Kratky, S. Günther, O. Tomanek, R. Zbořil, R. W. Fischer, R. A. Fischer, M. Cokoja, "Steric and Electronic Effects of Phosphane Additives on the Catalytic Performance of Colloidal Palladium Nanoparticles in the Semi‐Hydrogenation of Alkynes", *ChemCatChem* **2021**, *13*, 227–234, DOI: 10.1002/cctc.202001121.

[204] M. Spiekermann, T. Seidensticker (Technische Universität Dortmund), "Hydrierung ungesättigter Kohlenwasserstoffverbindungen", DE102024001564A1, **2024**.

[205] I. Cano, P. W. N. M. van Leeuwen, "Selective Hydrogenation of Aldehydes and Ketones" in *Recent Advances in Nanoparticle Catalysis*, *Vol. 1,* (Eds.: P. W. van Leeuwen, C. Claver), Springer International Publishing, Cham, **2020,** DOI: 10.1007/978-3-030-45823-2_11.

[206] J. Gaube, W. David, R. Sanchayan, N. Wuchter, H.-F. Klein, "Studies on partial hydrogenation of 1,5,9-cyclo-dodecatriene towards cyclo-dodecene", *Appl. Catal., A* **2011**, *409-410*, 21–27, DOI: 10.1016/j.apcata.2011.09.003.

[207] Á. Molnár, A. Sárkány, M. Varga, "Hydrogenation of carbon–carbon multiple bonds: chemo-, regio- and stereo-selectivity", *J. Mol. Catal. A: Chem.* **2001**, *173*, 185–221, DOI: 10.1016/S1381-1169(01)00150-9.

[208] L. Zhang, J. M. Winterbottom, A. P. Boyes, S. Raymahasay, "Studies on the hydrogenation of cinnamaldehyde over Pd/C catalysts", *J. Chem. Technol. Biotechnol.* **1998**, *72*, 264–272, DOI: 10.1002/(SICI)1097-4660(199807)72:3<264::AID-JCTB897>3.0.CO;2-2.

[209] A. Cabiac, T. Cacciaguerra, P. Trens, R. Durand, G. Delahay, A. Medevielle, D. Plée, B. Coq, "Influence of textural properties of activated carbons on Pd/carbon catalysts synthesis for

cinnamaldehyde hydrogenation", *Appl. Catal., A* **2008**, *340*, 229–235, DOI: 10.1016/j.apcata.2008.02.018.

[210] E. Boymans, M. Janssen, C. Müller, M. Lutz, D. Vogt, "Rh-catalyzed linear hydroformylation of styrene", *Dalton Trans.* **2013**, *42*, 137–142, DOI: 10.1039/c2dt31738a.

[211] C. G. McAlister (Columbian Carbon Company), "Selective Hydrogenation of Cyclododecatriene to Cyclododecene", US 3 400 164, **1966**.

[212] J. Herwig, N. Wilczok, M. Roos, R. Burghardt, J. Gaube, G. Oenbrink, B. Günzel (Degussa AG), "Selktivhydrierung von cyclododecatrien zu cyclododecen", EP1457476A1, **2003**.

[213] A. Behr, L. Johnen, "Myrcene as a natural base chemical in sustainable chemistry: a critical review", *ChemSusChem* **2009**, *2*, 1072–1095, DOI: 10.1002/cssc.200900186.

[214] E. Bogel-Łukasik, M. Da Gomes Silva, I. D. Nogueira, R. Bogel-Łukasik, M. Da Nunes Ponte, "Study on selectivity of β-myrcene hydrogenation in high-pressure carbon dioxide catalysed by noble metal catalysts", *Green Chem.* **2009**, *11*, 1847–1856, DOI: 10.1039/b916017p.

[215] M. G. Speziali, F. C. Moura, P. A. Robles-Dutenhefner, M. H. Araujo, E. V. Gusevskaya, E. N. dos Santos, "Selective hydrogenation of myrcene catalyzed by complexes of ruthenium, chromium, iridium and rhodium", *J. Mol. Catal. A: Chem.* **2005**, *239*, 10–14, DOI: 10.1016/j.molcata.2005.04.067.

[216] P. A. Robles-Dutenhefner, M. G. Speziali, E. M. Sousa, E. N. dos Santos, E. V. Gusevskaya, "Selective hydrogenation of myrcene catalyzed by sol–gel Pd/SiO2", *Appl. Catal., A* **2005**, *295*, 52–58, DOI: 10.1016/j.apcata.2005.08.005.

[217] G. Rubulotta, K. L. Luska, C. A. Urbina-Blanco, T. Eifert, R. Palkovits, E. A. Quadrelli, C. Thieuleux, W. Leitner, "Highly Selective Hydrogenation of R-(+)-Limonene to (+)-p-1-Menthene in Batch and Continuous Flow Reactors", *ACS Sustainable Chem. Eng.* **2017**, *5*, 3762–3767, DOI: 10.1021/acssuschemeng.6b02381.

[218] A. van Rooy, J. N. de Bruijn, K. F. Roobeek, P. C. Kamer, P. W. van Leeuwen, "Rhodium-catalysed hydroformylation of branched 1-alkenes; bulky phosphite vs. triphenylphosphine as modifying ligand", *J. Organomet. Chem.* **1996**, *507*, 69–73, DOI: 10.1016/0022-328X(95)05748-E.

[219] A. Behr, D. Obst, C. Schulte, T. Schosser, "Highly selective tandem isomerization–hydroformylation reaction of trans-4-octene to n-nonanal with rhodium-BIPHEPHOS catalysis", *J. Mol. Catal. A: Chem.* **2003**, *206*, 179–184, DOI: 10.1016/S1381-1169(03)00461-8.

[220] M. T. Reetz, R. Breinbauer, K. Wanninger, "Suzuki and Heck reactions catalyzed by preformed palladium clusters and palladiumnickel bimetallic clusters", *Tetrahedron Lett.* **1996**, *37*, 4499–4502, DOI: 10.1016/0040-4039(96)00924-0.

[221] M. T. Reetz, E. Westermann, "Phosphane-Free Palladium-Catalyzed Coupling Reactions: The Decisive Role of Pd Nanoparticles", *Angew. Chem. Int. Ed.* **2000**, *39*, 165–168, DOI: 10.1002/(SICI)1521-3773(20000103)39:1<165::AID-ANIE165>3.0.CO;2-B.

[222] Y. Li, X. M. Hong, D. M. Collard, M. A. El-Sayed, "Suzuki cross-coupling reactions catalyzed by palladium nanoparticles in aqueous solution", *Org. Lett.* **2000**, *2*, 2385–2388, DOI: 10.1021/ol0061687.

[223] Y. Li, M. A. El-Sayed, "The Effect of Stabilizers on the Catalytic Activity and Stability of Pd Colloidal Nanoparticles in the Suzuki Reactions in Aqueous Solution", *J. Phys. Chem. B* **2001**, *105*, 8938–8943, DOI: 10.1021/jp010904m.

[224] K. R. Gopidas, J. K. Whitesell, M. A. Fox, "Synthesis, Characterization, and Catalytic Applications of a Palladium-Nanoparticle-Cored Dendrimer", *Nano Lett.* **2003**, *3*, 1757–1760, DOI: 10.1021/nl0348490.

[225] L. Wu, Z.-W. Li, F. Zhang, Y.-M. He, Q.-H. Fan, "Air‐Stable and Highly Active Dendritic Phosphine Oxide‐Stabilized Palladium Nanoparticles: Preparation, Characterization and Applications in the Carbon‐Carbon Bond Formation and Hydrogenation Reactions", *Adv. Synth. Catal.* **2008**, *350*, 846–862, DOI: 10.1002/adsc.200700441.

[226] V. Calò, A. Nacci, A. Monopoli, F. Montingelli, "Pd nanoparticles as efficient catalysts for Suzuki and Stille coupling reactions of aryl halides in ionic liquids", *J. Org. Chem.* **2005**, *70*, 6040–6044, DOI: 10.1021/jo050801q.

[227] M. Pittelkow, K. Moth-Poulsen, U. Boas, J. B. Christensen, "Poly(amidoamine)-Dendrimer-Stabilized Pd(0) Nanoparticles as a Catalyst for the Suzuki Reaction", *Langmuir* **2003**, *19*, 7682–7684, DOI: 10.1021/la0348822.

[228] L. Strimbu, J. Liu, A. E. Kaifer, "Cyclodextrin-Capped Palladium Nanoparticles as Catalysts for the Suzuki Reaction", *Langmuir* **2003**, *19*, 483–485, DOI: 10.1021/la026550n.

[229] R. Majumdar, S. Tantayanon, B. G. Bag, "Synthesis of palladium nanoparticles with leaf extract of Chrysophyllum cainito (Star apple) and their applications as efficient catalyst for C–C coupling and reduction reactions", *Int. Nano Lett.* **2017**, *7*, 267–274, DOI: 10.1007/s40089-017-0220-4.

[230] S. Sawoo, D. Srimani, P. Dutta, R. Lahiri, A. Sarkar, "Size controlled synthesis of Pd nanoparticles in water and their catalytic application in C–C coupling reactions", *Tetrahedron* **2009**, *65*, 4367–4374, DOI: 10.1016/j.tet.2009.03.062.

[231] A. Verma, K. Tomar, P. K. Bharadwaj, "Nanosized Bispyrazole-Based Cryptand-Stabilized Palladium(0) Nanoparticles: A Reusable Heterogeneous Catalyst for the Suzuki-Miyaura Coupling Reaction in Water", *Inorg. Chem.* **2019**, *58*, 1003–1006, DOI: 10.1021/acs.inorgchem.8b03015.

[232] O. Altan, "A rare example of the in situ formation of palladium nanoparticles: The emergence of catalytically active palladium nanoparticles from Pd (II) phosphine complexes in the Suzuki–Miyaura coupling reaction", *Appl. Organometal. Chem.* **2022**, *36,* DOI: 10.1002/aoc.6690.

[233] E. M. Antunes, Y. A. Adegoke, S. Mgwigwi, J. J. Bolton, S. F. Malan, D. R. Beukes, "Balancing Yields and Sustainability: An Eco-Friendly Approach to Losartan Synthesis Using Green Palladium Nanoparticles", *Molecules* **2025**, *30*, 2314–2328, DOI: 10.3390/molecules30112314.

[234] M. T. Reetz, G. Lohmer, "Propylene carbonate stabilized nanostructured palladium clusters as catalysts in Heck reactions", *Chem. Commun.* **1996**, 1921–1922, DOI: 10.1039/CC9960001921.

[235] D. Prat, J. Hayler, A. Wells, "A survey of solvent selection guides", *Green Chem.* **2014**, *16*, 4546–4551, DOI: 10.1039/C4GC01149J.

[236] H. G. O. Becker, R. Beckert, G. Domschke, E. Fanghänel, W. D. Habicher, P. Metz, D. Pavel, K. Schwetlick, "Organikum. Organisch-chemisches Grundpraktikum", Wiley-VCH, Weinheim, **2001**.

[237] M. Moreno-Mañas, R. Pleixats, S. Villarroya, "Fluorous Phase Soluble Palladium Nanoparticles as Recoverable Catalysts for Suzuki Cross-Coupling and Heck Reactions", *Organometallics* **2001**, *20*, 4524–4528, DOI: 10.1021/om010442z.

[238] D. Prat, A. Wells, J. Hayler, H. Sneddon, C. R. McElroy, S. Abou-Shehada, P. J. Dunn, "CHEM21 selection guide of classical- and less classical-solvents", *Green Chem.* **2016**, *18*, 288–296, DOI: 10.1039/C5GC01008J.

[239] R. Martin, S. L. Buchwald, "Palladium-catalyzed Suzuki-Miyaura cross-coupling reactions employing dialkylbiaryl phosphine ligands", *Acc. Chem. Res.* **2008**, *41*, 1461–1473, DOI: 10.1021/ar800036s.

[240] C. A. Fleckenstein, H. Plenio, "Efficient Suzuki-Miyaura coupling of (hetero)aryl chlorides with thiophene- and furanboronic acids in aqueous n-butanol", *J. Org. Chem.* **2008**, *73*, 3236–3244, DOI: 10.1021/jo8001886.

[241] C. Adamo, C. Amatore, I. Ciofini, A. Jutand, H. Lakmini, "Mechanism of the palladium-catalyzed homocoupling of arylboronic acids: key involvement of a palladium peroxo complex", *J. Am. Chem. Soc.* **2006**, *128*, 6829–6836, DOI: 10.1021/ja0569959.

[242] R. Brückner, "Reaktionsmechanismen. Organische Reaktionen, Stereochemie, moderne Synthesemethoden", Springer Spektrum, Heidelberg, Berlin, **2004**.

[243] M. Häußler, M. Eck, D. Rothauer, S. Mecking, "Closed-loop recycling of polyethylene-like materials", *Nature* **2021**, *590*, 423–427, DOI: 10.1038/s41586-020-03149-9.

[244] N. Herrmann, K. Köhnke, T. Seidensticker, "Selective Product Crystallization for Concurrent Product Separation and Catalyst Recycling in the Isomerizing Methoxycarbonylation of Methyl

Oleate", *ACS Sustainable Chem. Eng.* **2020**, *8*, 10633–10638, DOI: 10.1021/acssuschemeng.0c03432.

[245] J. T. Christl, P. Roesle, F. Stempfle, P. Wucher, I. Göttker-Schnetmann, G. Müller, S. Mecking, "Catalyst activity and selectivity in the isomerising alkoxycarbonylation of methyl oleate", *Chemistry* **2013**, *19*, 17131–17140, DOI: 10.1002/chem.201301124.

[246] P. Roesle, C. J. Dürr, H. M. Möller, L. Cavallo, L. Caporaso, S. Mecking, "Mechanistic features of isomerizing alkoxycarbonylation of methyl oleate", *J. Am. Chem. Soc.* **2012**, *134*, 17696–17703, DOI: 10.1021/ja307411p.

[247] F. Zhang, J. Yi, W. Pan, G. Mei, "A new process for the production of second-generation biodiesel from waste oils and fats", *Biomass Conv. Bioref.* **2024**, *14*, 9013–9022, DOI: 10.1007/s13399-022-03149-x.

[248] V. Goldbach, L. Falivene, L. Caporaso, L. Cavallo, S. Mecking, "Single-Step Access to Long-Chain α,ω-Dicarboxylic Acids by Isomerizing Hydroxycarbonylation of Unsaturated Fatty Acids", *ACS Catal.* **2016**, *6*, 8229–8238, DOI: 10.1021/acscatal.6b02622.

[249] J. Vondran, A. I. Seifert, K. Schäfer, A. Laudanski, T. Deysenroth, K. Wohlgemuth, T. Seidensticker, "Progressing the Crystal Way to Sustainability: Strategy for Developing an Integrated Recycling Process of Homogeneous Catalysts by Selective Product Crystallization", *Ind. Eng. Chem. Res.* **2022**, *61*, 9621–9631, DOI: 10.1021/acs.iecr.2c00476.

[250] B. Mattson, W. Foster, J. Greimann, T. Hoette, N. Le, A. Mirich, S. Wankum, A. Cabri, C. Reichenbacher, E. Schwanke, "Heterogeneous Catalysis: The Horiuti–Polanyi Mechanism and Alkene Hydrogenation", *J. Chem. Educ.* **2013**, *90*, 613–619, DOI: 10.1021/ed300437k.

[251] J. Dong, J. Lau, S. A. Svoronos, B. M. Moudgil, "Continuous Synthesis of Precision Gold Nanoparticles Using a Flow Reactor", *KONA Powder Part. J.* **2022**, *39*, 262–269, DOI: 10.14356/kona.2022011.

[252] N. von Vietinghoff, "Gas-consuming triphasic gas-liquid-liquid reactions in segmented slug flow", *Dissertation*, Technische Universität Dortmund, Dortmund, **2023**.

[253] G. D. Mitchell, "A Review of Permeation Tubes and Permeators", *Sep. Purif. Methods* **2000**, *29*, 119–128, DOI: 10.1081/SPM-100100005.

[254] J. Son, S. Verma, J. H. Kang, H. S. Park, H. Song, Y.-S. Bae, "Solubility and selectivity behavior of methane and hydrogen in several solvents at 313.15 K", *J. Mol. Liq.* **2025**, *427*, 127327–127333, DOI: 10.1016/j.molliq.2025.127327.

[255] Deutsches Institut für Normung e.V., "DIN EN ISO 12966-4". *Tierische und pflanzliche Fette und Öle – Gaschromatographie von Fettsäuremethylestern – Teil 4: Bestimmung mittels Kapillargaschromatographie*, *67.200.10*, **2015**, Beuth, Berlin.

[256] C. Nishino, W. S. Bowers, "The stereoisomers of 3,7,11-trimethyldodeca-2,6,10-triene", *Tetrahedron* **1976**, *32*, 2875–2877, DOI: 10.1016/0040-4020(76)80139-1.

[257] N. Ohler, K. Fisher, J. K. Hong (Amyris, Inc.), "Olefins And Methods For Making The Same", WO 2012/141783 A1, **2012**.

[258] A. F. Thomas, B. Willhalm, "Les spectres de masse dans l'analyse. 3 e communication. Les spectres de masse des hydrocarbures monoterpéniques", *Helv. Chim. Acta* **1964**, *47*, 475–488, DOI: 10.1002/hlca.19640470215.

[259] A. F. Thomas, B. Willhalm, "Mass spectra and organic analysis. Part VII. The mass spectra of the menthols, carvomenthols, their acetates and related alcohols", *J. Chem. Soc.* **1966**, 219–227, DOI: 10.1039/J29660000219.

[260] E. Bogel-Łukasik, R. Bogel-Łukasik, M. N. Da Ponte, "Pt- and Pd-catalysed limonene hydrogenation in high-density carbon dioxide", *Monatsh. Chem.* **2009**, *140*, 1361–1369, DOI: 10.1007/s00706-009-0196-5.

[261] D. Bréard, G. Viault, M.-C. Mezier, S. Pagie, A. Bruguière, P. Richomme, B. Charreau, S. Derbré, "Additional Insights into Hypericum perforatum Content: Isolation, Total Synthesis, and Absolute Configuration of Hyperbiphenyls A and B from Immunomodulatory Root Extracts", *J. Nat. Prod.* **2018**, *81*, 1850–1859, DOI: 10.1021/acs.jnatprod.8b00325.

[262] N. Döben, H. Yan, M. Kischkewitz, J. Mao, A. Studer, "Intermolecular Acetoxyaminoalkylation of α-Diazo Amides with (Diacetoxyiodo)benzene and Amines", *Org. Lett.* **2018**, *20*, 7933–7936, DOI: 10.1021/acs.orglett.8b03504.

[263] A. Shiozuka, K. Sekine, Y. Kuninobu, "Photoinduced Deaminative Borylation of Unreactive Aromatic Amines Enhanced by CO2", *Org. Lett.* **2021**, *23*, 4774–4778, DOI: 10.1021/acs.orglett.1c01503.

# 13 List of Figures

# 14 List of Tables